Advances in Measuring Therapeutic Efficacy: Optimizing Translational Outcome Measures in Genetic Models of Neurodevelopmental Disorders

By

ANNA ADHIKARI
DISSERTATION

Submitted in partial satisfaction of the requirements for the degree of

DOCTOR OF PHILOSOPHY

in

Molecular, Cellular and Integrative Physiology

in the

OFFICE OF GRADUATE STUDIES

of the

UNIVERSITY OF CALIFORNIA

DAVIS

Approved:

Jill L. Silverman, Chair

Joseph S. Anderson

Kyle D. Fink

Committee in Charge

2021

Abstract

Neurodevelopmental disorders (NDDs) are a broad range of conditions characterized by abnormal development of the nervous system during "critical periods" of brain growth and neuronal migration leading to lifelong impairments that are severe and often debilitating. The clinical presentation of NDDs includes a wide range of complex symptoms such as intellectual disabilities, developmental delay, recurring, uncontrollable seizures, lack of communication, poor gross and fine motor abilities, and autism spectrum disorder. There are no cures nor corrective therapies currently available and traditional medicines for symptom alleviation are minimal. To understand the intricacies of the neurobiology underlying a variety of NDDs with similar phenotypes, and potentially identify overlapping common mechanisms, while simultaneously addressing the grand unmet clinical need of efficacious therapeutics, we used and, in some cases, generated, novel preclinical genetic mouse models to identify disease-relevant translational outcome measures. Mouse models provide a valuable system to closely investigate symptoms analogous to human disease phenotypes. With the growing knowledge in genetics, NDD-relevant mouse models (knockout, knockin, humanized, etc.) with high construct validity have been generated to study the causal role of specific genes and how the loss of function contributes to NDD etiology and symptom manifestation. The research herein investigates mouse models of four distinct genetic NDDs and defines robust phenotypes that can be employed to evaluate novel therapeutic approaches. Chapter 1 investigates a novel mouse model harboring a deletion of the regulatory region 1b of the *Scn1a* gene which encodes for $Na_v1.1$ sodium channel. Haploinsufficiency of *SCN1A* is associated with epilepsy, including Dravet Syndrome. We discovered that both heterozygous and homozygous deletion of the regulatory element led to behavioral and seizure deficits as well as electroencephalogram phenotypes, such as elevated

spontaneous spiking events and spike trains, indicating that the 1b deletion model provides strong evidence to investigate the epilepsy risk gene *Scn1a* and highlights the importance of functional studies following modulation of regulatory elements in haploinsufficiency-related disorders. Chapter 2 focuses on *CDKL5* Deficiency Disorder (CDD), a rare X-linked NDD caused by the deficiency of the gene *CDKL5* (cyclin-dependent kinase-like 5), which is essential for normal brain development. Previous studies focused on male subjects from two unique mouse models to avoid any potential confounds of variable CDKL5 expression that results from X chromosome mosaicism in females; however, about 90% of individuals living with CDD are females. We performed comprehensive characterization in both sexes of the two mouse models to reproduce earlier studies in males and extend to the translationally relevant population, females. We discovered clinically relevant phenotypes including hyperactivity, learning and memory deficits, and susceptibility to seizures and abnormal EEG that will allow investigators to advance preclinical testing of therapeutics candidates for CDD in females. Chapter 3 expands on the characterization of the *Snord116* deletion model of the NDD Prader-Willi Syndrome, which is caused by a loss of paternal genes on chromosome 15q11-q13a. *SNORD116* is a paternally expressed imprinted gene cluster that encodes multiple copies of small nucleolar RNA. We focused on an understudied and key behavioral domain of cognition, using a heterozygous deletion of *Snord116* and identified learning and memory impairments, highlighting a broader role of *SNORD116,* beyond the numerous previous reports focused hyperphagic and metabolic phenotypes. Finally, chapter 4 utilizes the rigorous methodologies we implemented in the earlier chapters spanning a range of behavioral domains, seizures, and electroencephalographic outcome measures to investigate a novel cell-based gene therapy for Angelman Syndrome (AS). AS is caused by the deficiency of the gene *UBE3A* (ubiquitin protein ligase E3A). To evaluate *in vivo*

efficacy of our approach, we generated an immunodeficient AS mouse model capable of accepting human hematopoietic stem cells for engraftment and multilineage hematopoiesis. Upon delivery of functional UBE3A via transplantation and engraftment of CD34+ cells transduced with a *Ube3a* lentivector, we demonstrated rescue of AS deficits in the immunodeficient AS mouse model across two developmental time points. Currently, this study is in IND-enabling studies after a thorough review of the pre-IND package submitted to the FDA. Taken together, this research advances our understanding of NDDs and highlights the importance of neurodevelopmental behavior research in identifying clinically relevant phenotypes to meet the ultimate goal of therapeutic rescue.

Table of Contents

Chapter 1

Deletion of a non-canonical regulatory sequence causes loss of *Scn1a* expression and epileptic phenotypes in mice

This chapter has been published as: Jessica L. Haigh †, Anna Adhikari †, Nycole A. Copping, Tyler Stradleigh, A. Ayanna Wade, Rinaldo Catta-Preta, Linda Su-Feher, Iva Zdilar, Sarah Morse, Timothy A. Fenton, Anh Nguyen, Diana Quintero, Samrawit Agezew, Michael Sramek, Ellie J. Kreun, Jasmine Carter, Andrea Gompers, Jason T. Lambert, Cesar P. Canales, Len A. Pennacchio, Axel Visel, Diane E. Dickel, Jill L. Silverman* & Alex S. Nord* (2021). *Genome Medicine* 13:69.

† Authors contributed equally

***Authors are co-corresponding**

Abstract

Background: Genes with multiple co-active promoters appear common in brain, yet little is known about functional requirements for these potentially redundant genomic regulatory elements. *SCN1A*, which encodes the $Na_V1.1$ sodium channel alpha subunit, is one such gene with two co-active promoters. Mutations in *SCN1A* are associated with epilepsy, including Dravet syndrome (DS). The majority of DS patients harbor coding mutations causing *SCN1A* haploinsufficiency; however, putative causal non-coding promoter mutations have been identified.

Methods: To determine the functional role of one of these potentially redundant *Scn1a* promoters, we focused on the non-coding *Scn1a* 1b regulatory region, previously described as a non-canonical alternative transcriptional start site. We generated a transgenic mouse line with deletion of the extended evolutionarily conserved 1b non-coding interval and characterized changes in gene and protein expression, and assessed seizure activity and alterations in behavior.

Results: Mice harboring a deletion of the 1b non-coding interval exhibited surprisingly severe reductions of *Scn1a* and $Na_V1.1$ expression throughout the brain. This was accompanied by electroencephalographic and thermal evoked seizures, and behavioral deficits.

Conclusions: This work contributes to functional dissection of the regulatory wiring of a major epilepsy risk gene, *SCN1A*. We identified the 1b region as a critical disease-relevant regulatory element and provide evidence that noncanonical and seemingly redundant promoters can have essential function.

Background

A large proportion of brain-expressed and, indeed, all mammalian genes are believed to rely on multiple alternative promoters [1–3]. For many genes, the alternative promoters produce distinct 5′ untranslated regions but otherwise similar mRNA products, leading to identical proteins from distinct transcription start sites (TSSs) [4, 5]. Much of the focus on understanding the role of alternative promoters in mammalian transcriptional regulation has been on the potential for discrete function via producing specific isoforms or compartmentalized expression in specific cells or tissues [6–9]. However, TSS activity mapping has found many genes where alternative promoters are also active in the same tissue [10, 11]. More recent evidence from single-cell RNA sequencing and chromosome conformation suggests that annotated alternative promoters are frequently co-active in the same cells and physically interact in the nucleus [12– 14]. However, in contrast to work on the requirement for alternative promoters with presumed discrete activity, studies investigating the functional requirement for apparently redundant co-active promoters are lacking.

Epilepsy is one of the most common neurological disorders, with both rare highly penetrant and common variants contributing to genetic etiology. Mutations in *SCN1A*, which encodes the $Na_V1.1$ sodium channel alpha subunit, result in a range of epilepsy phenotypes from generalized febrile seizures to Dravet syndrome (DS), a severe childhood-onset disorder [15–17]. The majority of DS cases are caused by heterozygous de novo mutations in *SCN1A* resulting in truncation of the protein, with haploinsufficiency of $Na_V1.1$ presumed to underlie pathology [18, 19]. Mouse models with heterozygous coding mutations in *Scn1a* recapitulate features of DS, including seizures and sudden unexpected death in epilepsy (SUDEP) [20–26]. DS remains pharmacoresistant, with generalized tonic-clonic seizures beginning in the first year of life and

common comorbid neurodevelopmental disorder (NDD) behavioral phenotypes including cognitive impairments and ataxia [27–29].

SCN1A transcripts have a variable 5′ untranslated region (UTR) containing one of two TSSs, 1a and 1b, that are conserved between human and mouse [30, 31]. The proteins produced from 1a and 1b are expected to be identical. 1a was found to be the majority TSS for SCN1A transcripts across human and mouse (54% and 52% RACE transcripts, respectively). No strong region-specific differences in 1a versus 1b TSS usage across brain regions have been identified in previous work [30, 32]. 1a (also referred to as h1u) has been defined as the major *SCN1A* promoter; however, comparison across brain tissues in human and mouse suggests that 1a and 1b are co-active, with ~ 35% of transcripts arising from 1b [30]. The apparent functional redundancy of 1a and 1b promoter activity and 1a- and 1b-associated *SCN1A* transcripts raises the question of whether there are distinct roles or requirements of the 1a and 1b UTR and regulatory DNA sequences.

In addition to serving as an example in which to dissect the role of multiple co-active promoters, there is significant disease relevance for understanding the functional requirements for *SCN1A* regulatory DNA elements. *SCN1A* is one of the most common and well-documented genes associated with severe medical consequences of haploinsufficiency. Further, genome-wide association studies (GWAS) have implicated non-coding *SCN1A* DNA variants as contributing to epilepsy risk [33, 34], presumably via more subtle perturbation to transcriptional regulation, and non-coding promoter deletions have been found in DS patients [35, 36]. A recent study of common variation in the promoter regions of *SCN1A* found that promoter variant haplotypes reduced luciferase in cells and that such non-coding variants in the functional *SCN1A* allele may modify DS severity [37]. Based on these findings, it is plausible that pathogenic variation in regulatory

regions modulates *SCN1A* transcription, contributing to epilepsy. Functional studies are needed to determine the consequences of perturbations to *SCN1A* expression caused by mutations in non-coding DNA.

Here, we investigate *Scn1a* as a model for examining transcriptional and phenotypic consequences associated with loss of a potentially redundant co-active promoter. Combining genomics, neuropathology, behavior, seizure susceptibility, and EEG, we show that the *Scn1a* 1b noncanonical promoter and flanking conserved non-coding DNA sequence is independently essential for expression and brain function via characterizing the impact of deletion in $1b^{+/-}$ and $1b^{-/-}$ mice. In addition to mapping an essential regulatory region of a critical disease-relevant gene, our findings provide evidence that non-canonical promoters can play essential roles in general transcriptional activation.

Methods

Analysis of existing datasets

Chromosome conformation (Hi-C), histone posttranslational modification (PTM), ChIP-seq, and chromatin accessibility (ATAC-seq) analyses were performed using published data. For human brain, chromatin contacts were displayed as a heatmap of pseudo-log contact matrix scores obtained at 10-kb resolution from the PsychEncode.org resource website [38]. Differential Hi-C comparisons were conducted with contact matrices at 40-kb resolution for prefrontal cortex (PFC), right ventricle, hippocampus, lung, and pancreas with data obtained from Schmitt et al. [39], NCBI Gene Expression Omnibus (GEO) dataset GSE87112. The heatmaps for individual tissues were generated with the pseudo-log of the scores in the contact matrices, while the inter-tissue comparisons were composed with the log likelihood of scores of one tissue against each other. Frontal lobe histone PTMs were assessed using ChIP-seq coverage from the Roadmap

Epigenomics Consortium [40] as integrated in the UCSC Genome Browser [41], data available at https://egg2.wustl.edu/roadmap/web_portal/. Assessment of chromatin accessibility for dorsolateral PFC neuronal and non-neuronal ATAC-seq data was made in the same way with data from Fullard et al. [42], GSE96949. For mouse brain, assessment of chromatin accessibility was performed using ATAC-seq data from purified excitatory, and parvalbumin (PV) and vasoactive intestinal peptide (VIP) expressing neurons obtained from Mo et al. [43], GSE63137.

Generation of 1b mutant mice

We used Cas9-mediated mutagenesis of C56BL/6N oocytes to generate a mouse line harboring deletion of a conserved portion on the non-coding region of *Scn1a* containing the previously described 1b [30] regulatory region. Guide RNA was designed and synthesized according to described methods [44], pooled with Cas9 mRNA and injected into mouse oocytes. The gRNA sequences were GGAGATCTGGGTAGTCCTCG and GCTTTTCATACTATAGTGAG. Initial Cas9 targeting was performed at Lawrence Berkeley National Laboratory. F0s (induced on C57BL/6N background) carrying mutations were genotyped and bred to expand a line harboring a 3063-bp deletion at the 1b interval (mm10 - chr2:66407567-66410630).

The colony was rederived and maintained by crossing male 1b deletion carriers with C57BL/6N wildtype females (Charles River). Extensive crossing of heterozygous mutation carriers to wildtype animals vastly reduces the likelihood that any potential off-target mutations caused by Cas9 targeting would persist in our 1b deletion line. Genotypes were identified via PCR and sequence-verified for all animals included in analyses, with the primers in **Table 1**. All mouse studies were approved by the Institutional Animal Care and Use Committees at the University of California Davis and the Lawrence Berkeley National Laboratory. Mice were housed in a temperature-controlled vivarium maintained on a 12-h light–dark cycle. Efforts were made to

minimize pain and distress and the number of animals used. Survival was monitored and log-rank Mantel Cox used to assess survival rate. Table 2 summarizes the sex, genotype, age, and n for each experiment.

RNA collection

Cortex, hippocampus, and cerebellum were regionally dissected from one hemisphere of P7, P32, and 3- month-old homozygous deletion, heterozygous, and wildtype mice following anesthesia with isoflurane and decapitation. The other hemisphere was used for Western blot analysis. Both male and female mice were used, though there was no equal sex representation across genotypes. Total RNA was isolated using RNAqueous kit (Ambion) and assayed using an Agilent BioAnalyzer instrument.

qRT-PCR

Differential expression of *Scn1a* was verified by qRT-PCR at 3 months old. Primers are reported in **Table 3**, and qPCR was performed with SYBR green PCR master mix (Applied Biosystems). Samples were excluded if technical replicates failed. Cycle counts were normalized to *Gapdh*. Statistical analysis was performed using ANOVA followed by Tukey's on relative gene expression between genotypes using ΔΔCT.

RNA-seq

RNA from P7 forebrain and P32 hippocampus was collected as described above. Samples included males and females of each genotype when possible. Stranded mRNA sequencing libraries were prepared using TruSeq Stranded mRNA kits (Illumina). Each round of sequencing was quantified, pooled, and sequenced in one lane on the Illumina HiSeq platform using a single-end 50-bp (P7, P32 homozygous) or paired-end 150 (P32 heterozygous) strategy at the UC Davis DNA Technologies Core. The transcriptomic analysis was performed as before [45]. Reads from RNA-

seq were aligned to the mouse genome (mm9) using STAR (version 2.7.2) [46]. Aligned reads mapping to genes were counted at the gene level using subreads featureCounts [47]. The mm9 knownGene annotation track and aligned reads were used to generate quality control information using the full RSeQC tool suite [48]. Unaligned reads were quality checked using FastQC.

Differential expression analysis

Raw count data for all samples were used for differential expression analysis using edgeR [49]. Genes with at least 1 read per million in at least one sample were included for analysis, resulting in a final set of 15589, 14631, and 15002 genes for differential testing in P7 and P32 mice, respectively. Multidimensional scaling analysis indicated that *Scn1a* expression and sex were the strongest driver of variance across samples. Tagwise dispersion estimates were generated and differential expression analysis was performed using a generalized linear model with genotype as the variable for testing. Effect of genotype was modeled as individual comparison of heterozygous and homozygous 1b deletion mice with the respective WT controls. Normalized expression levels were generated using the edgeR pseudocount and rpkm functions. Aligned reads contained in BAM files from each sample were counted to calculate the overlap of sequencing reads with each locus. The coordinates for each locus were m1a: chr2:66,278,753-66,278,887, the m1b deletion region: chr2:66245632-66248697, and m1c: chr2:66,249, 400-66,249,514. Mouse gene ontology (GO) data was downloaded from Bioconductor (org. Mm.eg.db). We used the goseq package to test for enrichment of GO terms indicating parent:child relationships. For GO analysis, we examined down- and upregulated genes separately for genes meeting an FDR < 0.05. For the enrichment analysis, the test set of differentially expressed genes was compared against the background set of genes expressed in our study.

Immunofluorescence

All histological experiments were performed at least in triplicate and experimenters were blinded to genotype. Following anesthesia with isoflurane, P28 male and female mice were transcardially perfused with 4% paraformaldehyde (PFA) in HEPES, followed by overnight fixation in the same solution. After fixation, brains were removed from the skull, embedded in 2% LTE agarose/ Tris-buffered saline (TBS) and cut coronally in 50-µm sections on a vibratome (VT 1000S, Leica). Sections underwent antigen retrieval in a solution of 0.1 M sodium citrate (pH 6), 200 mM sucrose, and 1% (v/v) hydrogen peroxide at 60 °C for 1 h. Subsequently, sections were permeabilized and blocked in TBS with 0.1% Triton X-100 and 5% normal donkey serum for 24 h at room temperature. Immunolabeling was carried out using primary antibodies directed against $Na_V1.1$ (K74/ 71, mouse, IgG1, 1:100, NeuroMab) and parvalbumin (L114/3, 75-455, mouse, IgG2a, 1:100, NeuroMab). Subclass-specific secondary antibodies (488 and RRX) were used at 1:200 (Jackson ImmunoResearch Laboratories Inc.). All imaging was carried out on a Nikon A1 laser scanning confocal microscope. FIJI (National Institutes of Health) was used for image processing with settings consistently applied to across samples.

Western blot

Flash frozen samples (n = 3 per genotype) were prepared for Western blot using the Mem-PER Plus protein extraction kit (89842, Thermo Scientific) to isolate membrane and cytoplasmic protein fractions from mice aged P29-32. We ran 40 µg of protein on 10% gels using the Mini-PROTEAN Tetra Cell Western blotting system (Bio-Rad). Anti-NaV1.1 (Ab5204a, rabbit, 1:1000, Millipore) and anti-beta-actin (Ab8227, rabbit, 1:5000, Abcam) primary antibodies were incubated overnight in Odyssey blocking buffer (LI-COR). Secondary antibodies (IRDye 800CW Donkey anti-Rabbit IgG Secondary Antibody) were used at 1:5000 in Odyssey blocking buffer (LI-COR) for 1 h at room temperature. Blots were visualized using a LI-COR Odyssey CLx system and quantified in

FIJI. Protein levels assayed via Western blot were compared by one-way ANOVA and Tukey's post hoc.

Mouse colony at UC Davis Medical Center

Heterozygous (+/−) breeders were transferred from the UC Davis Center of Neuroscience to the UC Davis Medical Center. Offspring were maintained on the C57BL/ 6N background from The Jackson Laboratory (Bar Harbor, ME). Colonies were maintained with two breeding paradigms: wildtype ($1b^{+/+}$) by heterozygous ($1b^{+/-}$) and heterozygous ($1b^{+/-}$) by heterozygous ($1b^{+/-}$) crosses, giving rise to wildtype ($1b^{+/+}$), heterozygous ($1b^{+/-}$), and homozygous mice ($1b^{-/-}$). After weaning on PND 21, mice were socially housed in groups of 2–4 by sex. Cages were housed in ventilated racks in a temperature (68–72 °F) and humidity (~ 25%) controlled vivarium on a 12:12 light/dark cycle with lights on at 07:00, off at 19: 00 h. Standard rodent chow and tap water were available ad libitum. In addition to standard bedding, a Nestlet square, shredded brown paper, and a cardboard tube were provided. All subjects were tested between 2 and 5 months of age. All measures were conducted by an experimenter blind to genotype.

Behavioral assay design

Both male and female subjects were used in this study. Subjects ($1b^{+/+}$ − males N = 12, females N = 14, $1b^{+/-}$ − males N = 15, females N = 15, and $1b^{-/-}$ − males N = 6, females N = 6) began the behavioral battery at 6 weeks of age. All behavioral tests were performed between 09: 00 and 17:00 h during the light phase of the 12:12 light/ dark cycle. Mice were brought to an empty holding room adjacent to the testing area at least 1 h prior to the start of behavioral testing. To minimize the carryover effects from repeated testing, assays were performed in the order of least to the most stressful tasks. Subjects were sampled from $1b^{+/-} \times 1b^{+/-}$ and $1b^{+/-} \times 1b^{+/+}$ pairings.

The order and age of testing was as follows with at least 48-h separating tasks: (1) Elevated-plus maze at 6 weeks of age, (2) light dark conflict at 6 weeks of age, (3) open field at 7 weeks of age, (4) beam walking at 7 weeks of age, (5) rotarod at 8 weeks of age, (6) novel object recognition at 9 weeks of age, (7) spontaneous alternation at 10 weeks of age, (8) self-grooming at 11 weeks of age, (9) social approach at 11 weeks of age, (10) male–female social interaction at 12 weeks of age, (11) acoustic startle at 13 weeks of age, (12) prepulse inhibition at 13 weeks of age, and (13) fear conditioning at 14 weeks of age.

Developmental milestones

Developmental milestones were measured on postnatal day (PND) 2, 4, 6, 8, 10, and 12, as previously described [50, 51]. Body weight, length (nose to edge of tail), and head width were measured using a scale (grams) and a digital caliper (cm). Cliff avoidance was tested by placing each pup near the edge of a cardboard box, gently nudging it towards the edge, and measuring the time for it to turn and back away from the edge. Failures to avoid the cliff was recorded as a maximum score of 30 s. Righting reflex was tested by placing each pup on its back, releasing it, and measuring the time for it to fully flip over onto four paws on each developmental day. Negative geotaxis was tested by placing each pup, facing downwards, on a screen angled at 45° from parallel, and measuring the time for it to completely turn and to climb to the top of the screen. Failures to turn and climb were recorded as a maximum score of 30 s. Circle transverse was tested by placing each pup in the center of a circle with a 5″ (12.5 cm) diameter drawn on a laminated sheet of 8.5″ × 11″ white paper and measuring the time for it to exit the circle. Failures to exit the circle were recorded as a maximum score of 30 s.

Elevated-plus maze

The assay was performed using a mouse EPM (model ENV-560A) purchased from Med Associates (St. Albans, VT) and performed as previously described [52].

Light↔dark conflict

The light↔dark assay was performed in accordance with previously described procedures [52]. The mouse was allowed to explore freely for 10 min. Time in the dark side chamber and total number of transitions between the light and dark side chambers were automatically recorded during the 10-min session.

Open field

General exploratory locomotion in a novel open field arena was evaluated as previously described [45, 50, 52]. Total distance traversed, horizontal activity, vertical activity, and time spent in the center were automatically measured to assess gross motor abilities in mice. Repeated measures ANOVA was used to detect differences in horizontal, vertical, total, and center time activity obtained during the open field assay. Multiple comparisons were corrected for using Sidak post hoc methods and F, degrees of freedom, and p values are reported.

Spontaneous alternation in a Y-maze

Spontaneous alternation was assayed using methods modified based from previous studies [45] in mice. Oneway ANOVA was used to detect differences in alternation. Multiple comparisons were corrected for using Sidak post hoc methods and F, degrees of freedom, and p values are reported.

Novel object recognition

The novel object recognition test was conducted as previously described [50, 53, 54]. The assay consisted of four sessions: a 30-min habituation session, a second 10-min habituation phase, a 10-min familiarization session, and a 5-min recognition test. Sniffing was defined as head facing the object with the nose point within 2 cm from the object. Time spent sniffing each object was scored by an investigator blind to both genotype and treatment. Recognition memory was evaluated by time spent sniffing the novel object versus the familiar object and innate side bias was accounted for by comparing sniff time of the two identical objects during familiarization. Within genotype repeated measures ANOVA was used to analyze novel object recognition using novel versus familiar objects as comparison. F, degrees of freedom, and p values are reported.

Balance beam walking

Balance beam walking is a standard measure of motor coordination and balance [55, 56]. We followed a procedure similar to methods previously described using our behavioral core [57]. Latency to traverse the length of the beam, number of footslips off the edge of the beam, and falls (if any) are scored by the investigator from coded video recordings. Approximately four trials per day for 3 days represents a standard training protocol.

Rotarod

Motor coordination, balance, and motor learning were assessed using an accelerating rotarod (Ugo Basile, Schwenksville, PA) as previously described [58, 59]. The task requires the mice to walk forward in order to remain on top of the rotating cylinder rod. Mice were given 3 trials per day with a 30–60-min intertrial rest interval. Mice were tested over two consecutive days for a total of 6 trials. Latency to fall was recorded with a 300-s maximum latency.

Repetitive self-grooming

Spontaneous repetitive self-grooming behavior was scored as previously described [45, 52, 58, 60, 61]. Each mouse was placed individually into a standard mouse cage (46 cm long × 23.5 cm wide × 20 cm high). The first 10-min was habituation and was unscored. Each subject was scored for cumulative time spent grooming all the body regions during the second 10 min of the test session.

Three-chambered social approach

Social approach was tested in an automated three-chambered apparatus using methods similar to those previously described [45, 50, 52, 61, 62]. Three zones, defined using the EthoVision XT software, detected time in each chamber for each phase of the assay. Direction of the head, facing towards the cup enclosure, defined sniff time. The subject mouse was first contained in the center chamber for 10 min, then allowed to explore all three empty chambers during a 10-min habituation session, then allowed to explore the three chambers containing a novel object in one side chamber and a novel mouse in the other side chamber. Lack of innate side preference was confirmed during the initial 10 min of habituation to the entire arena. Novel stimulus mice were 129Sv/ImJ, a relatively inactive strain, aged 10–14 weeks, and matched to the 1b mice by sex. Number of entries into the side chambers served as a within-task control for levels of general exploratory locomotion.

Male–female social interaction

The male–female reciprocal social interaction test was conducted as previously described [45, 52, 58, 60, 61]. Briefly, each freely moving male subject was paired for 5 min with a freely moving unfamiliar estrous WT female. Duration of nose-to-nose sniffing, nose-to-anogenital sniffing, and following were scored using Noldus Observer 8.0XT event recording software (Noldus, Leesburg,

VA). Ultrasonic vocalization spectrograms were displayed using Avisoft software, and calls were identified manually by a highly trained investigator blinded to genotype.

Fear conditioning

Delay contextual and cued fear conditioning was conducted using an automated fear-conditioning chamber (Med Associates, St Albans, VT, USA) as previously described [45, 50, 52]. Training consisted of a 2-min acclimation period followed by three tone–shock (CS–US) pairings (80-dB tone, duration 30 s; 0.5-mA footshock, duration 1 s; intershock interval, 90 s) and a 2.5-min period during which no stimuli were presented. The environment was well lit (~ 100 lx), with a stainless steel grid floor and swabbed with vanilla odor cue (prepared from vanilla extract; McCormick; 1:100 dilution). A 5- min test of contextual fear conditioning was performed 24 h after training, in the absence of the tone and footshock but in the presence of 100 lx overhead lighting, vanilla odor, and chamber cues identical to those used on the training day. Cued fear conditioning, conducted 48 h after training, was assessed in a novel environment with distinct visual, tactile, and olfactory cues. The cued test consisted of a 3-min acclimation period followed by a 3-min presentation of the tone CS and a 90-s exploration period. Cumulative time spent freezing in each condition was quantified by VideoFreeze software (Med Associates).

Acoustic startle and prepulse inhibition

Subjects were tested in San Diego Instruments startle chambers using standard methods as described previously [58, 63]. One trial type measured the response to no stimulus (baseline movement). The other five trial types measured startle responses to 40 ms sound bursts of 80, 90, 100, 110, or 120 dB. The maximum startle amplitude over this sampling period was taken as the dependent variable. For prepulse inhibition of acoustic startle, mice were presented with each of

seven trial types across six discrete blocks of trials for a total of 42 trials, over 10.5 min. One trial type measured the response to no stimulus (baseline movement) and another measured the startle response to a 40 ms, 110 dB sound burst. The other five trial types were acoustic prepulse stimulus plus acoustic startle stimulus trials. The trial types were presented in pseudorandom order such that each trial type was presented once within a block. Prepulse stimuli were 20 ms tones of 74, 78, 82, 86, and 92 dB intensity, presented 100 ms before the 110 dB startle stimulus. The maximum startle amplitude over this sampling period was taken as the dependent variable. A background noise level of 70 dB was maintained over the duration of the test session.

Seizure susceptibility following administration of pentylenetetrazole

Subjects were weighed then administered pentylenetetrazole (80 mg/kg) intraperitoneally. Dosing was conducted in the morning (9:00–12:00) in a dim (~ 30 lx) empty holding room. Directly after administration of the convulsant, subjects were placed in a clean, empty cage, and subsequent seizure stages were live-scored for 30 min. Seizure stages were scored using latencies to (1) first jerk/ Straub's tail, (2) loss of righting, (3) generalized clonic-tonic seizure, and (4) death. Time to each stage was taken in seconds and compared by genotype. Unpaired Student's t tests were used to analyze latencies to first jerk, loss of righting, generalized clonic-tonic seizure, and death.

Thermal induction of seizures in juveniles (febrile seizure paradigm)

Subjects were acclimated to an arena for 10 min maintaining temperature at 37.5 °C. Temperature was increased 0.5 °C every 2 min until animal showed behavioral seizure or a max temperature of 42.5 °C was reached. Observer recorded the type of seizure, and the temperature at which the behavioral seizure was observed using the Racine score from the literature for febrile seizures: 1.

Staring 2. Head nodding 3. Unilateral forelimb clonus 4. Bilateral forelimb clonus 5. Rearing and falling 6. Clonic seizure

EEG implantation

Wireless EEG transmitters were implanted in anesthetized test animals using continuous isoflurane (2–4%). A 2–3-cm midline incision was made over the skull and trapezius muscles, then expanded to expose the subcutaneous space. Implants were placed in the subcutaneous pocket lateral to the spine to avoid discomfort of the animal and displacement due to movement. Attached to the implant were 4 biopotential leads made of a NickelColbalt-based alloy insulated in medical-grade silicone, making up two channels that included a signal and reference lead. These leads were threaded towards the cranial part of the incisions for EEG and EMG placement. The periosteum was cleaned from the skull using a sterile cotton-tip applicator and scalpel then two 1-mm diameter burr holes were drilled (1.0 mm anterior and 1.0 mm lateral; − 3.0 mm posterior and 1.0 mm lateral) relative to bregma. This lead placement allowed for measurement of EEG activity across the frontal cortical area. Steel surgical screws were placed in the burr holes and the biopotential leads were attached by removing the end of the silicone covering and tying the lead to its respective screw. Once in place, the skull screws and lead connections were secured using dental cement. For EMG lead placement, the trapezius muscles of the animal were exposed, and each lead was looped through and sutured to prevent displacement. Finally, the incision was sutured using non-resorbable suture material and the animals were placed in a heated recovery cage where they received Carprofen (5 mg/kg; i.p.) directly after surgery and 24 h post-surgery as an analgesic. Subjects were individually caged with ad libitum access to food and water for 1-week before EEG acquisition and monitored daily to ensure proper incision healing and recovery. Each implantation surgery took < 45 min, and no fatalities were observed.

EEG acquisition

EEG data was acquired using Ponemah (Data Sciences International, St. Paul, MN, USA) and subsequently analyzed using the Neuroscore automated software (Data Sciences International, St. Paul, MN, USA). Subjects were recorded for 24-h baseline in their home cage before administration of 80 mg/kg pentylenetetrazole (Sigma Aldrich, St. Louis, MO, USA) injected intraperitoneally. EEG and EMG were continuously sampled at 500 Hz. Spiking was defined as activity above an absolute threshold of 200–1000 μV that lasted between 0.5 and 100 ms, while spike trains had a minimum duration of 0.5 s, a minimum spike interval of 0.05 s, and a minimum of 4 consecutive spikes. Power spectral densities were determined using a periodogram transformation from amplitude to frequency domains then log transformed for clearer data illustration. Latency to seizure onset and subsequent death following administration of PTZ was first quantified by observed latencies then confirmed by spectral EEG and amplitude response readouts. One-way ANOVA was used to analyze bouts of spike train activity and latency to seizure onset and death between genotypes. An overall ANOVA was used to detect a genotype difference across power bands, then genotype differences were analyzed within power bands using multiple comparisons.

Luciferase assay

We constructed luciferase reporter plasmids by cloning a ~ 900-bp region containing human 1b [30] into the pGL4.24 vector (Promega) upstream of the minP, primers in **Table 4**. HEK293 cells or SK-N-SH cells (40– 60% confluent) were transfected using Lipofectamine 3000 (Invitrogen) with each construct (400 ng) and the Renilla luciferase expression vector pRL-TK (40 ng; Promega) in triplicate. After 24 h, the luciferase activity in the cell lysates was determined using the Dual Luciferase Reporter System (Promega). Firefly luciferase activities were normalized to

that of Renilla luciferase, and expression relative to the activity of an inactive region of noncoding DNA (NEG2) was noted.

CRISPR/dCas9 in HEK293 cells

HEK293 cells were transfected with 500 ng of equimolar pooled SCN1A_h1b sgRNAs (**Table 5**) and 500 ng dCas9p300Core (Addgene, plasmid #61357) using Lipofectamine 3000. After 24 h, media was refreshed. Forty eight hours following transfection, RNA was collected using RNAqueous kit (Ambion) and cDNA was generated using Superscript III reverse transcriptase (Invitrogen). Changes in gene expression were quantified via qPCR using SYBR green, and primers are listed in **Table 3**.

Results

Scn1a 1a and 1b chromosomal regions physically interactand share chromatin signatures indicating pan-neuronal transcriptional activator regulatory activity. To define the regulatory landscape of the *SCN1A* locus, we examined publicly available chromosome conformation (Hi-C), transcriptomic and epigenomic data obtained from analysis of human and mouse brain tissues (**Fig. 1a, d, S1**). We generated contact heatmaps from published Hi-C from prefrontal cortex [64] (PFC) at 10-kb resolution (Additional file 1: Fig. S1a), and for additional tissues at 40-kb resolution [64] (**Additional file 1: Fig. S1c**). In PFC, *SCN1A* was located at the boundary of two major TADs (topological associated domains), with extensive local interactions within the *SCN1A* locus. Differential analysis of Hi-C from PFC versus lung showed stronger local interactions in PFC (Additional file 1: Fig. S1b), while there were no major differences between the PFC and hippocampus, suggesting brain-specific local *SCN1A* chromosomal interactions (**Additional file 1: Fig. S1c**).

Previous work using 5′ RACE [30] and luciferase as- says defined regulatory sequences at *SCN1A*, including two genomic intervals, non-coding exons 1a and 1b, that are conserved between human and mouse and where the majority of *SCN1A* transcripts originate [30] (Fig. 1a). The locations of the 1a (GenBank: DQ993522) and 1b (GenBank: DQ993523) TSSs are shown as mapped in earlier work [30, 32]. DNA sequence at 1a and 1b is highly evolutionarily conserved across vertebrates. Not- ably, conservation at 1b extends nearly 3 kb downstream of the defined UTR transcribed sequence. Interaction models from an independent capture Hi-C dataset [64] also suggested physical interaction between 1a and 1b as well as between 1b and the nearby *TTC21B* promoter (**Fig. 1a**).

We examined chromatin state at the SCN1A locus across seven histone post-translational modifications (PTMs) from human mid frontal lobe [40] (**Fig. 1a**). The strongest chromatin signatures for regulatory elements were at the previously defined 1a and 1b loci, with H3K27ac, H3K4me3 and H3K9ac, weak H3K4me1, and absence of H3K27me3, H3k9me3, and H3K36me3 in these regions. In ATAC-seq and H3K27ac across the majority of non-CNS tissues profiled in the ENCODE or Roadmap projects [40], 1a and 1b show reduced or absent signal, further indicating primary importance in the nervous system. In addition to 1a and 1b, there were several other non-coding regions showing weaker, but still significant enrichment for H3K27ac in brain, representing potential additional *SCN1A* regulatory elements. ATAC-seq from neuronal and non-neuronal cells from dorsolateral PFC (DLPFC) [42] showed that neuronal cells have increased chromatin accessibility across *SCN1A* generally (**Fig. 1a**), with specific enrichment at 1a, 1b, and a third region also within the first intron of *SCN1A*. Comparing human neuronal data with mouse ATAC-seq and histone PTM data [43], accessibility and chromatin states appeared largely conserved (**Fig. 1a, d**). Finally, ATAC-seq data [43] from sorted neuronal subtypes in mouse,

including excitatory neurons and parvalbumin (PV) and vasoactive intestinal peptide (VIP) interneurons, indicated consistent open chromatin at *Scn1a* 1a and 1b across neuron types (**Fig. 1d**).

The evolutionarily conserved Scn1a 1b non-coding region acts as a Scn1a transcriptional activator and is essential for survival. Taken together, the comparative and functional genomics data indicates evolutionarily conserved brain-specific pan-neuronal regulatory and TSS activity of 1a and 1b, with evidence for chromosomal physical interaction be- tween the two promoters. The 1b region has been annotated as an alternative TSS, yet the extended region surrounding the annotated transcribed UTR also shows the strongest enrichment for evolutionary conservation and for chromatin signatures associated with strong enhancer activity (i.e., H3K27ac and H3K4me3) across non-coding regions of the *SCN1A* locus. We sought to validate the specific role of 1b DNA in activation of *SCN1A* expression. We used luciferase assay to function- ally test the core human 1b (h1b) region in cell lines. A 941-bp region containing 1b and conserved flanking sequence induced expression in HEK293 and SK-N-SH cells when cloned into a vector with a minimal promoter (**Fig. 1b**). To further demonstrate the regulatory role of 1b in *SCN1A* expression, we showed that a pool of 6 sgRNAs targeted to human 1b sequence and delivered along with dCas9-p300, an inactivated Cas9-histone acetyltransferase fusion protein [65], was sufficient to in- duce *SCN1A* expression 2.5-fold in HEK293 cells compared to non-transfected control (**Fig. 1c**).

The strength of evolutionary conservation and tran- scriptional activation-associated epigenomic signatures at the extended 1b interval is paradoxical considering its presumed role as a secondary TSS. Thus, we sought to test whether the extended 1b regulatory region is essen-

tial for *Scn1a* expression, and whether loss of this elem-ent is sufficient to produce seizures and DS-relevant phenotypes in mice. We used CRISPR/Cas9 targeting of C57BL/6N oocytes to generate mice harboring a 3063- bp deletion of the interval flanking the 1b regulatory element of *Scn1a*, removing the entire mammalian con- served region (**Fig. 1e**). We expanded this *Scn1a 1b* dele- tion line (hereafter referred to as 1b) via at least six generations of breeding to wildtype C57BL/6N (WT) mice, eliminating potential off-target Cas9-induced mutations.

Previous studies have found that mice harboring homozygous coding mutations to *Scn1a* die in the third postnatal week and mice with heterozygous coding mutation exhibit reduced survival [20, 26]. In comparison,46 female WT by heterozygous male ($1b^{+/-}$) harem triopairings yielded 41 litters, and survival rates of $1b^{+/-}$ and WT littermate pups were indistinguishable (log-rank $p = 0.8458$); however, female $1b^{+/-}$ by $1b^{+/-}$ male harem trios required nearly double the number of pairings ($n = 74$) to produce only 13 litters. This was caused by both reduced rates of pregnancy, as determined via regularlyweighing females, and by increased litter cannibalism in the neonatal period. Among the 13 litters that were produced, the three genotypes were born at expected Mendelian frequencies (**Additional file 2: Table S1**). While survival rates for $1b^{+/-}$ and WT littermate pups from these litters were indistinguishable (log-rank $p = 0.5455$), 48% of homozygous 1b deletion ($1b^{-/-}$) mice died by weaning (**Fig. 1f**, log-rank $p < 0.0001$). Thus, $1b^{+/-}$ mice survive, but female carriers were less efficient at producing viable litters, severely impacting generation of homozygous 1b deletion offspring. $1b^{-/-}$ pups were visibly smaller and failed to thrive, though around half survived to maturity. In addition, $1b^{-/-}$ exhibited spontaneous seizures during routine handling, consistent with expected neurological impact of significant decreasein *Scn1a* expression.

We tested $1b^{+/-}$ mice for measures of general health and utilized a Fox developmental

battery [51] and found no deficits in growth, reflexes, and limb strength (**Additional file 3: Table S2**). $1b^{-/-}$ pups were not evaluated for these milestones, as spontaneous seizures were observed, so handling was minimized to increase survival.

Loss of extended 1b interval causes loss of $Na_V1.1$ across postnatal brain regions. We first sought to test if 1b ablation resulted in changes in amount and regional distribution of *Scn1a* transcript and $Na_V1.1$ protein in mouse brain. Expression of *Scn1a*/$Na_V1.1$ begins in the early postnatal period and reaches high expression throughout the brain by 4 weeks of age [66]. We focused on the cerebellum, hippocampus, and cortex, where we detected $Na_V1.1$ by immunohistochemistry in WT mice by P28 (**Fig. 2a–c**). We tested for reduced *Scn1a* RNA expression via quantitative reverse-transcription PCR (qRT-PCR) performed on cortex, hippocampus, and cerebellum of 3-month-old *Scn1a* 1b deletion carriers and WT littermates (WT $n = 4$, $1b^{+/-}$ $n = 5$, $1b^{-/-}$ $n = 7$) (**Fig. 2d**). In agreement with GTEx [32] and previous studies [30], we observed the highest level of WT *Scn1a* expression in the cortex with expression in cerebellum and hippocampus 34% and 60% lower, respectively. When comparing 1b deletion to WT mice (ANOVA with Tukey's post hoc), there was a reduction in *Scn1a* expression as measured by qPCR in $1b^{-/-}$ mice in all 3 regions tested (reduced by 57% in the cortex, 62% in the hippocampus and 59% in the cerebellum). $1b^{+/-}$ *Scn1a* expression was not significantly reduced versus WT, but did show a trend towards an intermediate level between WT and $1b^{-/-}$ levels (**Fig. 2d**).

Reduction in protein expression across the mouse brain was evaluated by Western blot analysis of the membrane fraction from prepared cortex, hippocampus, and cerebellum from mice aged P29–32 ($n = 3$ each genotype). $1b^{-/-}$ mice had significantly decreased $Na_V1.1$ protein

expression (ANOVA with Tukey's post hoc) compared to WT in all three regions, and $1b^{+/-}$ showed significant decreased expression in cortex and hippo- campus and a trend towards reduced levels in cerebellum (**Fig. 2e**). $Na_V1.1$ expression was reduced by 45% in $1b^{+/-}$ mice and 76% in $1b^{-/-}$ mice in the cortex, 35% in $1b^{+/-}$ mice and 75% in $1b^{-/-}$ mice in the hippocampus, and by 23% in $1b^{+/-}$ mice and 67% in $1b^{-/-}$ in the cere- bellum (**Fig. 2e**). Raw Western blots including blots of the cytoplasmic fraction can be seen in **Additional file 1: Fig. S2**. These results are consistent with qPCR results and show that deletion of the extended 1b interval had a larger than expected impact on *Scn1a* and $Na_V1.1$ expression considering the proportion of transcripts expected to originate at this element.

With immunofluorescence (IF), we compared qualitative distribution of expression of $Na_V1.1$ along with the interneuron marker parvalbumin across $1b^{-/-}$, $1b^{+/-}$, and $1b^{+/+}$ mice at P28 ($n = 3$ each genotype) (**Fig. 2f and raw images in Additional file 1: Fig. S3**). Notably, deletion of 1b appeared to generally reduce $Na_V1.1$ expression, rather than specifically impact certain brain regions, consistent with 5′ RACE TSS activity [30]. Consistent with Western blot quantifications, there was subtle apparent reduction in $Na_V1.1$ IF in the brainstem and midbrain between WT and $1b^{+/-}$ mice, while $1b^{-/-}$ mice had obvious reduction of expression in the brainstem, midbrain, cerebellum, and hippocampus.

Adult mice harboring heterozygous 1b deletion are susceptible to seizures and exhibit abnormal EEG activity. Given the general failure to thrive, developmental lethality, and spontaneous behavioral seizures in homozygous $1b^{-/-}$ mice, we focused on heterozygous $1b^{+/-}$ mice to test for more subtle phenotypes associated with two seizure induction paradigms, exposure to heat and the chemoconvulsant pentylenetetrazole (PTZ), paired with EEG recording.

Thermal-evoked seizures are a hallmark of DS and *SCN1A*-associated epilepsy models [67, 68], and thus, we tested whether these were induced in $1b^{+/-}$ mice. P22 $1b^{+/-}$ mice and WT littermates ($n = 9$ per genotype of mixed sex) were subjected to a gradual 0.5 °C increase in body temperature every 2 min from 37.5 °C to 42.5 °C, mimicking the increase in body temperature during a fever. $1b^{+/-}$ mice displayed heat- induced behavioral seizures at 41.5 °C (**Fig. 3a**) as measured by the Racine scale (**Fig. 3b**) while WT did not present with seizures (**Fig. 3a, b**).

To corroborate and further characterize induced seizure susceptibility, we used a second paradigm, PTZ seizure induction [69]. First, we performed a dose response analysis on mice of the C57BL/6 N background strain to identify a PTZ dose that allowed for observations of all stages of behavioral seizure in addition to EEG seizures (**Additional file 1: Fig. S4**). To test for induced seizure susceptibility, male and female $1b^{+/-}$ and WT littermate mice were intraperitoneally administered 80 mg/kg of PTZ. After administration, latencies to first jerk, loss of righting, generalized clonic-tonic seizure, and full tonic extension were measured. In comparison to WT litter- mates, PTZ-treated $1b^{+/-}$ mice exhibited increased seizure susceptibility across all measures (**Fig. 4a–d**: firstjerk $t_{(1,\ 30)} = 2.171$, $p = 0.038$; loss of righting $t_{(1,\ 30)} = 2.160$, $p = 0.039$; generalized clonic-tonic seizure $t_{(1,\ 30)} = 2.128$, $p = 0.042$; full tonic extension $t_{(1,\ 30)} = 2.207$, $p = 0.035$, unpaired Student's t tests).

Finally, to test for spontaneous neurophysiological phenotypes in $1b^{+/-}$ mice and to link PTZ-induced behavioral seizures with electrophysiological activity, skull screws for EEG and EMG were implanted in a second group of animals of both sexes and recordings were made over a 24-h interval, with PTZ induction at the end of the recording period. Comparison of EEG signatures for $1b^{+/-}$ and WT littermates prior to PTZ administration show elevated spontaneous spiking events and spike trains in $1b^{+/-}$ mice and increased power spectral density signatures (**Fig.**

4e, f). Spiking activity measured by bouts of spike trains was significantly higher in $1b^{+/-}$ when compared to WT littermate controls (**Fig. 4g**: t (1,8) = 3.812, p = 0.005), indicating heightened excitability. $1b^{+/-}$ deletion subjects also had higher power detected across all frequency bins when compared to WT (**Fig. 4h**:F (1, 8) = 423.9, $p < 0.0001$, multiple comparisons all had$p < 0.0001$). At the end of the recording period, PTZ ad- ministration in implanted mice reproduced the faster latency to seizure onset and trends towards faster latencyto death (**Fig. 4i**, j: t (1, 8) = 3.920, p = 0.004, t (1, 8) =2.103, p = 0.068, compared to WT by unpaired t tests),and revealed corresponding increases in EEG activity in response to PTZ. There were no sex differences in induced seizure or EEG outcomes in $1b^{+/-}$ mice. Overall, these experiments revealed elevated spontaneous EEG spiking and irregular neural signatures, and link PTZ- induced behavioral seizures with increased neurophysiological activity in $1b^{+/-}$ mice.

Homozygous but not heterozygous 1b deletion causes cognitive deficits in novel object recognition (NOR) and spontaneous alternation in the Y-maze. To investigate the impact of 1b deletion on behavior, we performed a tailored battery focused on learning and memory and motor abilities on $1b^{+/-}$ and surviving $1b^{-/-}$ male and female mice (see "Methods" section for details). $1b^{+/-}$ mice of both sexes were additionally tested in a comprehensive behavioral battery of standard assays of overall physical health across development, sensori- motor reflexes, motor coordination, anxiety-like, and so- cial behavior to test for subtler phenotypes that might be present in the heterozygous mutants. Details of the ad- ministration of behavioral testing are described in "Methods", and results from these experiments are summarized in **Additional file 4: Table S3**.

Cognitive deficits were observed in $1b^{-/-}$ but not $1b^{+/-}$ mice in two corroborating assays of learning and memory, NOR, and Y-maze. Following established NOR methods [50, 53], manual

scoring by a highly trained observer blinded to genotype indicated WT and $1b^{+/-}$ mice spent more time investigating the novel object versus the familiar object, as expected. In contrast, $1b^{-/-}$ homozygous mice did not exhibit typical novel object preference (**Fig. 5a**: within genotype repeated measures (paired *t*-test) WT $p = 0.002$; $1b^{+/-}$ mice $p = 0.018$, *, novel versus familiar), illustrating recall of the familiar object and learning. Yet the $1b^{-/-}$ mice did not exhibit this typical learning and memory ($p = 0.8698$). Sexes were combined since there was no sex difference observed on time spent sniffing objects (**Additional file 5: Table S4**). Control data illustrating no preference for the left or right objects and sufficient time spent investigating the objects is shown in **Fig. 5b**. $1b^{-/-}$ mice were also impaired on the Y-maze, making less alternation triads compared to WT and $1b^{+/-}$ mice (**Fig. 5c**: $F_{(2, 62)} = 5.693$, $p < 0.005$). Sidak's multiple comparisons indicated the $1b^{-/-}$ differed from the WT ($p = 0.0192$) and $1b^{+/-}$ ($p = 0.0047$) mice.

Most parameters of gross motor skills and motor co- ordination were similar across genotypes (**Additional file 4: Table S3**). In the open field novel arena assay of loco- motion, $1b^{-/-}$ were hyperactive during 10 min of the 30- min session. The time course for horizontal, total, and vertical activity was as expected across time, showing normal acclimation to the arena in all genotypes. Horizontal and vertical activity did not differ between genotypes (**Fig. 5d, e**; $F_{(2, 80)} = 0.1401$, $p > 0.05$). However, $1b^{-/-}$ mice were hyperactive in total activity (**Fig. 5f**; $F_{(2, 80)} = 5.117$, $p < 0.008$, Two-way repeated measures ANOVA, genotype × time). Sidak's multiple comparisons indicated comparisons between the $1b^{-/-}$ versus the WT mice differed at time of bins 11–15 ($p = 0.0014$) and differed between the $1b^{-/-}$ and $1b^{+/-}$ mice at time bins of 11–15 ($p < 0.0001$) and 16–20 ($p = 0.0270$). In addition to highlighting a clear hyperactive phenotype in the $1b^{-/-}$ mice, linked to DS and numerous NDDs [70, 71], these results indicate that there were no gross motor abnormalities, inability to rear, or hindlimb weakness

that would prevent movement in the learning and memory assays that utilized objects and maze exploration.

$1b^{+/-}$ mice did not exhibit significant consistent phenotypes in a comprehensive battery of assays standard for examining mouse models of NDDs (**Additional file 4: Table S3**). For example, $1b^{+/-}$ mice spent less time in the dark chamber in the light-dark assay ($t_{(1, 69)} = 2.121$, $p = 0.0375$, unpaired two-tailed *t*-test) suggesting elevated anxiety-like behavior, yet no corroborative significance was observed in the plus maze. Reduced male–female ultrasonic vocalizations in $1b^{+/-}$ males in the reciprocal social interaction test alludes to aberrant social communication but no corroborative social behavior events were detected ($t_{(1,25)} = 2.143$, $p = 0.0420$, unpaired two-tailed *t*-test). Also, a three-chambered approach was typical. Applying rigorous standards used for behavioral studies of NDD models, the absence of two corroborating assays or indices of anxiety-like behavior and sociability precludes us from interpreting these findings as robust phenotypes [72, 73]. For all behavioral assays, no sex differences were identified between male and female 1b deletion mice (**Additional file 5: Table S4**).

Differential gene expression in Scn1a 1b deletion mouse hippocampus. We used RNA sequencing (RNA-seq) at P7 and P32 to examine *Scn1a* isoform expression and transcriptional pathology associated with 1b deletion. At P7, forebrain from WT ($n = 2$), $1b^{+/-}$ ($n = 4$), and $1b^{-/-}$ ($n = 2$) mice was compared. At P32, analysis was performed on microdissected hippocampus tissue in two rounds. We focused on hippocampus as an example P32 tissue, as hippocampal ablation of *Scn1a* has been specifically linked to seizure and DS-relevant cognitive deficits in mice [74]. For P32, we first compared $1b^{-/-}$ ($n = 2$) and WT ($n = 2$) mice using 50 bp single-end

read approach. Next, we compared of WT (n = 3) and 1b$^{+/-}$ (n = 4) mice using 150 bp paired-end read methods in order to more deeply sample reads covering the 1a and 1b UTR region of the *Scn1a* transcript.

At both P7 and P32, *Scn1a* expression showed significant 1b dosage-dependent decrease using an additive model (**Additional file 6: Table S5–7**). *Scn1a* expression was reduced compared to WT in 1b$^{+/-}$ and 1b$^{-/-}$ mice at P7, though this decrease was only independently significant in 1b$^{-/-}$ mice and failed to pass stringent FDR threshold (P = 0.0047, FDR = 0.28). At P32, where we had increased power due to higher coverage and larger sample numbers and where *Scn1a* expression is much higher in WT, *Scn1a* was significantly lower in both heterozygous and homozygous 1b deletion mice (FDR = 0.00028 and 1.97 × 10 [11], respectively; **Fig. 6a, b, Additional file 1: Fig. S5a**).

To compare transcripts arising from 1a and 1b at P32, when *Scn1a* expression in WT brain is high, we measured the number of splice junction reads that linked the 1a and 1b non-coding exons with the first *Scn1a* coding exon and the number of total reads that mapped unambiguously to 1a or 1b (**Fig. 6c**). As expected, splice junction and overlapping reads associated with mouse 1b were reduced in 1b$^{+/-}$ mice and abolished in 1b$^{-/-}$ mice (**Fig. 6d, Additional file 1: Fig. S5b**). Mouse 1a splice junction and overlapping reads appeared reduced in 1b$^{-/-}$ mice, though there were relatively low numbers of reads mapping to these intervals (**Fig. 6d top, Additional file 1: Fig. S5b left**). In contrast, 1a-associated reads in heterozygous 1b deletion carriers were in- creased (**Fig. 6d bottom, Additional file 1: Fig. S5b right**). The increased 1a transcripts present in the 1b$^{+/-}$, but not the 1b$^{-/-}$ mice, is consistent with *trans* compensation by increased expression from the second *Scn1a* allele, but not with compensation of the deleted 1b in *cis* via increased 1a usage. The change in total *Scn1a* reads from RNA-seq at P32 (**Fig. 6d**) was

stronger than identified in adult brain tissues via qRT-PCR and $Na_V1.1$ Western blot. Our findings suggest decreases in RNA and protein levels in 1b deletion mice that are higher than predicted based on the proportion of *Scn1a* transcripts originating at 1b observed here and in previous work [30].

We tested for differential expression across 15589, 14631, and 15002 genes that were robustly expressed in the P7, P32 heterozygous comparison, and P32 homozygous comparison RNA-seq datasets, respectively (RPKM values in **Additional file 6: Table S5–7**). No genes flanking *Scn1a* showed consistent robust differential ex- pression (DE) in $1b^{+/-}$ and $1b^{-/-}$ mice at P7 or P32, indicating that the major regulatory effects of the deleted *Scn1a 1b* interval are specific to *Scn1a* expression (**Additional file 1: Fig. S5a**). At P7, we identified 21 mostly downregulated DE genes in $1b^{+/-}$ carriers and 47 down- regulated and 61 upregulated DE genes in $1b^{-/-}$ mice meeting an FDR < 0.05 threshold (**Additional file 6: Table S8, S9**). The small effect of 1b deletion on differential gene expression at P7 is consistent with the low expression and non-essential role of *Scn1a* in early post- natal development [75]. Later in development, P32 heterozygous *1b* deletion was associated with 223 DE genes (175 downregulated, 48 upregulated) at FDR < 0.05 (**Fig. 6e, Additional file 6: Table S10**). Homozygous *1b* deletion carriers exhibited much stronger transcriptional impact, with a total of 723 DE genes (337 downregulated, 386 upregulated) DE at FDR < 0.05 **(Fig. 6f, Additional file 6: Table S11**). Volcano plots that show log2 fold change effect sizes and significance values for DE genes in 1b deletion mice shown in **Fig. 6e, f**. Gene set enrichment analysis of Gene Ontology (GO) found general synaptic signaling and function were enriched among downregulated DE genes in P32 heterozygous carriers, with no terms passing FDR < 0.05 criteria for upregulated genes. In P32 homozygous *1b* carriers, enriched terms for neuron development and differentiation were

associated with upregulated DE genes while synaptic signaling and mature neuronal function terms were enriched among downregulated DE genes (**Fig. 6g**). Heterozygous and homozygous *1b* deletion mutants shared 104 DE genes (**Additional file 1: Fig. S5c**), which were primarily downregulated and enriched for synaptic and differentiation terms (**Additional file 1: Fig. S5d**).

Discussion

The majority of functional studies of alternative promoters have been on genes where the multiple alternative TSSs are predicted to have discrete cell-type or tissue-specific activity [6–9]. However, recent studies ofTSS usage and promoter interactions suggest a model where alternative promoters interact physically and are co-active in the same cells [12–14]. In these situations, it is largely unknown what the requirement for individual TSS and associated regulatory DNA may be. Here we focus on one specific putative non-canonical disease- relevant alternative promoter, a 3-kb evolutionarily con- served DNA region including the previously described *Scn1a* 1b TSS. We show that full deletion of this interval from the mouse genome causes significant decrease in *Scn1a* expression and $Na_V1.1$ protein and results inspontaneous seizures and high developmental lethality with significant cognitive and behavioral deficits in surviving mice. While phenotypes were less severe in heterozygous $1b^{+/-}$ mice, presence of temperature and PTZ-induced behavioral seizures and elevated observations of epileptiform indices in EEG in these mice indicate a milder phenotype with relevance to SCN1A-associated epilepsies [76–78]. Our results define 1b as an essential disease-relevant *Scn1a* regulatory region and show that loss of regulatory DNA associated with a non- canonical TSS can have a surprisingly strong and translationally relevant phenotypic impact.

There are multiple possible explanations for the observed strong impact of loss of the 1b interval

on *Scn1a* expression. First, 1a and 1b isoforms may indeed be discretely regulated, but previous measures of 1b- originating transcripts must have significantly underestimated the actual contribution of 1b transcripts to *Scn1a* expression. However, there is no evidence that earlier studies were incorrect and our estimates of *Scn1a* overall and 1a and 1b RNA-seq read frequency in 1b deletion mice do not support this simple model. Alternatively, the 1b TSS could have increased activity earlier in development or 1b-associated regulatory DNA activity could also be required for 1a transcription. These models are both plausible and consistent with our results. Considering the frequency of promoter-promoter interaction and reported common co-expression of alterative TSSs in single neurons, many brain genes could share similar regulatory structure as *Scn1a*. Our findings are consistent with models suggesting regulatory DNA at putative alternative promoters and associated regulatory sequences contributes to transcriptional activation across interacting TSSs. Further experiments are needed to resolve the specific cellular, molecular, and developmental function and potential co-dependence of the 1a and 1b intervals and associated transcripts, and studies of other genes are needed to test if this phenomenon is wide-spread. Our findings represent initial insights into the essential regulatory roles of non-canonical promoters even when such TSSs produce mRNA encoding identical amino acid products.

Annotation of the genome has led to major gains in understanding transcriptional wiring, yet it has been surprisingly difficult to predict the sufficiency and necessity of specific regulatory elements, even those expected to be critical based on comparative and functional genomics [3, 10, 79]. Knockout mouse models have been a gold standard for testing the phenotypic consequences of mutations, and recent efforts deleting non-coding DNA have provided critical insights into the role of regulatory DNA [79–82]. Here, we used CRISPR/Cas9-mediated deletion to assess the role of the evolutionarily conserved 1b interval on higher-order neurological

phenotypes in mice. Homozygous 1b deletion caused spontaneous seizures and behavioral deficits and had a strong impact on survival, demonstrating the essential nature of the deleted interval. Further studies are needed to define the minimal and core nucleotides within the 1b interval and to define proteins that bind and participate in regulation. In addition, similar functional studies of other *Scn1a* regulatory DNA elements, and specifically of the 1a region, are necessary to determine which regulatory DNA regions are necessary and sufficient for expression in the brain.

Heterozygous loss of the 1b interval appears to have a less severe impact compared to truncating *Scn1a* mutations, which are sufficient to reduce survival and cause behavioral and cognitive deficits relevant to DS and NDD in mice [20, 26]. It is possible that phenotypes are milder in heterozygous 1b deletion mice in this study compared to other *Scn1a* mouse models due to differences in genetic background or environment. In a review of $Scn1a^{+/-}$ mouse models of Dravet syndrome [83], it was noted that those bred on a 6N background were more susceptible to hyperthermia-induced seizures, yet had milder spontaneous seizures and improved survival rates relative to 6J crosses. DS-model mice bred on 129/SvJ genetic background have a higher threshold for thermally induced seizures, no cognitive impairments, and reduced rates of premature death [84]. The 1b deletion mouse line was generated on a C57BL/6N background and thus it is possible that phenotypes are milder due to this compared to if they were bred with C57BL/6J. However, there is also evidence that the milder phenotypes in 1b deletion mice relative to *Scn1a* coding loss-of- function mutants is due to the different impacts on *Scn1a* dosage. Previously reported phenotypes of mice harboring heterozygous DS-associated *Scn1a* truncating mutations are similar to or less severe than homozygous 1b deletion phenotype identified here, suggesting stronger phenotypic impact in line with haploinsufficiency is produced by the more severe reduction in *Scn1a* expression caused by homozygous 1b deletion. In support of this, the P32

homozygous DE signatures of downregulated synaptic expression and upregulated expression of earlier neuronal differentiation and maturation genes are consistent with previous data on *Scn1a* truncating mutants [85]. Notably, these DE results could be driven by either developmental changes or reflect seizure pathology in 1b deletion mice [85]. Further studies of 1b deletion and *Scn1a* coding mutant mouse lines on the same genetic background will be needed to directly compare phenotype severity associated with 1b deletion.

While we did not identify spontaneous behavioral seizures or corroborated behavioral phenotypes in heterozygous 1b deletion mice, our characterization of $1b^{+/-}$ mice showed general epilepsy relevance. Heterozygous 1b deletion mice exhibited spontaneous spike trains and abnormal EEG spectral bandwidths. In particular, the EEG results with increased spike trains observed $1b^{+/-}$ mice are indicative of general seizure relevance. It is likely that the increased spike events at baseline are associated with susceptibility to thermally induced seizures seen in $1b^{+/-}$ mice. At 41.5 °C, the temperature of seizure onset is higher than those observed for global $Scn1a^{+/-}$ mice (38.5 ± 0.2 °C) [86] and hippocampal $Na_V1.1$ deletion mice (40.3 ± 0.2 °C) [74]. There are neurodevelopmental disorder genetic models where spontaneous behavioral seizures are not seen in mice while they are in humans [87–89]. As female $1b^{+/-}$ failed to efficiently reproduce, it is possible that milder but still DS- relevant behavioral and cognitive deficits are present in heterozygous 1b deletion mice. The degree to which 1b deletion is directly relevant to DS will require further studies. Regardless, our findings show the relevance of this novel *Scn1a* regulatory deletion mouse line to *SCN1A*-associated epilepsy.

The EEG spectral phenotypes in heterozygous 1b deletion mice overlap with other neurodevelopmental disorder and epilepsy models, and represent a potential translational biomarker for future investigation. Elevated delta spectral power is a biomarker of Angelman

syndrome (AS) [90] and elevated beta spectral power is posited to be a biomarker of Dup15q syndrome [91, 92]. These disorders are of interest as there are co-occurring features with DS and epilepsy. AS and Dup15q both have high rates of seizures, cognitive disruption, and comorbid diagnosis with autism. Neural signatures in EEG by power bands can be similarly measured in both rodents and humans, and thus our findings have translational relevance [76–78]. Analysis of spike-firing and oscillatory activity during rewarded trials in touchscreen assays have recently been described in detail [93]. Given the behavioral deficits in cognitive function and firing activity identified here, future studies investigating behavioral outcomes and neurophysiological signals are warranted and will shed light on relationship between 1b deletion, EEG spectral phenotypes, and behavior.

SCN1A-associated epilepsies, including DS, remain difficult to treat as conventional sodium channel blockers are usually ineffective and may even exacerbate the disease [29, 94]. Precision therapies that rescue $Na_V1.1$ haploinsufficiency in relevant cell types would be preferred to ameliorate symptoms and reduce side effects compared to more globally acting therapies. Using CRISPR/dCas9 induction, we increased *SCN1A* expression in HEK293 cells by targeting the 1b region. Application of a similar synthetic transcriptional activation therapeutic strategy has shown exciting promise in vivo in mice, where a dCas9-based activator combined with locus-specific guide RNA delivered to hypothalamus was capable of rescuing obesity phenotypes in *Sim1* and *Mc4r* heterozygous mutant mice [95]. dCas9-VP160 activation of *Scn1a* 1b, but not 1a, by a single sgRNA was able to enhance *Scn1a* expression in P19 cells [96]. Delivery of the guide and dCas9-VP64 via AAV intracerebroventricular injections to forebrain GABAergic interneurons in a model of Dravet syndrome ameliorated hyperthermia- induced seizures [96]. Our data demonstrates that 1b is an essential and important regulator of *Scn1a* expression and highlights a potential target for

epigenomic intervention in *SCN1A*-related epilepsies. Studies characterizing the regulatory DNA at disease-relevant loci, as we have done here with the *Scn1a* 1b region, will be required to properly design therapies using targeted expression rescue.

Conclusions

The work here on the *Scn1a* 1b regulatory region contributes to functional dissection of the regulatory wiring of a major epilepsy risk gene. Our findings show that *Scn1a* 1b regulatory deletion mice represent a general epilepsy-relevant model that will be valuable for understanding the relationship between *Scn1a* dosage and neurological phenotypes in a genetic preclinical model. Our study justifies increased focus on non-coding regulatory DNA in genetic screening of DS and epilepsy patients, and highlights the need for more in-depth functional studies of regulatory DNA elements in general and specifically in haploinsufficiency-associated disorders.

References

1. Landry, J.-R., Mager, D. L. & Wilhelm, B. T. Complex controls: the role of alternative promoters in mammalian genomes. *Trends Genet.* **19**, 640–8 (2003).

2. Forrest, A. R. R. *et al.* A promoter-level mammalian expression atlas. *Nature* **507**, 462–470 (2014).

3. Carninci, P. *et al.* The transcriptional landscape of the mammalian genome. *Science* **309**, 1559–63 (2005).

4. Yamashita, R. *et al.* Genome-wide characterization of transcriptional start sites in humans by integrative transcriptome analysis. *Genome Res.* **21**, 775–89 (2011).

5. Davuluri, R. V., Suzuki, Y., Sugano, S., Plass, C. & Huang, T. H. M. The functional consequences of alternative promoter use in mammalian genomes. *Trends in Genetics* **24**, 167–177 (2008).

6. Kimura, K. *et al.* Diversification of transcriptional modulation: large-scale identification and characterization of putative alternative promoters of human genes. *Genome Res.* **16**, 55–65 (2006).

7. de Klerk, E. & 't Hoen, P. A. C. Alternative mRNA transcription, processing, and translation: insights from RNA sequencing. *Trends Genet.* **31**, 128–39 (2015).

8. Tzvetkov, M. V., Meineke, C., Oetjen, E., Hirsch-Ernst, K. & Brockmöller, J. Tissue-specific alternative promoters of the serotonin receptor gene HTR3B in human brain and intestine. *Gene* **386**, 52–62 (2007).

9. Reyes, A. & Huber, W. Alternative start and termination sites of transcription drive most transcript isoform differences across human tissues. *Nucleic Acids Res.* **46**, 582–592 (2018).

10. Kim, T. H. *et al.* A high-resolution map of active promoters in the human genome. *Nature* **436**, 876–80 (2005).

11. Sandelin, A. *et al.* Mammalian RNA polymerase II core promoters: insights from genome-wide studies. *Nat. Rev. Genet.* **8**, 424–36 (2007).

12. Karlsson, K., Lönnerberg, P. & Linnarsson, S. Alternative TSSs are co-regulated in single cells in the mouse brain. *Mol. Syst. Biol.* **13**, 930 (2017).

13. Li, G. *et al.* Extensive promoter-centered chromatin interactions provide a topological basis for transcription regulation. *Cell* **148**, 84–98 (2012).

14. Zhang, Y. *et al.* Chromatin connectivity maps reveal dynamic promoter–enhancer long-range associations. *Nature* **504**, 306–310 (2013).

15. Claes, L. R. *et al.* The *SCN1A* variant database: a novel research and diagnostic tool. *Hum. Mutat.* **30**, E904–E920 (2009).

16. Lossin, C. A catalog of SCN1A variants. *Brain Dev.* **31**, 114–130 (2009).

17. Parihar, R. & Ganesh, S. The SCN1A gene variants and epileptic encephalopathies. *J. Hum. Genet.* **58**, 573–580 (2013).

18. McArdle, E. J., Kunic, J. D., George, A. L. & Jr. Novel SCN1A frameshift mutation with absence of truncated Nav1.1 protein in severe myoclonic epilepsy of infancy. *Am. J. Med. Genet. A* **146A**, 2421–3 (2008).

19. Meng, H. *et al.* The SCN1A mutation database: updating information and analysis of the relationships among genotype, functional alteration, and phenotype. *Hum. Mutat.* **36**, 573–80 (2015).

20. Yu, F. H. *et al.* Reduced sodium current in GABAergic interneurons in a mouse model of severe myoclonic epilepsy in infancy. *Nat. Neurosci.* **9**, 1142–1149 (2006).

21. Ogiwara, I. *et al.* Nav1.1 haploinsufficiency in excitatory neurons ameliorates seizure-associated sudden death in a mouse model of Dravet syndrome. *Hum. Mol. Genet.* **22**, 4784–804 (2013).

22. Miller, A. R., Hawkins, N. A., McCollom, C. E. & Kearney, J. A. Mapping genetic modifiers of survival in a mouse model of Dravet syndrome. *Genes. Brain. Behav.* **13**, 163–72 (2014).

23. Tai, C., Abe, Y., Westenbroek, R. E., Scheuer, T. & Catterall, W. A. Impaired excitability of somatostatin- and parvalbumin-expressing cortical interneurons in a mouse model of Dravet syndrome. *Proc. Natl. Acad. Sci.* **111**, E3139–E3148 (2014).

24. Dutton, S. B. *et al.* Preferential inactivation of Scn1a in parvalbumin interneurons increases seizure susceptibility. *Neurobiol. Dis.* **49**, 211–20 (2013).

25. Cheah, C. S. *et al.* Specific deletion of NaV1.1 sodium channels in inhibitory interneurons causes seizures and premature death in a mouse model of Dravet syndrome. *Proc. Natl. Acad. Sci. U. S. A.* **109**, 14646–51 (2012).

26. Ogiwara, I. *et al.* Nav1.1 Localizes to Axons of Parvalbumin-Positive Inhibitory Interneurons: A Circuit Basis for Epileptic Seizures in Mice Carrying an Scn1a Gene Mutation. *J. Neurosci.* **27**, 5903–5914 (2007).

27. Kalume, F. Sudden unexpected death in Dravet syndrome: Respiratory and other physiological dysfunctions. *Respir. Physiol. Neurobiol.* **189**, 324–328 (2013).

28. Shmuely, S., Sisodiya, S. M., Gunning, W. B., Sander, J. W. & Thijs, R. D. Mortality in Dravet syndrome: A review. *Epilepsy Behav.* **64**, 69–74 (2016).

29. Wirrell, E. C. Treatment of Dravet Syndrome. *Can. J. Neurol. Sci. / J. Can. des Sci. Neurol.* **43**, S13–S18 (2016).

30. Martin, M. S., Tang, B., Ta, N. & Escayg, A. Characterization of 5′ untranslated regions of the voltage-gated sodium channels SCN1A, SCN2A, and SCN3A and identification of cis-conserved noncoding sequences. *Genomics* **90**, 225–235 (2007).

31. Long, Y.-S. *et al.* Identification of the promoter region and the 5′-untranslated exons of the human voltage-gated sodium channel $Na_v1.1$ gene (*SCN1A*) and enhancement of gene expression by the 5′-untranslated exons. *J. Neurosci. Res.* **86**, 3375–3381 (2008).

32. Lonsdale, J. *et al.* The Genotype-Tissue Expression (GTEx) project. *Nat. Genet.* **45**, 580 (2013).

33. International League Against Epilepsy Consortium on Complex Epilepsies. Electronic address: epilepsy-austin@unimelb.edu.au. Genetic determinants of common epilepsies: a meta-analysis

of genome-wide association studies. *Lancet Neurol.* **13**, 893–903 (2014).

34. ILAE, T. I. L. A. E. C. on C. E. Genome-wide mega-analysis identifies 16 loci and highlights diverse biological mechanisms in the common epilepsies. *Nat. Commun.* **9**, 5269 (2018).

35. Gao, Q.-W. *et al.* A Point Mutation in SCN1A 5′ Genomic Region Decreases the Promoter Activity and Is Associated with Mild Epilepsy and Seizure Aggravation Induced by Antiepileptic Drug. *Mol. Neurobiol.* **54**, 2428–2434 (2017).

36. Nakayama, T. *et al.* Deletions of SCN1A 5′ genomic region with promoter activity in Dravet syndrome. *Hum. Mutat.* **31**, 820–829 (2010).

37. Lange, I. M. *et al.* Influence of common *SCN1A* promoter variants on the severity of *SCN1A* -related phenotypes. *Mol. Genet. Genomic Med.* e727 (2019). doi:10.1002/mgg3.727

38. PsychENCODE Consortium, S. *et al.* The PsychENCODE project. *Nat. Neurosci.* **18**, 1707–12 (2015).

39. Schmitt, A. D. *et al.* A Compendium of Chromatin Contact Maps Reveals Spatially Active Regions in the Human Genome. *Cell Rep.* **17**, 2042–2059 (2016).

40. Roadmap Epigenomics Consortium, A. *et al.* Integrative analysis of 111 reference human epigenomes. *Nature* **518**, 317–30 (2015).

41. Fullard, J. F. *et al.* An atlas of chromatin accessibility in the adult human brain. *Genome Res.* **28**, 1243–1252 (2018).

42. Mo, A. *et al.* Epigenomic Signatures of Neuronal Diversity in the Mammalian Brain. *Neuron* **86**, 1369–84 (2015).

43. Mali, P. *et al.* RNA-guided human genome engineering via Cas9. *Science (80-.).* **339**, 823–826 (2013).

44. Gompers, A. L. *et al.* Germline Chd8 haploinsufficiency alters brain development in mouse. *Nat. Neurosci.* **20**, 1062–1073 (2017).

45. Dobin, A. *et al.* STAR: ultrafast universal RNA-seq aligner. *Bioinformatics* **29**, 15–21 (2013).

46. Liao, Y., Smyth, G. K. & Shi, W. FeatureCounts: An efficient general purpose program for assigning sequence reads to genomic features. *Bioinformatics* **30**, 923–930 (2014).

47. Wang, L., Wang, S. & Li, W. RSeQC: quality control of RNA-seq experiments. *Bioinformatics* **28**, 2184–5 (2012).

48. MD, R., DJ, M. & GK, S. edgeR: a Bioconductor package for differential expression analysis of digital gene expression data. *Bioinformatics* **26**, 139–40 (2009).

49. Adhikari, A. *et al.* Cognitive deficits in the Snord116 deletion mouse model for Prader-Willi syndrome. *Neurobiol. Learn. Mem.* (2018). doi:10.1016/j.nlm.2018.05.011

50. Fox, W. M. Reflex-ontogeny and behavioural development of the mouse. *Anim. Behav.* **13**, 234-IN5 (1965).

51. Copping, N. A. *et al.* Neuronal overexpression of Ube3a isoform 2 causes behavioral impairments and neuroanatomical pathology relevant to 15q11.2-q13.3 duplication syndrome. *Hum. Mol. Genet.* **26**, 3995–4010 (2017).

52. Flannery, B. M. *et al.* Behavioral assessment of NIH Swiss mice acutely intoxicated with tetramethylenedisulfotetramine. *Neurotoxicol. Teratol.* **47**, 36–45 (2015).

53. Yang, M., Lewis, F. C., Sarvi, M. S., Foley, G. M. & Crawley, J. N. 16p11.2 Deletion mice display cognitive deficits in touchscreen learning and novelty recognition tasks. *Learn. Mem.* **22**, 622–32 (2015).

54. Brooks, S. P., Pask, T., Jones, L. & Dunnett, S. B. Behavioural profiles of inbred mouse strains used as transgenic backgrounds. I: motor tests. *Genes. Brain. Behav.* **3**, 206–15 (2004).

55. Carter, R. J., Morton, J. & Dunnett, S. B. Motor Coordination and Balance in Rodents. *Curr. Protoc. Neurosci.* **15**, 8.12.1-8.12.14 (2001).

56. Vogel Ciernia, A. *et al.* Early motor phenotype detection in a female mouse model of Rett syndrome is improved by cross-fostering. *Hum. Mol. Genet.* **26**, 1839–1854 (2017).

57. Yang, M. *et al.* Reduced excitatory neurotransmission and mild autism-relevant phenotypes in adolescent Shank3 null mutant mice. *J. Neurosci.* **32**, 6525–41 (2012).

58. Silverman, J. L. *et al.* Sociability and motor functions in Shank1 mutant mice. *Brain Res.* **1380**, 120–37 (2011).

59. Silverman, J. L. *et al.* GABAB Receptor Agonist R-Baclofen Reverses Social Deficits and Reduces Repetitive Behavior in Two Mouse Models of Autism. *Neuropsychopharmacology* **40**, 2228–39 (2015).

60. Dhamne, S. C. *et al.* Replicable in vivo physiological and behavioral phenotypes of the Shank3B null mutant mouse model of autism. *Mol. Autism* **8**, 26 (2017).

61. Copping, N. A. *et al.* Touchscreen learning deficits and normal social approach behavior in the Shank3B model of Phelan–McDermid Syndrome and autism. *Neuroscience* **345**, 155–165 (2017).

62. Papaleo, F. *et al.* Working memory deficits, increased anxiety-like traits, and seizure susceptibility in BDNF overexpressing mice. *Learn. Mem.* **18**, 534–44 (2011).

63. Wang, D. *et al.* Comprehensive functional genomic resource and integrative model for the human brain. *Science (80-.).* **362**, eaat8464 (2018).

64. Consortium, R. E. *et al.* Integrative analysis of 111 reference human epigenomes. *Nature* **518**, 317 (2015).

65. Kundaje, A. *et al.* Integrative analysis of 111 reference human epigenomes. *Nature* **518**, 317–330 (2015).

66. Hilton, I. B. *et al.* Epigenome editing by a CRISPR-Cas9-based acetyltransferase activates genes from promoters and enhancers. *Nat. Biotechnol.* **33**, 510–7 (2015).

67. Cheah, C. S. *et al.* Correlations in timing of sodium channel expression, epilepsy, and sudden death in Dravet syndrome. *Channels* (2013). doi:10.4161/chan.26023

68. Dravet, C. The core Dravet syndrome phenotype. *Epilepsia* (2011). doi:10.1111/j.1528-1167.2011.02994.x

69. Escayg, A. & Goldin, A. L. Sodium channel SCN1A and epilepsy: Mutations and mechanisms.

Epilepsia (2010). doi:10.1111/j.1528-1167.2010.02640.x

70. NA Copping, A Adhikari, SP Petkova, and J. S. Genetic Backgrounds Have Unique Seizure Response Profiles and Behavioral Outcomes Following Convulsant Administration. *Epilepsy Behav.* (2019).

71. Genton, P., Velizarova, R. & Dravet, C. Dravet syndrome: The long-term outcome. *Epilepsia* **52**, 44–49 (2011).

72. Rubinstein, M. *et al.* Dissecting the phenotypes of Dravet syndrome by gene deletion. *Brain* **138**, 2219–2233 (2015).

73. Silverman, J. L., Yang, M., Lord, C. & Crawley, J. N. Behavioural phenotyping assays for mouse models of autism. *Nat. Rev. Neurosci.* **11**, 490–502 (2010).

74. Sukoff Rizzo, S. J. & Silverman, J. L. Methodological Considerations for Optimizing and Validating Behavioral Assays. *Curr. Protoc. Mouse Biol.* **6**, 364–379 (2016).

75. Stein, R. E., Kaplan, J. S., Li, J. & Catterall, W. A. Hippocampal deletion of NaV1.1 channels in mice causes thermal seizures and cognitive deficit characteristic of Dravet Syndrome. *Proc. Natl. Acad. Sci. U. S. A.* (2019). doi:10.1073/pnas.1906833116

76. Cheah, C. S. *et al.* Channels Correlations in timing of sodium channel expression, epilepsy, and sudden death in Dravet syndrome. *Channels* **7**, 468–472

77. Featherstone, R. E. *et al.* EEG biomarkers of target engagement, therapeutic effect, and disease process. *Ann. N. Y. Acad. Sci.* **1344**, 12–26 (2015).

78. Modi, M. E. & Sahin, M. Translational use of event-related potentials to assess circuit integrity in ASD. *Nat. Rev. Neurol.* **13**, 160–170 (2017).

79. Dickinson, A. *et al.* Interhemispheric alpha-band hypoconnectivity in children with autism spectrum disorder. *Behav. Brain Res.* **348**, 227–234 (2018).

80. Cunningham, T. J. *et al.* Genomic Knockout of Two Presumed Forelimb Tbx5 Enhancers Reveals They Are Nonessential for Limb Development. *Cell Rep.* **23**, 3146–3151 (2018).

81. Dickel, D. E. *et al.* Ultraconserved Enhancers Are Required for Normal Development. *Cell* **172**, 491-499.e15 (2018).

82. Hewitt, S. C. *et al.* A distal super enhancer mediates estrogen-dependent mouse uterine-specific gene transcription of Igf1 (insulin-like growth factor 1). *J. Biol. Chem.* **294**, 9746–9759 (2019).

83. Johnson, K. R. *et al.* Deletion of a long-range Dlx5 enhancer disrupts inner ear development in mice. *Genetics* **208**, 1165–1179 (2018).

84. Kang, S. K., Hawkins, N. A. & Kearney, J. A. C57BL/6J and C57BL/6N substrains differentially influence phenotype severity in the *Scn1a* $^{+/-}$ mouse model of Dravet syndrome. *Epilepsia Open* **4**, epi4.12287 (2018).

85. Rubinstein, M. *et al.* Genetic background modulates impaired excitability of inhibitory neurons in a mouse model of Dravet syndrome. *Neurobiol. Dis.* (2015). doi:10.1016/j.nbd.2014.09.017

86. Hawkins, N. A., Calhoun, J. D., Huffman, A. M. & Kearney, J. A. Gene expression profiling in a mouse model of Dravet syndrome. *Exp. Neurol.* **311**, 247–256 (2019).

87. Oakley, J. C., Kalume, F., Yu, F. H., Scheuer, T. & Catterall, W. A. Temperature- and age-dependent seizures in a mouse model of severe myoclonic epilepsy in infancy. *Proc. Natl. Acad. Sci. U. S. A.* (2009). doi:10.1073/pnas.0813330106

88. Terzic, B. *et al.* X-linked cellular mosaicism underlies age-dependent occurrence of seizure-like events in mouse models of CDKL5 deficiency disorder. *Neurobiol. Dis.* (2021). doi:10.1016/j.nbd.2020.105176

89. Fallah, M. S. & Eubanks, J. H. Seizures in Mouse Models of Rare Neurodevelopmental Disorders. *Neuroscience* (2020). doi:10.1016/j.neuroscience.2020.01.041

90. Colic, S., Wither, R. G., Zhang, L., Eubanks, J. H. & Bardakjian, B. L. Characterization of seizure-like events recorded in vivo in a mouse model of Rett syndrome. *Neural Networks* (2013). doi:10.1016/j.neunet.2013.05.002

91. Sidorov, M. S. *et al.* Delta rhythmicity is a reliable EEG biomarker in Angelman syndrome: a parallel mouse and human analysis. *J. Neurodev. Disord.* **9**, 17 (2017).

92. Frohlich, J. *et al.* Mechanisms underlying the EEG biomarker in Dup15q syndrome. *Mol. Autism* **10**, 29 (2019).

93. Frohlich, J. *et al.* A Quantitative Electrophysiological Biomarker of Duplication 15q11.2-q13.1 Syndrome. *PLoS One* **11**, e0167179 (2016).

94. Marquardt, K., Sigdel, R. & Brigman, J. L. Touch-screen visual reversal learning is mediated by value encoding and signal propagation in the orbitofrontal cortex. *Neurobiol. Learn. Mem.* **139**, 179–188 (2017).

95. Guerrini, R. *et al.* Lamotrigine and seizure aggravation in severe myoclonic epilepsy. *Epilepsia* **39**, 508–12 (1998).

96. Matharu, N. *et al.* CRISPR-mediated activation of a promoter or enhancer rescues obesity caused by haploinsufficiency. *Science (80-.).* **363**, eaau0629 (2019).

97. Colasante, G. *et al.* dCas9-Based Scn1a Gene Activation Restores Inhibitory Interneuron Excitability and Attenuates Seizures in Dravet Syndrome Mice. *Mol. Ther.* **28**, 235–253 (2019).

Tables

Primer name	Sequence (5'-3')
L_outer_Scn1a	AGATCAGGCCTTCTTGCTGA
R_outer_Scn1a	GGGCTCCTCATTGTTTTGGG
R_interal_Scn1a	CACACACAGGCACATGATGA

Table 1: Scn1a 1b deletion genotyping primers

Experiment	n	Region	Age
qPCR	WT=4F, $1b^{+/-}$=5 (4F, 1M), $1b^{-/-}$=7 (2F, 5M)	Cortex Hippocampus Cerebellum	3 months
Western blot	WT=3M, $1b^{+/-}$=3M, $1b^{-/-}$=3M	Cortex Hippocampus Cerebellum	P29-P32
IF	WT=3, $1b^{+/-}$=3, $1b^{-/-}$=3	Brain	P28
RNA-seq	WT=2M, $1b^{+/-}$=4 (2M, 2F), $1b^{-/-}$=2F	Forebrain	P7
	WT=2F, $1b^{-/-}$=2 (1M, 1F); WT=3M, $1b^{+/-}$=4 (3M, 1F)	Hippocampus	P32
Behavior	WT=26(12M, 14F), $1b^{+/-}$=30(15M, 15F), $1b^{-/-}$=12 (6M, 6F)		Started at 6 weeks
Thermal-induced seizures	WT=9(5M, 4F) $1b^{+/-}$=9 (6M, 3F)		P22

Table 2: sex, genotype, age and n for each experiment

Target	Sequence (5'-3')
Human Gapdh	F-CAATGACCCCTTCATTGACC
	R-TTGATTTTGGAGGGATCTCG
Mouse Gapdh	F-TCACCACCATGGAGAAGGC
	R-GCTAAGCAGTTGGTGGTGCA
Scn1a (mouse and human)	F-CTCGTTCCTGATCGTGTTCC
	R-ATCCTGTCCACAGCAATCTG

Table 3: qPCR primers

Target	Sequence (5'-3')
human 1b	F-ttaattaagagctcCGGAAATCATTGCCCCTTCC
	R-ttaattaactcgagAATCTGGATTGTGAGAAAGTGTTT
Human NEG2	F-ccggagctcTGGTATGGGTGAAAACGGCT
	R-cggctcgagGAGGTTTGTGGGGAGGAGTG

Table 4: Primers for cloning regions from human DNA

Target	Sequence (5'-3')	Location (hg19)
h1b_1	GCTATTTGCTGATTTGTATTAGG	Chr2: 166128022 166128044
h1b_2	GAGGATACTGCAGAGGTCTCTGG	Chr 2: 166984479-166984501
h1b_3	GGAAGGTTGAGAGAGGAGGGGGG	Chr 2: 166984086-166984108
h1b_4	AGTATCTGCAGTATCATTGCTGG	Chr 2: 166983556 166983578
h1b_5	GGAAAATTCCATGCTGAGGTTGG	Chr 2: 166983037 166983059
h1b_6	TGAATGGCCACAGAGATTTACGG	Chr 2: 166982669 166982691

Table 5: sgRNA sequences for CRISPR dCas9 induction

Figures

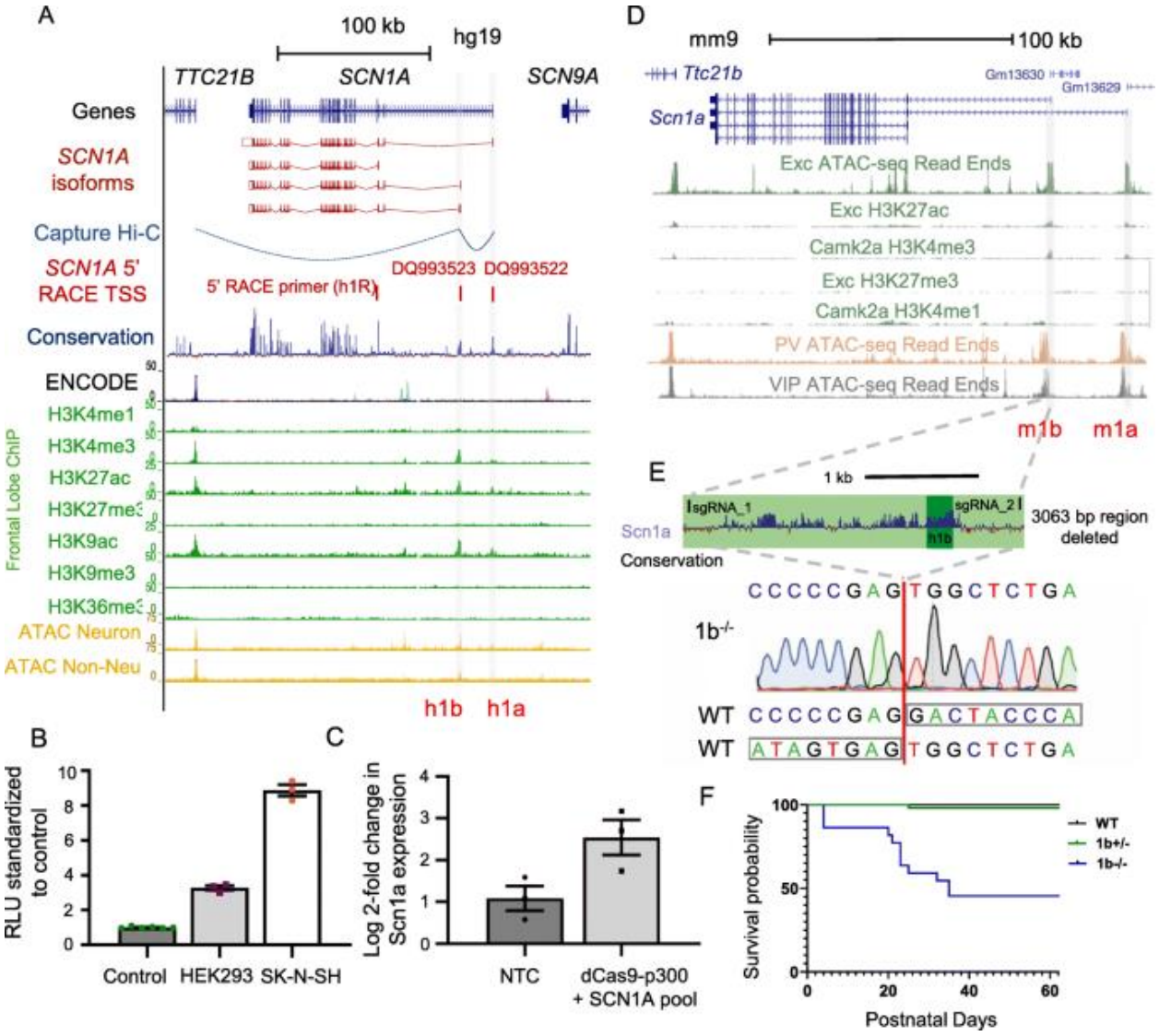

Figure 1: Genomic context of *SCN1A* gene and Scn1a 1b deletion mouse model generation. (a) Human (hg19) *SCN1A* locus showing signal for histone PTMs and ATAC-seq for neuronal and non-neuronal cells derived from dorsolateral PFC. (b) Activity of human 1b region in luciferase assay with minimal promoter in HEK293 (****P < 0.0001) and SK-N-SH cells (****P < 0.0001) shown as mean ± SEM. (c) Transcriptional activation of *SCN1A* using gRNAs targeting 1b co-transfected with dCas9-p300 in HEK293 cells increases *SCN1A* expression (*P = 0.047) when compared to empty vector (EV) as measured by qPCR and normalized to non-transfected control, shown as mean ± SEM. (d) Mouse (mm10) *Scn1a* locus showing signal for histone PTMs and ATAC-seq for neuronal cell types. (e) Mouse Scn1a 1b locus showing guideRNA sequence targets for Cas9-directed deletion of mouse 1b removal of entire 3063 bp conserved region and sequence trace validating deleted region. (f) Survival curve for offspring from $1b^{+/-}$ by $1b^{+/-}$ breeding pairs. Data is from 13 litters that dropped from 3 generations of pairings combined. $1b^{+/-}$ and $1b^{+/+}$ Logrank p value = 0.5455; $1b^{+/+}$ versus $1b^{-/-}$ Logrank p value < 0.0001. For panels a and d see text for data sources.

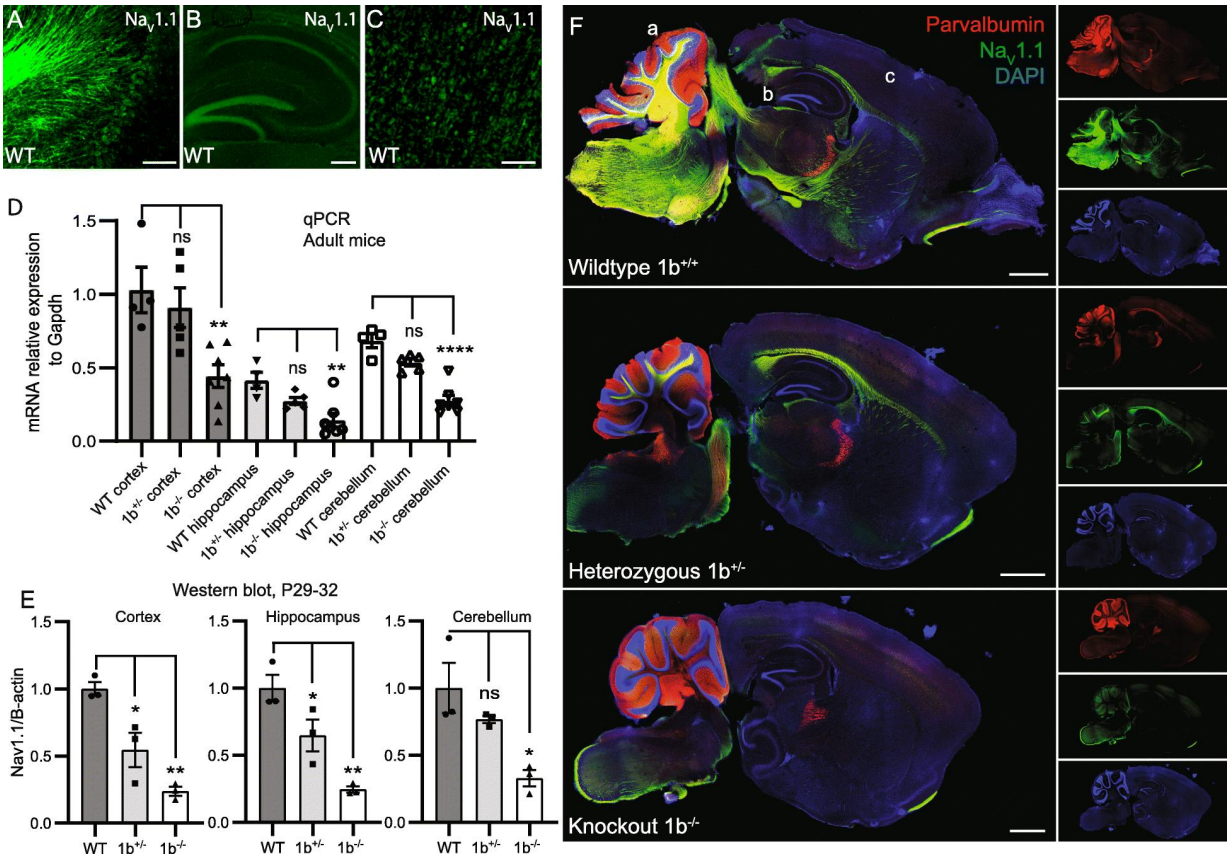

Figure 2: *Scn1a* expression is reduced in 1b deletion mouse model. (a-c) Immunofluorescent analysis of Na$_V$1.1 in wildtype mice across cerebellum (a), hippocampus (b) and cortex (c), regions taken from wildtype in panel f. Scale bars a and b = 100 µm, c = 250 µm. (d) Bar plot showing relative expression of *Scn1a* using qPCR in 3-month-old mice (mean ± SEM), values normalized to WT cortex. *Scn1a* expression reduced in $1b^{-/-}$ cortex vs WT cortex (**P = 0.0092), $1b^{-/-}$ hippocampus vs WT hippocampus (**P = 0.0029), and $1b^{-/-}$ cerebellum vs WT cerebellum (****P < 0.0001). (e) Western blots of P29-32 mouse brain membrane fractions, showing reduction of Na$_V$1.1 protein in cortex of $1b^{+/-}$ (*P=0.0174) and $1b^{-/-}$ (**P=0.0014) mice, hippocampus of $1b^{+/-}$ (*P = 0.0445) and $1b^{-/-}$ (**P = 0.0025) mice and cerebellum of $1b^{-/-}$ (*P = 0.0142) mice. (f) Immunofluorescent analysis of sagittal sections of P28 mice revealed a reduction in Na$_V$1.1 (green) expression in homozygous versus WT mice with no changes in parvalbumin (red) expression. Scale bars = 1 mm.

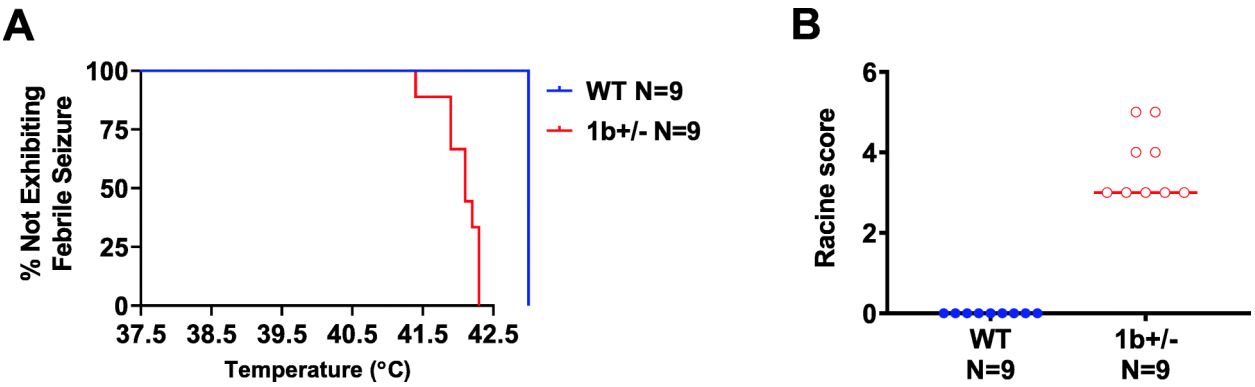

Figure 3: Thermal-evoked febrile seizures in 1b$^{+/-}$ mice and WT littermates. a) The 1b$^{+/-}$ mice began to have seizures at 41.5 °C b) as measured by the Racine scale.

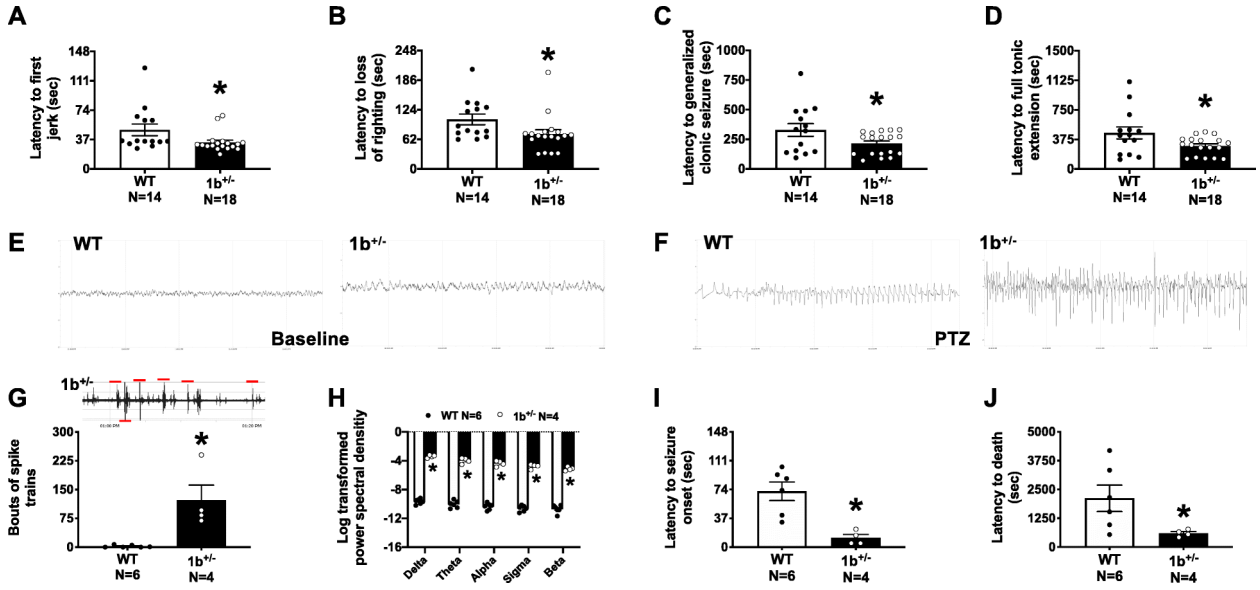

Figure 4: Increased seizure susceptibility and abnormal EEG in heterozygous 1b deletion mice. (a-d) Latency measures were observed after an i.p. injection of 80 mg/kg PTZ over the course of a 30-min trial. Reduced latencies to first jerk, loss of righting, generalized clonic seizure, and full tonic extension were observed in Het mice when compared to WT littermate controls. EEG was collected using a wireless telemetry system before and after an i.p. injection of 80 mg/kg PTZ. (e-f) Representative EEG traces of WT and $1b^{+/-}$ mice during baseline EEG recording and subsequent PTZ response. Powerband calculations and spiking events were automatically scored. (g) $1b^{+/-}$ mice had significantly more spiking events and spike trains during baseline EEG acquisition when compared to WT. Scored spiking events are shown on a $1b^{+/-}$ representative trace and indicated by red lines. (h) $1b^{+/-}$ mice also had significantly higher power across all frequency bins, Delta (0-4 Hz), Theta (4-8 Hz), Alpha (8-12 Hz), Sigma (12-16 Hz), and Beta (16-30) during baseline when compared to controls. Finally, seizure susceptibility was confirmed with EEG after PTZ administration. (i-j) Reduced latencies to seizure onset and death were observed in $1b^{+/-}$mice. *, $p < 0.05$, t-test

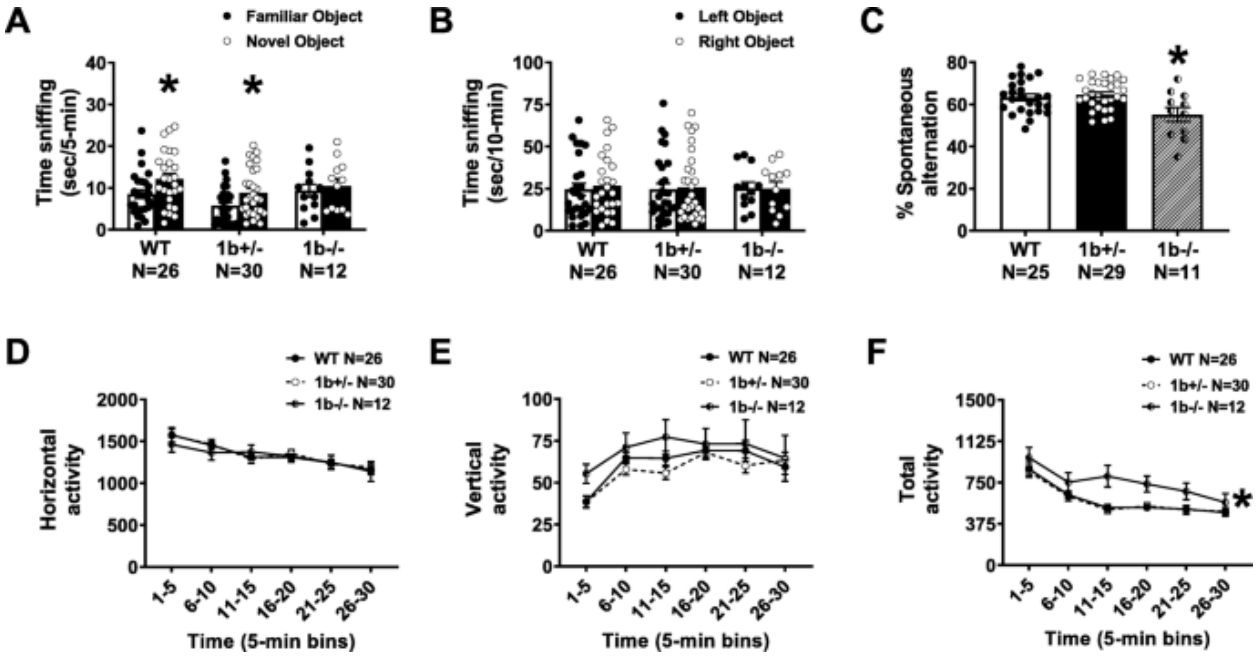

Figure 5: *Scn1a* 1b homozygous deletion mice exhibit learning and memory impairments without confounds in gross motor abilities. Recognition memory was assessed using a novel object recognition assay. (a) $1b^{-/-}$ mice did not spend more time sniffing the novel object over the familiar object. $1b^{+/-}$ and WT performed with typical preference. (b) All genotypes showed no preference for either the left or right object during the familiarization phase indicating no innate side bias confounds of lack of object exploration, in the novel object recognition trials. *, $p < 0.05$, paired-test within genotype using the familiar versus novel object for comparison. (c) Working memory impairments were observed by lower percentages of spontaneous alternation in the Y-Maze. *, $p < 0.05$, One-way ANOVA. (d) No genotype differences in horizontal (d) or (e) vertical activity counts in the $1b^{+/-}$ and $1b^{-/-}$ mice compared to their wildtype littermate controls. (f) $1b^{-/-}$ deletion mice were hyperactive in total activity during two different 5-min bins of the 30-min assay. Moreover, when total activity is summed and re-graphed as a bar graph, comparisons between $1b^{-/-}$ versus WT and $1b^{+/-}$ in total movement were observed. Analyses include both males and females. *$p < 0.05$, repeated measures ANOVA, main effect of genotype.

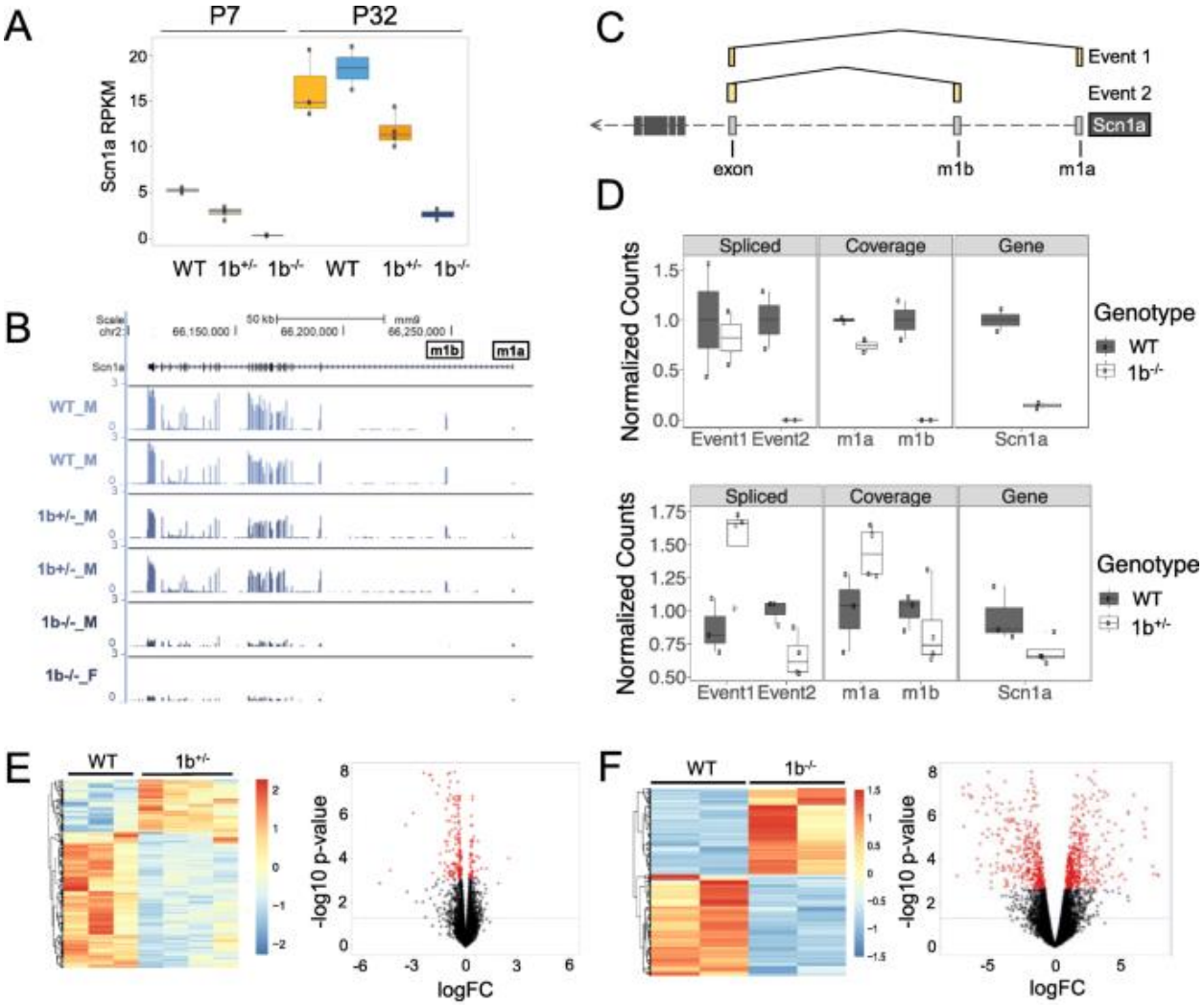

G

Category	1b+/- Terms	#DE	p-val	FDR
GO:0099536	synaptic signaling	31	2.34E-10	5.83E-07
GO:0007186	GPCR signaling path.	26	2.83E-10	6.04E-07
GO:0007268	chemical syn. transmission	30	5.27E-10	9.36E-07
GO:0051480	reg. of cytosolic ca ion conc.	19	7.74E-10	1.11E-06
GO:0005216	ion channel activity	20	3.44E-09	3.67E-06
GO:0038023	signaling receptor activity	27	1.44E-10	9.33E-06
GO:0007268	chemical syn. transmission	11	5.08E-05	0.312654
GO:0098916	antero. trans-syn. signaling	11	5.08E-05	0.312654
GO:0099537	trans-synaptic signaling	11	5.62E-05	0.312654
GO:0099536	synaptic signaling	11	6.23E-05	0.312654
GO:0007267	cell-cell signaling	15	8.40E-05	0.312654
GO:0099055	int. comp. of postsyn. mem.	6	8.80E-05	0.312654

Category	1b-/- Terms	#DE	p-val	FDR
GO:0007610	behavior	52	1.29E-15	1.39E-11
GO:0007186	GPCR signaling path.	39	1.41E-11	7.57E-08
GO:0043269	reg. of ion transport	38	9.35E-09	1.26E-05
GO:0042391	reg. of mem. potential	29	2.44E-08	2.39E-05
GO:0043005	neuron proj.	63	6.66E-08	5.51E-05
GO:0007268	chemical syn. transmission	38	2.49E-07	0.000137
GO:0097485	neuron proj. guidance	26	3.42E-11	1.22E-07
GO:0061564	axon development	37	5.45E-10	1.25E-06
GO:0038023	signaling receptor activity	44	1.95E-09	3.50E-06
GO:0031012	extracellular matrix	28	3.59E-07	0.000193
GO:0048468	cell development	83	5.34E-07	0.00026
GO:0099699	int. comp. of syn. mem.	19	1.35E-06	0.000558

Figure 6: Differential gene expression with *Scn1a* 1b deletion. (a) Bar plot indicating RPKM *Scn1a* expression between WT and $1b^{+/-}$ or $1b^{-/-}$ mutants in postnatal day (P) 7 forebrain or P32 hippocampus, (mean ± SEM). (b) Mouse (mm9) *Scn1a* locus showing decrease in coverage in representative P32 heterozygous and homozygous 1b deletion carriers compared to wild-type controls. (c) Schematic showing splicing of m1a and m1b sequences with first *Scn1a* coding exon

in reference. (d) Bar plots showing the number of sequencing reads that overlap each splicing event, m1b or m1a locus, and the entire *Scn1a* locus along the x-axis for P32 WT, $1b^{+/-}$, and $1b^{-/-}$ mice. The full table is included in the supplement. (e) Heatmap and scatterplot of differentially-expressed genes in P32 $1b^{+/-}$ mice. In the scatterplot, genes with FDR < 0.05 are in red while the dashed line indicates a p-value < 0.05. (f) Heatmap and scatterplot of differentially-expressed genes in P32 1b-/- mice. In the scatterplot, genes with FDR < 0.05 are in red while the dashed line indicates a p-value < 0.05. (g) Table showing select pathways enriched in differentially-expressed genes for P32 $1b^{+/-}$ (left) or $1b^{-/-}$ (right) mice. Pathways enriched in down-regulated genes are shown in grey. Pathways enriched in up-regulated genes are shown in white. Ontologies are biological pathways (BP), molecular function (MF), or cellular component (CC).

Additional files

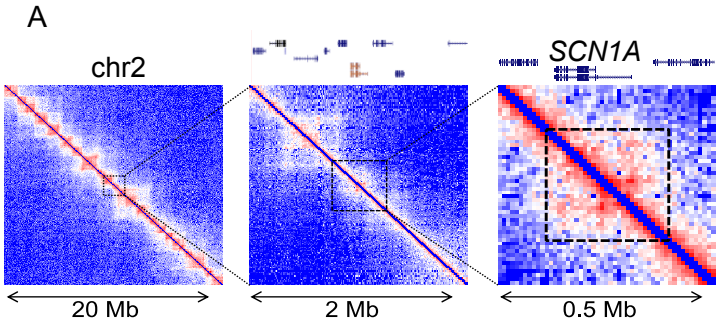

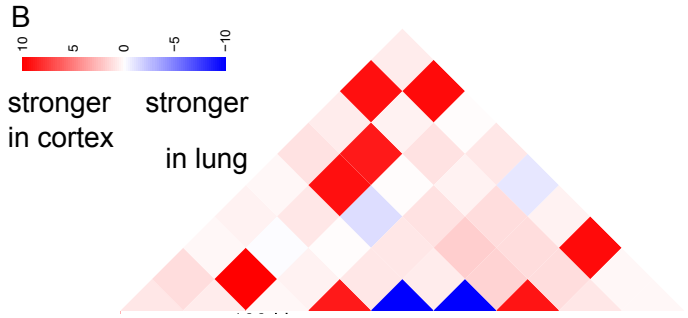

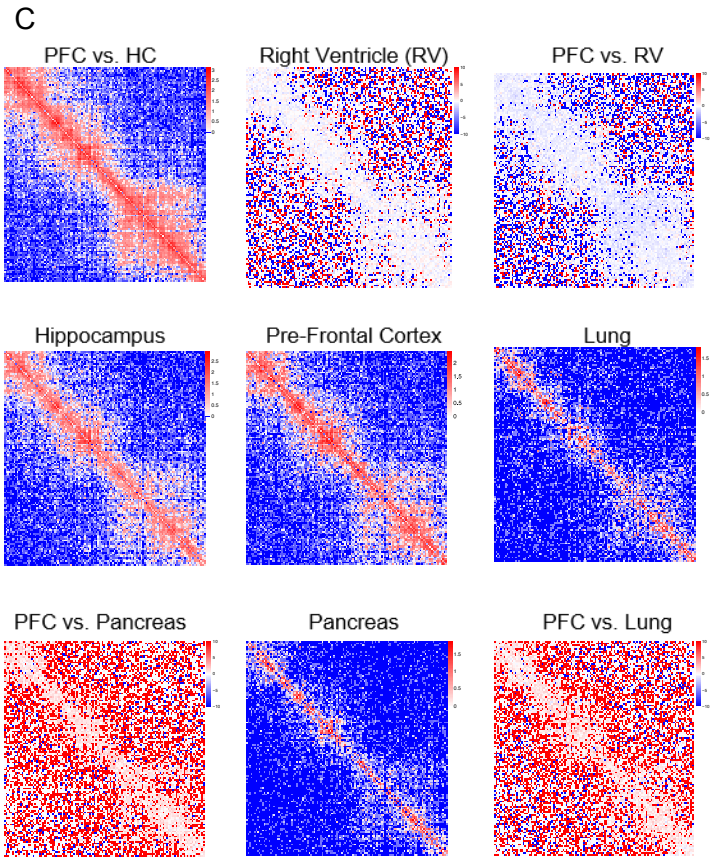

Figure S1: Tissue and brain regional differences in chromatin conformation. (A) Hi-C contact heatmaps showing chromosomal neighborhood of SCN1A at different ranges. (B) Contrasting differential Hi-C contact heatmaps showing differences between PFC and lung. (C) Hi-C contact map heatmaps at 40-kb resolution for a 5-Mb region around SCN1A gene. In the central rows and columns are the absolute contact maps, while the corner plots represent the differential contact maps between pre-frontal cortex (PFC) and the indicated tissue. For the latter, red color indicates stronger contacts in PFC in relation to the other tissue, and blue color the opposite.

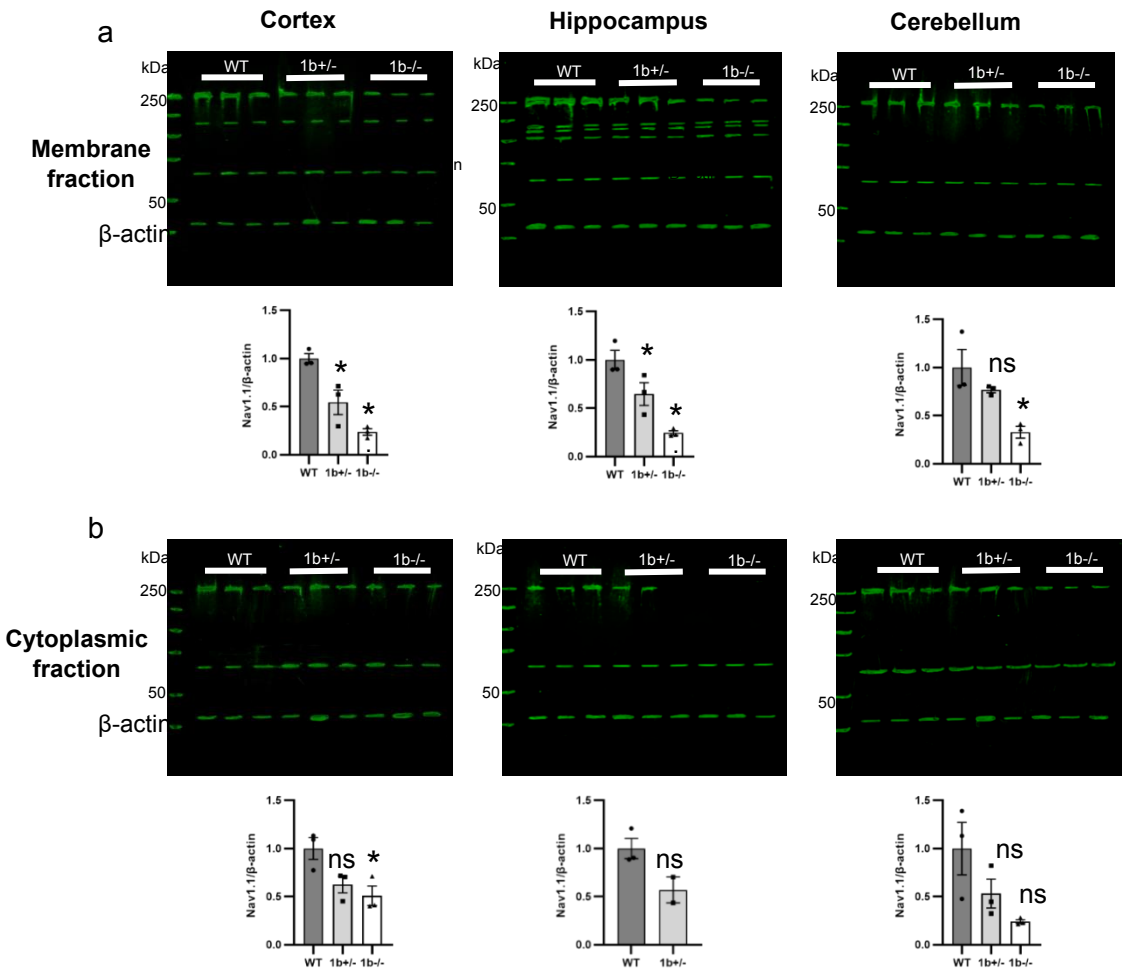

Figure S2: Western blots of Na$_V$1.1 (250 kDa) and β-actin (45 kDa) proteins in P29-32 brain lysates, membrane and cytoplasmic fractions ran separately. A) Membrane fraction western blot for cortex shows decrease in Na$_V$1.1 protein abundance in $1b^{+/-}$ (*P=0.0174) and $1b^{-/-}$ (**P=0.0014) mice. In the hippocampus there is also a decrease in $1b^{+/-}$ (*P=0.0445) and $1b^{-/-}$ (**P=0.0025) mice. In the cerebellum there was a decrease in Na$_V$1.1 in $1b^{-/-}$ (*P=0.0142) compared to WT. B) Cytoplasmic fraction western blot shows a decrease in NaV1.1 in $1b^{-/-}$ (*P=0.0321) versus wildtype, no other significant changes. $1b^{+/+}$ n=3, $1b^{+/-}$ n=3, $1b^{-/-}$ n=3. ANOVA with Tukey's post-hoc, significance is versus WT. Error bars represent mean ± SEM. Bands not at 250 and 45 kDa are non-specific and do not show significant changes between genotypes.

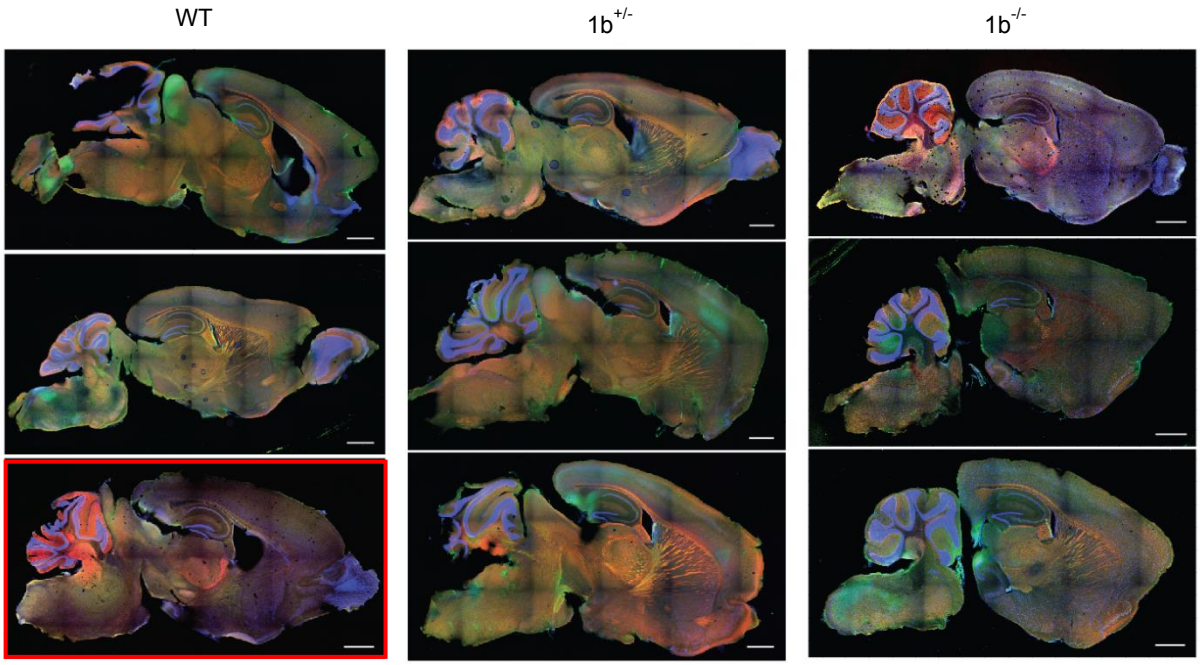

Figure S3: Immunofluorescent analysis of sagittal sections of P28 mice. WT, heterozygous ($1b^{+/-}$) and knockout ($1b^{-/-}$) 1b mice (n=3 each genotype) underwent immunohistochemistry (IHC) for $Na_V1.1$ (green) and parvalbumin (red) expression (DAPI shown in blue). No observable difference between WT and $1b^{+/-}$. In $1b^{-/-}$ mice $Na_V1.1$ appears reduced in brainstem (2/3 $1b^{-/-}$), corpus callosum (3/3) and hippocampus (3/3). No observable difference at the IF level in the cortex. WT in red box presented patchy labelling. Scale bars = 1 mm.

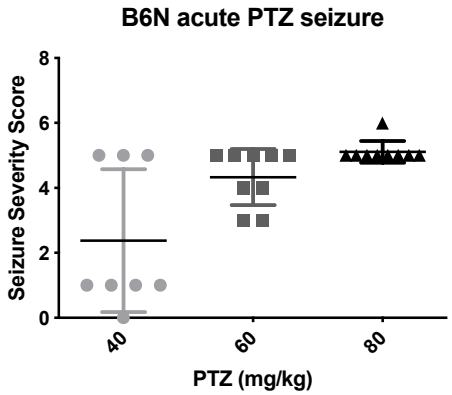

Figure S4: Seizure severity following Pentylenetetrazole (PTZ) administration in C57BL6/N mice. 80 mg/kg was chosen to ensure all seizure stages were reached.

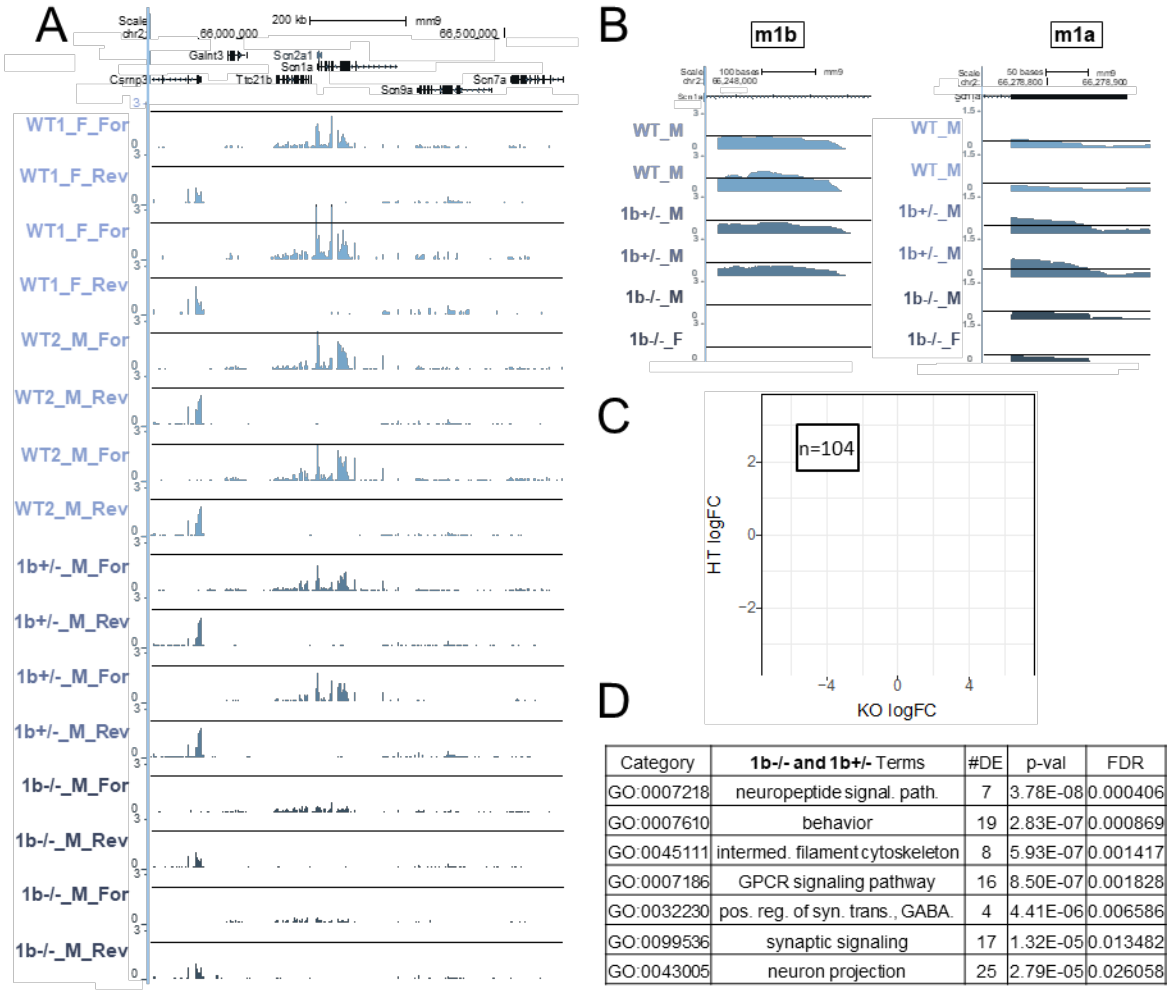

Category	**1b-/- and 1b+/-** Terms	#DE	p-val	FDR
GO:0007218	neuropeptide signal. path.	7	3.78E-08	0.000406
GO:0007610	behavior	19	2.83E-07	0.000869
GO:0045111	intermed. filament cytoskeleton	8	5.93E-07	0.001417
GO:0007186	GPCR signaling pathway	16	8.50E-07	0.001828
GO:0032230	pos. reg. of syn. trans., GABA.	4	4.41E-06	0.006586
GO:0099536	synaptic signaling	17	1.32E-05	0.013482
GO:0043005	neuron projection	25	2.79E-05	0.026058

Figure S5: Differential gene expression with *Scn1a 1b* deletion in P32 hippocampus. (a) Mouse (mm9) *Scn1a* and nearby-gene loci for P32 wild-type, $1b^{+/-}$, and $1b^{-/-}$ mice. WT1 refers to mice sequenced with the $1b^{-/-}$ mutants. WT2 refers to mice sequenced with $1b^{+/-}$ mutants. (b) Coverage of the m1b (left) and m1a (right) loci across representative P32 wild-type and mutant mice. (c) Scatterplot of differentially-expressed genes meeting a p-value < 0.05 and fold-change > 1.5 threshold in both P32 heterozygous and homozygous 1b deletion datasets. (d) Table showing select pathways enriched in genes having shared differential-expression in both P32 mutant mouse datasets. Ontologies are biological pathways (BP), molecular function (MF), or cellular component (CC).

Genotypes	Expected	Observed
$1b^{+/-}$	47	52
$1b^{-/-}$	23	23
WT	23	19

Table S1: Expected Mendelian ratios and observed number of pups born
The genotypes were born at expected Mendelian ratios, 13 $1b^{+/-}$ x $1b^{+/-}$ litters dropped from 3 generations of pairings combined. 14 litters were cannibalized.

Domain	Assay	Sample size	Statistical test	Statistic	p-value	Significant (p<0.05)?	Sidak's multiple comparisons (WT vs $1b^{+/-}$)	p-value
Physical	Weight	WT N = 24 $1b^{+/-}$ N = 28	Two Way Repeated Measures ANOVA	F (1, 50) = 0.1063	p = 0.7457	No	PND 2	p > 0.9999
							PND 4	p = 0.9998
							PND 6	p = 0.9928
							PND 8	p = 0.9956
							PND 10	p = 0.9518
							PND 12	p = 0.9856
	Total length	WT N = 24 $1b^{+/-}$ N = 28	Two Way Repeated Measures ANOVA	F (1, 50) = 0.1158	p = 0.7350	No	PND 2	p > 0.9999
							PND 4	p = 0.9995
							PND 6	p = 0.9998
							PND 8	p > 0.9999
							PND 10	p > 0.9999
							PND 12	p = 0.0931
	Body length	WT N = 24 $1b^{+/-}$ N = 28	Two Way Repeated Measures ANOVA	F (1, 50) = 0.01835	p = 0.8928	No	PND 2	p > 0.9999
							PND 4	p > 0.9999
							PND 6	p = 0.8910
							PND 8	p > 0.9999
							PND 10	p = 0.9991
							PND 12	p = 0.5872
	Head width	WT N = 24 $1b^{+/-}$ N = 28	Two Way Repeated Measures ANOVA	F (1, 50) = 0.3327	p = 0.5667	No	PND 2	p = 0.9987
							PND 4	p = 0.9953
							PND 6	p = 0.9790
							PND 8	p = 0.8293
							PND 10	p > 0.9999
							PND 12	p = 0.9974

Reflex	Negative geotaxis	WT N = 24 $1b^{+/-}$ N = 28	Two Way Repeated Measures ANOVA	F (1, 50) = 0.04947	p = 0.8249	No	PND 2	p = 0.9921
							PND 4	p = 0.3794
							PND 6	p = 0.9992
							PND 8	p = 0.9994
							PND 10	p = 0.9759
							PND 12	p = 0.9982
	Righting reflex	WT N = 24 $1b^{+/-}$ N = 28	Two Way Repeated Measures ANOVA	F (1, 50) = 0.2493	p = 0.6198	No	PND 2	p = 0.9981
							PND 4	p = 0.9791
							PND 6	p > 0.9999
							PND 8	p = 0.9981
							PND 10	p > 0.9999
							PND 12	p = 0.9756
	Circle traverse	WT N = 24 $1b^{+/-}$ N = 28	Two Way Repeated Measures ANOVA	F (1, 50) = 2.323	p = 0.1338	No	PND 2	p > 0.9999
							PND 4	p = 0.9995
							PND 6	p = 0.1302
							PND 8	p = 0.8712
							PND 10	p = 0.9977
							PND 12	p = 0.7909
	Cliff aversion	WT N = 24 $1b^{+/-}$ N = 28	Two Way Repeated Measures ANOVA	F (1, 50) = 2.225	p = 0.1421	No	PND 2	p = 0.9368
							PND 4	p = 0.9303
							PND 6	p = 0.1077
							PND 8	p = 0.9995
							PND 10	p = 0.9997
							PND 12	p > 0.9999
Limb strength	Forelimb hang	WT N = 24 $1b^{+/-}$ N = 28	Two Way Repeated Measures ANOVA	F (1, 50) = 2.704	p = 0.1064	No	PND 2	p > 0.9999
							PND 4	p > 0.9999
							PND 6	p = 0.4166

							PND 8	p > 0.9999
							PND 10	p = 0.0158
							PND 12	p = 0.9990
	Hindlimb hang	WT N = 24 $1b^{+/-}$ N = 28	Two Way Repeated Measures ANOVA	F (1, 50) = 1.946	p = 0.1692	No	PND 2	p = 0.8967
							PND 4	p = 0.7164
							PND 6	p = 0.9996
							PND 8	p = 0.1313
							PND 10	p = 0.9614
							PND 12	p > 0.9999

Table S2: Summary of measures of general health and development in wildtype and heterozygous 1b deletion mice

	Assay	**Metric**	**Sample size**	**Statistical test**	**Statistic**	**p-value**	**Significant (p<0.05)?**	**Sidak's multiple comparisons WT vs 1b$^{+/-}$**	**p-value**
Anxiety-like	Elevated-plus maze	%Open arm time	WT = 26 1b$^{+/-}$ = 30	Unpaired Two-Tailed T-Test	T (54) = 0.2605	p = 0.7955	No		
		Total entries	WT = 26 1b$^{+/-}$ = 30	Unpaired Two-Tailed T-Test	T (54) = 0.3618	p = 0.7189	No		
	Light-dark	Time in dark chamber	WT = 26 1b$^{+/-}$ = 30	Unpaired Two-Tailed T-Test	T (54) = 2.067	**p = 0.0436**	Yes		
		Total transitions	WT = 26 1b$^{+/-}$ = 30	Unpaired Two-Tailed T-Test	T (54) = 0.9267	p = 0.3582	No		
Motor	Beam walking	Latency to cross	WT = 25 1b$^{+/-}$ = 29	Two Way Repeated Measures ANOVA	F (1, 52) = 0.5912	p = 0.4454	No	Rod 1	p = 0.9999
								Rod 2	p = 0.7336
								Rod 3	p = 0.7859
	Rotarod	Latency to fall	WT = 26 1b$^{+/-}$ = 29	Two Way Repeated Measures ANOVA	F (1, 53) = 1.125	p = 0.2937	No	Day 1	p = 0.3252
								Day 2	p = 0.4701
								Day 3	p = 0.9989
Learning and Memory	Fear conditioning	Freeze time -training	WT = 24 1b$^{+/-}$ = 28	Two Way Repeated Measures ANOVA	F (1, 50) = 0.008692	p = 0.9261	No	Pre-training vs Post-training	WT **p < 0.0001**
									1b$^{+/-}$ **p < 0.0001**
		Freeze time -context	WT = 24 1b$^{+/-}$ = 28	Unpaired Two-Tailed T-Test	T (50) = 0.8902	p = 0.3776	No		
		Freeze time -cue	WT = 24 1b$^{+/-}$ = 28	Two Way Repeated Measures ANOVA	F (1, 50) = 0.07299	p = 0.7881	No	Pre-cue vs Post-cue	WT **p < 0.0001**
									1b$^{+/-}$ **p < 0.0001**
Social	3-chambered social approach	Time in chamber	WT = 25 1b$^{+/-}$ = 29	Two Way Repeated Measures ANOVA	Genotype F (1, 52) = 2.068	p = 0.1564	No	Novel object vs Novel mouse	WT **p < 0.0001**
					Chamber F (2, 104) = 262.8	**p<0.0001**	Yes		
									1b$^{+/-}$ **p < 0.0001**

		Time sniffing	WT = 25 1b$^{+/-}$ = 29	Two Way Repeated Measures ANOVA	Genotype F (1, 52) = 0.1736	p = 0.6786	No Yes	Novel object vs Novel mouse	WT **p < 0.0001**
					Chamber F (1, 52) = 90.48	**p<0.0001**			1b$^{+/-}$ **p < 0.0001**
		Transitions	WT = 25 1b$^{+/-}$ = 29	Two Way Repeated Measures ANOVA	Genotype F (1, 52) = 2.441	p = 0.1243	No	WT	p = 0.2881
					Chamber F (2, 104) = 0.6140	p = 0.4368	No	1b$^{+/-}$	p = 0.9053
	Male-female social interaction	Nose to nose sniffing	WT = 12 1b$^{+/-}$ = 15	Unpaired Two-Tailed T-Test	T (25) = 0.08607	p = 0.9321	No		
		Nose to anogenital sniffing	WT = 12 1b$^{+/-}$ = 15	Unpaired Two-Tailed T-Test	T (25) = 1.374	p = 0.1817	No		
		Following	WT = 12 1b$^{+/-}$ = 15	Unpaired Two-Tailed T-Test	T (25) = 0.2615	p = 0.7958	No		
		Exploring	WT = 12 1b$^{+/-}$ = 15	Unpaired Two-Tailed T-Test	T (25) = 1.009	p = 0.3224	No		
		Sum ultrasonic vocalizations	WT = 12 1b$^{+/-}$ = 15	Unpaired Two-Tailed T-Test	T (25) = 2.143	p = 0.0420	Yes		
Repetitive	Self-groom	Time grooming	WT = 26 1b$^{+/-}$ = 30	Unpaired Two-Tailed T-Test	T (54) = 0.2345	p = 0.8155	No		
Sensorymotor reflex	Acoustic startle	Startle amplitude	WT = 26 1b$^{+/-}$ = 27	Two Way Repeated Measures ANOVA	F (1, 51) = 0.3275	p = 0.5696	No		
	Pre-pulse inhibition	Startle amplitude	WT = 26 1b$^{+/-}$ = 27	Two Way Repeated Measures ANOVA	F (1, 51) = 0.3244	p = 0.5715	No		

Table S3: Summary of the battery of behavioral tests

Assay	Metric	Sample size	Statistical test	Statistic	p-value	Significant (p<0.05)?
Open field	Horizontal activity	WT M = 12 WT F = 14	Two Way Repeated Measures ANOVA	F (1, 24) = 2.874	p = 0.1030	No
		$1b^{+/-}$ M = 15 $1b^{+/-}$ F = 15	Two Way Repeated Measures ANOVA	F (1,28) = 3.225	p = 0.0833	No
		$1b^{-/-}$ M = 6 $1b^{-/-}$ F = 6	Two Way Repeated Measures ANOVA	F (1, 10) = 0.2820	p = 0.6070	No
	Vertical activity	WT M = 12 WT F = 14	Two Way Repeated Measures ANOVA	F (1, 24) = 1.549	p = 0.2253	No
		$1b^{+/-}$ M = 15 $1b^{+/-}$ F = 15	Two Way Repeated Measures ANOVA	F (1,28) = 0.1632	p = 0.6893	No
		$1b^{-/-}$ M = 6 $1b^{-/-}$ F = 6	Two Way Repeated Measures ANOVA	F (1, 10) = 4.398	p = 0.0624	No
	Total activity	WT M = 12 WT F = 14	Two Way Repeated Measures ANOVA	F (1, 24) = 3.477	p = 0.0745	No
		$1b^{+/-}$ M = 15 $1b^{+/-}$ F = 15	Two Way Repeated Measures ANOVA	F (1,28) = 1.627	p = 0.2125	No
		$1b^{-/-}$ M = 6 $1b^{-/-}$ F = 6	Two Way Repeated Measures ANOVA	F (1, 10) = 7.226	**p = 0.0228***	Yes
Novel Object Recognition	Novel-Familiar sniff Novel phase	WT M = 12 WT F = 14	Unpaired Two-Tailed T-Test	T (24) = 1.497	p = 0.1475	No
		$1b^{+/-}$ M = 15 $1b^{+/-}$ F = 15	Unpaired Two-Tailed T-Test	T (28) = 0.3861	p = 0.7023	No
		$1b^{-/-}$ M = 6 $1b^{-/-}$ F = 6	Unpaired Two-Tailed T-Test	T (10) = 1.764	p = 0.1081	No
Spontaneous alternation		WT M = 12	Unpaired Two-Tailed T-Test	T (23) = 1.176	p = 0.2516	No

	% Spontaneous alternation	WT F = 13				
		$1b^{+/-}$ M = 15 $1b^{+/-}$ F = 14	Unpaired Two-Tailed T-Test	T (27) = 0.5110	p = 0.6135	No
		$1b^{-/-}$ M = 6 $1b^{-/-}$ F = 5	Unpaired Two-Tailed T-Test	T (9) = 0.8541	p = 0.4152	No

Table S4: Lack of sex difference between wildtype, $1b^{+/-}$ and $1b^{-/-}$ mice in behavioral assays

Table S5–11. Table S5. RPKM values for P7 samples. Table S6. RPKM values for P32 $1b^{+/-}$ samples. Table S7. RPKM values for P32 $1b^{-/-}$ samples. Table S8. Differentially expressed genes between WT and $1b^{+/-}$ mice at P7. Table S9. Differentially expressed genes between WT and $1b^{-/-}$ mice at P7. Table S10. Differentially expressed genes between WT and $1b^{+/-}$ mice at P32. Table S11. Differentially expressed genes between WT and $1b^{-/-}$ mice at P32.

Chapter 2

Touchscreen Cognitive Deficits, Hyperexcitability, and Hyperactivity in Males and Females Using Two Models of CDKL5 Deficiency Disorder

Anna Adhikari, Fiona K. B. Buchanan, Timothy Fenton, David Cameron , Julian A.N.M. Halmai, Nycole A. Copping, Kyle D. Fink and Jill L. Silverman

Abstract

Many neurodevelopmental disorders (NDDs) are the result of mutations on the X chromosome. One severe NDD resulting from mutations on the X chromosome is *CDKL5* Deficiency Disorder (CDD). CDD is a monogenic, severe NDD, characterized by severe neurodevelopmental delay, treatment-resistant epilepsy and seizures leading to epileptic encephalopathy, intellectual disabilities (ID), sleep disorders or abnormal sleep patterns, apnea, and/or respiratory dysfunction. CDD is a rare condition with an estimated incidence of 1 in 40,000 to 60,000 newborns. Approximately 90 % of those diagnosed with CDD are girls. CDD is driven by the loss of cyclin-dependent kinase-like 5 (*CDKL5*), a serine/threonine kinase that is essential for standard brain development and is for, synapse formation and signal transmission. Previous studies focused on male subjects from two unique animal models, to avoid the complexity of X mosaicism. For the first time, we report translationally relevant behavioral phenotypes in young adult (8 weeks-20 weeks) with robust signal size, including impairments in learning and memory, substantial hyperactivity, increased susceptibility to seizures/reduced seizure thresholds, and increased frequency and amplitude in electroencephalographic oscillations, in both sexes, and in two models of CDD preclinical mice, one with a general loss of function mutation and one that is a patient-derived mutation.

Introduction

Numerous genetic causal factors have been shown to confer risk for neurodevelopmental disorders (NDDs), including autism spectrum disorder (ASD) and intellectual disabilities (ID). Many NDDs are the result of mutations on the X chromosome, as it accounts for ~1000 more gene products than its ancestral homologue, the Y chromosome (1-4). One severe NDD resulting from a mutation on the X chromosome is *CDKL5* Deficiency Disorder (CDD) (5-7). CDD is a monogenic, severe NDD characterized by developmental delays, seizures and treatment-resistant epilepsy, leading to epileptic encephalopathy. CDD also has moderate to severe ID, sleep disorders and abnormal sleep patterns, with apnea, and respiratory dysfunction (8-12). CDD is a rare condition with an estimated incidence of 1 in 40,000 to 60,000 newborns. About 90% of those diagnosed with CDD are girls. CDD is driven by loss-of-function mutations in the cyclin-dependent kinase-like 5 (*CDKL5*) gene, which encodes a serine/threonine kinase that is essential for brain development (5, 13), including synapse formation and signal transmission. As in Rett Syndrome, another NDD specific to the X chromosome, females with CDD are mosaics, with cells expressing either the mutant or wild-type *CDKL5* allele, which increases complexity; however, this complexity can be leveraged with innovative gene therapeutic technologies. CDD may be one of the few potentially treatable or "curable" NDDs, via reactivation of endogenous healthy copies of *CDKL5*, which may significantly alleviate symptom severity. In fact, proof of concept studies using an inducible Cdkl5 model found that many of the disease associated deficits could be reversed in adulthood (14). Recently, the first study outlining the targeted reactivation of *CDKL5* from the inactive X allele in a human neuronal cell line (15) has energized research efforts for this unique genetic rare disorder. Corroborative findings using a conditional mouse model that restored Cdkl5 after the early stages of brain development highlighted the potential for disease reversal in CDD, and suggested a broad therapeutic time window (14).

Within the past decade, CDD now has a uniform consensus as a unique NDD, distinct from Rett or Angelman syndromes and/or ASD although CDD was previously classified as an atypical form of Rett syndrome, as these conditions have common features including seizures, ID, co-morbid ASD, and other problems with development. CDD was previously classified as the early-onset-seizure variant of Rett syndrome, since a catalogue of CDKL5 sequence variations, including pathogenic mutations, nonpathogenic polymorphisms, and sequence variations of uncertain significance can be found at the RettBASE website (http://mecp2.chw.edu.au). Its distinct diagnosis is warranted, as one study of CDD (13) demonstrated that less than a quarter of those affected met clinical criteria for early-onset Rett syndrome with symptoms associated with CDD and its genetic cause distinct from those of Rett syndrome.

Unfortunately, with respect to CDD, there are no approved therapies, or treatments and standard of care is not effective at managing seizures nor preventing neurodevelopmental delays and/or failure to make gains or declines with age in motor and cognitive milestones. To examine the specific and functional loss of *CDKL5*, mouse models were generated to investigate and discover functional effects of *Cdkl5* deficiency to evaluate potential therapeutics for the most severe symptom domains. The first model from the Zhou laboratory, deleted exon 6, and observed substantial behavioral alterations resulting in hyperactivity, abnormal social approach and reduced contextual fear conditioning (16), in male subjects. In 2019, a novel mouse line was created from the Jensen group used a common patient variant R59X, to create a knock-in mouse model line. This novel model, also only tested in males, reported hyperactivity, reduced contextual fear conditioning, unusual motor coordination and less directed social behavior (17). Both laboratories are continuing to pursue the cell-type specificity of these phenotypes (18) and screening various therapeutics using *ex vivo* slice electrophysiology. Neither of these mouse models exhibited

spontaneous behavioral seizures when evaluated as young adults, which is not unreasonable, given there has been a failure to detect this key phenotype on the C57BL/6J for other NDD and seizure disorder models, such as Angelman and Dravet Syndromes (19-22). C57BL/6J have been repeatedly illustrated to be seizure resistant, published by our group (23) and others (21, 24-28).

Given the latest advances in gene editing technology, *CDKL5*, Rett, *CNSKR2*, and *CASK* Syndromes have been of emerging interest to translational researchers. In X-linked disorders caused by *de novo* mutations, female patients are heterozygous because they have both a healthy allele and a mutant allele comprising their XX genotype (29). Most females are mosaics, having a mixture of cells expressing either their mother's or father's X-linked genes (30-32). Often, cell mosaicism is advantageous, ameliorating the deleterious effects of X-linked mutations and contributing to physiological diversity. As a consequence, most X-linked mutations produce male-only diseases. Yet, in some cases the dynamic interactions between cells in mosaic females lead to female-specific disease manifestations (32). As a result of random X chromosome inactivation (XCI), these patients end up with approximately 50% of their cells expressing the mutant allele while the present healthy allele is epigenetically silenced. Multiple studies of XCI have revealed that genes expressed from the active X chromosome have a unique epigenetic signature when compared to the inactive X chromosome (33). More interestingly, genes that "escape" XCI and express from the inactive chromosome resemble the epigenetics of the active allele with a signature that is defined by the presence of active histones and the absence of promoter methylation. Our team has developed a strategy to recruit epigenetic modifiers to the promoter of genes on the inactive X chromosome, resulting in increased transcription (34). In addition, to our work with epigenetic editing (35, 36), other novel precision-based therapeutics that target the underlying genetic loss of *CDKL5/Cdkl5* via cutting-edge technologies include CDKL5 protein substitution

therapy (37), AAV delivered gene replacement therapy of CDKL5 (38), and approaches that combine gene editing strategies such as treatment with a small-molecule inhibitors of DNA methylation and an antisense oligonucleotide (ASO) against X inactive specific transcript RNA (39).

To assess efficacy of these novel therapeutics, our laboratory has been focused identifying rigorous, reproducible, translationally relevant phenotypes or outcome measures. Over twenty years, our behavioral neuroscience laboratory has transformed focus to translational neurogenetics, concentrating on outcome indices in mice and rats that are translatable to the clinic, and include a range of behavioral domains, seizures, neuroanatomy, electroencephalographic (EEG) signatures, and the correlation of these metrics across the lifespan, from development to age related declines in motor, learning, and memory function (23, 40-44). Our strategy has reported and validated translational phenotypes using Angelman and Phelan McDermid Syndromes and an Scn1a-regulator model of Dravet Syndrome/epilepsy (41, 45). This report is the first description of translationally relevant phenotypes in male and female young adult (8-16 week) mice using two etiologically distinct preclinical CDD models. Observations included robust impairments in touchscreen pairwise discrimination and spatial learning and memory, hyperactivity, increased susceptibility to seizures, and visibly increased frequency and amplitude in electroencephalographic oscillations. These data highlight novel, rigorous phenotypes in two preclinical models of CDD in both sexes. Findings are critical, as they can be utilized as outcome measure indices for a wide variety of novel gene editing and small molecule therapeutics that are currently in the pipeline as potential therapeutic interventions for CDD.

Materials and Methods

Animals

Cdkl5^{exon6} mice were generated by crossing *Cdkl5*$^{exon\ 6-/+}$ females (JAX stock #021967) with congenic C57BL/6J males. *Cdkl5*^{R59X} mice were generated by crossing *Cdkl5*$^{R59X-/+}$ females (JAX stock #028856) with congenic C57BL/6J males. To identify mice, neonates were labelled by paw tattoo on postnatal day (PND) 2-3 using non-toxic animal tattoo ink (Ketchum Manufacturing Inc., Brockville, ON, Canada). At PND 5-7, tails of pups were clipped (0.5 cm) for genotyping, following the UC Davis IACUC policy regarding tissue collection. Genotyping was performed with RED Extract-N-Amp (Sigma Aldrich, St. Louis, MO) using primers 34149 5'-GGAAGAAATGCCAAATGGAG-3' ,34150 5′-GGAGACCTGAAGAGCAAAGG-3, 34151 5′-CCCTCTCAGTAAGGCAGCAG-3, and 34152 5′-TGGTTTTGAGGTGGTTCACA-3 for *Cdkl5*^{exon6}, and 5′-GCTGCTTACATTAGGAGAGACTGC-3′ and 5′-GTCACATGACCAGCCAGCGT-3′ for *Cdkl5*^{R59X}. After weaning on PND21, mice were socially housed in groups of 2-4 by sex.

Tissue extraction

Adult wild-type and heterozygous CDKL5 mice, of both sexes, were cervically dislocated and brains were rapidly extracted. The cerebral cortex, hippocampus, and cerebellum were dissected and flash frozen over dry ice. Tissue was later homogenized and separated for genomic DNA, RNA, or protein.

Western blots

Protein was extracted using Pierce RIPA Buffer (ThermoFisher, Waltham, MA) with Protease & Phosphatase Inhibitor Cocktail (ThermoFisher, Waltham, MA). Protein concentrations were measured using Pierce Bicinchoninic Acid Assay Kit (ThermoFisher, Waltham, MA). 25 ug of

whole brain protein lysate per sample was separated on 4–20% Stacking TGX Gels (BioRad, Hercules, CA) and transferred overnight at 30 V onto Immobilon-FL PVDF membranes (Millipore Sigma, Burlington, MA). PVDF membranes were blocked for 1 h with Intercept (PBS) Blocking Buffer (LI-COR, Lincoln, NE). Following blocking, PVDF membranes were incubated with anti-CDKL5 (1:1000, MRC-PPU Reagents, S957D) and anti-beta actin (1:10000, Sigma-Aldrich, A5441) antibodies in a 1:1 dilution of Intercept and 0.2% PBS Tween (PBST) at 4°C overnight. Following incubation, membranes were washed in 0.1% PBST 5× for 5 min. Membranes were then incubated with IRDye 800 Donkey Anti-Goat IgG Secondary Antibody (1:15000, LI-COR Biosciences, 926-32214) and IRDye 680 Goat Anti-Mouse IgG Secondary Antibody (1:20000, LI-COR Biosciences, 926-68070) in the same Intercept dilution as described previously. Following incubation, membranes were washed 5× in 0.1% PBST and 1× in PBS before storing in fresh PBS. Membranes were imaged on Odyssesy CLx imager (LI-COR, Lincoln, NE). Quantitative analysis was performed using Image Studio Lite software (LI-COR, Lincoln, NE).

Subjects for Behavior and Neurophysiology

All mice were housed in Techniplast cages (Techniplast, West Chester, PA, USA). Cages were housed in ventilated racks in a temperature (68-72°F) and humidity (~25%) controlled colony room on a 12:12 light/dark cycle. Standard rodent chow and tap water were available *ad libitum*. In addition to standard bedding, a Nestlet square, shredded brown paper, and a cardboard tube (Jonesville Corporation, Jonesville, MI) were provided in each cage. All experimental procedures were performed in accordance with the National Institutes of Health Guide for Care and Use of Laboratory Animals and were approved by the Institutional Animal Care and Use Committees (IACUC) #21494 (PI, Silverman) of the University of California, Davis.

Order of Testing

Two cohorts of mice were tested per strain as follows: Cohort 1 of *Cdkl5*^{exon6} deletion mice was sampled from 11 litters. The order and age of testing were as follows: (1) Open field at 6 weeks of age, (2) DigiGait at 6 weeks of age, (3) Rotarod at 7 weeks of age, (4) Spontaneous Alternation at 8 weeks of age, (5) Novel Object Recognition at 8 weeks of age, (6) Touchscreen pairwise discrimination from 12 to 20 weeks of age. Cohort 2 was sampled from 4 litters and tested in PTZ-induced seizures at 8 weeks of age. Cohort 1 of *Cdkl5*^{R59X} knock-in mice was sampled from 13 litters. The order and age of testing were as follows: (1) Open field at 6 weeks of age, (2) DigiGait at 6 weeks of age, (3) Rotarod at 7 weeks of age, (4) Spontaneous Alternation at 8 weeks of age, (5) Novel Object Recognition at 8 weeks of age, (6) Touchscreen pairwise discrimination from 12 to 20 weeks of age. Cohort 2 was sampled from 3 litters and tested in PTZ-induced seizures at 8 weeks of age.

Behavioral Assays

Open field

General exploratory locomotion in a novel open field arena was evaluated as previously described (46-48). Briefly, each subject was tested in a VersaMax Animal Activity Monitoring System (Accuscan, Columbus, OH, USA) for 30-min in a ~30 lux testing room. Total distance traversed, horizontal activity, vertical activity, and time spent in the center were automatically measured to assess gross motor abilities in mice.

Rotarod

Motor coordination, balance, and motor learning were tested with an accelerating rotarod (Ugo Basile, Gemonio, Italy) as previously described (40, 49). Mice were placed on a rotating cylinder that slowly accelerated from 5 to 40 revolutions per min over 5 min. Mice were given three trials

per day with a 60-min inter-trial rest interval and tested for 3 consecutive days for a total of nine trials. Performance was scored as latency to fall off the cylinder with a maximum latency of 5 min.

Spontaneous alternation in a Y-maze

Spontaneous alternation was assayed using methods based on previous studies (50) in mice. The Y-shaped apparatus was made of non-reflective matte white finished acrylic (P95 White, Tap Plastics, Sacramento, CA, USA). Subjects were placed in the middle of the apparatus and transitions between the three arms were scored by an investigator blind to genotype. Mice are placed midway of the start arm, facing the center of the Y for an 8-minute test period and the sequence of entries into each arm are recorded via a ceiling mounted camera integrated with behavioral tracking software (Noldus Ethovision). % Spontaneous alternation is calculated as the number of triads (entries into each of the 3 different arms of the maze in a sequence of 3 without returning to a previously visited arm) relative to the number of alteration opportunities.

Novel Object Recognition

The novel object recognition test was conducted as previously (47, 51-53)described in opaque matte white (P95 White, Tap Plastics, Sacramento, CA, USA) arenas (41 cm *l* x 41 cm *w* x 30 cm *h*)(40, 47, 48, 50, 54). The assay consisted of four sessions: a 30-min habituation session, a second 10-min habituation phase, a 10-min familiarization session, and a 5-min recognition test. On day 1, each subject was habituated to a clean empty arena for 30-min. 24-h later, each subject was returned to the empty arena for an additional 10-min habituation session. The mouse was then removed from testing arena and was placed in a clean temporary holding cage while two identical objects were placed in the arena. Subjects were returned to the testing arena and given a 10-min of familiarization period in which they had time to investigate the two identical objects. After the familiarization phase subjects were returned to their holding cages for a 1-h interval period. One

familiar object and one novel object were placed in the arena, where the two identical objects had been located during the familiarization phase. After the 1-h interval, each subject was returned to the arena for a 5-min recognition test. The familiarization session and the recognition test were recorded using Ethovision XT video tracking software (version 9.0, Noldus Information Technologies, Leesburg, VA, USA). Sniffing was defined as head facing the object with the nose point within 2 cm or less from the object. Time spent sniffing each object was scored by an investigator blind to both genotype and treatment. Recognition memory was defined as spending significantly more time sniffing the novel object compared to the familiar object. Total time spent sniffing both objects was used as a measure of general exploration. Time spent sniffing two identical objects during the familiarization phase confirmed the lack of an innate side bias. Within genotype repeated-measures ANOVA was used to analyze novel object recognition using novel versus familiar objects as comparison. *F*, degrees of freedom, and *p*-values are reported.

Touchscreen pairwise discrimination

An efficient pre-training regimen was validated based on previously published work (42, 48, 55). The pre-training consisted of four stages. Stage 1 consisted of two days of habituation to the chamber under overhead lighting (60 lux). Stage 2 was a single 45-min session in which entering and exiting the magazine triggers reinforcement under overhead lighting. During Stage 3, subjects were trained in daily 45-min sessions during which an image (a random picture from a selection of 40 images) was presented in one of the two windows, and remained on the screen until it was touched. Mice must complete 30 trials/day for two consecutive days to advance to the next stage. In Stage 4, subjects were trained in 45-min daily sessions in which touching the blank side of the screen was discouraged with a 5-s time-out during which the overhead lighting turned off. Completion of at least 30 trials, at an average accuracy of 80%, on two consecutive days, is required for advancement. Images used in Stages 3 and 4 were not used in the subsequent

discrimination task. Only mice that completed all stages of pre-training were advanced to the pairwise visual discrimination task. Bussey–Saksida touchscreen apparatus for mice (Campden Instruments Ltd/Lafayette Instruments, Lafayette, IL, USA), using a procedure modified from original methods described previously (46, 55-59). Subjects were trained to discriminate between two novel images, a spider and an airplane presented in a spatially pseudo-randomized manner in the two windows of the touchscreen. The reinforcer was 20 ul of a palatable liquid nutritional supplement (Strawberry Ensure Plus, Abbott, IL, USA) diluted to 50% with water. A standard tone cue was used to signal the delivery of the reinforcer during pre-training and acquisition. Prior to pre-training, subject mice were weighed, and placed on a restricted diet of 2–4 g of rodent chow per mouse per day, to induce a 15% weight loss. Body weight was carefully monitored throughout the experiment, to ensure that a minimum of 85% of free feeding body weight was maintained for each mouse. Completion of at least 30 trials, at an average accuracy of 80%, on two consecutive days, is required for completion. Days to completion, percent accuracy during a session is defined as (# correct trials/# total trials) * 100, percentage of mice reaching criterion on each day were compared between genotypes, total trials performed across session and correction trials are collected as data, as information on motor abilities and motivation to complete task. Each 45-min session consisted of unlimited number of trials separated by 15-s intertrial intervals (ITI). Designation of the correct and incorrect images were counterbalanced across mice within each genotype. Correct responses were reinforced. Each incorrect response was followed by a correction trial in which the images were presented in an identical manner to the previous trial, until a correct response was made.

Pentylenetetrazol-induced seizures

In a separate cohort, behavioral assessment of seizure threshold in mice was performed with intraperitoneal injections of 80 mg/kg of pentylenetetrazol (PTZ) (Sigma Aldrich, St. Louis, MO, USA) as described previously (23, 43, 50, 60). Dosing was conducted in a dim light setting (~30 lux). Directly after administration of PTZ, subjects were placed in a clean, empty cage and subsequent seizure stages were live-scored for 30-min. Seizure stages were scored using a modified Racine scale where 0 = normal exploratory behavior, 1 = immobility, 2 = generalized spasm, 3 = Straub's tail, 4 = forelimb clonus, 5 = generalized clonus, 6 = clonic-tonic seizure, and 7 = full tonic extension/death.

Perfusions

At the conclusion of behavior testing, mice were euthanized by CO_2 asphyxiation followed by bilateral thoracotomy. Mice were perfused with 10mL PBS (HyClone) followed by 10mL 4% paraformaldehyde (Fisher Healthcare, Pittsburg, PA). Brains were harvested, fixed in formalin for 24 hours, then transferred to 30% sucrose (Fisher Chemical, Fair Lawn, NJ) for 24-48 hours at 4°C. Brains were then frozen for 3 minutes in 100% isopropanol bath on dry ice at -77°C and then stored at -80°C until further processing.

Immunohistochemistry

Brains were serially sectioned at 30μm in the sagittal plane using a Cryotome FSE (Precisionary Instruments) and placed into a 12-well plate filled with PBS with 0.1% sodium azide (NaN3) with 8-12 sections per well. The wells were incubated in PBS with 10% SEA BLOCK Blocking Buffer (Thermo Scientific) for an hour on an orbital shaker at 60 rpm. Sections were transferred into the primary antibody solution (5% SEA BLOCK in PBS with anti-TMEM119: 1:250, Cell Signaling, 90840; anti-GFAP: 1:2000, Abcam, ab10062; and anti-NeuN: 1:1000, EMD Millipore, ABN90) and placed on an orbital shaker at 4°C overnight. Sections were then washed with 0.1% PBST 3

times and placed into a secondary antibody solution (5% SEA BLOCK in PBS with Alexa Fluor 488 Goat Anti-Rabbit IgG (H+L): 1:2000, Invitrogen; Alexa Fluor 594 Goat Anti-Mouse IgG (H+L): 1:2000, Invitrogen; and Alexa Fluor 647 Goat Anti-Guinea Pig IgG (H+L) on an orbital shaker at room temperature for one hour. After incubation, the wells were incubated with Hoescht (1:2000) for 5 minutes on an orbital shaker, then transferred to 0.1% PBST and washed 3 times. To utilize the autodetection software on the AxioScan, sections were immersed in 0.01% Sudan Black in 70% EtOH, gently agitated for 1 minute, and then transferred into PBS prior to mounting. The sections were then mounted onto microscope slides (Thermo Scientific) sequentially from lateral to midline and coverslipped using Fluoromount (Sigma). Whole brain sections were then scanned at 20x and stitched together using a Zeiss AxioScan. Image analysis was performed in Zen 2 (blue edition) (Zeiss) and ImageJ.

Statistical analysis

All statistical analysis were carried out using Prism 9 software (GraphPad Software, San Diego, CA). All significance levels were set at $p < 0.05$ and all *t* tests were two-tailed. Two-way ANOVAs were used to analyze the effects of both genotype and sex. Multiple comparisons were corrected for using Holm-Sidak posthoc methods and F, degrees of freedom, and p-values are reported. Log-rank Mantel-Cox test was used to analyze the percentage of animals that reached criteria in the survival analysis for the touchscreen test. Data are presented as mean ± standard error of the mean (S.E.M) unless otherwise noted.

Results

Given that 90% of those affected by CDD are females (61, 62)and that the majority of CDD mouse model research has focused on male mice, we performed an in-depth translationally-relevant behavioral and physiological comparison of two different lines that lack functional Cdkl5 in both sexes, lack of expression in *Cdkl5*$^{exon\ 6-/y}$ males and a 68% reduction in expression in *Cdkl5*$^{exon\ 6-/+}$ females versus *Cdkl5*$^{exon\ 6+/y}$ males and *Cdkl5*$^{exon6+/+}$ females, respectively. Lack of expression in *Cdkl5*$^{R59X-/y}$ males and a 50% reduction of expression in *Cdkl5* $^{R59X\ +/-}$ females were verified in whole-brain protein lysate Western blotting (**Fig. S1**), corroborating what was previously described (16, 63). Volumetric analysis of brain regions associated with neurological impairments in CDD and quantification of the expression of two markers of neuroinflammation (TMEM119 and GFAP) via fluorescent immunohistochemistry on sagittal brain sections showed no phenotypes in either model (**Fig. S2** and **S3**).

Motor function is highly translational and consists of many nuanced components, including gross exploration and motor abilities, balance, coordination, gait, and fine motor skills. We utilized a tailored motor battery to perform comprehensive outcome assessment that may be useful for clinical trials. *Cdkl5* mutants exhibited a large main effect of genotype using total activity by a Two-Way ANOVA (**Fig 1A**; $F_{(3, 40)} = 22.36$, $p < 0.0001$; **Fig 1E**; $F_{(3, 40)} = 18.63$, $p < 0.0001$), exhibiting hyperactivity when compared to wild-type, sex-matched littermate controls. Holm-Sidak corrected posthoc analysis for multiple comparisons highlighted the significant effect in *Cdkl5*$^{exon\ 6-/y}$ males ($p < 0.0001$) differing from *Cdkl5*$^{exon\ 6+/y}$**,** at every 5-minute time bin across the 30-minute activity assay (0-5min, $p < 0.0005$; 6-10min, $p < 0.0001$; 11-15min, $p < 0.0001$; 16-20min, $p < 0.0001$; 21-25min, $p < 0.0001$; and 26-30min $p < 0.0001$). In females, Holm-Sidak corrected posthoc analysis for multiple comparisons revealed the significance, *Cdkl5*$^{exon\ 6-/+}$ ($p =$

0.0287) versus *Cdkl5*$^{exon\ 6+/+}$ mice, limited to the first two 5-minute time bins across the 30-minute activity assay (0-5min, $p = 0.0468$; 6-10min, $p < 0.002$). As hypothesized, males were slightly more severely affected due to the total loss of Cdkl5 protein. *Cdkl5*$^{R59X+/y}$ and $^{-/y}$ males exhibited significance using total activity following posthoc analysis ($p < 0.0001$), while females did not pass posthoc correction analysis ($p = 0.955$). *Cdkl5*$^{R59X-/y}$ differed from *Cdkl5*$^{R59X+/y}$ during four of six 5-minute time bins across the 30-minute activity assay (0-5min, $p = 0.0764$; 6-10 min, $p < 0.0001$; 11-15 min, $p < 0.0001$; 16-20 min, $p < 0.0001$; 21-25 min, $p < 0.0001$; and 26-30 min $p < 0.0001$). Activity summed over the 30 min session illustrated robust *Cdkl5*^{exon6} and *Cdkl5*^{R59X} main effects of genotype by One-Way ANOVA (**Fig 1B**; $F_{(3, 40)} = 13.33$, $p < 0.0001$; **Fig 1F**; $F_{(3, 40)} = 20.97$, $p < 0.0001$), with mice of both models exhibiting hyperactivity when compared to their wild-type, sex-matched littermate controls. Holm-Sidak corrected posthoc analysis for multiple comparisons, highlighted significant effects in *Cdkl5*$^{exon\ 6-/y}$ ($p < 0.0001$) versus *Cdkl5*$^{exon\ 6+/y}$ males and *Cdkl5*$^{exon6\ -/+}$ ($p = 0.0338$) versus *Cdkl5*$^{exon\ 6+/+}$ females. Males and females with the R59X mutation were hyperactive when analyzed by Holm-Sidak corrected posthoc analysis for multiple comparisons in *Cdkl5*$^{R59X-/y}$ ($p < 0.0001$) versus *Cdkl5*$^{R59X+/y}$ males and *Cdkl5*$^{R59-/+}$ ($p = 0.0268$) versus *Cdkl5*$^{R59X+/+}$ females. *Cdkl5*^{exon6} and *Cdkl5*^{R59X} exhibited a large main effect of genotype by a Two-Way ANOVA using horizontal activity in a novel open field (**Fig 1C**; $F_{(3, 40)} = F_{(3, 40)} = 22.15$, $p < 0.0001$; **Fig 1G**; $F_{(3, 40)} = 10.75$, $p < 0.0001$), with deletion and knockin mice of both models exhibiting hyperactivity compared to wild-type, sex-matched, littermate controls. Holm-Sidak corrected posthoc analysis for multiple comparisons highlighted the significant effect of *Cdkl5*$^{exon\ 6-/y}$ males ($p < 0.0001$) differed from *Cdkl5*$^{exon\ 6+/y}$ during five of the six 5-minute time bins across the 30-minute activity assay (0-5min, $p = 0.0512$; 6-10min, $p < 0.0006$; 11-15min, $p < 0.0006$; 16-20min, $p < 0.0002$; 21-25min, $p < 0.0172$; and 26-30min $p < 0.0001$). In females,

horizontal activity showed hyperactivity in the heterozygous females *Cdkl5*$^{exon6-/+}$ as compared to wild-types ($p = 0.0183$). Further, when analyzed by Holm-Sidak corrected posthoc analysis for multiple comparisons, highlights were clear in two middle bins of the of the six 5-minute time bins across the 30-minute activity assay (10-15min, $p = 0.0512$; 16-20min, $p < 0.0006$). The R59X model showed hyperactivity in both males ($p = 0.0006$) and females ($p = 0.0183$). Holm-Sidak corrected posthoc analysis for multiple comparisons found mutant males were hyperactive during five of six 5-min time bins across the 30 min assay (0-5min, $p = 0.0512$; 6-10min, $p < 0.0006$; 11-15min, $p < 0.0006$; 16-20min, $p < 0.0002$; 21-25min, $p < 0.0172$; and 26-30min $p < 0.0001$). In females, horizontal activity also showed hyperactivity when *Cdkl5*$^{R59X-/+}$ mice were compared to wild-type ($p = 0.0183$). Furthermore, when analyzed by Holm-Sidak corrected posthoc analysis for multiple comparisons, highlights were clear in two middle bins of the six 5-minute time bins across the 30-minute activity assay (10-15min, $p = 0.0069$; 16-20min, $p = 0.0039$).

A corroborating assay of motor abilities, coordination and motor learning is the rotarod. As observed previously by others (16, 64, 65), *Cdkl5*^{exon6} and *Cdkl5*^{R59X} mutants exhibited large main effects of genotype using Two-Way ANOVAs (*Cdkl5*^{exon6} **Fig 1D**; $F_{(3, 40)} = 5.890$, $p < 0.0002$; *Cdkl5*^{R59X} **Fig 1H**; $F_{(3, 40)} = 3.835$, $p < 0.0167$), with affected mice of both models exhibiting shorter latencies to fall off the accelerating rod, illustrating deficits in motor coordination and balance when compared to wild-type, sex-matched littermate controls. *Cdkl5*^{exon6} but not *Cdkl5*^{R59X} mutants exhibited a main effect of time using Two-Way ANOVAs (*Cdkl5*^{exon6} **Fig 1D**; $F_{(3, 40)} = 3.228$, $p < 0.05$; *Cdkl5*^{R59X} **Fig 1H**; $F_{(3, 40)} = 1.045$, $p = 0.353$), suggesting a motor learning deficit in one of the two models.

Cognitive deficits were observed in the Y-maze, an assay of learning and memory that has been validated by experiments in which scopolamine (0.56 and 1 mg/kg; 30 min pre, i.p.) produced

significant reductions in spontaneous alternation behavior relative to vehicle-treated C57Bl/6J mice (communication with Dr. Sukoff-Rizzo and open access https://www.jax.org/MNBF). An overall genotype effect was observed in both *Cdkl5*^{exon6} and *Cdkl5*^{R59X}, in which mutant mice made fewer alternation triads than wild-type, sex-matched littermates (**Fig** 2C; $F_{(3, 40)} = 11.34$, $p < 0.001$ and **Fig. 2G;** $F_{(3, 39)} = 12.45$, $p < 0.001$). *Cdkl5*$^{exon6\ -/y}$ males ($p < 0.001$) and *Cdkl5*$^{exon6\ -/+}$ females ($p = 0.0154$) differed from *Cdkl5*$^{exon6+/y}$ males and *Cdkl5*$^{exon6\ +/+}$ females, respectively, by making fewer alternation triads as described in the methods section. As would be predicted from the hyperactivity described above, both *Cdkl5*^{exon6} and *Cdkl5*^{R59X} (**Fig 2D**; $F_{(3, 40)} = 3.475$, $p = 0.0184$ and **Fig. 2H;** $F_{(3, 39)} = 3.049$, $p = 0.0399$) mutant mice made a greater number of total transitions. Holm-Sidak corrected posthoc analysis for multiple comparisons did not find an effect of a single between group comparison.

A corroborating assay of learning and memory, novel object recognition (NOR), was manually scored by a highly trained observer blinded to genotype. Scores indicated both *Cdkl5*^{exon6} and *Cdkl5*^{R59X} wild-type mice of both sexes spent more time investigating the novel object versus the familiar object, as expected (*Cdkl5*$^{exon6\ +/y}$ **Fig 2A**; $t_{(20)} = 2.317$, $p < 0.003$; *Cdkl5*$^{exon6+/+}$ $t_{(20)} = 3.194$, $p < 0.0046$; *Cdkl5*$^{R59X\ -/y}$ $t_{(20)} = 2.164$, $p < 0.0139$; *Cdkl5*$^{R59X\ +/+}$ $t_{(20)} = 2.323$, $p < 0.028$). Scores from the *Cdkl5*^{exon6} line indicated that mutant mice of both sexes did not spend more time investigating the novel object versus the familiar object (*Cdkl5*$^{exon6\ -/y}$ **Fig 2A**; $t_{(20)} = 1.141$, $p = 0.2673$; *Cdkl5*$^{exon6-/+}$ $t_{(20)} = 0.5904$, $p = 0.5618$), highlighting a corroborating deficit in learning and memory. However, scores from the *Cdkl5*^{R59X} line indicate that mutant mice spent more time investigating the novel object versus the familiar object (*Cdkl5*$^{R59X-/y}$ Fig 2C; $t_{(20)} = 3.201$, $p < 0.005$; *Cdkl5*$^{R59X-/+}$ $t_{(20)} = 2.723$, $p = 0.0134$), indistinguishable from control mice. This finding is a unique observation of differing phenotypes across the two mouse models in which the etiology

of *Cdkl5* loss differs. Our methods utilized were consistent with other NOR literature (40, 51). Data illustrating no preference for the left or right objects and sufficient time spent investigating the objects is also shown, to confirm a lack of inherent preference bias (**Fig. 2B** $Cdkl5^{exon6\ +/y}$; $t_{(20)} = 0.0818$, $p > 0.05$; $Cdkl5^{exon6+/+}$ $t_{(20)} = 0.5358$, $p < 0.05$; $Cdkl5^{R59X\ +/y}$ $t_{(20)} = 0.7402$, $p > 0.05$; $Cdkl5^{R59X\ +/+}$ $t_{(20)} = 0.4422$, $p > 0.05$ and **Fig 2D**; $Cdkl5^{exon6\ -/y}$ $t_{(20)} = 0.9218$, $p > 0.05$; $Cdkl5^{exon6-/+}$ $t_{(20)} = 0.2359$, $p > 0.05$; $Cdkl5^{R59X\ -/y}$ $t_{(20)} = 0.9306$, $p > 0.05$; $Cdkl5^{R59X\ -/+}$ $t_{(20)} = 0.2443$, $p > 0.05$).

We utilized innovative computerized touchscreen assays with high translational relevance to evaluate visual discrimination attributable to cortical circuitry and glutamatergic neurotransmission (66-69) . Mutant male and female mice from the exon 6 deletion exhibited robust learning and memory impairments (**Fig. 3B** $Cdkl5^{exon6\ -/y}$; $t_{(20)} = 3.936$, $p < 0.0009$**; Fig. 3A** $Cdkl5^{exon6-/+}$ ($t_{(20)} = 3.950$, $p < 0.0009$)**,** requiring significantly fewer sessions to a stringent criterion of completing at least 30 trials, at an accuracy of 80% or higher, on two consecutive days, when compared to wild-type, sex-matched littermate controls. Analysis of survival curves, i.e., percentage of mice that reached the 80% accuracy criterion on each training day, indicated that the percentage of mice that reached this criterion was significantly higher in wild-type, sex matched controls (**Fig. 3D** $Cdkl5^{exon6\ -/y}$; Log-rank Mantel-Cox test $X^2_{(54)} = 11.78$, $p < 0.0006$; **Fig. 3C** $Cdkl5^{exon6-/+}$ Log-rank Mantel-Cox test $X^2_{(52)} = 10.78$, $p < 0.001$). Analysis of additional parameters indicated that $Cdkl5^{exon6\ -/y}$ male mice required more trials to reach criterion, compared to $Cdkl5^{exn6+/y}$ controls (**Fig. 3F** $Cdkl5^{exon6\ -/y}$; $t_{(20)} = 4.249$, $p < 0.0001$; **Fig. 3E** $Cdkl5^{exon6-/+}$ $t_{(20)} = 1.167$, $p < 0.248$) and required greater correction trials, suggesting a slower rate of learning (**Fig. 3H** $Cdkl5^{exon6\ -/y}$; $t_{(20)} = 6.34$, $p < 0.0001$; **Fig. 3G** $Cdkl5^{exon6-/+}$ $t_{(20)} = 3.806$, $p < 0.0004$).

Mutant male and female R59X mice also exhibited robust learning and memory impairments (**Fig. 4B** *Cdkl5*$^{R59X-/y}$; $t_{(19)} = 7.195$, $p < 0.0001$; **Fig. 4A** *Cdkl5*$^{R59X-/+}$ $t_{(19)} = 3.742$, $p = 0.0014$), requiring significantly fewer sessions to a stringent criterion of completing at least 30 trials, at an accuracy of 80% or higher, on two consecutive days, when compared to wild-type, sex-matched littermate controls. Analysis of survival curves indicated that the percentage of mice that reached this criterion was significantly higher in wild-type, sex-matched controls (**Fig. 4D** *Cdkl5*$^{R59X-/y}$; Log-rank Mantel-Cox test $X^2_{(54)} = 17.61$, $p < 0.0001$; **Fig. 4C** *Cdkl5*$^{R59X-/+}$ Log-rank Mantel-Cox test $X^2_{(53)} = 10.73$, $p = 0.0011$). Analysis of additional parameters indicated that *Cdkl5*$^{R59X-/y}$ male mice required more trials to reach criterion, compared to *Cdkl5*$^{R59X+/y}$ controls (**Fig. 4F** *Cdkl5*$^{R59X-/y}$; $t_{(19)} = 4.866$, $p < 0.0001$; **Fig. 4E** *Cdkl5*$^{R59X-/+}$ $t_{(19)} = 2.635$, $p = 0.011$) and required greater correction trials, suggesting a slower rate of learning (**Fig. 4H** *Cdkl5*$^{R59X-/y}$; $t_{(19)} = 9.920$, $p < 0.0001$; **Fig. 4G** *Cdkl5*$^{R59X-/+}$ $t_{(19)} = 6.949$, $p < 0.0001$).

Behavioral assessment of seizure threshold in female mice of both lines was performed with injections of 80 mg/kg of pentylenetetrazol (PTZ) as described previously (23, 43, 47, 48, 50, 60, 70). PTZ-induced convulsions were used to gauge susceptibility to primary generalized seizures and as a gross approximation of excitation–inhibitory balance. Seizures were provoked using pentylenetetrazol (PTZ; 80 mg/kg, i.p.) in *Cdkl5*$^{exon6-/+}$ females. Latencies to myoclonic jerk and generalized clonic seizure (loss of righting reflex) (**Fig. 5A** *Cdkl5*$^{exon6-/+}$; $t_{(15)} = 2.660$, $p = 0.0178$; **Fig. 5B** *Cdkl5*$^{exon6-/+}$; $t_{(15)} = 2.410$, $p = 0.0292$), were faster and shorter. They illustrate preliminary characterization of seizure, subthreshold epileptiform activity, and imbalances in the excitatory/inhibitory homeostasis. Administration of PTZ, a non-competitive $GABA_A$ antagonist, leads to brain hyperexcitability. Female *Cdkl5*$^{R59X-/+}$ mice exhibited faster latencies to myoclonic jerk and loss of righting reflex/time to clonic seizure (**Fig. 5C** *Cdkl5*$^{R59X-/+}$; $t_{(17)} = 2.309$, $p =$

0.0338; **Fig. 5D** *Cdkl5*$^{R59X-/+}$; $t_{(17)} = 3.095$, $p = 0.0066$). Multiple previous studies in male hemizygous *Cdkl5* mutant mice have failed to show spontaneous seizures leading to epilepsy in mice younger than 4 months of age (17, 71-74).

Discussion

The X chromosome is highly enriched for genes that are critical in brain function and linked to neurological disease. This is highlighted by the fact that there are ~140 known genes that are causative for X-linked intellectual disabilities (ID) (3, 4). CDD is a X-linked NDD with debilitating ID and pervasive seizures leading to epileptic encephalopathy and severe sleep disruption. The goal of the proposed studies was to provide quantifiable translational phenotypes in females and males using two in vivo model systems, one with an exon deletion mutation and one with a patient-derived knockin mutation. We discovered hyperactivity in both sexes, in both lines, and substantial learning and memory deficits in two of the three tests and in some cases three of three assays that capture cognitive dysfunction. We also report, for the first time, seizure susceptibility, accompanied by representative EEG traces, confirming the biology underlying the behavioral phenomenon in this unique rare genetic NDD. While no gross neuroanatomical changes were observed via immunohistochemistry to correlate behavioral abnormalities with distinct structural changes, more sensitive methodologies aiming at brain connectivity, white matter tracts, and subtler volumetric differences are being pursued in ongoing work. Additionally, it is now well known that the role of microglia in typical and atypical neurodevelopment is critically important (75-77). However, as no differences were observed, in this study that utilized a single time point, it is quite possible that effects of Cdkl5 mutations in microglia activation and/or reactivity may be nuanced or occur at critical windows of development, that were not observed in our initial characterization (76, 78, 79). Previous research has behaviorally and biochemically characterized

male mice from numerous CDD models, including the two lines used here, which do not spontaneously seize as young adults during the average duration of their lifespan. Less work has been performed on female mice, resulting in a relative lack of informative and quantifiable translational phenotypes with sizeable effects. Our teams focused on sensitive behavioral and neurophysiological assays, with a large signal: noise ratio across four major functional domains (motor, cognition, behavioral seizures, and EEG) which will allow for the assessment of future novel therapeutic interventions, informing IND approval(s). The studies were the first to identify translationally relevant cross-species phenotypes with ultrasensitive, touchscreen technology for cognitive deficits like NIH Toolbox in clinical trials of ID, hyperactivity, neurophysiology, and heightened seizure susceptibility in females in two models of CDD preclinical mice.

Clinically relevant outcome measures are required to demonstrate the utility of innovative therapeutic designs, as well as to validate other traditional medicinal therapies that may be in the discovery pipeline of biotechnology and pharmaceutical companies. The first model from the Zhou laboratory, a deletion of Cdkl5 exon 6, demonstrated substantial behavioral alterations in hyperactivity, abnormal social approach and reduced contextual fear conditioning in deletion males (16). These data were collected on male mice to avoid the confounding effects of X-linked mosaicism in the females. However, this perpetuates an inherent lack of translational relevance to the affected females of the CDD community. Our data presented herein, indicate robust hyperactivity deficits in both sexes of both the exon 6 deletion and the R59X knockin mice. The robust signal of hyperactivity was corroborated. We cannot compare fear conditioning data to earlier reports, as many behavioral neuroscience laboratories, including ours, consider hyperactivity a confounding variable when evaluating/interpreting the reduction in freezing percentages in the fear conditioning data (80-82). The novel mouse model that recreated the

patient variant R59X, also reported hyperactivity, reduced contextual fear conditioning, abnormal motor coordination, and less directed social behavior (17). Similar comments as above regarding females and the hyperactivity confound during fear learning, apply to this characterization. Both of these renowned laboratories are continuing to pursue the critical work of examining cell-type specificity of these phenotypes (63, 83) (18) and screening various therapeutics using ex vivo slice electrophysiology and behavioral assays. Our data corroborates the earlier findings, extends the results to females, defines a novel, robust cognitive phenotype, reports abnormal hyperexcitability and provides translational relevance. We also corroborated the profound hyperactivity in both lines and in both sexes.

Over the past five years, our group has optimized sensitive assays across functional domains that allow for the assessment of novel therapeutic interventions (52). In addition, we also employ gold-standard behavioral assays such as open field, rotarod, novel object recognition and the Y-maze. In this study, we also used our highly translational, touchscreen assay to assess cortical-dependent learning via pairwise visual discrimination, as many other renowned laboratories (42, 57-59, 66-69, 84-87), as touchscreen assays are idyllic for simple and complex cognition assessments with limited motor confounds. We have utilized these assays in rat and mouse models of Angelman Syndrome (85, 88) and models of Phelan-McDermid Syndrome, (Shank3+/- mutations) both which have motor hypo-dysfunction (46, 88). We have also observed utilized touchscreen learning testing in a model of another NDD, Coffin-Siris Syndrome, mice with mutations in Arid1b+/- have gross physical delays, and are substantial smaller than aged, sex-matched wildtype littermates. Interesting, despite their smaller stature (analogous to the patient community), Arid1b+/- have normal motor activity levels and normal, intact visual discrimination (35). A fascinating, unique observation of these Cdkl5 model lines is that although they exhibit substantial hyperactivity,

indicated by ~30% increased transitions (Fig. 2D,H) in the Y-maze, ~50% increased activity in the open field (Fig. 1B,F)data and increased trial number in the touchscreen (Figs. 3E,F and 4E,F), they exhibit clear and robust learning impairments and learning delays, contrasting the NDD models of Chd8 and Arid1b (47, 48) and Fragile X Syndrome (86). This means that despite more attempts at the learning and memory tasks, their ability is deficient. Not only does this study, for the first time, report cognitive dysfunction in females, but it reports these learning and memory impairments are not confounded by their inherent hyperactivity. This is the first observation, to our knowledge, of such a unique detectable, sizeable impairment, uninfluenced by the physical activity and sensory processing of the subject mice and similar to clinical observations.

We utilized electroencephalogram (EEG) via an untethered implant system to allow for free movement of the animal over the course of data collection. Our group has focused on a surface EEG acquisition approach rather than region-specific depth recordings, to more closely parallel EEG collection seen clinically and to encourage a global characterization of underlying neural activity. Epileptic activity is captured through EEG as sudden, excessive synchronous neuronal firing of excessive frequency and increased amplitude, across the cortex called spiking activity. This activity is sufficient in the detection and diagnosis of epilepsy and, preclinically, is observed in many mouse models of epilepsy. Bahi-Buisson and colleagues (5-7, 89) have several reports on the early onset and natural history of epilepsy in patients with CDKL5 mutations describing early epilepsy in the first stage (median age of 4 weeks), epileptic encephalopathy in the second stage and tonic seizures and late myoclonic epilepsy in the third. Representative traces from data in Cdkl5 deletion mice highlight visible anomalies in the preclinical surface EEG (Fig. 5A,B). A comprehensive manuscript on the intricate, nuanced indices of EEG, during light/dark cycles, and active versus sleep stages is being prepared for a subsequent report. Here, we observed several

metrics of heightened seizure susceptibility including reduced latencies to generalized seizure in female Cdkl5 mutant mice. Mice were tested as adults (~16 weeks), far younger than a recent reports of seizure properties with aged Cdkl5 mice (72, 90).

Recently, anecdotal and published reports of myoclonic seizure events, provoked by handling, had been observed in aged female Cdkl5 mice by 42 weeks of age (72, 74). These new studies monitored video and four-channel EEG recordings, within a cohort of > 42 week old female Cdkl5exon6-/+ and Cdkl5R59X-/+ mutant mice compared to wild-type littermates, similar to the design herein, except our mice never aged beyond 20 weeks. Mulcahey et al (2020) observed a high frequency of epileptic spasms (72). These events appeared to myoclonic, in nature, as they were characterized by sudden-onset, brief myoclonic jerks involving the limbs or trunk and correlated with the amplitude of the epileptiform activity on EEG (72). The data presented herein corroborate and extend that Cdkl5 knockout mice display decreased latency to the first stages of seizure progression upon low-dose PTZ administration (17), suggesting that seizure susceptibility is altered in the absence of Cdkl5. Yet, our PTZ data contrast with other reports that used high-dose kainic acid seizure induction of overt seizures since Cdkl5 hemizygous knockout males exhibited similar latencies to wild-type littermates, following KA (71). The first study of seizures in females observed myoclonic jerks involving sudden and repetitive movement of the head and neck with or without tail stiffening from 20 weeks of age and older, concluding similar results as other reports that seizures increase with aging (74). However, as seizures increase in frequency and seizure thresholds are reduced, concomitant with natural aging in C57BL/6J mice, we are enthusiastic for our ongoing bioinformatic analysis using extended EEG recording data to quantify and analyze comprehensive epileptiform, power spectrum and seizure characterization in both models in both sexes prior to 20 weeks of age, as the PTZ susceptibility and representative tracings

suggest these substantial aging paradigms, may not be essential for phenotypic detection and are less translational by lifespan timepoints.

Summary

Our report demonstrated quantifiable translational behavioral phenotypes in females and males using two in vivo model systems, one with an exon deletion mutation and one with a patient-derived knockin mutation of CDD. We discovered hyperactivity, substantial learning and memory deficits using touchscreen technology which captures translational cognitive dysfunction, and hyperexcitability, by reduced seizure thresholds

References

1 des Portes, V. (2013) X-linked mental deficiency. Handb Clin Neurol, 111, 297-306.

2 Laumonnier, F., Bonnet-Brilhault, F., Gomot, M., Blanc, R., David, A., Moizard, M.P., Raynaud, M., Ronce, N., Lemonnier, E., Calvas, P. et al. (2004) X-linked mental retardation and autism are associated with a mutation in the NLGN4 gene, a member of the neuroligin family. Am J Hum Genet, 74, 552-557.

3 Skuse, D. (2003) X-linked genes and the neural basis of social cognition. Novartis Found Symp, 251, 84-98; discussion 98-108; 109-111, 281-197.

4 Turkmen, A. and Lin, B. (2021) Detecting X-linked common and rare variant effects in family-based sequencing studies. Genetic Epidemiology, in press.

5 Bahi-Buisson, N. and Bienvenu, T. (2012) CDKL5-Related Disorders: From Clinical Description to Molecular Genetics. Mol Syndromol, 2, 137-152.

6 Bahi-Buisson, N., Kaminska, A., Boddaert, N., Rio, M., Afenjar, A., Gerard, M., Giuliano, F., Motte, J., Heron, D., Morel, M.A. et al. (2008) The three stages of epilepsy in patients with CDKL5 mutations. Epilepsia, 49, 1027-1037.

7 Bahi-Buisson, N., Villeneuve, N., Caietta, E., Jacquette, A., Maurey, H., Matthijs, G., Van Esch, H., Delahaye, A., Moncla, A., Milh, M. et al. (2012) Recurrent mutations in the CDKL5 gene: genotype-phenotype relationships. Am J Med Genet A, 158A, 1612-1619.

8 Ho, N.T., Kroner, B., Grinspan, Z., Fureman, B., Farrell, K., Zhang, J., Buelow, J., Hesdorffer, D.C. and Rare Epilepsy Network Steering, C. (2018) Comorbidities of Rare Epilepsies: Results from the Rare Epilepsy Network. J Pediatr, 203, 249-258 e245.

9 Arican, P., Gencpinar, P. and Olgac Dundar, N. (2019) A new cause of developmental and epileptic encephalopathy with continuous spike-and-wave during sleep: CDKL5 disorder. Neurocase, 25, 59-61.

10 Lo Martire, V., Alvente, S., Bastianini, S., Berteotti, C., Silvani, A., Valli, A., Viggiano, R., Ciani, E. and Zoccoli, G. (2017) CDKL5 deficiency entails sleep apneas in mice. J Sleep Res, 26, 495-497.

11 Hagebeuk, E.E., van den Bossche, R.A. and de Weerd, A.W. (2013) Respiratory and sleep disorders in female children with atypical Rett syndrome caused by mutations in the CDKL5 gene. Dev Med Child Neurol, 55, 480-484.

12 Lee, K.Z. and Liao, W. (2018) Loss of CDKL5 disrupts respiratory function in mice. Respir Physiol Neurobiol, 248, 48-54.

13 Fehr, S., Wilson, M., Downs, J., Williams, S., Murgia, A., Sartori, S., Vecchi, M., Ho, G., Polli, R., Psoni, S. et al. (2013) The CDKL5 disorder is an independent clinical entity associated with early-onset encephalopathy. Eur J Hum Genet, 21, 266-273.

14 Terzic, B., Davatolhagh, M.F., Ho, Y., Tang, S., Liu, Y.T., Xia, Z., Cui, Y., Fuccillo, M.V. and Zhou, Z. (2021) Temporal manipulation of Cdkl5 reveals essential postdevelopmental functions and reversible CDKL5 deficiency disorder-related deficits. J Clin Invest, 131.

15 JANM, H., P, D., CE, G., NB, C., CD, C., Buchanan, Waldo, Lock, Anderson, O'Geen et al. (2020) Artificial escape from XCI by DNA methylation editing of the CDKL5 gene. Nucleic acids research, in press.

16 Wang, I.T., Allen, M., Goffin, D., Zhu, X., Fairless, A.H., Brodkin, E.S., Siegel, S.J., Marsh, E.D., Blendy, J.A. and Zhou, Z. (2012) Loss of CDKL5 disrupts kinome profile and event-related potentials leading to autistic-like phenotypes in mice. Proc Natl Acad Sci U S A, 109, 21516-21521.

17 Yennawar, M., White, R.S. and Jensen, F.E. (2019) AMPA Receptor Dysregulation and Therapeutic Interventions in a Mouse Model of CDKL5 Deficiency Disorder. J Neurosci, 39, 4814-4828.

18 Tang, S., Terzic, B., Wang, I.J., Sarmiento, N., Sizov, K., Cui, Y., Takano, H., Marsh, E.D., Zhou, Z. and Coulter, D.A. (2019) Altered NMDAR signaling underlies autistic-like features in mouse models of CDKL5 deficiency disorder. Nat Commun, 10, 2655.

19 Kang, S.K., Hawkins, N.A. and Kearney, J.A. (2019) C57BL/6J and C57BL/6N substrains differentially influence phenotype severity in the Scn1a (+/-) mouse model of Dravet syndrome. Epilepsia Open, 4, 164-169.

20 Rubinstein, M., Westenbroek, R.E., Yu, F.H., Jones, C.J., Scheuer, T. and Catterall, W.A. (2015) Genetic background modulates impaired excitability of inhibitory neurons in a mouse model of Dravet syndrome. Neurobiol Dis, 73, 106-117.

21 Born, H.A., Dao, A.T., Levine, A.T., Lee, W.L., Mehta, N.M., Mehra, S., Weeber, E.J. and Anderson, A.E. (2017) Strain-dependence of the Angelman Syndrome phenotypes in Ube3a maternal deficiency mice. Sci Rep, 7, 8451.

22 Sun, W., Wagnon, J.L., Mahaffey, C.L., Briese, M., Ule, J. and Frankel, W.N. (2013) Aberrant sodium channel activity in the complex seizure disorder of Celf4 mutant mice. J Physiol, 591, 241-255.

23 Copping, N.A., Adhikari, A., Petkova, S.P. and Silverman, J.L. (2019) Genetic backgrounds have unique seizure response profiles and behavioral outcomes following convulsant administration. Epilepsy Behav, 101, 106547.

24 Ferraro, T.N., Golden, G.T., Smith, G.G. and Berrettini, W.H. (1995) Differential susceptibility to seizures induced by systemic kainic acid treatment in mature DBA/2J and C57BL/6J mice. Epilepsia, 36, 301-307.

25 Ferraro, T.N., Smith, G.G., Schwebel, C.L., Doyle, G.A., Ruiz, S.E., Oleynick, J.U., Lohoff, F.W., Berrettini, W.H. and Buono, R.J. (2010) Confirmation of multiple seizure susceptibility QTLs on chromosome 15 in C57BL/6J and DBA/2J inbred mice. Physiol Genomics, 42A, 1-7.

26 Jazrawi, S.P. and Horton, R.W. (1986) Brain adrenoceptor binding sites in mice susceptible (DBA/2J) and resistant (C57 Bl/6) to audiogenic seizures. J Neurochem, 47, 173-177.

27 Spyrou, N.A., Prestwich, S.A. and Horton, R.W. (1984) Synaptosomal [3H]GABA uptake and [3H]nipecotic acid binding in audiogenic seizure susceptible (DBA/2) and resistant (C57 B1/6) mice. Eur J Pharmacol, 100, 207-210.

28 Hertz, L., Schousboe, A., Formby, B. and Lennox-Buchthal, M. (1974) Some age-dependent biochemical changes in mice susceptible to seizures. Epilepsia, 15, 619-631.

29 Ahn, J. and Lee, J. (2008) X chromosome: X inactivation. . Nature Education, 1(1):24.

30 Hagerman, R.J. and Hagerman, P.J. (2006) X inactivation and cellular mosaicism. JAMA, 296, 930-931; author reply 931.

31 Migeon, B.R. (2006) The role of X inactivation and cellular mosaicism in women's health and sex-specific diseases. JAMA, 295, 1428-1433.

32 Migeon, B.R. (2020) X-linked diseases: susceptible females. Genet Med, 22, 1156-1174.

33 Renthal, W., Boxer, L.D., Hrvatin, S., Li, E., Silberfeld, A., Nagy, M.A., Griffith, E.C., Vierbuchen, T. and Greenberg, M.E. (2018) Characterization of human mosaic Rett syndrome brain tissue by single-nucleus RNA sequencing. Nat Neurosci, 21, 1670-1679.

34 Halmai, J., Deng, P., Gonzalez, C.E., Coggins, N.B., Cameron, D., Carter, J.L., Buchanan, F.K.B., Waldo, J.J., Lock, S.R., Anderson, J.D. et al. (2020) Artificial escape from XCI by DNA methylation editing of the CDKL5 gene. Nucleic Acids Res, 48, 2372-2387.

35 O'Geen, H., Bates, S.L., Carter, S.S., Nisson, K.A., Halmai, J., Fink, K.D., Rhie, S.K., Farnham, P.J. and Segal, D.J. (2019) Ezh2-dCas9 and KRAB-dCas9 enable engineering of epigenetic memory in a context-dependent manner. Epigenetics Chromatin, 12, 26.

36 Segal, D.J. (2019) Grand Challenges in Gene and Epigenetic Editing for Neurologic Disease. Front Genome Ed, 1, 1.

37 Trazzi, S., De Franceschi, M., Fuchs, C., Bastianini, S., Viggiano, R., Lupori, L., Mazziotti, R., Medici, G., Lo Martire, V., Ren, E. et al. (2018) CDKL5 protein substitution therapy rescues neurological phenotypes of a mouse model of CDKL5 disorder. Hum Mol Genet, 27, 1572-1592.

38 Gao, Y., Irvine, E.E., Eleftheriadou, I., Naranjo, C.J., Hearn-Yeates, F., Bosch, L., Glegola, J.A., Murdoch, L., Czerniak, A., Meloni, I. et al. (2020) Gene replacement ameliorates deficits in mouse and human models of cyclin-dependent kinase-like 5 disorder. Brain, 143, 811-832.

39 Carrette, L.L.G., Wang, C.Y., Wei, C., Press, W., Ma, W., Kelleher, R.J., 3rd and Lee, J.T. (2018) A mixed modality approach towards Xi reactivation for Rett syndrome and other X-linked disorders. Proc Natl Acad Sci U S A, 115, E668-E675.

40 Adhikari, A., Copping, N.A., Onaga, B., Pride, M.C., Coulson, R.L., Yang, M., Yasui, D.H., LaSalle, J.M. and Silverman, J.L. (2018) Cognitive Deficits in the Snord116 Deletion Mouse Model for Prader-Willi Syndrome. Neurobiol Learn Mem, in press.

41 Copping, N. and Silverman, J. (2020) Abnormal electrophysiological and sleep deficits in a mouse model of Angelman Syndrome Molecular Autism in press.

42 Copping, N.A., Berg, E.L., Foley, G.M., Schaffler, M.D., Onaga, B.L., Buscher, N., Silverman, J.L. and Yang, M. (2016) Touchscreen learning deficits and normal social approach behavior in the Shank3B model of Phelan-McDermid Syndrome and autism. Neuroscience, in press.

43 Copping, N.A., Christian, S.G.B., Ritter, D.J., Islam, M.S., Buscher, N., Zolkowska, D., Pride, M.C., Berg, E.L., LaSalle, J.M., Ellegood, J. et al. (2017) Neuronal overexpression of Ube3a isoform 2 causes behavioral impairments and neuroanatomical pathology relevant to 15q11.2-q13.3 duplication syndrome. Hum Mol Genet, 26, 3995-4010.

44 Dhamne, S.C., Silverman, J.L., Super, C.E., Lammers, S.H.T., Hameed, M.Q., Modi, M.E., Copping, N.A., Pride, M.C., Smith, D.G., Rotenberg, A. et al. (2017) Replicable in vivo physiological and behavioral phenotypes of the Shank3B null mutant mouse model of autism. Mol Autism, 8, 26.

45 Haigh, J.L., Adhikari, A., Copping, N.A., Stradleigh, T., Wade, A.A., Catta-Preta, R., Su-Feher, L., Zdilar, I., Morse, S., Fenton, T.A. et al. (2021) Deletion of a non-canonical regulatory sequence causes loss of Scn1a expression and epileptic phenotypes in mice. Genome Med, 13, 69.

46 Copping, N.A., Berg, E.L., Foley, G.M., Schaffler, M.D., Onaga, B.L., Buscher, N., Silverman, J.L. and Yang, M. (2017) Touchscreen learning deficits and normal social approach behavior in the Shank3B model of Phelan-McDermid Syndrome and autism. Neuroscience, 345, 155-165.

47 Gompers, A.L., Su-Feher, L., Ellegood, J., Copping, N.A., Riyadh, M.A., Stradleigh, T.W., Pride, M.C., Schaffler, M.D., Wade, A.A., Catta-Preta, R. et al. (2017) Germline Chd8 haploinsufficiency alters brain development in mouse. Nat Neurosci, 20, 1062-1073.

48 Ellegood, J., Petkova, S.P., Kinman, A., Qiu, L.R., Adhikari, A., Wade, A.A., Fernandes, D., Lindenmaier, Z., Creighton, A., Nutter, L.M.J. et al. (2021) Neuroanatomy and behavior in mice with a haploinsufficiency of AT-rich interactive domain 1B (ARID1B) throughout development. Mol Autism, 12, 25.

49 Flannery, B.M., Silverman, J.L., Bruun, D.A., Puhger, K.R., McCoy, M.R., Hammock, B.D., Crawley, J.N. and Lein, P.J. (2015) Behavioral assessment of NIH Swiss mice acutely intoxicated with tetramethylenedisulfotetramine. Neurotoxicol Teratol, 47, 36-45.

50 Haigh, J.L., Adhikari, A., Copping, N.A., Stradleigh, T., Wade, A.A., Catta-Preta, R., Su-Feher, L., Zdilar, I., Morse, S., Fenton, T.A. et al. (2021) Deletion of a non-canonical regulatory sequence causes loss of Scn1a expression and epileptic phenotypes in mice. Genome Med, 13, 69.

51 Gulinello, M., Mitchell, H.A., Chang, Q., Timothy O'Brien, W., Zhou, Z., Abel, T., Wang, L., Corbin, J.G., Veeraragavan, S., Samaco, R.C. et al. (2018) Rigor and reproducibility in rodent behavioral research. Neurobiol Learn Mem, in press.

52 Adhikari, A., Copping, N.A., Beegle, J., Cameron, D.L., Deng, P., O'Geen, H., Segal, D.J., Fink, K.D., Silverman, J.L. and Anderson, J.S. (2021) Functional rescue in an Angelman syndrome model following treatment with lentivector transduced hematopoietic stem cells. Hum Mol Genet, 30, 1067-1083.

53 Adhikari, A., Copping, N.A., Onaga, B., Pride, M.C., Coulson, R.L., Yang, M., Yasui, D.H., LaSalle, J.M. and Silverman, J.L. (2019) Cognitive deficits in the Snord116 deletion mouse model for Prader-Willi syndrome. Neurobiol Learn Mem, 165, 106874.

54 Vogel Ciernia, A., Pride, M.C., Durbin-Johnson, B., Noronha, A., Chang, A., Yasui, D.H., Crawley, J.N. and LaSalle, J.M. (2017) Early motor phenotype detection in a female mouse model of Rett syndrome is improved by cross-fostering. Hum Mol Genet, 26, 1839-1854.

55 McTighe, S.M., Mar, A.C., Romberg, C., Bussey, T.J. and Saksida, L.M. (2009) A new touchscreen test of pattern separation: effect of hippocampal lesions. Neuroreport, 20, 881-885.

56 Bussey, T.J., Muir, J.L., Everitt, B.J. and Robbins, T.W. (1997) Triple dissociation of anterior cingulate, posterior cingulate, and medial frontal cortices on visual discrimination tasks using a touchscreen testing procedure for the rat. Behav Neurosci, 111, 920-936.

57 Graybeal, C., Bachu, M., Mozhui, K., Saksida, L.M., Bussey, T.J., Sagalyn, E., Williams, R.W. and Holmes, A. (2014) Strains and stressors: an analysis of touchscreen learning in genetically diverse mouse strains. PLoS One, 9, e87745.

58 Horner, A.E., Heath, C.J., Hvoslef-Eide, M., Kent, B.A., Kim, C.H., Nilsson, S.R., Alsio, J., Oomen, C.A., Holmes, A., Saksida, L.M. et al. (2013) The touchscreen operant platform for testing learning and memory in rats and mice. Nat Protoc, 8, 1961-1984.

59 Morton, A.J., Skillings, E., Bussey, T.J. and Saksida, L.M. (2006) Measuring cognitive deficits in disabled mice using an automated interactive touchscreen system. Nat Methods, 3, 767.

60 Copping, N.A. and Silverman, J.L. (2021) Abnormal electrophysiological phenotypes and sleep deficits in a mouse model of Angelman Syndrome. Mol Autism, 12, 9.

61 Mangatt, M., Wong, K., Anderson, B., Epstein, A., Hodgetts, S., Leonard, H. and Downs, J. (2016) Prevalence and onset of comorbidities in the CDKL5 disorder differ from Rett syndrome. Orphanet J Rare Dis, 11, 39.

62 Olson, H.E., Daniels, C.I., Haviland, I., Swanson, L.C., Greene, C.A., Denny, A.M.M., Demarest, S.T., Pestana-Knight, E., Zhang, X., Moosa, A.N. et al. (2021) Current neurologic treatment and emerging therapies in CDKL5 deficiency disorder. J Neurodev Disord, 13, 40.

63 Tang, S., Wang, I.J., Yue, C., Takano, H., Terzic, B., Pance, K., Lee, J.Y., Cui, Y., Coulter, D.A. and Zhou, Z. (2017) Loss of CDKL5 in Glutamatergic Neurons Disrupts Hippocampal Microcircuitry and Leads to Memory Impairment in Mice. J Neurosci, 37, 7420-7437.

64 Okuda, K., Takao, K., Watanabe, A., Miyakawa, T., Mizuguchi, M. and Tanaka, T. (2018) Comprehensive behavioral analysis of the Cdkl5 knockout mice revealed significant enhancement in anxiety- and fear-related behaviors and impairment in both acquisition and long-term retention of spatial reference memory. PloS one, 13, e0196587.

65 Sivilia, S., Mangano, C., Beggiato, S., Giuliani, A., Torricella, R., Baldassarro, V.A., Fernandez, M., Lorenzini, L., Giardino, L., Borelli, A.C. et al. (2016) CDKL5 knockout leads to altered inhibitory transmission in the cerebellum of adult mice. Genes Brain Behav, 15, 491-502.

66 Brigman, J.L., Daut, R.A., Saksida, L., Bussey, T.J., Nakazawa, K. and Holmes, A. (2015) Impaired discrimination learning in interneuronal NMDAR-GluN2B mutant mice. Neuroreport, 26, 489-494.

67 Brigman, J.L., Feyder, M., Saksida, L.M., Bussey, T.J., Mishina, M. and Holmes, A. (2008) Impaired discrimination learning in mice lacking the NMDA receptor NR2A subunit. Learn Mem, 15, 50-54.

68 Marquardt, K., Josey, M., Kenton, J.A., Cavanagh, J.F., Holmes, A. and Brigman, J.L. (2019) Impaired cognitive flexibility following NMDAR-GluN2B deletion is associated with altered orbitofrontal-striatal function. Neuroscience, 404, 338-352.

69 Kenton, J.A., Castillo, R., Holmes, A. and Brigman, J.L. (2018) Cortico-hippocampal GluN2B is essential for efficient visual-spatial discrimination learning in a touchscreen paradigm. Neurobiol Learn Mem, 156, 60-67.

70 Born, H.A., Martinez, L.A., Levine, A.T., Harris, S.E., Mehra, S., Lee, W.L., Dindot, S.V., Nash, K.R., Silverman, J.L., Segal, D.J. et al. (2021) Early Developmental EEG and Seizure Phenotypes in a Full Gene Deletion of Ubiquitin Protein Ligase E3A Rat Model of Angelman Syndrome. eNeuro, 8.

71 Amendola, E., Zhan, Y., Mattucci, C., Castroflorio, E., Calcagno, E., Fuchs, C., Lonetti, G., Silingardi, D., Vyssotski, A.L., Farley, D. et al. (2014) Mapping pathological phenotypes in a mouse model of CDKL5 disorder. PloS one, 9, e91613.

72 Mulcahey, P.J., Tang, S., Takano, H., White, A., Davila Portillo, D.R., Kane, O.M., Marsh, E.D., Zhou, Z. and Coulter, D.A. (2020) Aged heterozygous Cdkl5 mutant mice exhibit spontaneous epileptic spasms. Exp Neurol, 332, 113388.

73 Okuda, K., Kobayashi, S., Fukaya, M., Watanabe, A., Murakami, T., Hagiwara, M., Sato, T., Ueno, H., Ogonuki, N., Komano-Inoue, S. et al. (2017) CDKL5 controls postsynaptic localization of GluN2B-containing NMDA receptors in the hippocampus and regulates seizure susceptibility. Neurobiol Dis, 106, 158-170.

74 Terzic, B., Cui, Y., Edmondson, A.C., Tang, S., Sarmiento, N., Zaitseva, D., Marsh, E.D., Coulter, D.A. and Zhou, Z. (2021) X-linked cellular mosaicism underlies age-dependent

occurrence of seizure-like events in mouse models of CDKL5 deficiency disorder. Neurobiol Dis, 148, 105176.

75 Bilbo, S.D. (2018) The diverse culinary habits of microglia. Nat Neurosci, 21, 1023-1025.

76 Dziabis, J.E. and Bilbo, S.D. (2021) Microglia and Sensitive Periods in Brain Development. Curr Top Behav Neurosci, in press.

77 Smith, C.J. and Bilbo, S.D. (2019) Microglia Sculpt Sex Differences in Social Behavior. Neuron, 102, 275-277.

78 Mao, Y., Evans, E.E., Mishra, V., Balch, L., Eberhardt, A., Zauderer, M. and Gold, W.A. (2021) Anti-Semaphorin 4D Rescues Motor, Cognitive, and Respiratory Phenotypes in a Rett Syndrome Mouse Model. International journal of molecular sciences, 22.

79 Veselinovic, A., Petrovic, S., Zikic, V., Subotic, M., Jakovljevic, V., Jeremic, N. and Vucic, V. (2021) Neuroinflammation in Autism and Supplementation Based on Omega-3 Polyunsaturated Fatty Acids: A Narrative Review. Medicina (Kaunas), 57.

80 Silverman, J.L., Nithianantharajah, J., Der-Avakian, A., Young, J.W. and Sukoff Rizzo, S.J. (2020) Lost in translation: At the crossroads of face validity and translational utility of behavioral assays in animal models for the development of therapeutics. Neurosci Biobehav Rev, 116, 452-453.

81 Sukoff Rizzo, S.J., Anderson, L.C., Green, T.L., McGarr, T., Wells, G. and Winter, S.S. (2018) Assessing Healthspan and Lifespan Measures in Aging Mice: Optimization of Testing Protocols, Replicability, and Rater Reliability. Curr Protoc Mouse Biol, 8, e45.

82 Sukoff Rizzo, S.J. and Silverman, J.L. (2016) Methodological Considerations for Optimizing and Validating Behavioral Assays. Curr Protoc Mouse Biol, 6, 364-379.

83 Lupori, L., Sagona, G., Fuchs, C., Mazziotti, R., Stefanov, A., Putignano, E., Napoli, D., Strettoi, E., Ciani, E. and Pizzorusso, T. (2019) Site-specific abnormalities in the visual system of a mouse model of CDKL5 deficiency disorder. Hum Mol Genet, 28, 2851-2861.

84 Bussey, T.J., Padain, T.L., Skillings, E.A., Winters, B.D., Morton, A.J. and Saksida, L.M. (2008) The touchscreen cognitive testing method for rodents: how to get the best out of your rat. Learn Mem, 15, 516-523.

85 Leach, P.T. and Crawley, J.N. (2018) Touchscreen learning deficits in Ube3a, Ts65Dn and Mecp2 mouse models of neurodevelopmental disorders with intellectual disabilities. Genes Brain Behav, 17, e12452.

86 Leach, P.T., Hayes, J., Pride, M., Silverman, J.L. and Crawley, J.N. (2016) Normal Performance of Fmr1 Mice on a Touchscreen Delayed Nonmatching to Position Working Memory Task. eNeuro, 3.

87 Yang, M., Lewis, F.C., Sarvi, M.S., Foley, G.M. and Crawley, J.N. (2015) 16p11.2 Deletion mice display cognitive deficits in touchscreen learning and novelty recognition tasks. Learn Mem, 22, 622-632.

88 Berg, E.L., Pride, M.C., Petkova, S.P., Lee, R.D., Copping, N.A., Shen, Y., Adhikari, A., Fenton, T.A., Pedersen, L.R., Noakes, L.S. et al. (2020) Translational outcomes in a full gene deletion of ubiquitin protein ligase E3A rat model of Angelman syndrome. Transl Psychiatry, 10, 39.

89 Bahi-Buisson, N., Nectoux, J., Rosas-Vargas, H., Milh, M., Boddaert, N., Girard, B., Cances, C., Ville, D., Afenjar, A., Rio, M. et al. (2008) Key clinical features to identify girls with CDKL5 mutations. Brain, 131, 2647-2661.

90 Gennaccaro, L., Fuchs, C., Loi, M., Pizzo, R., Alvente, S., Berteotti, C., Lupori, L., Sagona, G., Galvani, G., Gurgone, A. et al. (2021) Age-Related Cognitive and Motor Decline in a Mouse Model of CDKL5 Deficiency Disorder is Associated with Increased Neuronal Senescence and Death. Aging Dis, 12, 764-785.

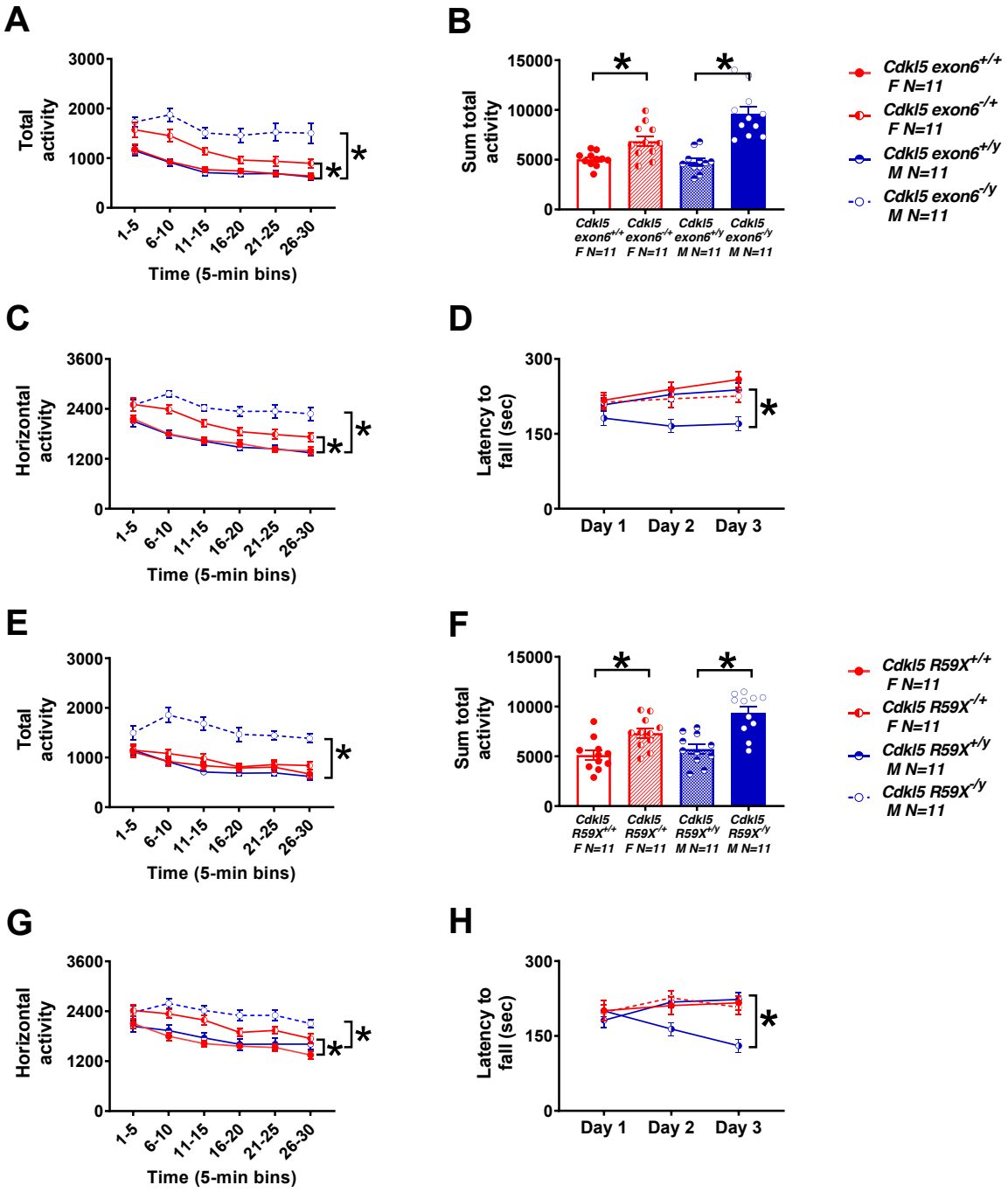

Figure 1. Hyperactivity and motor learning deficits in *Cdkl5* deletion and knockin mice. (A-C) *Cdkl5*$^{exon6-/+}$ females and *Cdkl5*$^{exon6-/y}$ males exhibited increased activity by total activity over 5-mins time bins, summed total activity, and horizontal activity metrics. (D) *Cdkl5*$^{exon6-/y}$ males, but not *Cdkl5*$^{exon6-/+}$ females, had significantly lower latencies to fall off the rotarod compared to wildtype littermate controls. (E-G) *Cdkl5*$^{R59X-/+}$ females showed significantly increased activity by summed total activity, and horizontal activity metrics but not total activity over 5-mins time bins. *Cdkl5*$^{R59X-/y}$ males showed increased activity by all three activity metrics. (H) *Cdkl5*$^{R59X-/y}$ males

had lower latencies to fall off the rotarod compared to wildtype littermate controls exhibiting a motor learning deficit.

Data are expressed as mean +/- S.E.M. *$p<0.05$ indicates when the *Cdkl5* mutant mice differ from sex-matched wildtype littermate controls.

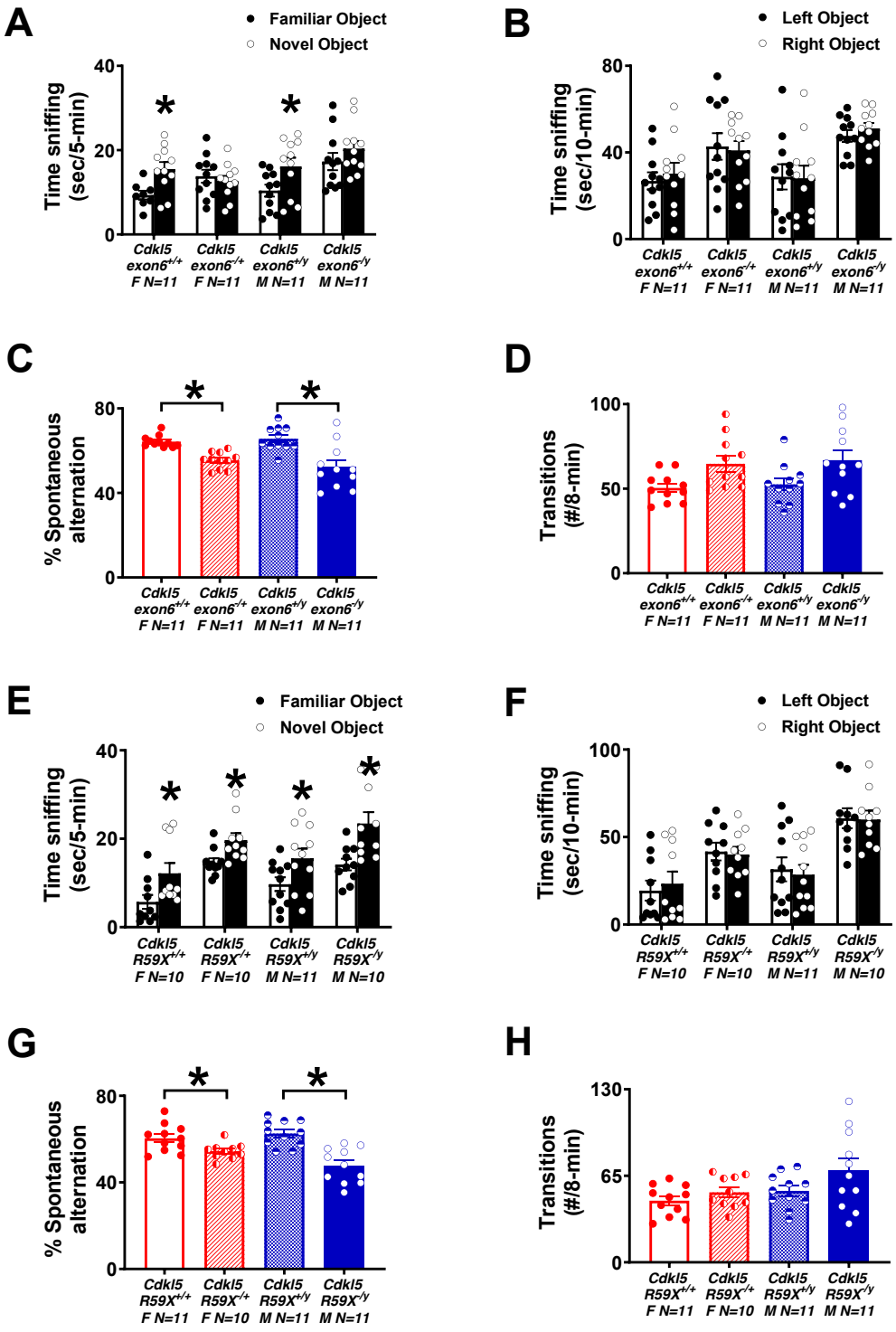

Figure 2. Cognitive deficits in *Cdkl5* deletion and knockin mice. (A) *Cdkl5*$^{exon6-/+}$ females and *Cdkl5*$^{exon6-/y}$ males exhibited a lack of recognition memory following a one-hour delay compared to wildtype controls that exhibited more time with the novel object, exhibiting intact object recognition. (B) All groups explored the two objects similarly during the familiarization phase.

(C) *Cdkl5*$^{exon6-/+}$ females and *Cdkl5*$^{exon6-/y}$ males exhibited working memory impairments by lower percentage of spontaneous alternation in Y-maze. (D) *Cdkl5*$^{exon6-/+}$ females and *Cdkl5*$^{exon6-/y}$ males made greater total transition in Y-maze compared to wildtype littermate controls. (E) *Cdkl5*$^{R59X-/+}$ females and *Cdkl5*$^{R59X-/y}$ males exhibited intact recognition memory following a one-hour delay similar to wildtype controls. (F) All groups explored the two objects similarly during the familiarization phase. (G) *Cdkl5*$^{R59X-/+}$ females and *Cdkl5*$^{R59X-/y}$ males exhibited working memory impairments by lower percentage of spontaneous alternation in Y-maze. (H) *Cdkl5*$^{R59X-/y}$ males but not *Cdkl5*$^{R59X-/+}$ females made greater total transitions in Y-maze compared to wildtype littermate controls.

Data are expressed as mean +/- S.E.M. *$p<0.05$ indicates when the *Cdkl5* mutant mice differ from sex-matched wildtype littermate controls.

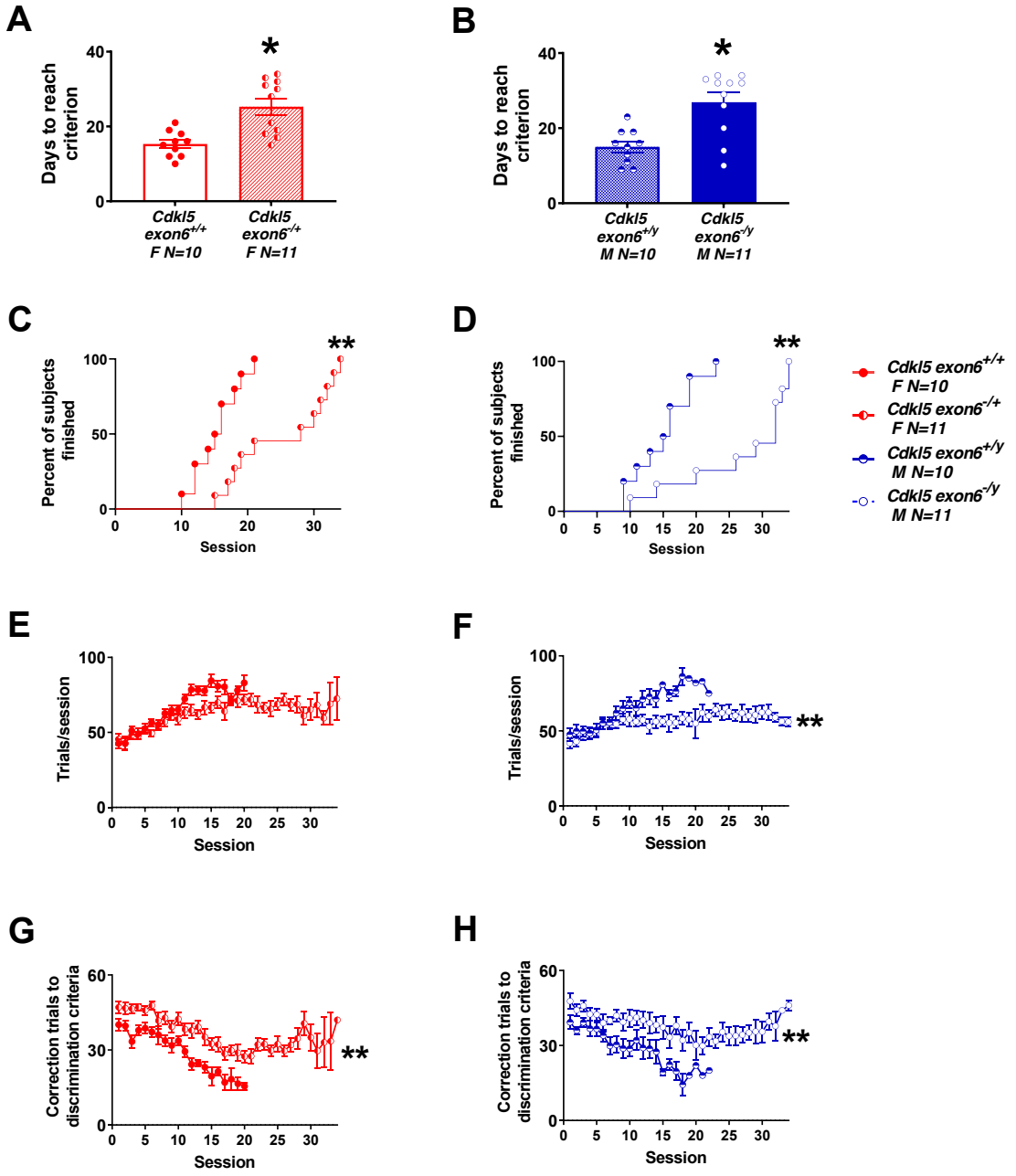

Figure 3. Delayed touchscreen learning in *Cdkl5* deletion mice. (A,B) *Cdkl5*$^{exon6-/+}$ females and *Cdkl5*$^{exon6-/y}$ males took significantly longer to reach a criterion of completing at least 30 trials with 80% or higher accuracy on two consecutive days compared to sex-matched wildtype littermates. (C,D) The percentage of mice that reached criterion was significantly higher in sex-matched wildtype controls than *Cdkl5*$^{exon6-/+}$ females and *Cdkl5*$^{exon6-/y}$ males suggesting a delayed rate of learning. (E,F) *Cdkl5*$^{exon6-/+}$ females and *Cdkl5*$^{exon6-/y}$ males had fewer trials per session. (G,H) *Cdkl5*$^{exon6-/+}$ females and *Cdkl5*$^{exon6-/y}$ males required higher correction trials to reach criterion.

Data are expressed as mean +/- S.E.M. *p<0.05, **p<0.001, ***p<0.0001 indicate when the *Cdkl5* mutant mice differ from sex-matched wildtype littermate controls.

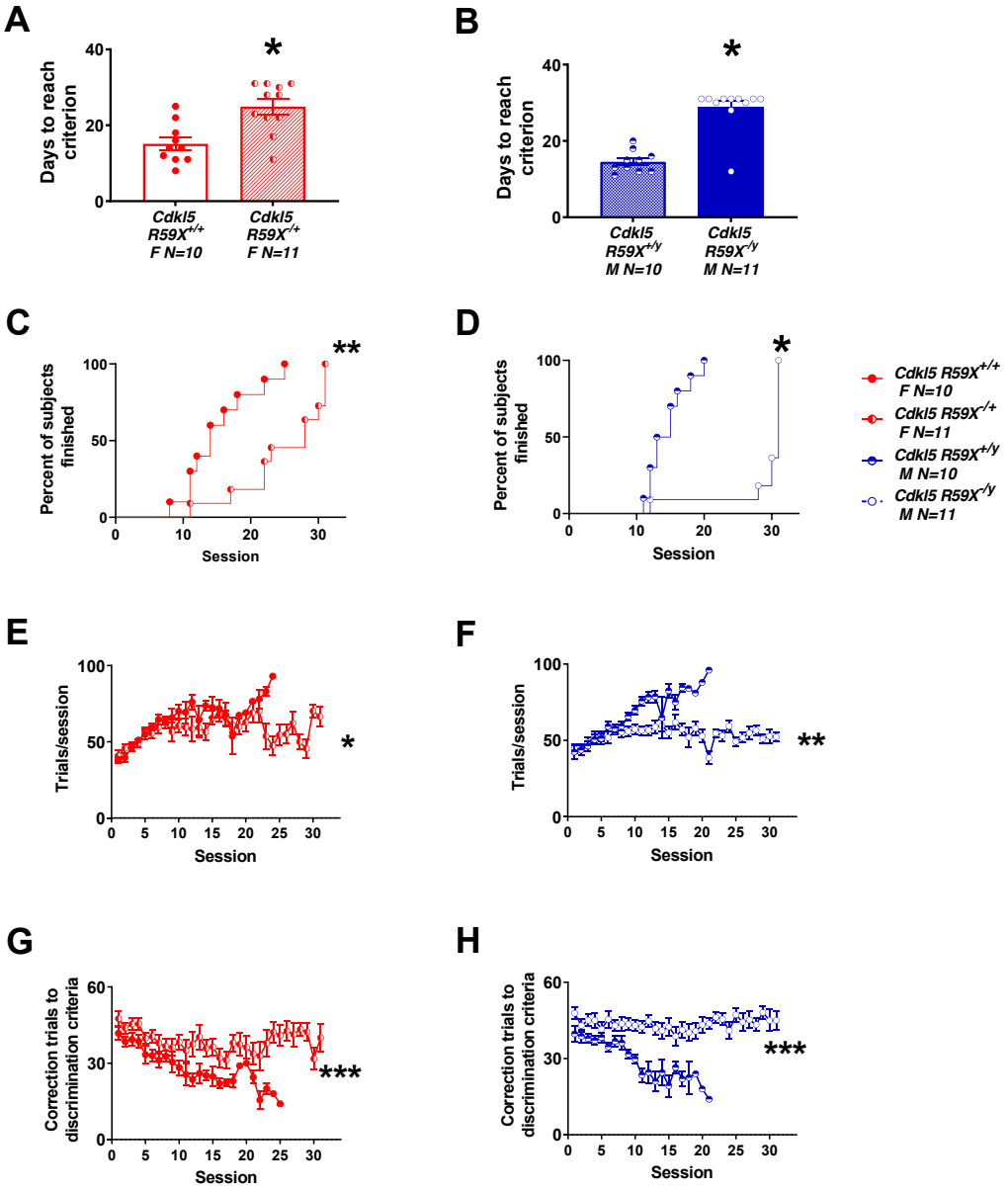

Figure 4. Delayed touchscreen learning in *Cdkl5* knockin mice. (A,B) *Cdkl5*$^{R59X-/+}$ females and *Cdkl5*$^{R59X-/y}$ males took significantly longer to reach a criterion of completing at least 30 trials with 80% or higher accuracy on two consecutive days compared to sex-matched wildtype littermates. (C,D) The percentage of mice that reached criterion was significantly higher in sex-matched wildtype controls than *Cdkl5*$^{R59X-/+}$ females and *Cdkl5*$^{R59X-/y}$ males suggesting a delayed rate of learning. (E,F) *Cdkl5*$^{R59X-/+}$ females and *Cdkl5*$^{R59X-/y}$ males had fewer trials per session. (G,H) *Cdkl5*$^{R59X-/+}$ females and *Cdkl5*$^{R59X-/y}$ males required higher correction trials to reach criterion.

Data are expressed as mean +/- S.E.M. *p<0.05, **p<0.001, ***p<0.0001 indicate when the *Cdkl5* mutant mice differ from sex-matched wildtype littermate controls.

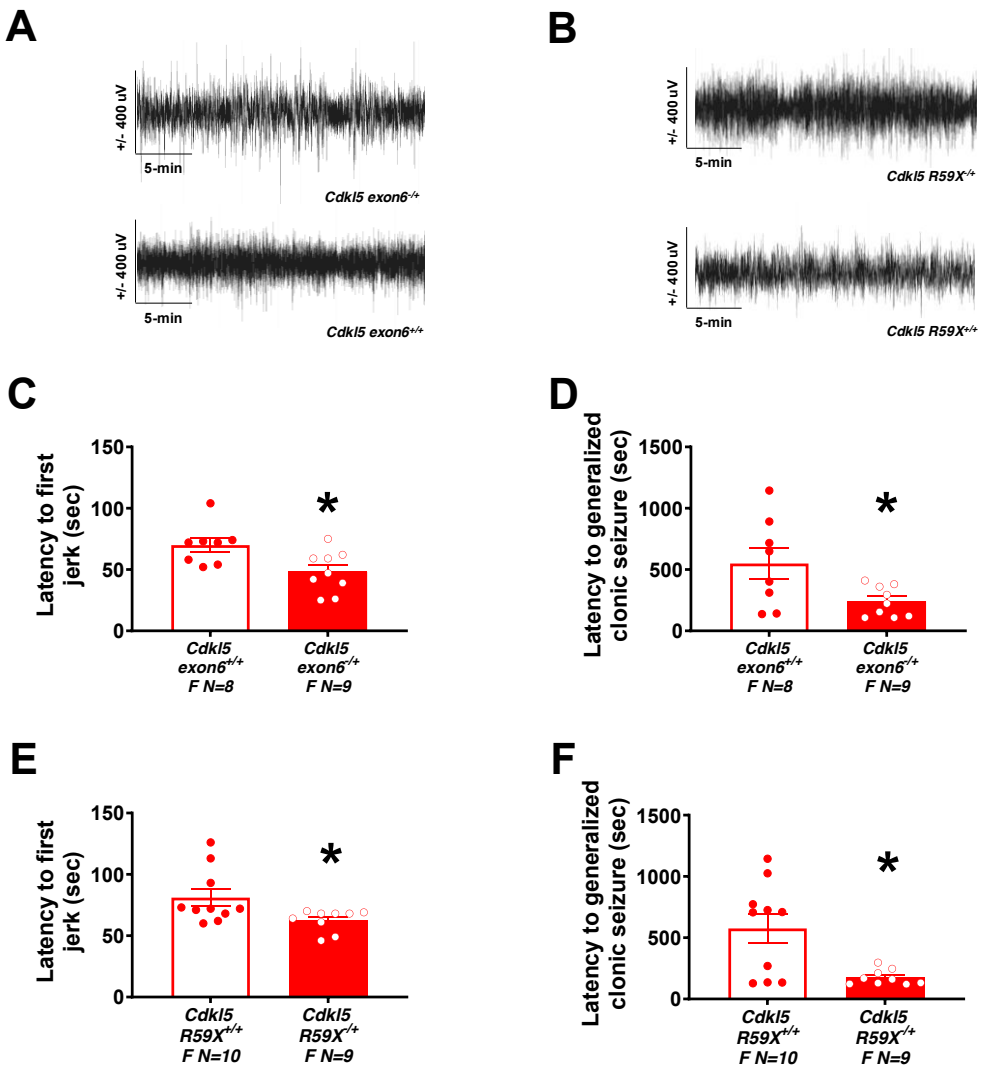

Figure 5. Increased seizure susceptibility in *Cdkl5* deletion and knockin female mice. (A) Representative EEG traces of *Cdkl5*$^{exon6-/+}$ and their wildtype littermates over 4 days of baseline recording. (B) (C,D) Reduced latencies to first jerk and generalized clonic seizures were observed in *Cdkl5*$^{exon6-/+}$ females after an i.p. injection of 80 mg/kg PTZ over the course of a 30-min trial. (E,F) Reduced latencies to first jerk and generalized clonic seizures were observed in *Cdkl5*$^{R59X-/+}$ females after an i.p. injection of 80 mg/kg PTZ over the course of a 30-min trial.

Data are expressed as mean +/- S.E.M. *p<0.05 indicates when the *Cdkl5* mutant mice differ from sex-matched wildtype littermate controls.

Additional files

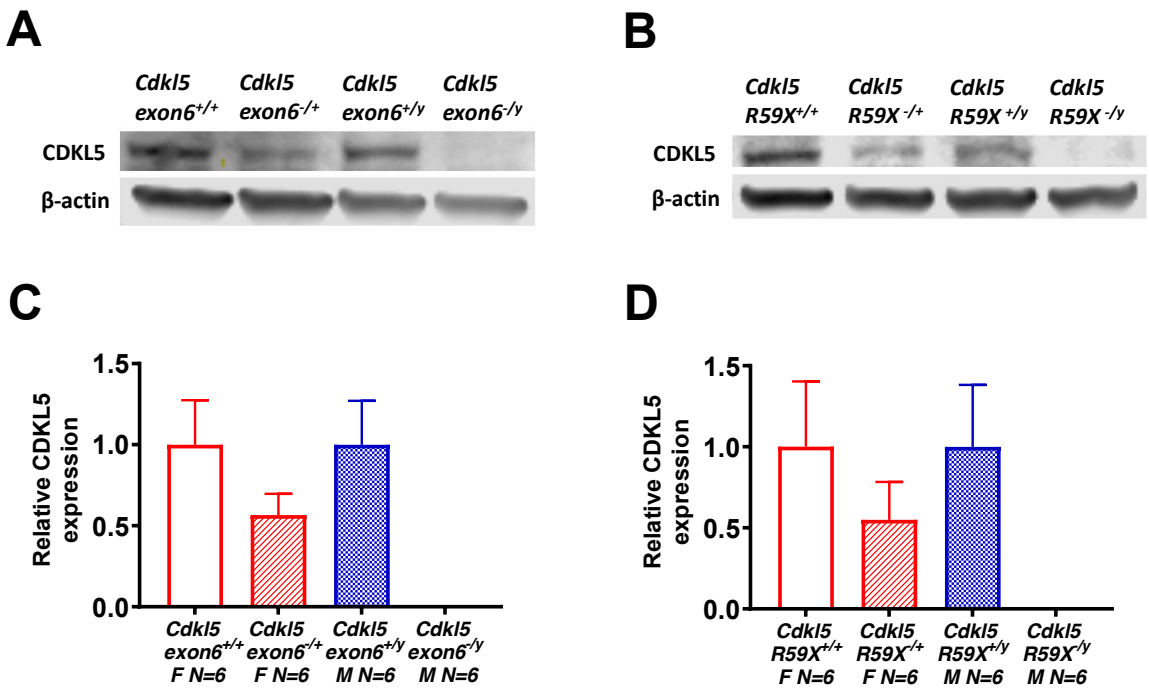

Figure S1. Validation of CDKL5 deficiency by Western Blotting. Representative images of Western blots and quantitation showing the expression of CDKL5 and beta actin in whole-brain lysates across genotypes in both mouse models. (A,C) the exon 6 deletion model, (B,D) the R59X model.

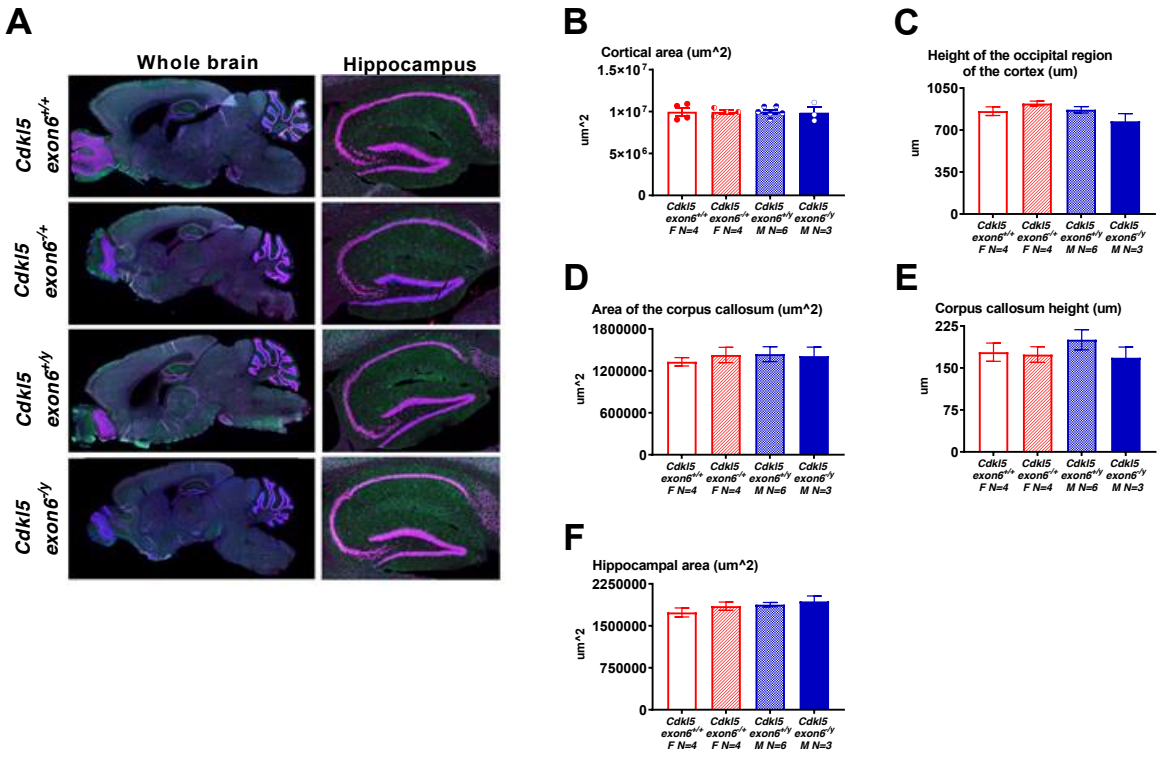

Figure S2. Volumetric analysis of critical brain regions across genotypes shows no disease phenotype in *Cdkl5* deletion mice. (A) representative images of whole-brain sagittal sections (left) and hippocampi (right) by genotype. Fluorescent immunohistochemistry was performed to differentiate neuroanatomical substructures: blue, Hoechst; green, TMEM119; red, GFAP; violet, NeuN. (B-F) comparative analyses of the area and height of various brain regions. N=3 sections per animal, 3-6 animals per genotype.

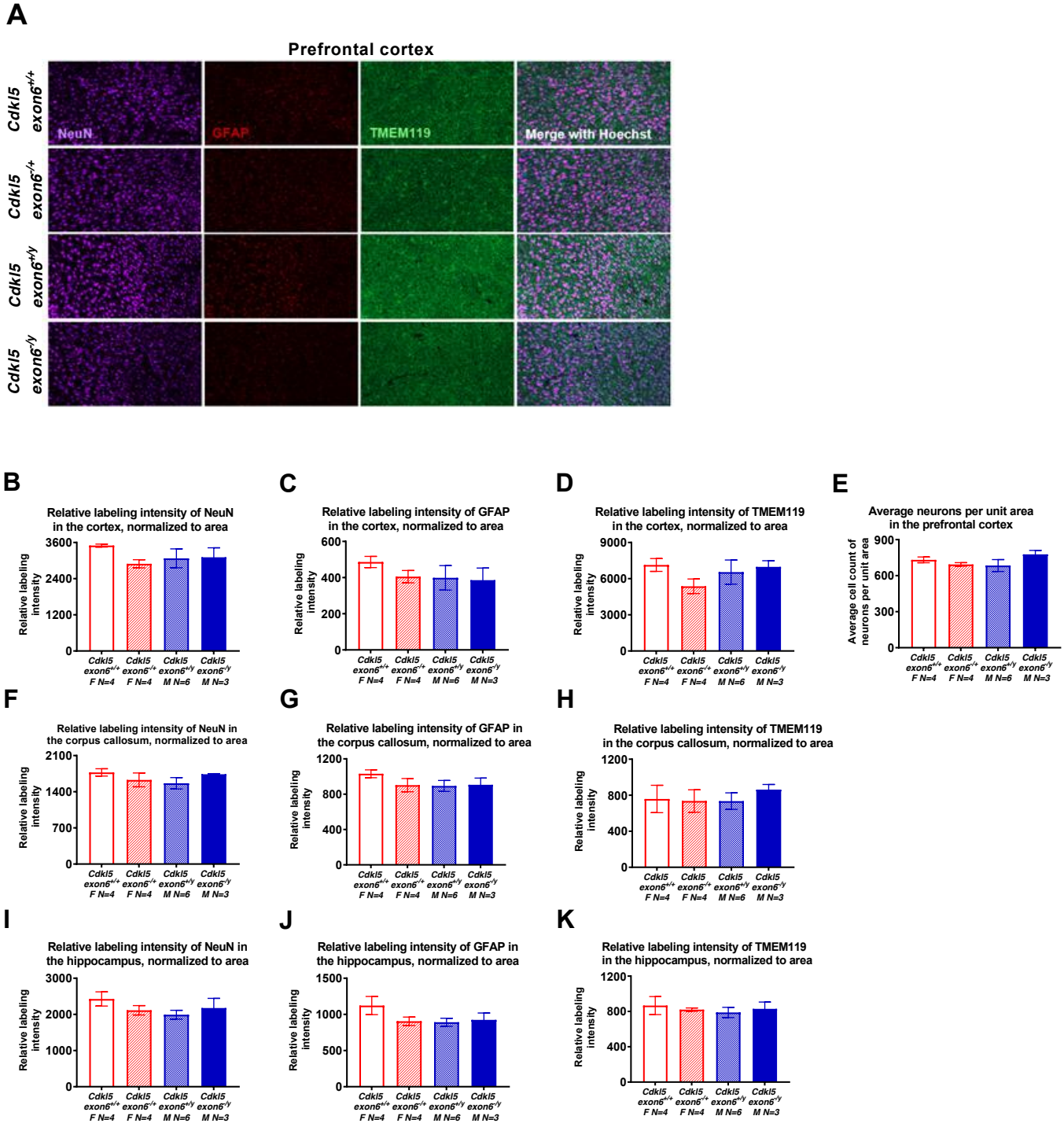

Figure S3. Quantification of protein expression analysis across genotypes shows no neuroinflammatory phenotype in *Cdkl5* deletion mice. (A) representative images of the prefrontal cortex by genotype. Fluorescent immunohistochemistry was performed for markers of neuroinflammation and to label neurons and nuclei: blue, Hoechst; green, TMEM119; red, GFAP; violet, NeuN. (B-K), comparative analyses of the relative labeling intensity of each protein via fluorescent immunohistochemistry. N=3 sections per animal, 3-6 animals per genotype.

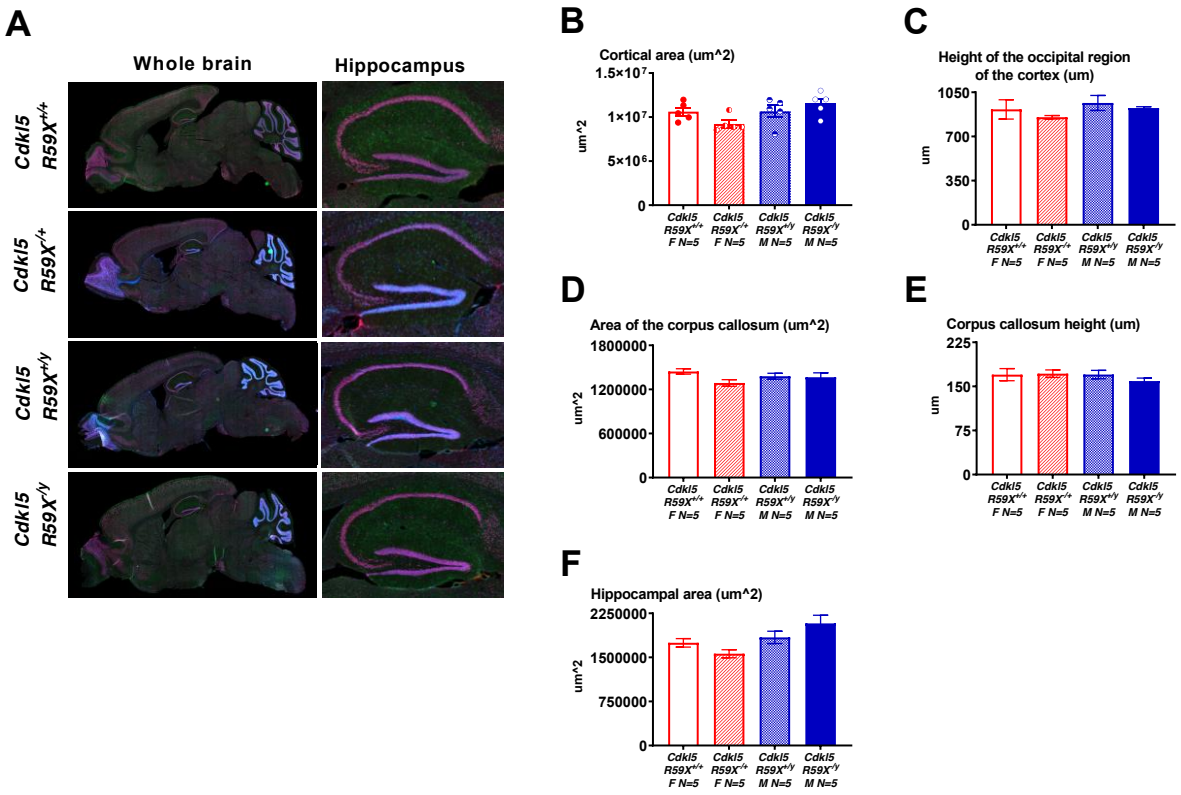

Figure S4. Volumetric analysis of critical brain regions across genotypes shows no disease phenotype in *Cdkl5* knockin mice. (A) representative images of whole-brain sagittal sections (left) and hippocampi (right) by genotype. Fluorescent immunohistochemistry was performed to differentiate neuroanatomical substructures: blue, Hoechst; green, TMEM119; red, GFAP; violet, NeuN. (B-F) comparative analyses of the area and height of various brain regions. N=3 sections per animal, 5 animals per genotype.

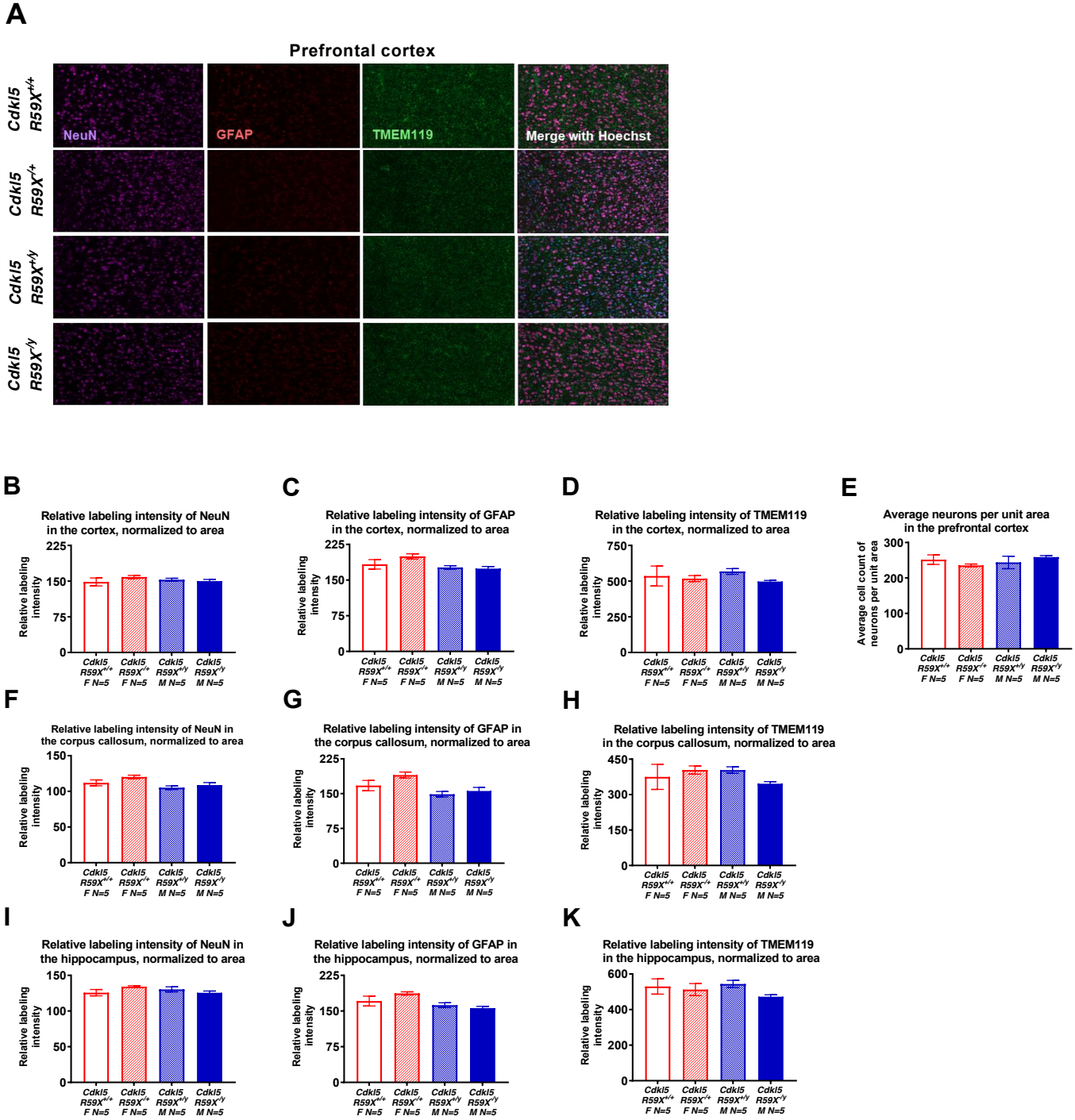

Figure S5. Quantification of protein expression analysis across genotypes shows no neuroinflammatory phenotype in *Cdkl5* knockin mice. (A) representative images of the prefrontal cortex by genotype. Fluorescent immunohistochemistry was performed for markers of neuroinflammation and to label neurons and nuclei: blue, Hoechst; green, TMEM119; red, GFAP; violet, NeuN. (B-K), comparative analyses of the relative labeling intensity of each protein via fluorescent immunohistochemistry. N=3 sections per animal, 5 animals per genotype.

Chapter 3

Cognitive deficits in the *Snord116* deletion mouse model for Prader-Willi syndrome

This chapter has been published as: Anna Adhikari, Nycole A. Copping, Beth Onaga, Michael C. Pride, Rochelle L. Coulson, Mu Yang, Dag H. Yasui, Janine M. LaSalle, Jill L. Silverman (2019). *Neurobiology of Learning and Memory.*165:106874.

Abstract

Prader-Willi syndrome (PWS) is an imprinted neurodevelopmental disease caused by a loss of paternal genes on chromosome 15q11-q13. It is characterized by cognitive impairments, developmental delay, sleep abnormalities, and hyperphagia often leading to obesity. Clinical research has shown that a lack of expression of *SNORD116,* a paternally expressed imprinted gene cluster that encodes multiple copies of a small nucleolar RNA (snoRNA) in both humans and mice, is most likely responsible for many PWS symptoms seen in humans. The majority of previous research using PWS preclinical models focused on characterization of the hyperphagic and metabolic phenotypes. However, a crucial understudied clinical phenotype is cognitive impairments and thus we investigated the learning and memory abilities using a model of PWS, with a heterozygous deletion in *Snord116*. We utilized the novel object recognition task, which doesn't require external motivation, or exhaustive swim training. Automated findings were further confirmed with manual scoring by a highly trained blinded investigator. We discovered deficits in *Snord116* +/– mutant mice in the novel object recognition, location memory and tone cue fear conditioning assays when compared to age-, sex- matched, littermate control *Snord116* +/+ mice. Further, we confirmed that despite physical neo-natal developmental delays, *Snord116* +/− mice had normal exploratory and motor abilities. These results show that the *Snord116* + /– deletion murine model is a valuable preclinical model for investigating learning and memory impairments in individuals with PWS without common confounding phenotypes.

Introduction

Prader-Willi syndrome (PWS) is a rare genetic disorder that occurs in approximately 1:15,000 live births. PWS is characterized by neonatal failure to thrive, developmental delay, lack of satiety cues, lack of control of food intake and metabolic abnormalities that lead to obesity. In addition to obesity, PWS affected individuals usually exhibit low to moderate intellectual disability and issues with numerous tasks related to executive function (e.g., response inhibition, set-shifting and planning) (Dykens, Hodapp, Walsh, & Nash, 1992a, 1992b; Dykens, Leckman, & Cassidy, 1996; Dykens et al., 2017; Dykens and Shah, 2003; Martin et al., 1998; Schwartz et al., 2016).

Due to the imprinted status of the 15q11-q13 locus, allele-specific mutations lead to the development of two distinct neurodevelopmental disorders. PWS results from genetic mutations leading to deficient gene expression from the paternal allele of chromosome 15 (15q11-q13), while Angelman Syndrome (AS) results from mutations inherited from the maternal allele of the same locus, emphasizing a critical neurological function of these genes (Jiang, Tsai, Bressler, & Beaudet, 1998). Numerous mutant mouse models were generated by targeting different portions of the orthologous mouse region. The first model deleted the entire PWS/AS locus, similar to the vast majority of PWS and/or AS patients (Gabriel et al., 1999; Stefan, Portis, Longnecker, & Nicholls, 2005). Follow-up model systems highlighted the PWS imprinting center and informed the essential nature of the epigenetic processes (Yang et al., 1998). Several smaller deletion and single gene mutant model systems have been created to delineate the contribution of each gene in the region to aspects of the PWS phenotype. These include models deleting exons in the small nuclear ribonucleoprotein polypeptide N (*Snrpn*), an RNA-protein complex that forms an RNA spliceosome (Bressler et al., 2001; Dubose, Smith, Yang, Johnstone, & Resnick, 2011; Tsai, Jiang, et al., 1999), necdin (*Ndn*), which can influence multiple pathways involved in neuronal survival,

differentiation and outgrowth and *Magel2,* a *Ndn* homolog that is expressed in the hypothalamus, cerebral cortex and spinal cord and key in circadian timekeeping (Kozlov et al., 2007; Lee et al., 2000).

While many genes are likely involved in the entire complicated PWS phenotype (including developmental failure to thrive, metabolic anomalies, obesity, cognitive deficits, obsessive-compulsive behaviors, and other psychiatric co-morbidities), analyses of rare PWS patients have determined that a ~ 200 kb deletion of a cluster of small nucleolar/noncoding RNAs (snoRNAs) within this locus is sufficient to cause PWS (Bieth et al., 2015; de Smith et al., 2009; Duker et al., 2010; Sahoo et al., 2008). Thus, investigation into the loss of this particular group of snoRNA genes, known as the *Snord116* cluster, as contributing factors is an essential step toward elucidating the neurobiology of the PWS phenotype.

Ding et al. (2008) derived a novel mouse model for PWS by deleting the paternal copies of *Snord116.* Mice with paternally inherited *Snord116* +/− deletions had growth delays in the first three postnatal weeks, hyperphagia, prolonged mealtime and increased circulating ghrelin but normal pain sensitivity, motor abilities and working memory measured by the spontaneous alternation task (Ding et al., 2008). Lassi, Maggi, et al. (2016) observed significant changes in working-for-food behavioral responses at various timescales in a home cage behavioral system in *Snord116* +/− mice (Lassi, Maggi, et al., 2016). It is unknown how or if the missing *Snord116* cluster contributes to other components of the intellectual disability behavioral diagnosis in clinical populations since the overwhelming majority of previous research using PWS preclinical models focused on characterization of the hyperphagic and metabolic phenotypes. The following report carefully investigated learning and memory abilities in the heterozygous deletion *Snord116* +/− model of PWS. We discovered that *Snord116* +/− mice exhibited learning

and memory impairments compared to their wildtype littermates on the low stress-standard assays of novel object recognition (NOR) and object location memory (OLM). Second, we illustrated data that were quantified with reasonable signal to noise ratio by automated tracking software, and confirmed and fine-tuned by human manual scoring. We also discovered that the *Snord116* +/− group showed deficits in cued but not contextual fear conditioning. Finally, we confirmed our results were not confounded by physical or motor dysfunction.

Materials and methods

Subjects

All animals were housed in a temperature-controlled vivarium maintained on a 12:12 light-dark cycle. All procedures were approved by the Institutional Animal Care and Use Committee at the University of California Davis and were conducted in accordance with the National Institutes of Health Guide for the Care and Use of Laboratory Animals. B6(Cg)-Snord116^{tm11Uta}/J *(Snord116* +/–) mice were obtained from The Jackson Laboratory (Bar Harbor, ME, USA) and fed a standard diet of Teklad global 18% protein rodent diets 2918 (Envigo, Hayward, CA, USA). Heterozygous deletion male mice were bred with C57BL/6J females to generate paternal deletion *Snord116* +/− and wildtype (*Snord116* +/+) littermates. To identify mice, pups were labelled by paw tattoo over postnatal days (PND) 2–4 using non-toxic animal tattoo ink (Ketchum Manufacturing Inc., Brockville, ON, Canada). Tails of pups were clipped (1–2 mm) for genotyping, following the UC Davis IACUC policy regarding tissue collection. Genotyping was performed with REDExtract-N-Amp (Sigma Aldrich, St. Louis, MO, USA) using primers oIMR7958 AAT CCC CAA CCT ACT TCA AAC AGT C, oIMR7959 TGG ATC TCT CCT TGC TTG TTT TCT C, and oIMR7960 TTT ACG GTA CAT GAC AGC ACT CAA G.

Behavioral assays

Order of behavioral testing and description of cohorts.

To determine if findings were robust and reproducible 2 cohorts were used for the novel object recognition assessment. The second cohort was also used to assess developmental milestones at PND10, 12 and 14, elevated plus maze, light ↔ dark conflict, open field behavior, balance beam walking, object location memory and fear conditioning. To minimize the carry-over effects from repeated testing, assays were performed in the order of least to the most stressful tasks. Cohort 1 was sampled from 7 litters and was tested in novel object recognition (NOR). Cohort 2 was sampled from 6 litters and was tested in elevated plus-maze, light ↔ dark, open field, beam walking, NOR, object location memory (OLM), and context and cued fear conditioning. All male and female mice were used from every litter. In cohort 1, the order and age of testing was as follows: (1) NOR at 7 weeks of age. In cohort 2, the order of testing was as follows with at least 48-hrs separating tasks: (1) PND 10, 12, 14 developmental milestones, (2) elevated plus-maze at 6 weeks of age, (3) light ↔ dark exploration task at 6 weeks of age, (4) open field locomotion at 7 weeks of age, (5) balance beam walking at 8 weeks of age, (6) NOR at 8 weeks of age, (7) OLM at 10 weeks of age, and (8) fear conditioning at 12 weeks of age. All behavioral assays in all cohorts were performed between 9 am-4 pm PST (ZT2-ZT9).

Developmental milestones

Developmental milestones were measured on postnatal days (PND) 10, 12 and 14, similar to those previously described (Fox, 1965; Vogel Ciernia et al., 2017; Yang et al., 2012). All measures were conducted by an experimenter blind to genotype. Body weight, length (nose to edge of tail), and head width were measured using a scale (grams) and a digital caliper (cm). Cliff avoidance was

tested by placing each pup near the edge of a cardboard box, gently nudging it towards the edge, and measuring the time for it to turn and back away from the edge. Failures to avoid the cliff was recorded as a maximum score of 30-s. Righting reflex was tested by placing each pup on its back, releasing it, and measuring the time for it to fully flip over onto four paws on each developmental day. Negative geotaxis was tested by placing each pup, facing downwards, on a screen angled at 45° from parallel, and measuring the time for it to completely turn and to climb to the top of the screen. Failures to turn and climb were recorded as a maximum score of 30-s. Circle transverse was tested by placing each pup in the center of a circle with a 5″ (12.5 cm) diameter drawn on a laminated sheet of 8.5″ × 11″ white paper, and measuring the time for it to exit the circle. Failures to exit the circle were recorded as a maximum score of 30-s.

Novel object recognition (NOR)

The NOR test was conducted in opaque matte white (P95 White, Tap Plastics, Sacramento, CA) open field arenas (41 cm × 41 cm × 30 cm), using methods similar to those previously described (Copping, Christian, et al., 2017; Gompers et al., 2017). The experiment consisted of four sessions: a 30-min exposure to the open field arena the day before the test, a 10-min re-habituation on test day, a 10-min familiarization session and a 5-min recognition test. On day 1, each subject was habituated to a clean, empty open field arena for 30-min. 24-hr later, each subject was returned to the open field arena for another 10- min for the habituation phase. The mouse was then removed from the open field and placed in a clean temporary holding cage for approximately 2-min. Two identical objects were placed in the arena. Each subject was returned to the open field in which it had been habituated and allowed to freely explore for 10-min. After the familiarization session, subjects were returned to their holding cages, which were transferred from the testing room to a nearby holding area. The open field was cleaned with 70% ethanol and let dry. One clean familiar

object and one clean novel object were placed in the arena, where the two identical objects had been located during in the familiarization phase. 60-min after the end of the familiarization session, each subject was returned to its open field for a 5-min recognition test, during which time it was allowed to freely explore the familiar object and the novel object. The familiarization session and the recognition test were recorded and scored with Ethovision XT videotracking software (Version 9.0, Noldus Information Technologies, Leesburg, VA). Object investigation was defined as time spent sniffing the object when the nose was oriented toward the object and the nose–object distance was 2-cm or less. Recognition memory was defined as spending significantly more time sniffing the novel object compared to the familiar object via a Student's paired *t*-test. Total time spent sniffing both objects was used as a measure of general exploration. Time spent sniffing two identical objects during the familiarization phase confirmed the lack of an innate side bias. Objects used were plastic toys: a small soft plastic orange safety cone and a hard plastic magnetic cone with ribbed sides, as previously described (Gompers et al., 2017; Gulinello et al., 2018).

Open field locomotion

General exploratory locomotion in a novel open field environment was assayed in an arena sized 40 cm × 40 cm × 30.5 cm, as previously described (Copping, Berg, et al., 2017; Copping, Christian, et al., 2017; Gompers et al., 2017). Open field activity was considered an essential control for effects on physical activity, for example, sedation or hyperactivity which could confound the interpretation of result of interaction with objects, arena and object exploration, and sniffing and investigation times. The testing room was illuminated at ~ 40 lx.

Beam walking

A beam walking motor task was conducted as previously described, with some modifications as outlined (Carter et al., 2001, chap. 8; Vogel Ciernia et al., 2017). 59 cm long round rods were suspended 68 cm above a cushioned landing pad. A goal box at the end of the beam consisted of a 12 cm diameter cylinder to provide motivation to cross the beam. Each mouse was placed at one end of the beam and the time to cross to the goal box on the other end was measured. Testing sequence moved from largest diameter to smallest diameter rods in order of increased difficulty. On the day prior to testing, all animals were given two practice trials on the largest diameter round beam in order to become accustom to the procedure. On the test day, each animal was sequentially tested on three round rods (35, 18 and 13 mm). Testing sequence was based on presentations of decreasing diameter to present increasing levels of difficulty. Each mouse was given two trials on each beam, separated by approximately 30 min. The time to transverse the beam was recorded and averaged across the two trials for each beam. A maximum time of 60 s was assigned to individuals that failed to cross the beam in that duration. In the small number of cases where mice fell from the beam, a score of 60-s was assigned.

Elevated plus-maze

The assay was performed using a mouse EPM (model ENV-560A) purchased from Med Associates (St. Albans, VT) and performed as previously described (Copping, Christian, et al., 2017; Flannery et al., 2015). The EPM contained two open arms (35.5 cm × 6 cm) and two closed arms (35.5 cm × 6 cm) radiating from a central area (6 cm × 6 cm). The maze was cleaned with 70% ethanol before the beginning of the first test session and after each subject mouse was tested with sufficient time for the ethanol odor to dissipate before the start of the next test session. Room illumination was ~ 30 lx.

Light ↔ dark conflict

The light ↔ dark assay was performed in accordance with previously described procedures (Copping, Christian, et al., 2017; Flannery et al., 2015). The test began by placing the mouse in the light side (~ 320 lx; 28 cm × 27.5 cm × 27 cm) of an automated 2-chambered apparatus, in which the enclosed/dark side (~5lx; 28 cm × 27.5 cm × 19 cm) was reached by traversing the small opening of the partition between the two chambers. The mouse was allowed to explore freely for 10-min. Time in the dark side chamber and total number of transitions between the light and dark side chambers were automatically recorded during the 10-min session using Labview 8.5.1 software (National Instruments, Austin, TX).

Contextual and cued fear conditioning

Delay contextual and cued fear conditioning was conducted using an automated fear-conditioning chamber (Med Associates, St Albans, VT, USA). The conditioning chamber was interfaced to a PC installed with VideoFreeze software (version 1.12.0.0, Med Associates) and enclosed in a sound-attenuating cubicle. Training consisted of a 2-min acclimation period followed by three tone-shock (CS–US) pairings (80 dB tone, duration 30-s; 0.5 mA footshock, duration 1 s; intershock interval 90-s) and a 2.5-min period, during which no stimuli were presented. The environment was well lit (~ 100 lx), with a stainless steel grid floor and swabbed with almond odor cue (prepared from almond extract; McCormick; 1:100 dilution). A 5-min test of contextual fear conditioning was performed 24-hr after training, in the absence of the tone and footshock, but in the presence of 100 lx overhead lighting, almond odor and chamber cues identical to those used on the training day. Cued fear conditioning, conducted 48-hr after training, was assessed in a novel environment with distinct visual, tactile and orange olfactory cues. Overhead lighting was turned off. The cued test consisted of a 3-min acclimation period followed by a 3-min presentation of the

tone CS and a 90-s exploration period. Cumulative time spent freezing in each condition was quantified by VideoFreeze software (Med Associates).

Statistical analysis

Data were analyzed with Statistica software (Tulsa, OK, USA) and Graphpad Prism. Statistical testing was performed using established assay-specific methods, including Student's *t*-test for single parameter comparisons between genotypes, and one-way or two-way repeated-measures ANOVA for comparisons across time points (e.g., development, pre- and post- fear conditioning, open field and beam walking). All significance levels were set at $p < 0.05$ and all *t*-tests were two-tailed. Groups sizes were chosen based on past experience and power analyses (Sukoff Rizzo and Silverman, 2016). Significant ANOVAs were followed by Bonferroni-Dunn posthoc testing. Behavioral analysis passed distribution normality tests, was collected using continuous variables and thus was analyzed via parametric analysis in all assays. For all behavioral analyses, variances were similar between groups and data points within 2 standard deviations of the mean were included in analysis.

Results

Snord116+/− mice were delayed in their early physical development and neurological reflexes. Table 1 shows delayed early physical development and neurological reflexes in various parameters in *Snord116 +/−* compared to *Snord116 +/+* littermates. All subjects gained weight and grew in length over time (weight: $F_{2,50} = 120.7$, $p < 0.0001$ and length: $F_{2,50} = 67.51$, $p < 0.0001$). However, *Snord116 +/−* mice weighed less at all three time points collected ($F_{1,25} = 26.55$, $p < 0.0001$, Bonferroni-Dunn posthoc) and were shorter by total length (body plus tail) at PND 12 and 14 ($F_{1,25} = 13.84$, $p < 0.002$, Bonferroni-Dunn posthoc). *Snord116 +/−* mice also had smaller head widths at all three time points ($F_{1,25} = 13.84$, $p < 0.001$, Bonferroni-Dunn posthoc). Reflexes including negative geotaxis ($F_{1,25} = 0.074$, $p > 0.05$), cliff aversion ($F_{125} = 0.19$, $p > 0.05$) and the righting reflex ($F_{1,25} = 1.196$, $p > 0.05$) did not differ between genotypes. Onset of ability to walk developed over time by traversing out of the center of a circle ($F_{2,50} = 49.68$, $p < 0.0001$). *Snord116 +/−* mice had longer times to traverse out of the center of a circle at PND12 ($F_{1,25} = 12.61$, $p < 0.002$, Bonferroni-Dunn posthoc).

Snord116+/− mice exhibit impaired novel object recognition. Cognitive abilities as measured by the NOR task were tested in two independent cohorts of *Snord116+/−* compared to *Snord116 +/+* mice. In Cohort 1, manual scoring by a highly trained observer blinded to genotype indicated *Snord116 +/+* spent more time investigating the novel object versus the familiar object, as expected. In contrast, *Snord116 +/−* mice did not exhibit typical novel object preference (**Fig. 1A**: *Snord116 +/+ ;* $t_{(19)} = 4.59$, $p < 0.002$ and *Snord116+/−;* $t_{(13)} = 1.58$, $p > 0.05$). In this cohort, using manual scores, both genotypes explored the two identical objects similarly during the familiarization phase (**Fig. 1B**: *Snord116+/+ ;* $t_{(19)} = 0.43$, $p > 0.05$ and *Snord116 +/–*; $t_{(13)} = 0.845$, $p > 0.05$). Sexes were combined since there was no sex difference observed on time spent

sniffing objects in the novel phase of the test by automated and manual scoring methods in two cohorts (cohort 1 auto: $F(1, 50) = 0.000$, $p > 0.05$; cohort 1 manual: $F_{(1,50)} = 0.567$, $p > 0.05$; cohort 2 auto: $F_{(1,50)} = 0.064$, $p > 0.05$; cohort 2 manual: $F_{(1,50)} = 0.003$, $p > 0.05$), consistent with other NOR literature (Gulinello et al., 2018). *Snord116 +/+* also displayed normal NOR when quantified by automated tracking software, spending more time in the defined zone with the novel object than in the zone surrounding the familiar object, whereas *Snord116 +/−* mice did not exhibit typical novel object preference (**Fig. 1C**: *Snord116 +/+ ;* $t_{(18)} = 2.08$, $p = 0.065$ and *Snord116 +/–*; $t_{(13)} = 0.52$, $p > 0.05$). Both genotypes explored the two identical objects similarly during the automated familiarization phase (**Fig. 1D**: *Snord116+/+ ;* $t_{(19)} = 0.43$, $p > 0.05$ and *Snord116 +/–* ; $t_{(13)} = 0.845$, $p > 0.05$). In automated analysis of the novel phase, data from one *Snord116+/+* mouse was removed because of a loss of tracking data.

In Cohort 2, manual and automated scoring indicated *Snord116+/+*spent more time investigating the novel object versus the familiar object whereas *Snord116+/−* mice did not exhibit typical novel object preference (**Fig. 1E**: *Snord116 +/+ ;* $t_{(10)} = 3.16$, $p < 0.02$ and *Snord116 +/–*; $t_{(15)} = 1.74$, $p > 0.05$ and **Fig. 1G**: *Snord116 +/+ ;* $t_{(10)} = 2.186$, $p < 0.05$ and *Snord116 +/–*; $t_{(15)} = 1.034$, $p > 0.05$). Once again, manual and automated scoring illustrated that both genotypes explored the two identical objects similarly during the familiarization phase that tested for side bias and object salience (**Fig. 1F**: *Snord116 +/+ ;* $t_{(10)} = 0.439$, $p > 0.05$ and *Snord116 +/− ;* $t_{(15)} = 0.324$, $p > 0.05$ and **Fig. 1H**: *Snord116 +/+ ;* $t_{(10)} = 0.203$, $p > 0.05$ and *Snord116+/− ;* $t_{(14)} = 0.007$, $p > 0.05$). During automated analysis of side bias, data from one *Snord116+/−* mouse was removed because of loss of video tracking data. These results indicated that the NOR deficit in *Snord116 +/−* mice is replicable in different cohorts with

differing laboratory personnel and when scored either from videos by human observer or by automated video tracking methods.

Snord116+/- mice exhibit impaired object location memory. OLM was defined as spending significantly more time sniffing the relocated object than sniffing the object in the original location. Manual scoring of object investigation by sniffing indicated *Snord116*+/+ spent more time investigating an object displaced to a novel location versus the familiar location whereas *Snord116*+/– mice did not exhibit this location memory (**Fig. 2A**: *Snord116*+/+ ;$t_{(10)}$ = 2.254, $p < 0.05$ and *Snord116* +/– ;$t_{(15)} = 0.203$, $p > 0.05$). Automated video tracking corroborated the manual methods confirming that *Snord116* +/+ spent more time investigating an object displaced to a novel location versus the familiar location whereas *Snord116*+/– mice did not exhibit this location memory (**Fig. 2B**: *Snord116* +/+ ; $t_{(10)} = 4.169$, $p < 0.02$ and *Snord116*+/– ;$t_{(15)} = 1.654$, $p > 0.05$). Sexes were combined since there was no sex difference observed on time spent sniffing objects in the novel phase of the test by automated and manual scoring methods (auto: $F(1, 50) = 2.211$, $p > 0.05$; manual: $F(1, 50) = 1.175$, $p > 0.05$).

Snord116+/- mice have deficits in tone cued fear conditioning. Learning and memory was further evaluated using two measures of Pavlovian fear conditioning with a 24-hr contextual component and a tone cued fear conditioning. High levels of freezing were observed, subsequent to the conditioned stimulus (CS) – unconditioned stimulus (UCS) pairings, on the training day, in both genotypes (**Fig. 3A**: main effect of training, $F_{(1, 25)} = 31.62$, $p < 0.0001$; no genotype difference in training freeze scores $F_{(1, 25)} = 0.919$, $p > 0.05$), indicating no confounds and no deficits in the learning of the associations between the context stimuli and tone cues. No genotype difference was observed 24-hrs following CS-UCS training between *Snord116* +/– and *Snord116* +/+ freezing (**Fig. 3B**: $t_{(25)} = 0.176$, $p > 0.05$), when placed in the context chamber from

conditioning training with identical stimulus cues. No sex difference was observed in context freezing ($F_{(1, 50)} = 0.671$, $p > 0.05$).

Levels of freezing, between the pre- and post-cue presentation 48-hrs after training, revealed significant main effects of cued training (main effect of cue, $F_{(1, 25)} = 75.86$, $p < 0.001$). *Snord116 +/–* froze less than *Snord116 +/+* when the tone was presented in the novel contextual arena (**Fig. 3C**: $t_{(25)} = 2.49$, $p < 0.0199$). No sex difference was observed in pre or post cue freezing (pre cued: $F_{(1, 50)} = 3.228$, $p > 0.05$ and post-cued: $F_{(1, 50)} = 0.387$, $p > 0.05$).

Snord116+/- mice have normal motor abilities in open field locomotion and balance beam walking. Normal motor function in *Snord116 +/−* mice was confirmed by lack of genotype effect in the open field exploratory locomotion task across a 30-min session. The time course for total distance traversed in the novel open field, was significant, representing normal habituation to the novelty of the open field **(Fig. 4A**: $F_{(5,125)} = 63.81$, $p < 0.0001$). No sex difference was observed in activity metrics ($F_{(1, 50)} = 0.649$, $p > 0.05$). No genotype effects were observed in total distances traversed (**Fig. 4A**; $F_{(1, 25)} = 0.187$, $p > 0.05$), horizontal activity scores (**Fig. 4B**: $F_{(1, 25)} = 2.479$, $p > 0.05$), vertical activity counts (**Fig. 4C**: $F_{(1, 25)} = 1.094$, $p > 0.05$), nor time spent in the center of the arena (**Fig. 4D**: $F_{(1, 25)} = 0.0439$, $p > 0.05$) between *Snord116+/− and Snord116 +/+* mice. No genotype effect was observed when the activity over the 30-min session was summed (**Fig. 4E**: $t_{(25)} = 0.433$, $p > 0.05$). Both groups showed longer latencies to cross the rod shaped beams as they became thinner and more difficult to traverse, as expected across the task (**Fig. 4F**: $F_{(2, 50)} = 35.98$, $p < 0.0001$). No genotype effects were observed in time to traverse any of the various widths of beams $F_{(1, 25)} = 0.342$, $p > 0.05$). Sexes were combined since there was no sex difference observed on time to cross the beams ($F_{(1, 50)} = 2.53$, $p > 0.05$).

Snord116+/-- mice showed inconsistent and/or mild anxiety-like phenotypes. Anxiety-like behavior was assessed with the elevated plus-maze and the light ↔ dark conflict assay. As compared to *Snord116 +/+* , *Snord116 +/−* mice spent less time on the open arm of the maze (**Fig. 5A**: $t_{(25)} = 3.056$, $p < 0.006$). *Snord116 +/−* also made fewer total arm entries calculated by open arm entries + closed arm entries (**Fig. 5B**: $t_{(25)} = 2.142$, $p > 0.05$), suggesting less overall navigational motion during this short task in the mutants. No sex differences were observed in the percent time spent on the open arm ($F_{(1,50)} = 2.8733$, $p > 0.05$), or the total entries ($F_{(1>50)} = 1.50$, $p > 0.05$). In the light« dark conflict assay, no genotype effects were observed on the amount of time spent in the dark chamber (**Fig. 5C**: $t_{(25)} = 0.124$, $p > 0.05$) nor the number of transitions between chambers (**Fig. 5D**: $t_{(25)} = 0.948$, $p > 0.05$), suggesting that anxiety-like phenotypes are either subtle or absent in our examination. No sex differences were observed in the parameters of light↔dark conflict ($F_{(1,50)} = 1.75$, $p > 0.05$), or the total transitions ($F(1,50) = 2.55$, $p > 0.05$).

Discussion

Basic research to discover highly specific intervention targets requires well-controlled *in vivo* studies in model organisms with high construct validity. PWS arises by paternal 15q11–13 deletions, maternal uniparental disomy, or imprinting errors which lead to aberrant methylation and downregulation of paternally expressed transcripts. Genetic mapping data from unique "microdeletion" patients suggest *SNORD116,* is a critical mediator of the neurodevelopmental phenotypes. Therefore, we evaluated a mouse model of paternally inherited *Snord116* deletion on physical characteristics and functional outcome measures. For the first time, we reliably identified the clinically relevant phenotype of cognitive deficits due to the loss of *Snord116* using several standard behavioral metrics of learning and memory. Further, we corroborated earlier reports of postnatal failure to thrive. Our data highlight a functional cognitive contribution of this critical

snoRNA complex and suggest a broader role for *Snord116/SNORD116,* beyond known cellular processes.

We discovered that *Snord116* +/− mice exhibited robust learning and memory impairments in the low stress standard assay of NOR using optimized methods of our laboratory and the MIND Institute's Intellectual and Developmental Disabilities Research Center (IDDRC) Rodent Behavioral Core, recently highlighted as a collaborative effort by numerous prominent neuroscientists (Gulinello et al., 2018). The outcome parameter of time spent in zone of close proximity using Noldus 9.0XT automated tracking software was corroborated by an expert technician blinded to genotype that scored time spent sniffing the objects manually. Both methods produced quantifiable data with reasonable signal to noise ratio. However, we discovered that only manual observation was able to eliminate misdetections in the automated tracking such as subjects knocking over objects, subjects sitting on objects, subjects grooming next to objects, and/or when the nose and tail detection indicator points switch amongst one another.

Our study also discovered deficits of the *Snord116*+/− mutants in learning and memory by OLM on which rodents are presented with two identical, familiar objects, one of which is in its previous location while the other is in a new location. Rodents spend more time exploring the object in the novel location (Ennaceur & Meliani, 1992). The NOR and OLM impairments were detected in the typical short-term range by a 1-hr time interval between familiarization and testing. This window is thought to occur within the consolidation phase of memory formation and may not be dependent on protein synthesis. *Snord116*+/− mutants showed impairments in cued but not contextual fear conditioning. The cued conditioning deficits but intact responses in context learning and memory were detected 48-hr post-training and therefore were transcriptionally and translationally dependent learning and memory as previously shown by this Pavlovian paradigm

(Schafe and LeDoux, 2000; Schafe et al., 2000), and as further suggested by studies performed using a latent inhibition cued conditioning protocol (Lewis & Gould, 2007). Our detection of impairments in the short and longer term intervals implicate the multiple biochemical mechanisms that underlie learning and memory.

These cognitive behavioral deficiencies are intriguing and lend suggestions toward the role of the well-studied underlying neural circuitry. OLM and NOR both heavily rely on the spontaneous exploratory behavior of rodents towards objects (Bevins and Besheer, 2006; Ennaceur and Delacour, 1988; Vogel-Ciernia and Wood, 2014). Broadly, neuroanatomical substrates implicated in these functional outcomes include the hippocampus and its supporting limbic regions, such as the medial prefrontal, anterior cingulate, and retrosplenial cortices. In fact, an array of lesions in limbic sites connected with the hippocampus did not disrupt performance on a 15-min retention test of NOR while similar studies in OLM revealed impairments from lesions of the fornix and the cingulate cortex but not the medial prefrontal cortex (Ennaceur, Neave, & Aggleton, 1997). The amygdala is important for associating objects or spatial relationships with positive or aversive outcomes and appears to mediate fear responses to novel stimuli or neophobia (Ennaceur, Michalikova, & Chazot, 2009). For example, rodents with amygdala lesions show attenuated neophobia for novel food (Burns, Annett, Kelley, Everitt, & Robbins, 1996). Moreover, a rich literature of lesion work indicated that specific but different brain regions appear to regulate cued versus contextual fear conditioning. Although the responses of behavioral freezing elicited by contextual and cued fear conditioning are identical, the processing demands underlying the two forms of fear conditioning are different. The preponderance of the evidence supports the hypothesis that primary sensory information from the auditory thalamus into the lateral amygdala mediate cued fear conditioning (Phillips and LeDoux, 1992; Schafe and LeDoux, 2000) while

contextual fear conditioning require both the amygdala and the hippocampus (Phillips and LeDoux, 1995; Maren and Holt, 2000). Given our reported impairments in *Snord116*+/− mice using novelty-based tasks and cued fear conditioning, we hypothesize a broad range of neural substrates underlying the dysfunction. A study by Lassi, Priano et al. (2016)also supports our suggestion of subcortical and limbic anomalies with evidence of morphological changes measured by structal MRI. Moreover, they discovered a major reduction in the size of the hippocampus in *Snord116* +/− mice and PWS patients (Lassi, Priano, et al., 2016).

We corroborated the previously reported physical neo-natal developmental delays in weight and growth in *Snord116* +/− (Ding et al., 2008; Powell et al., 2013). We extended these phenotypic outcomes by also quantifying smaller body lengths and smaller head circumferences. Development of walking measured by the animals' skills to traverse outward of a circle disk was delayed in the *Snord116* +/− mice. Interestingly, other standard neonatal neurological reflexes such as negative geotaxis, righting reflex and cliff aversion remained intact. We confirmed that the cognitive deficits observed in *Snord116* +/− mice were not the result of confounding motor hypo activity, despite the substantial growth delays in the first 2 weeks of postnatal life. In extension of earlier work, we also examined anxiety-related phenotypes. Earlier characterization studies had reported an increased anxiety-like phenotype measured by increased ratio of time spent in the closed arm by the *Snord116* +/− mice (Ding et al., 2008). We corroborated this finding by the standard measure of anxiety-like behavior on the plus- maze of percent time spent on the open arm. While a mild anxiety-like phenotype was observed on the elevated plus-maze, it was not supported by data from the light-dark conflict task nor the center time in the open field, which suggested to us a very mild anxiety-like phenotype which probably did not confound learning and memory results.

Earlier research using the same *Snord116 +/−* mutation mice reported disrupted circadian rhythms, sleep-wake cycles, frontal cortical transcriptional and epigenetic regulation, as well as reduced forebrain neuronal and cerebellar cellular sizes, which could mechanistically contribute to the behavioral phenotypes reported (Burnett et al., 2017; Coulson et al., 2018; Lassi, Priano, et al., 2016). Other *in vivo* model systems of PWS deleted the entire critical imprinting center and reported low locomotor abilities and impairments in the frontal cortical dependent five choice serial reaction time task (Relkovic et al., 2010). Given the number of genes in the critical imprinting region, other models were generated that focused on mutations of single paternally expressed genes. Necdin *(Ndn)* null mutants were the first to be generated and characterized since Necdin protein is postulated to govern the permanent arrest of cell growth of post-mitotic neurons during development. *Ndn* mutant mouse models were generated from multiple laboratories and displayed highly variable functional phenotypes, that ranged from no abnormality to respiratory distress and lethality, depending on the background strain of mouse (Gerard, Hernandez, Wevrick, & Stewart, 1999; Kuwako et al., 2005; Muscatelli et al., 2000; Tsai, Armstrong, et al., 1999). The other gene in the region that is highly homologous to *Ndn,*paternally expressed and has multiple key cell cycle regulatory functions is *Magel2*. *Magel2* mutant mice have disrupted circadian rhythm and reduced brain volumes however relatively normal motor and learning abilities (Fountain, Tao, Chen, Yin, & Schaaf, 2017; Kozlov et al., 2007; Mercer et al., 2009) in contrast to the learning and memory deficits reported herein.

Conclusion

Prader-Willi syndrome (PWS) is a complex neurodevelopmental disease caused by a loss of imprinted paternal genes on chromosome 15q11-q13 and is characterized by cognitive impairments, developmental delay, hyperphagia, and obesity. The majority of previous research

using PWS preclinical models focused on characterization of the hyperphagic and metabolic phenotypes. This work reports the clinically relevant phenotype of cognitive impairments on three different learning and memory behavioral assays in the *Snord116*+/− model of PWS. These deficits in the *Snord116* +/− mouse model highlight the critical role of *Snord116* +/− in PWS and extend validity of the model as a valuable preclinical tool for investigating learning and memory impairments in PWS.

References

1. Bevins RA, & Besheer J (2006). Object recognition in rats and mice: A one-trial non-matching-to-sample learning task to study 'recognition memory'. *Nature Protocols*, 1, 1306–1311.

2. Bieth E, Eddiry S, Gaston V, Lorenzini F, Buffet A, Conte Auriol F, … Tauber M (2015). Highly restricted deletion of the SNORD116 region is implicated in Prader- Willi syndrome. *European Journal of Human Genetics: EJHG*, 23, 252–255.

3. Bressler J, Tsai TF, Wu MY, Tsai SF, Ramirez MA, Armstrong D, & Beaudet AL (2001). The SNRPN promoter is not required for genomic imprinting of the Prader- Willi/Angelman domain in mice. *Nature Genetics*, 28, 232–240.

4. Burnett LC, Hubner G, LeDuc CA, Morabito MV, Carli JFM, & Leibel RL (2017). Loss of the imprinted, non-coding Snord116 gene cluster in the interval deleted in the Prader Willi syndrome results in murine neuronal and endocrine pancreatic developmental phenotypes. *Human Molecular Genetics*, 26, 4606–4616.

5. Burns LH, Annett L, Kelley AE, Everitt BJ, & Robbins TW (1996). Effects of lesions to amygdala, ventral subiculum, medial prefrontal cortex, and nucleus accumbens on the reaction to novelty: Implication for limbic-striatal interactions. *Behavioral Neuroscience*, 110, 60–73.

6. Carter RJ, Morton J, & Dunnett SB (2001). Motor coordination and balance in rodents. *Current Protocols in Neuroscience*, 8–12.

7. Copping NA, Berg EL, Foley GM, Schaffler MD, Onaga BL, Buscher N, … Yang M (2017). Touchscreen learning deficits and normal social approach behavior in the Shank3B model of Phelan-McDermid Syndrome and autism. *Neuroscience*, 345, 155–165.

8. Copping NA, Christian SGB, Ritter DJ, Islam MS, Buscher N, Zolkowska D,… Dindot SV (2017). Neuronal overexpression of Ube3a isoform 2 causes behavioral impairments and neuroanatomical pathology relevant to 15q11.2-q13.3 duplication syndrome. *Human Molecular Genetics*, 26, 3995–4010.

9. Coulson R, Yasui D, Dunaway K, Laufer B, Vogel-Ciernia A, Mordaunt C, … LaSalle J (2018). Snord116-dependent diurnal rhythm of DNA methylation in mouse cortex. *Nature Communications*, 9(1), 1616 10.1101/184788.
10. de Smith AJ, Purmann C, Walters RG, Ellis RJ, Holder SE, Van Haelst MM, … Blakemore AI (2009). A deletion of the HBII-85 class of small nucleolar RNAs (snoRNAs) is associated with hyperphagia, obesity and hypogonadism. *Human Molecular Genetics*.

11. Ding F, Li HH, Zhang S, Solomon NM, Camper SA, Cohen P, & Francke U (2008). SnoRNA Snord116 (Pwcr1/MBII-85) deletion causes growth deficiency and hyperphagia in mice. *PloS One*, 3, e1709.

12. Dubose AJ, Smith EY, Yang TP, Johnstone KA, & Resnick JL (2011). A new deletion refines the boundaries of the murine Prader-Willi syndrome imprinting center. *Human Molecular Genetics*, 20, 3461–3466.

13. Duker AL, Ballif BC, Bawle EV, Person RE, Mahadevan S, Alliman S, … Sahoo T (2010). Paternally inherited microdeletion at 15q11.2 confirms a significant role for the SNORD116 C/D box snoRNA cluster in Prader-Willi syndrome. *European Journal of Human Genetics*, 18(11), 1196–1201. 10.1038/ejhg.2010.102.

14. Dykens EM, Hodapp RM, Walsh K, & Nash LJ (1992a). Adaptive and maladaptive behavior in Prader-Willi syndrome. *Journal of the American Academy of Child & Adolescent Psychiatry*, 31, 1131–1136.

15. Dykens EM, Hodapp RM, Walsh K, & Nash LJ (1992b). Profiles, correlates, and trajectories of intelligence in Prader-Willi syndrome. *Journal of the American Academy of Child & Adolescent Psychiatry*, 31, 1125–1130.

16. Dykens EM, Leckman JF, & Cassidy SB (1996). Obsessions and compulsions in Prader-Willi syndrome. *Journal of Child Psychology and Psychiatry*, 37, 995–1002.

17. Dykens EM, Roof E, Hunt-Hawkins H, Dankner N, Lee EB, Shivers CM, … Kim SJ (2017). Diagnoses and characteristics of autism spectrum disorders in children with Prader-Willi syndrome. *J Neurodev Disord*, 9, 18.

18. Dykens E, & Shah B (2003). Psychiatric disorders in Prader-Willi syndrome: Epidemiology and management. *CNS Drugs*, 17, 167–178.

19. Ennaceur A, & Delacour J (1988). A new one-trial test for neurobiological studies of memory in rats. 1: Behavioral data. *Behavioural Brain Research*, 31, 47–59.

20. Ennaceur A, & Meliani K (1992). A new one-trial test for neurobiological studies of memory in rats. III. Spatial vs. non-spatial working memory. *Behavioural Brain Research*, 51(1), 83–92.

21. Ennaceur A, Michalikova S, & Chazot PL (2009). Do rats really express neophobia towards novel objects? Experimental evidence from exposure to novelty and to an object recognition task in an open space and an enclosed space. *Behavioural Brain Research*, 197, 417–434.

22. Ennaceur A, Neave N, & Aggleton JP (1997). Spontaneous object recognition and object location memory in rats: The effects of lesions in the cingulate cortices, the medial prefrontal cortex, the cingulum bundle and the fornix. *Experimental Brain Research*, 113, 509–519.

23. Flannery BM, Silverman JL, Bruun DA, Puhger KR, McCoy MR, Hammock BD, Lein PJ (2015). Behavioral assessment of NIH Swiss mice acutely intoxicated with tetramethylenedisulfotetramine. *Neurotoxicology and Teratology*, 47, 36–45.

24. Fountain MD, Tao H, Chen CA, Yin J, & Schaaf CP (2017). Magel2 knockout mice manifest altered social phenotypes and a deficit in preference for social novelty. *Genes, Brain and Behavior*, 16, 592–600.

25. Fox WM (1965). Reflex-ontogeny and behavioural development of the mouse. *Animal Behaviour*, 13, 234–241.

26. Gabriel JM, Merchant M, Ohta T, Ji Y, Caldwell RG, Ramsey MJ, … Nicholls RD (1999). A transgene insertion creating a heritable chromosome deletion mouse model of Prader-Willi and angelman syndromes. *Proceedings of the National Academy of Sciences of the United States of America*, 96, 9258–9263.
27. Gerard M, Hernandez L, Wevrick R, & Stewart CL (1999). Disruption of the mouse necdin gene results in early post-natal lethality. *Nature Genetics*, 23, 199–202.

28. Gompers AL, Su-Feher L, Ellegood J, Copping NA, Riyadh MA, Stradleigh TW, … Zdilar, I. (2017). Germline Chd8 haploinsufficiency alters brain development in mouse. *Nature Neuroscience*, 20, 1062–1073.

29. Gulinello M, Mitchell HA, Chang Q, Timothy O'Brien W, Zhou Z, Abel T, … Crawley JN (2018). Rigor and reproducibility in rodent behavioral research. *Neurobiology of Learning and Memory*.

30. Jiang Y, Tsai TF, Bressler J, & Beaudet AL (1998). Imprinting in Angelman and Prader-Willi syndromes. *Current Opinion in Genetics & Development*, 8, 334–342.

31. Kozlov SV, Bogenpohl JW, Howell MP, Wevrick R, Panda S, Hogenesch JB, … Stewart CL (2007). The imprinted gene Magel2 regulates normal circadian output. *Nature Genetics*, 39, 1266–1272.

32. Kuwako K, Hosokawa A, Nishimura I, Uetsuki T, Yamada M, Nada S, … Yoshikawa K (2005). Disruption of the paternal necdin gene diminishes TrkA signaling for sensory neuron survival. *The Journal of Neuroscience: The Official Journal of the Society for Neuroscience*, 25, 7090–7099.

33. Lassi G, Maggi S, Balzani E, Cosentini I, Garcia-Garcia C, & Tucci V (2016). Working-for-food behaviors: a preclinical study in Prader-Willi Mutant mice. *Genetics*, 204, 1129–1138.

34. Lassi G, Priano L, Maggi S, Garcia-Garcia C, Balzani E, El-Assawy N, … Tucci V (2016). Deletion of the Snord116/SNORD116 alters sleep in mice and patients with Prader-Willi Syndrome. *Sleep*, 39, 637–644.

35. Lee S, Kozlov S, Hernandez L, Chamberlain SJ, Brannan CI, Stewart CL, & Wevrick R (2000). Expression and imprinting of MAGEL2 suggest a role in Prader- willi syndrome and the homologous murine imprinting phenotype. *Human Molecular Genetics*, 9, 1813–1819.

36. Lewis MC, & Gould TJ (2007). Signal transduction mechanisms within the entorhinal cortex that support latent inhibition of cued fear conditioning. *Neurobiology of Learning and Memory*, 88(3), 359–368.

37. Maren S, & Holt W (2000). The hippocampus and contextual memory retrieval in Pavlovian conditioning. *Behavioural Brain Research*, 110, 97–108.

38. Martin A, State M, Koenig K, Schultz R, Dykens EM, Cassidy SB, & Leckman JF (1998). Prader-Willi syndrome. *American Journal of Psychiatry*, 155, 1265–1273.

39. Mercer RE, Kwolek EM, Bischof JM, van Eede M, Henkelman RM, & Wevrick R (2009). Regionally reduced brain volume, altered serotonin neurochemistry, and abnormal behavior in mice null for the circadian rhythm output gene Magel2. *American Journal of Medical Genetics Part B: Neuropsychiatric Genetics*, 150B, 1085–1099.

40. Muscatelli F, Abrous DN, Massacrier A, Boccaccio I, Le Moal M, Cau P, & Cremer H (2000). Disruption of the mouse Necdin gene results in hypothalamic and behavioral alterations reminiscent of the human Prader-Willi syndrome. *Human Molecular Genetics*, 9, 3101–3110.

41. Phillips RG, & LeDoux JE (1992). Differential contribution of amygdala and hippocampus to cued and contextual fear conditioning. *Behavioral Neuroscience*, 106, 274–285.

42. Phillips RG, & LeDoux JE (1995). Lesions of the fornix but not the entorhinal or perirhinal cortex interfere with contextual fear conditioning. *The Journal of Neuroscience: The Official Journal of the Society for Neuroscience*, 15, 5308–5315.

43. Powell WT, Coulson RL, Crary FK, Wong SS, Ach RA, Tsang P, … Lasalle JM (2013). A Prader-Willi locus lncRNA cloud modulates diurnal genes and energy expenditure. *Human Molecular Genetics*, 22, 4318–4328.

44. Relkovic D, Doe CM, Humby T, Johnstone KA, Resnick JL, Holland AJ, … Isles AR (2010). Behavioural and cognitive abnormalities in an imprinting centre deletion mouse model for Prader-Willi syndrome. *European Journal of Neuroscience*, 31, 156–164.

45. Sahoo T, del Gaudio D, German JR, Shinawi M, Peters SU, Person RE, … Beaudet AL (2008). Prader-Willi phenotype caused by paternal deficiency for the HBII-85 C/D box small nucleolar RNA cluster. *Nature Genetics*, 40, 719–721.

46. Schafe GE, Atkins CM, Swank MW, Bauer EP, Sweatt JD, & LeDoux JE (2000). Activation of ERK/MAP kinase in the amygdala is required for memory consolidation of pavlovian fear conditioning. *The Journal of Neuroscience: The Official Journal of the Society for Neuroscience*, 20, 8177–8187.

47. Schafe GE, & LeDoux JE (2000). Memory consolidation of auditory pavlovian fear conditioning requires protein synthesis and protein kinase A in the amygdala. *The Journal of Neuroscience: The Official Journal of the Society for Neuroscience*, 20, RC96.

48. Schwartz L, Holland A, Dykens E, Strong T, Roof E, & Bohonowych J (2016). Prader-Willi syndrome mental health research strategy workshop proceedings: The state of the science and future directions. *Orphanet Journal of Rare Diseases*, 11, 131.

49. Stefan M, Portis T, Longnecker R, & Nicholls RD (2005). A nonimprinted Prader-Willi Syndrome (PWS)-region gene regulates a different chromosomal domain in trans but the imprinted pws loci do not alter genome-wide mRNA levels. *Genomics*, 85, 630–640.

50. Sukoff Rizzo SJ, & Silverman JL (2016). Methodological considerations for optimizing and validating behavioral assays. *Current Protocols in Mouse Biology*, 6, 364–379.

51. Tsai TF, Armstrong D, & Beaudet AL (1999). Necdin-deficient mice do not show lethality or the obesity and infertility of Prader-Willi syndrome. *Nature Genetics*, 22, 15–16.

52. Tsai TF, Jiang YH, Bressler J, Armstrong D, & Beaudet AL (1999). Paternal deletion from Snrpn to Ube3a in the mouse causes hypotonia, growth retardation and partial lethality and provides evidence for a gene contributing to Prader-Willi syndrome. *Human Molecular Genetics*, 8, 1357–1364.

53. Vogel Ciernia A, Pride MC, Durbin-Johnson B, Noronha A, Chang A, Yasui DH, … LaSalle JM (2017). Early motor phenotype detection in a female mouse model of Rett syndrome is improved by cross-fostering. *Human Molecular Genetics*, 26, 1839–1854.

54. Vogel-Ciernia A, & Wood MA (2014). Examining object location and object recognition memory in mice. *Current Protocols in Neuroscience*, 69, 8–31.

55. Yang T, Adamson TE, Resnick JL, Leff S, Wevrick R, Francke U, … Brannan CI (1998). A mouse model for Prader-Willi syndrome imprinting-centre mutations. *Nature Genetics*, 19, 25–31.

56. Yang M, Bozdagi O, Scattoni ML, Wohr M, Roullet FI, Katz AM, … Crawley JN (2012). Reduced excitatory neurotransmission and mild autism-relevant phenotypes in adolescent Shank3 null mutant mice. *The Journal of Neuroscience: The Official Journal of the Society for Neuroscience*, 32, 6525–6541.

57. Yang M, Lewis FC, Sarvi MS, Foley GM, & Crawley JN (2015). 16p11.2 Deletion mice display cognitive deficits in touchscreen learning and novelty recognition tasks. *Learning & Memory*, 22, 622–632.

Tables

Milestones	Domain	Genotype	PND 10 Mean ± SE	PND 12 Mean ± SE	PND 14 Mean ± SE	F value	Significance @ $p < 0.05$
Weight (g)	Physical	*Snord116* +/+	5.845 ± 0.106	6.818 ± 0.364	8.073 ± 0.177	F(1,25) = 26.55	Yes, $p < 0.0001$
		Snord116 +/−	4.525 ± 0.205	5.281 ± 0.257	5.869 ± 0.256		
Length (mm)	Physical	*Snord116* +/+	69.027 ± 0.800	75.318 ± 2.186	81.618 ± 1.002	F(1,25) = 13.84	Yes, $p < 0.001$
		Snord116 +/−	65.063 ± 0.830	70.938 ± 1.142	75.581 ± 1.065		
Head width	Physical	*Snord116* +/+	11.491 ± 0.249	11.973 ± 0.288	12.318 ± 0.172	F(1,25) = 27.63	Yes, $p < 0.0001$
		Snord116 +/−	10.619 ± 0.232	10.706 ± 0.198	11.206 ± 0.166		
Circle transverse	Reflex	*Snord116* +/+	22.805 ± 3.096	15.791 ± 2.442	4.436 ± 1.127	F(1,25)= 12.61	Yes, $p < 0.002$
		Snord116 +/−	27.918 ± 1.313	22.751 ± 1.703	6.643 ± 1.612		
Negative geotaxis	Reflex	*Snord116* +/+	14.264 ± 3.785	6.972 ± 2.368	3.195 ± 0.690	F(1,25) = 0.074	NS, $p > 0.05$
		Snord116 +/−	14.201 ± 2.456	8.561 ± 1.713	3.095 ± 0.639		
Righting reflex	Reflex	*Snord116* +/+	9.257 ± 7.776	0.605 ± 0.073	0.607 ± 0.060	F(1,25) = 1.20	NS, $p > 0.05$
		Snord116 + /–	1.769 ± 0.177	0.939 ± 0.091	0.749 ± 0.061		
Cliff aversion	Reflex	*Snord116* +/+	4.735 ± 2.555	1.950 ± 0.685	0.499 ± 0.073	F(1,25) = 0.20	NS, $p > 0.05$
		Snord116 +/−	3.017 ± 0.884	2.617 ± 0.969	0.429 ± 0.029		

Table 1. Physical characteristics, milestone development and neurological reflexes at postnatal days 10, 12 and 14 in *Snord116* +/+ and *Snord116* +/- mice.

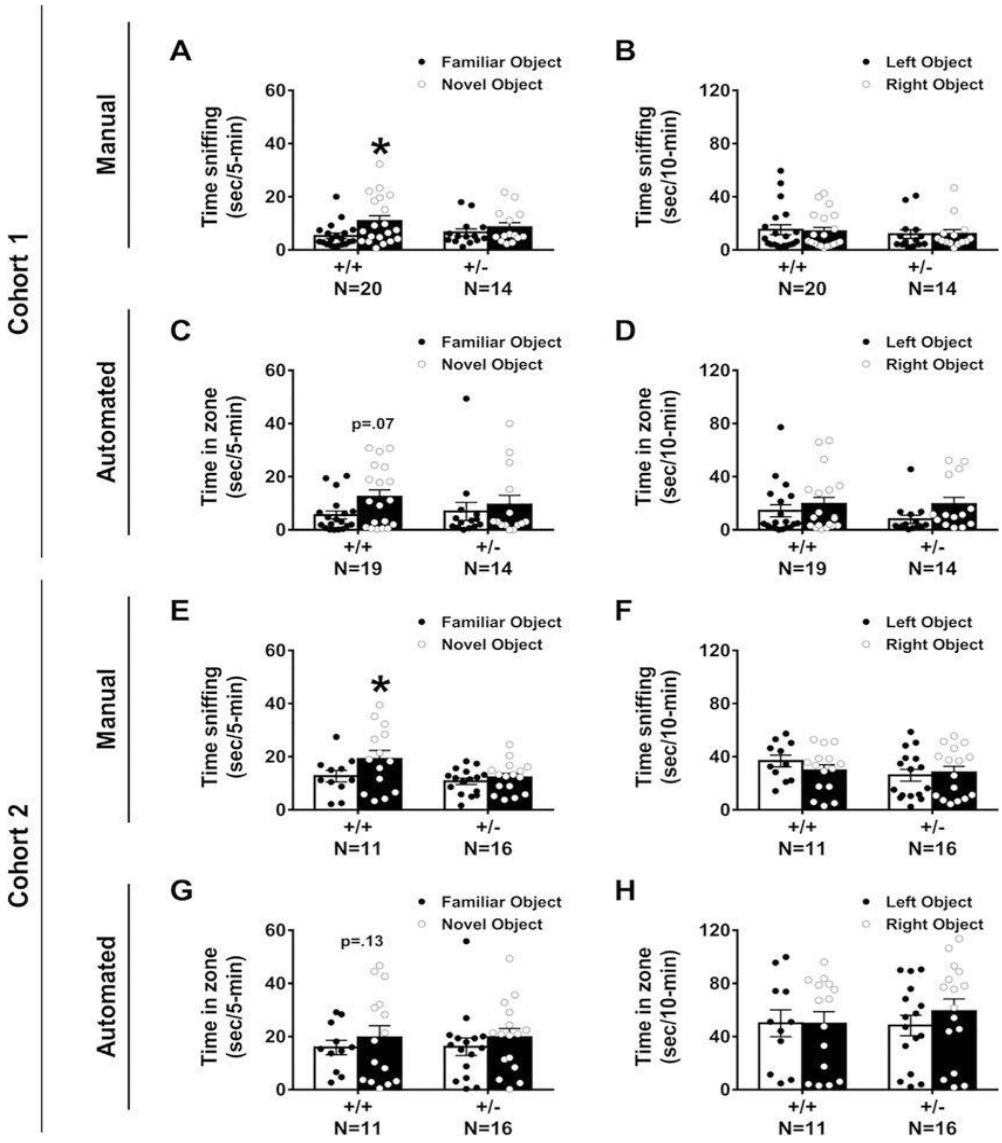

Fig 1. *Snord116* +/– displayed robust impairments on the novel object recognition (NOR) assay in two independent cohorts by manual and automated quantification measures. This version of NOR started with animal habituation to the open field testing arena for 30-min. After 24-hr, the mouse received another 10-min habituation session. Next, the subjects were given a 10-min familiarization session during which time spent sniffing each object was recorded. The objects were then cleaned and after a 1-hr inter-trial interval, the mouse was placed back into the arena with one familiar object and one novel object. (A) *Snord116* +/– mice do not spend more time sniffing the novel object as compared to the familiar object. *Snord116* +/+ litter- mates spend more time sniffing the novel object as compared to familiar object. (B) During the familiarization phase, manual scoring of objects revealed no left-right side bias in either *Snord116* + /+ or *Snord116* +/–. (C) Automated scoring via Noldus Ethovision 9.0XT illustrated *Snord116* +/– mice do not spend more time in the zone defined around the novel object versus the zone defined around the familiar object, while *Snord116* +/+ exhibit this typical object preference (p = 0.07) during the 5-min testing phase. (D) Similar to manual data, in the familiarization phase, automated tracings

confirmed the absence of a left-right side bias in *Snord116* +/+ and *Snord116* +/– mice. (E) Manual scoring of the 5-min testing phase in Cohort 2 confirmed that *Snord116* +/– mice do not spend more time sniffing the novel object as compared to the familiar object. Once again, *Snord116* +/+ littermates spend more time sniffing the novel object when compared to familiar object. (F) Reproducing Cohort 1, during the familiarization phase, manual scoring of objects revealed no left-right side bias in *Snord116*+/+ and *Snord116* +/–. (G) Similar to manual data and Cohort 1, automated scoring via Noldus Ethovision 9.0XT illustrated *Snord116* + /– mice do not spend more time in the zone defined around the novel object versus the zone defined around the familiar object, while *Snord116* +/+ exhibited a trend to toward novel object preference ($p = 0.13$) during the 5-min testing phase. (H) In the familiarization phase, automated tracings repeatedly confirmed the absence of a left-right side bias in either *Snord116* +/+ or *Snord116* +/– mice. *$p < 0.05$, novel object versus familiar object, paired t-test within genotype.

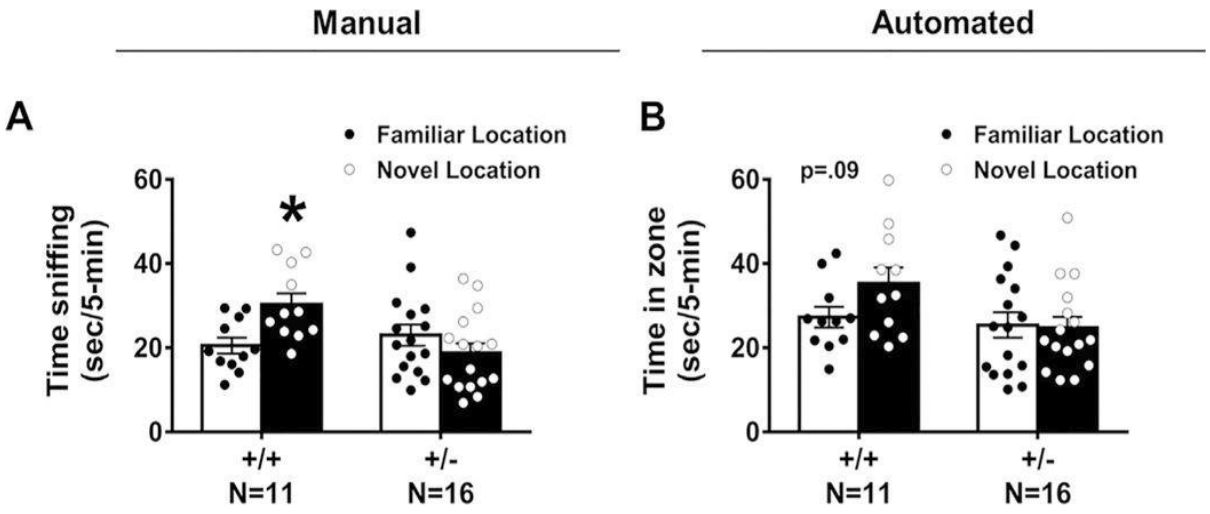

Fig 2. *Snord116* +/− displayed impairments on the object location memory (OLM) task by manual and automated quantification measures. This version of the OLM used the same apparatus that was used for testing NOR and used the same habituation and familiarization procedures. However, the subject was exposed to different objects. Two identical objects were placed 12-cm away from the wall and 18-cm from each other) for a 10-min familiarization session. (A) *Snord116* +/− mice do not spend more time sniffing the displaced object in the new location as compared to the object in the original location. *Snord116* +/+ littermates spend more time sniffing the displaced object in the new location when compared to familiar location. (B) Automated scoring via Noldus Ethovision 9.0XT illustrated *Snord116* +/− mice do not spend more time in the zone defined around the displaced object versus the zone defined around the familiar location, while *Snord116* +/+ exhibit this object location memory (p = 0.09) during the 5-min testing phase.

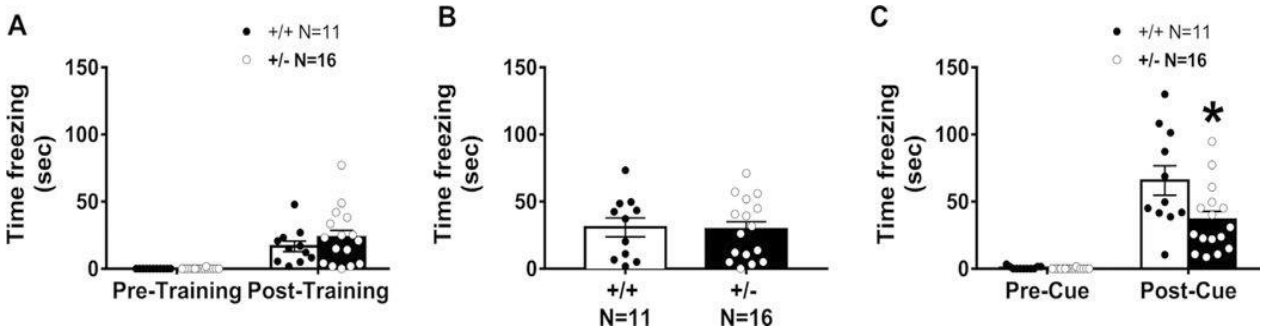

Fig 3. *Snord116* +/− displayed impairments in learning and memory in cued but not contextual fear conditioning. Learning and memory was evaluated by Pavlovian fear conditioning using two components, contextual cues and an auditory tone, with assessments of freezing time before and after the presentation of three tone-shock pairings. (A) Normal levels of freezing post-training indicate associations between tone and shock were made in all genotypes. In addition, both genotypes showed typical basal levels of freezing suggesting no confounds of deficits in sensory reactivity or pain threshold. (B) The 24-hr contextual component illustrated typical levels freezing, indicating no abnormal contextual learning and memory in either *Snord116* + /+ or *Snord116* +/− mice. (C) Cued conditioning freeze time 48-hr after initial training, before and after, the presentation of three tone-cues is illustrated. *Snord116* +/− mice had lower freezing scores compared to *Snord116* +/+ following the auditory reminder tone cue. *$p < 0.05$ versus *Snord116* +/+ by student's unpaired *t*-tests.

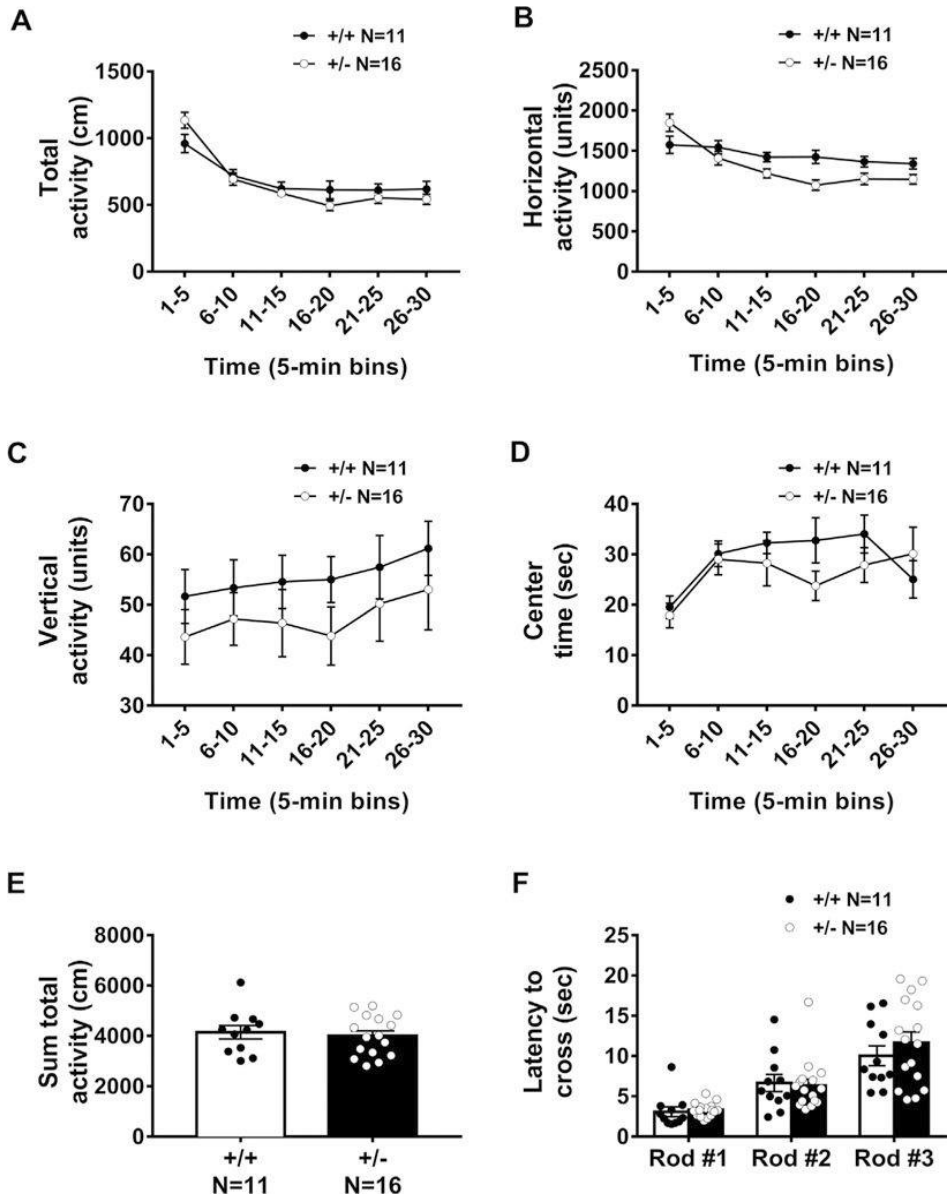

Fig 4. General motor ability and coordination in a novel open field and a balance beam assay were normal in *Snord116* +/− mice. Activity and motor abilities are essential controls because hypolocomotion could confound the interpretation of result of interaction with objects, arena and object exploration, and sniffing and investigation times. Motor abilities were measured by (A) total distance traversed, (B) horizontal activity, (C) vertical activity and (D) time spent in the center of an arena over the course of a 30-min trial. Data are shown in 5-min time bins. (E) Summed activity over the course of the 30-min session highlights similar exploratory levels in *Snord116* +/+ and *Snord116* +/− mice. (F) Both groups showed longer latencies to cross the rod-shaped beams as they became thinner and more difficult to traverse. However, no genotype effects were observed in latency to traverse any of the various widths of beams, regardless of difficulty.

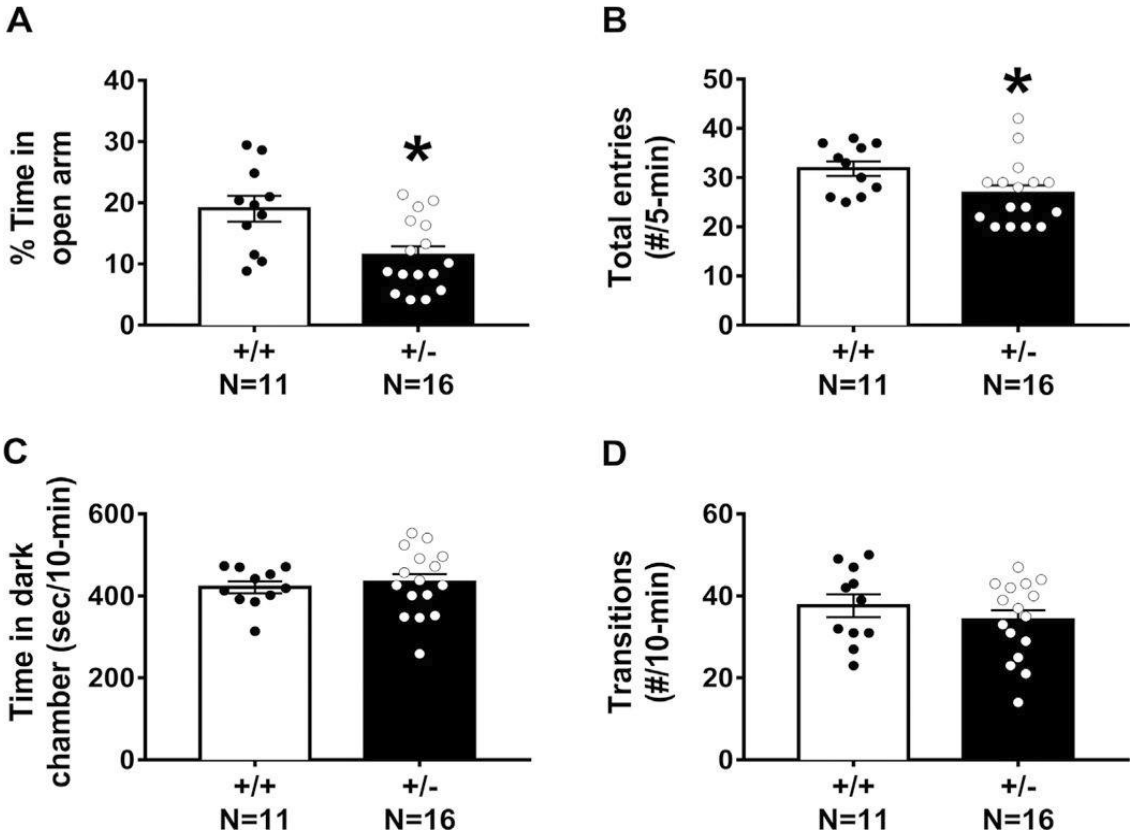

Fig 5. Anxiety-like behavioral testing illustrated inconsistent and confounded behavioral phenotypes in Snord116+/− mice. Anxiety-like behaviors were assessed in two gold standard assays: elevated plus-maze and light↔dark conflict. (A) During the elevated plus-maze, percent time spent on the open arm and (B) number of total arm entries (open+closed) were fewer in Snord116+/− mice as compared to Snord116+/ +. (C) In the light↔dark conflict assay, time spent in the dark chamber and (D) transitions between chambers did not differ between Snord116+/+ and Snord116+/− mice. *$p < 0.05$ versus Snord116+/+ by student's unpaired *t*-test.

Chapter 4

Functional rescue in an Angelman syndrome model following treatment with lentivector transduced hematopoietic stem cells

This chapter has been published as: Anna Adhikari, Nycole A. Copping, Julie Beegle, David L. Cameron, Peter Deng, Henriette O'Geen, David J. Segal, Kyle D. Fink, Jill L. Silverman, Joseph S. Anderson (2021). *Human Molecular Genetics*.30,1067-1083.

Abstract

Angelman syndrome (AS) is a rare neurodevelopmental disorder characterized by impaired communication skills, ataxia, motor and balance deficits, intellectual disabilities, and seizures. The genetic cause of AS is the neuronal loss of UBE3A expression in the brain. A novel approach, described here, is a stem cell gene therapy which uses lentivector-transduced hematopoietic stem and progenitor cells to deliver functional UBE3A to affected cells. We have demonstrated both the prevention and reversal of AS phenotypes upon transplantation and engraftment of human CD34+ cells transduced with a *Ube3a* lentivector in a novel immunodeficient $Ube3a^{mat-/pat+}$ $IL2rg^{-/y}$ mouse model of AS. A significant improvement in motor and cognitive behavioral assays as well as normalized delta power measured by electroencephalogram was observed in neonates and adults transplanted with the gene modified cells. Human hematopoietic profiles observed in the lymphoid organs by detection of human immune cells were normal. Expression of UBE3A was detected in the brains of the adult treatment group following immunohistochemical staining illustrating engraftment of the gene-modified cells expressing UBE3A in the brain. As demonstrated with our data, this stem cell gene therapy approach offers a promising treatment strategy for AS, not requiring a critical treatment window.

Introduction

Angelman syndrome (AS) is a rare neurodevelopmental disorder characterized by developmental delay, impaired communication skills, ataxia, motor and balance deficits, poor attention, intellectual disabilities, microcephaly, and seizures (1–3). The genetic cause of AS is loss of expression in the brain of UBE3A (ubiquitin-protein ligase E6-AP), due typically to a 4-Mb de novo deletion of the maternal 15q11-q13 region (4–6). Due to brain-specific imprinting, the paternal allele is silenced, thus loss of the maternal allele causes UBE3A deficiency throughout the brain (7).

Novel strategies to treat AS are critical as there is no FDA approved cure or corrective therapy available to patients. Therapies in development for genetic precision medicine for AS have resulted in: (1) silencing or cleavage of the paternal antisense transcript that stops expression of the maternal allele, (2) molecular reversal of Ube3a expression levels and (3) some degree of functional phenotypic rescue in a few but not all affected domains. These include therapies by antisense oligonucleotides (ASO), viral vector delivery and artificial transcription factors (ATFs) (8–12). In fact, two ASO compounds are in Phase I clinical trials (GeneTx NCT04259281; Roche NCT04428281**)**. These novel therapies are promising as treatment modalities for AS; however, a number of these approaches had limited functional phenotypic rescue preclinically, may have off-target genetic effects, and require repeated dosing. In addition, dietary and traditional pharmaceutical treatments have shown 'alleviation' of one or more symptom domains found in the mouse model, including but not limited to NNZ-2566, minocycline, ketone esters, dietary methylation, ErbB inhibitors and topoisomerase inhibitor drugs (13–19). However, despite various research attempts, clinical trials in AS have been limited.

A novel approach to corrective therapy being pursued by our laboratories is the use of hematopoietic stem and progenitor cells (HSPC), which offer a promising approach for life-long delivery of functional UBE3A to affected cells, i.e. neurons. This process would entail modifying autologous HSPC with a lentiviral vector expressing a modified form of UBE3A. The engrafted and genetically modified HSPC would produce cell progeny that systemically express the enzyme and provide functional UBE3A through a process called 'cross-correction' (20–22). Lentiviral vectors are highly effective in delivering transgenes to HSPC due to their ability to stably transduce both dividing and non-dividing cells (22–29). They provide long-term expression of the introduced genes due to their ability to integrate and are less prone to gene silencing or off-target effects in differentiated cells. Newly developed lentiviral vectors have undergone several refinements to increase safety and transgene expression. We chose to utilize human HSPC over mouse HSPC due to our desire to expedite into clinical translation and eliminate the need for bridging studies of mHSPC to hHSPC.

Transplantation of UBE3A-expressing HSPC has the potential to prevent, halt, or reverse symptoms associated with AS by providing UBE3A to the central nervous system from the engraftment of microglia derived from the vector transduced CD34+ cells (22,30–34). This was recently demonstrated for other metabolic diseases including metachromatic leukodystrophy, adrenoleukodystrophy and Tay-Sachs/Sandhoff disease, in which the hematopoietic system was used to deliver therapeutic levels of functional enzymes via engraftment of modified HSPC (22,30–32).

The experiments described herein took an innovative step to evaluate the concept of cross-correction for AS. First, we generated a lentiviral vector that expressed a modified form of the mouse Ube3a isoform 3 (mAS8) and confirmed its expression and functionality. In parallel, we

generated a novel immunodeficient AS mouse model Ube3a$^{mat-/pat+}$ IL2rg$^{-/y}$ that was capable of receiving human CD34+ HSPC for transplantation and engraftment followed by multi-lineage hematopoiesis throughout the hematopoietic system and also confirmed that no AS-relevant behavioral phenotypes presented in the new model, given the interleukin 2 gamma chain loss. Finally, we administered our therapeutic via HSPC transplantation in neonates and adults.

Our data illustrate robust functional prevention and rescue of AS phenotypes in both neonate and adult AS mice following treatment with human CD34+ HSPC transduced with an Ube3a-expressing lentiviral vector. This strongly suggests that cross-correction is a beneficial strategy to pursue and that this stem cell gene-therapy approach offers a potential therapeutic intervention for AS patients.

Results

Expression and functionality of the *Ube3a*-expressing lentiviral vector. A lentiviral vector backbone, CCLc-MNDU3-x, was used to develop the various constructs used in this study (**Fig. 1A**). A control EGFP-alone vector was created by inserting a PGK-EGFP expression cassette downstream from the MNDU3 promoter (**Fig. 1B**). A modified mouse Ube3a isoform 3 or a modified human Ube3a isoform 1 were inserted upstream of the PGK-EGFP expression cassette under the control of an MNDU3 promoter (**Fig. 1C and D**). To evaluate whether UBE3A was expressed from the lentiviral vector and whether it was functional at ubiquitinating a target protein, western blots and an in vitro S5A ubiquitination assay were performed, respectively. Human CD34+ cells were left non-transduced (NT) or were transduced with the EGFP control or a lentiviral vector expressing a modified form of the human Ube3a isoform 1 (hAS8) and derived into macrophages in vitro. Cell extracts were evaluated for UBE3A expression via western blot.

As displayed in **Figure 1E**, successful detection of UBE3A was observed in the cells transduced with the hAS8 lentiviral vector compared with the NT and EGFP control transduced cells. To determine whether the lentiviral vector expressed UBE3A was functional, an S5A ubiquitination assay was performed. As displayed in **Figure 1F**, ubiquitination of S5A, as determined by the banding pattern, was detected in the hAS8 lane compared with the control cell lanes which displayed no banding pattern. A similar banding pattern was observed in the positive (+) control lane.

Colony forming unit assay and the derivation of mature macrophages. To initially evaluate the safety of the Ube3a-expressing lentiviral vector after transduction of human CD34+ HSPC, a colony forming unit (CFU) assay was performed. This was performed to evaluate whether similar differentiation patterns, as demonstrated by the development of granulocyte/macrophage (GM), granulocyte/erythrocyte/megakaryocyte/macrophage (GEMM) and burst forming unit-erythroid colonies (BFU-E), were observed in all cultures. Transduced cells, either EGFP-control or hAS8 were first sorted based on EGFP expression and then cultured in methylcellulose media containing cytokines allowing for cell differentiation. As displayed in **Figure 2A**, similar GM, GEMM and BFU-E colony counts were observed in the hAS8 cultures as compared with the NT and EGFP control vector-transduced colonies. To further evaluate the differentiation potential of the hAS8 vector transduced CD34+ cells, the CFU colonies were cultured in macrophage specific media. After a 4-day incubation to allow for macrophage development, the cells were analyzed for macrophage cell-specific surface markers including CD14, CD4 and HLADR. hAS8 macrophages displayed, on average, 97.8, 97.9 and 99.2% expression of CD4, CD14 and HLADR, respectively. This compared with NT macrophages which displayed 97.6, 97.6 and 98.9% and EGFP control

macrophages, which displayed 98.2, 97.8 and 97.9% of CD4, CD14 and HLADR, respectively. Representative flow cytometry histograms are displayed in **Figure 2B.**

Generation and optimization of an immunodeficient *Ube3a*-deficient mouse model. For novel gene therapies to be translated into a clinical setting, *in vivo* studies in relevant disease-specific models evaluating the efficacy of genetically modified cells are essential. The Ube3a-deficient mouse model, which contains a deletion in exon 2 of *Ube3a* (AS mice), have been used to study AS and therapeutic interventions (**35**). Since the Ube3a gene is paternally imprinted, AS phenotypes occur only when the mutation is inherited on the maternal allele (**35**,**36**). This mouse model has pronounced behavioral phenotypes relevant to AS including robust motor deficits, cognitive impairments, seizure susceptibility, abnormal epileptiform discharges and spiking events in electroencephalogram (EEG), and a characteristic EEG signature of elevated delta spectral power (**31**,**33–35**). In order to evaluate our therapeutic candidate, human CD34+ cells transduced with a murine Ube3a lentiviral vector and an immunodeficient AS-specific model needed to be developed. We tested a suite of immunocompromised mice with various degrees of immunodeficiency for AS behavioral phenotypes and human cell engraftment. A partial degree of immunodeficiency was required to transplant human CD34+ HSPC without immune activation and rejection of these therapeutic cells to successfully reconstitute mice with human immune cells. To assess if immune deficiency, was causing deleterious behavioral deficits, we evaluated Rag2 (JAX #025730; B6.129S-Rag2^{tm1Fwa} CD47^{tm1Fpl} Il2rg^{tm1Wjl}/J), Rag1 (JAX #002216; B6.129S7-Rag1^{tm1Mom}/J) and IL2rg-null mice (JAX stock #003174; B6.129S4-IL2rg^{tm1Wjl}/J) on a battery of AS-relevant outcomes and quantified human cell engraftment, **Supplementary Material, Fig. S1A–F**, **2**. These studies revealed that the optimal immunodeficient strain to cross with Ube3a $^{mat-/pat+}$ mice were the IL2rg null mice (IL2rg$^{-/y}$),

generating a Ube3a$^{mat-/pat+}$ IL2rg$^{-/y}$ immunodeficient model for studying the in vivo efficacy of the Ube3a-expressing lentiviral vector in human CD34+ cells.

Experimental cohorts evaluating *in vivo* efficacy of the Ube3a vector transduced human CD34+ cells. Four treatment groups were analyzed for prevention or functional rescue in behavioral assays relevant to AS and reproduced rigorously in our laboratory and others (**31**,**36**,**37**). The treatment groups were: (1) WT = control wildtype that had an IL2rg null mutation (IL2rg $^{-/y}$) for appropriate control of the immune system influence and a WT (Ube3a$^{+/+}$) genotype, Ube3a$^{mat+/pat+}$ IL2rg$^{-/y}$, (2) HET = Ube3a$^{mat-/pat+}$ IL2rg$^{-/y}$, the innovative AS model with a maternal deletion of Ube3a and capable of human cell engraftment attributed to the IL2rg $^{-/y}$ null mutation, (3) NT-HET = Ube3a$^{mat-/pat+}$ IL2rg$^{-/y}$, the innovative AS model, transplanted with NT human CD34+ HSPC to control for the effect of HSPC alone and (4) Ube3a-HET = Ube3a$^{mat-/pat+}$ IL2rg$^{-/y}$ that are the novel immunodeficient AS model transplanted with Ube3a vector transduced human CD34+ HSPC.

Neonatal treatment with HSPC transduced with a *Ube3a*-expressing lentiviral vector prevented AS phenotypes in rigorous motor assessments. To evaluate whether AS phenotypes could be prevented prior to their initial onset, neonates were transplanted with the Ube3a vector transduced HSPC. Prevention of AS phenotypes in the Ube3a-HET treatment group was observed by these mice scoring indistinguishably from the WT group on multiple assays of motor deficits 8 weeks post-transplant. HET and NT-HET illustrated typical AS deficits of reduced motor activity and impaired motor coordination in four tests of motor abilities. This is the first report of significant gait impairments in an AS mouse model, although our group has previously reported this in the AS rat (**37**,**38**). Locomotion in a novel open field was collected by assessing the total

distance traversed and the horizontal movements using beam breaks in a novel arena. Group differences in horizontal activity counts were observed using a multi-factor repeated measure ANOVA (**Fig. 3A**; $F_{(3, 67)} = 8.194$, $P < 0.0001$). Holm-Sidak corrected posthoc analysis for multiple comparisons highlighted that both NT-HET ($P < 0.0001$) and HET ($P < 0.0028$) differed from WT while our treatment group, Ube3a-HET, did not differ from WT ($P > 0.05$). Holm-Sidak corrected posthoc analysis for multiple comparisons highlighted that both NT-HET ($P < 0.0001$) and HET ($P < 0.0002$) differed from WT while our treatment group, Ube3a-HET, did not differ from WT ($P = 0.191$). The rigor of this posthoc analysis is remarkable. The Ube3a-HET group did not differ from WT at any timepoint across the 30 min assay (0–5 min, $P = 0.389$, 6–10 min, $P = 0.5027$, 11–15 min, $P = 0.132$, 16–20 min, $P = 0.5418$, 21–25 min $P = 0.995$, 26–30 min $P = 0.8991$), while the HET and WT adjusted P's from Holm Sidak provided (0–5 min, $P < 0.0052$, 6–10 min, $P < 0.0076$, 11–15 min, $P < 0.004$, 16–20 min, $P < 0.024$, 21–25 min, 26–30 min) differed in four of the six 5-min time bins and the NT-HET and WT differ on every 5-min bin of the 30-min task (0–5 min, $P < 0.0002$, 6–10 min, $P < 0.000$, 11–15 min, $P < 0.0004$, 16–20 min, $P < 0.003$, 21–25 min, $P < 0.0287$, 26–30 min, $P < 0.0003$). In corroboration, the total distance also illustrated group differences using a multi-factor repeated measure ANOVA (**Fig. 3B**; $F_{(3, 67)} = 9.487$, $P < 0.0001$). Holm-Sidak corrected posthoc analysis for multiple comparisons highlighted that both NT-HET ($P < 0.0001$) and HET ($P < 0.0002$) differed from WT while our treatment group, Ube3a-HET, did not differ from WT ($P = 0.191$). The Ube3a-HET did not differ from WT at any timepoint across the 30-min assay, while the HET and WT adjusted P's from Holm Sidak differed in five of the six 5-min time bins and the NT-HET and WT differ on every 5-min bin of the 30-min task. Sexes were combined as there was no sex difference in any group in the open

field (**Fig. 3A**: WT $F_{(1, 14)} = 1.637$, $P > 0.05$; HET $F_{(1, 18)} = 0.002$, $P > 0.05$; NT-HET $F_{(1, 18)} = 3.062$, $P > 0.05$; Ube3a-HET $F_{(1, 13)} = 0.048$, $P > 0.05$).

A balance beam walking motor task was conducted as previously described (**39**). All groups displayed longer latencies to cross the rod-shaped beams as they became thinner and more difficult to traverse, as expected. Group differences were detected using a multi-factor repeated measure ANOVA (**Fig. 3C and D**; $F_{(3, 67)} = 17.02$, $P < 0.0001$). Interestingly, Ube3a-HET mice transplanted with the Ube3a lentivector transduced human CD34+ HSPC exhibited values that were not significantly different from the values seen in WT on the beam, illustrated via Holm-Sidak posthoc analysis. The Ube3a-HET did not differ from WT on rod #3 (**Fig. 3D**: rod #3, $P > 0.999$) while the HET ($P < 0.0001$) and NT-HET ($P < 0.227$) had much slower latencies to cross rod #3, highlighting the improved motor coordination of our treated group. Sexes were combined as there was no sex difference in any group in the beam walking assay (**Fig. 3C**: WT $F_{(1, 14)} = 0.9276$, $P > 0.05$; HET $F_{(1, 18)} = 0.563$, $P > 0.05$; NT-HET $F_{(1, 18)} = 0.314$, $P > 0.05$; Ube3a-HET $F_{(1, 13)} = 0.107$, $P > 0.05$). Another corroborating assay of motor coordination is the rotarod. AS mice have deficits in this task, reported by other laboratories (**36–40**). As expected, HET differed from WT in their latencies to fall from the accelerating rod (**Fig. 3E**; $F_{(3, 67)} = 8.395$, $P < 0.0001$) on days 2 ($P < 0.0098$) and 3 ($P < 0.0133$), illustrating poor motor coordination and a lack of motor learning. Strikingly, the Ube3a-HET group was similar to WT across all 3 days of testing using Holm-Sidak posthoc analyses (Day 1; $P = 0.8356$), (Day 2; $P = 0.9572$), and (Day 3; $P = 9979$). Group differences were detected using a multi-factor ANOVA (**Fig. 3F**; $F_{(3, 65)} = 5.782$, $P < 0.002$). Sexes were combined as there was no sex difference

in any group in the rotarod (**Fig. 3E**: WT $F_{(1, 14)} = 0.312$, $P > 0.05$; HET $F_{(1, 18)} = 1.163$, $P > 0.05$; NT-HET $F_{(1, 18)} = 1.196$, $P > 0.05$; Ube3a-HET $F_{(1, 13)} = 0.0571$, $P > 0.05$).

In multiple reports, AS patients exhibit wide stances on the Zenowalk Way (**41**). DigiGait analysis showed HET ($P < 0.0026$) and NT-HET ($P < 0.002$) differ from WT while the Ube3a-HET group showed a narrowing of these wide stances ($P = 0.3486$). Gait trajectories in the hindlimb and forelimb differ slightly, likely due to the differing functions between the fore and hind limbs in quadrupeds. Sexes were combined as there was no sex difference in any group in gait analysis (**Fig. 3F**: WT $F_{(1, 14)} = 5.486$, $P > 0.05$; HET $F_{(1, 18)} = 2.301$, $P > 0.05$; NT-HET $F_{(1, 18)} = 0.071$, $P > 0.05$; Ube3a-HET $F_{(1, 13)} = 0.6627$, $P > 0.05$).

Adult treatment with HSPC transduced with a Ube3a-secreting lentiviral vector rescued AS phenotypes in rigorous motor assessments. As described above, we have demonstrated prevention of AS phenotypes in *Ube3a*$^{mat-/pat+}$ *IL2rg*$^{-/y}$ neonates upon transplantation of human HSPC transduced with the *Ube3a* expressing lentivector. To evaluate whether AS phenotype progression could be halted or reversed, adult *Ube3a*$^{mat-/pat+}$ *IL2rg*$^{-/y}$ mice were transplanted with the Ube3a-expressing lentivector transduced cells after AS phenotypes were present. Rescue of AS phenotypes in the Ube3a-HET group was observed by these mice scoring indistinguishably from WT on multiple assays of motor deficits 6 weeks post-transplant. This was in contrast to the HET and NT-HET groups which illustrated typical AS deficits of reduced motor activity and impaired motor coordination in four tests of motor abilities. Locomotion in a novel open field was collected by assessing the total distance traversed and the horizontal movements using beam breaks in a novel arena. Group differences in horizontal activity counts were observed using a multi-factor repeated measure ANOVA (**Fig. 4A**; $F_{(3, 63)} = 9.650$, $P < 0.0001$), followed by the Holm-Sidak

posthoc test ($P = 0.3465$). Similar to the treated neonates, in the adult treated groups, Holm-Sidak corrected for multiple comparisons still clearly highlighted that both NT-HET ($P < 0.0397$) and HET ($P < 0.0001$) differed from WT while our Ube3a-HET treatment group did not differ from WT ($P = 0.3465$). The Ube3a-HET do not differ from WT at any timepoint across the 30-min assay, while the HET, adjusted P's from Holm Sidak differed in four of the six 5-min time bins. NT-HETs differed in three of the six 5-min time bins. In corroboration, the total distance also illustrated group differences using a multi-factor repeated measure ANOVA (**Fig. 4B**; $F_{(3, 61)} = 11.78$, $P < 0.0001$). Holm-Sidak corrected posthoc analysis for multiple comparisons highlighted that both NT-HET ($P < 0.0001$) and HET ($P < 0.0002$) differed from WT while our treatment group, Ube3a-HET, did not differ from WT ($P = 0.191$). The Ube3a-HET group did not differ from WT at any timepoint across the 30-min assay, while the HET, adjusted P's from Holm Sidak differed in five of the six 5-min time bins and the NT-HET differed on every 5-min bin of the 30-min task. Sexes were combined as there was no sex difference in any group in the open field (**Fig. 4A**: WT $F_{(1, 18)} = 0.332$, $P > 0.05$; HET $F_{(1, 15)} = 0.189$, $P > 0.05$; NT-HET $F_{(1, 11)} = 4.071$, $P > 0.05$; Ube3a-HET $F_{(1, 15)} = 0.562$, $P > 0.05$).

As observed in **Figure 4C**, the *WT* and *Ube3a-HET* groups were the fastest to cross the rods and were indistinguishable from one another by time across the rods, displaying substantial improvement in motor coordination. A balance beam walking motor task was conducted in adults. All groups showed longer latencies to cross the rod shaped beams as they became thinner and more difficult to traverse ($F_{(2, 124)} = 11.73$, $P < 0.0001$), as expected (**39**). Group differences using a multi-factor repeated measure ANOVA (**Fig. 4C and D**; $F_{(3, 62)} = 11.24$, $P < 0.0001$). Amazingly, Ube3a-HET exhibited values that were not significantly different from the values seen in WT on the rods,

illustrated via Holm-Sidak posthoc analysis. Ube3a-HET do not differ from WT on rod #3 (**Fig. 4D**: rod #3, $P = 0.9931$) while the HET ($P < 0.0164$) and NT-HET ($P < 0.0002$) had slower latencies to cross rod #3, highlighting improved motor coordination of our treated group. Sexes were combined as there was no sex difference in any group on the balance beam (**Fig. 4C**: WT $F_{(1, 18)} = 0.951$, $P > 0.05$; HET $F_{(1, 15)} = 0.175$, $P > 0.05$; NT-HET $F_{(1, 11)} = 0.132$, $P > 0.05$; Ube3a-HET $F_{(1, 15)} = 0.066$, $P > 0.05$). On the rotarod coordination assay, as expected, HET differed from WT in their latencies to fall from the accelerating rod (**Fig. 4E**, $F_{(3, 59)} = 3.30$, $P < 0.05$) on day 3 ($P < 0.05$), illustrating poor motor coordination and a lack of motor learning. Strikingly, the Ube3a-HET group was similar to WT across all 3 days of testing using Holm-Sidak posthoc analyses (Day 1; $P = 0.9321$), (Day 2; $P = 0.9691$), and (Day 3; $P = 0.9514$). Sexes were combined as there was no sex difference in any group in the rotarod (**Fig. 4E**: WT $F_{(1, 18)} = 0.558$, $P > 0.05$; HET $F_{(1, 15)} = 1.664$, $P > 0.05$; **NT**-HET $F_{(1, 11)} = 2.82$, $P > 0.05$; Ube3a-HET $F_{(1, 15)} = 3.825$, $P > 0.05$). In evaluating gait analysis, group differences were detected using a multi-factor ANOVA (**Fig. 4F**; $F_{(3, 65)} = 5.782$, $P < 0.002$). DigiGait analysis demonstrated that HET ($P < 0.0026$) and NT-HET ($P < 0.002$) groups differed from WT while the Ube3a-HET group demonstrated a narrowing of these wide stances ($P = 0.3486$). Gait trajectories in the hindlimb and forelimb differ slightly, likely due to the differing functions between the fore and hind limbs in quadrupeds. Sexes were combined as there was no sex difference in any group in gait metrics (**Fig. 4F**: WT $F_{(1, 18)} = 0.792$, $P > 0.05$; HET $F_{(1, 15)} = 0.368$, $P > 0.05$; NT-HET $F_{(1, 11)} = 0.588$, $P > 0.05$; Ube3a-HET $F_{(1, 15)} = 0.584$, $P > 0.05$).

Prevention and rescue of cognitive deficits in the novel AS model following transplantation with HSPC transduced with a *Ube3a*-expressing lentiviral vector. The AS rodent models

exhibit learning and memory deficits as observed by us and others (**36**,**37**,**42**). As displayed in **Figure 5**, we demonstrated both the prevention and reversal of cognitive impairments, in neonates and adults, respectively, following 6–8 weeks of treatment with human CD34+ HSPC transduced with the Ube3a expressing lentiviral vector. All data were collected with automated Ethovision software and subsequently manually scored. For the $Ube3a^{mat-/pat+}$ $IL2rg^{-/y}$ neonate transplantations, as anticipated, the WT group spent more time investigating the novel object versus the familiar object. In contrast, the HET and NT-HET groups did not exhibit typical novel object preference (**Fig. 5A**: WT; $t_{(15)} = 3.833$, $P < 0.0006$; HET; $t_{(14)} = 0.7699$, $P > 0.05$; NT-HET; $t_{(19)} = 0.8703$, $P > 0.05$). However, we observed cognitive rescue in the Ube3a-HET treated group (**Fig. 5A**: Ube3a-HET; $t_{(14)} = 3.302$, $P < 0.003$). There was no object or side bias exhibited by any group (**Fig. 5B**: WT; $t_{(15)} = 0.1100$, $P > 0.05$; HET; $t_{(14)} = 0.2968$, $P > 0.05$; NT-HET; $t_{(19)} = 0.7160$, $P > 0.05$; Ube3a-HET; $t_{(14)} = 0.5284$, $P > 0.05$) since all groups explored the two identical objects similarly during the familiarization phase. Sexes were combined as there was no sex difference in any group in the open field (**Fig. 5B**: WT $t_{(14)} = 0.400$, $P > 0.05$; HET $t_{(18)} = 0.265$, $P > 0.05$; NT-HET $t_{(18)} = 1.029$, $P > 0.05$; Ube3a-HET $t_{(13)} = 0.030$, $P > 0.05$).

As displayed in **Figure 5C and D**, we demonstrated functional reversal of cognitive behavioral impairments in adult $Ube3a^{mat-/pat+}$ $IL2rg^{-/y}$ mice following treatment with human CD34+ HSPC transduced with a Ube3a expressing lentiviral vector. As anticipated, the WT group spent more time investigating the novel object versus the familiar object. In contrast, the HET and NT-HET groups did not exhibit typical novel object preference (**Fig. 5C**: WT; $t_{(14)} = 2.626$, $P < 0.0139$; HET; $t_{(16)} = 0.1392$, $P > 0.05$; NT-HET; $t_{(12)} = 0.1331$, $P > 0.05$).

Impressively, we observed cognitive rescue in the Ube3a-HET mice (**Fig. 5C**: Ube3a-HET; $t_{(14)} = 3.271$, $P < 0.0026$). All groups explored the two objects similarly during the familiarization phase (**Fig. 5D**: WT; $t_{(14)} = 0.3698$, $P = 0.7193$; HET; $t_{(16)} = 0.2968$, $P = 0.8903$; NT-HET; $t_{(12)} = 0.1331$, $P = 0.8952$; Ube3a-HET; $t_{(14)} = 0.1392$, $P = 0.6488$). Sexes were combined as there was no sex difference in any group in the open field (**Fig. 5D**: WT $t_{(13)} = 0.036$, $P > 0.05$; HET $t_{(13)} = 0.723$, $P > 0.05$; NT-HET $t_{(11)} = 0.241$, $P > 0.05$; Ube3a-HET $t_{(15)} = 0.539$, $P > 0.05$).

Neonatal treatment with HSPC transduced with a *Ube3a* expressing lentiviral vector prevented the elevated delta power characteristic of AS. Several EEG abnormalities have been described in AS, including elevated delta power, which have been recapitulated in the Ube3a-deficent mouse models (**43–45**). To evaluate whether the CD34+ cells transduced with the Ube3a expressing lentivector rescued this deficit, the Ube3a-deficient mice were transplanted with these cells. As expected, we observed elevated delta power in the *HET* group when compared with *WT* littermate controls (**Fig. 6**: $F_{(25,\ 362)} = 4.312$, $P < 0.0001$). However, strikingly, we observed a reduction of delta power in the *Ube3a-HET* (**Fig. 6***:* $F_{(25,\ 300)} = 0.223$, $P > 0.999$) group that was significantly lower than the *NT-HET* and *HET* mice (**Fig. 6***:* $F_{(25,\ 475)} = 3.249$, $P < 0.0001$). These results confirmed that delta power elevation could be corrected upon treatment with Ube3a-expressing HSPC.

Immunohistochemical detection of UBE3A expression in the brains of $Ube3a^{mat-/pat+}$ $IL2rg^{-/y}$ mice transplanted with the Ube3a-expressing vector transduced HSPC. To determine if UBE3A expression could be restored in the brains of mice engrafted with

the Ube3a-epressing lentivector transduced human HSPC, transplanted mice were euthanized via transcardial perfusion and prepared for immunohistochemistry. Data suggest that the engrafted human cells were able to cross the blood brain barrier (BBB) when administered as adults, **Figure 7A and B**. **Figure 7A and B** highlights analysis of UBE3A expression in the cortex of the mouse brain 6-weeks post-HSPC transplant in adult mice. **Figure 7A** is an immunohistochemical image showing expression of UBE3A in the mouse cortex of non-transplanted *WT* mice, a *Ube3a-HET* (an AS mouse transplanted with Ube3a-epressing vector transduced human CD34+ HSPC), *NT-HET* (an AS mouse transplanted with NT human CD34+ HSPC) and a non-transplanted *HET*. **Figure 7B** shows the analysis that highlighted the significant increase in UBE3A positive cells, similar to the *WT* level, observed in transplanted *Ube3a-HET* mice compared with *NT-HET* and *HET*. Tukey's corrected post hoc analysis for multiple comparisons revealed that our treatment group *Ube3a-HET* differed from *HET* ($P = 0.0126$) but did not differ from *WT* ($P > 0.05$). This data highlights the groundbreaking potential for adult rescue by intense positive staining for UBE3A with UBE3A-specific antibodies demonstrating restored expression in the brains of transplanted mice.

Multi-lineage hematopoiesis of Ube3a vector transduced human CD34+ cells. To evaluate the in vivo engraftment and differentiation potential of Ube3a lentiviral vector transduced human CD34+ HSPC, cells were transplanted into immunodeficient NOD-$Rag1^{-/-}IL2rg^{-/y}$ (NRG) mice. These mice contain deletions in their Rag1 and IL2 receptor gamma chain genes causing their immunodeficiency and allowing for the transplantation and engraftment of human CD34+ cells in the peripheral blood and various lymphoid organs. Human CD34+ HSPC were left either NT, transduced with the EGFP control vector, or transduced with the hAS8 Ube3a vector and

transplanted into NRG mice. After 6-months post-transplant, mice were analyzed for engraftment in the peripheral blood, spleen, thymus and bone marrow.

Initial analyses determined that normal engraftment of hAS8 Ube3a lentiviral vector transduced CD34+ cells and development of human T cells was demonstrated in the peripheral blood of engrafted NRG mice. As displayed in **Figure 8A**, no significant difference ($P > 0.05$) in the development of CD3+/CD4+ T cells, CD3+/CD8+ T cells, or CD4+/CD8+ double positive T cells from hAS8 vector transduced human CD34+ cells was observed compared with EGFP-control vector transduced or NT human CD34+ cells. Similar levels of all T cells populations analyzed were observed in the peripheral blood of all mouse cohorts. On average, mice transplanted with the Ube3a vector-transduced cells displayed CD3+/CD4+ (76.1%), CD3+/CD8+ (38.2%), and CD3+/CD4+/CD8+ (24.4%) levels in the peripheral blood compared with mice transplanted with NT cells (CD3+/CD4+ (72.1%), CD3+/CD8+ (47.5%), and CD3+/CD4+/CD8+ (19.6%)) and EGFP alone vector transduced cells (CD3+/CD4+ (68.2%), CD3+/CD8+ (37.9%), and CD3+/CD4+/CD8+ (13.1%)). Similar to the peripheral blood, as displayed in **Figure 8B**, no significant difference ($P > 0.05$) in the development of CD3+/CD4+ T cells, CD3+/CD8+ T cells, or CD4+/CD8+ double positive T cells in the spleens of engrafted mice from hAS8 vector transduced human CD34+ cells was observed compared with EGFP control vector transduced or NT human CD34+ cells. On average, mice transplanted with the Ube3a vector transduced cells displayed CD3+/CD4+ (70.9%), CD3+/CD8+ (46.3%) and CD3+/CD4+/CD8+ (15.3%) levels in the spleen compared with mice transplanted with NT cells (CD3+/CD4+ (67.8%), CD3+/CD8+ (58.5%) and CD3+/CD4+/CD8+ (26.4%)) and EGFP control vector transduced cells (CD3+/CD4+ (57.9%), CD3+/CD8+ (52.0%) and CD3+/CD4+/CD8+ (19.1%)). We next analyzed the levels of T cells in the thymus of engrafted mice. As displayed

in **Figure 8C**, no significant difference ($P > 0.05$) in the development of CD3+/CD4+ T cells, CD3+/CD8+ T cells or CD4+/CD8+ double positive T cells in the thymus of engrafted mice from hAS8 vector transduced human CD34+ cells was observed compared with EGFP control vector transduced or NT human CD34+ cells. On average, mice transplanted with the Ube3a vector transduced cells displayed CD3+/CD4+ (66.1%), CD3+/CD8+ (54.4%) and CD3+/CD4+/CD8+ (27.7%) levels in the thymus compared with mice transplanted with NT cells (CD3+/CD4+ (74.3%), CD3+/CD8+ (53.6%) and CD3+/CD4+/CD8+ (28.0%)) and EGFP control vector transduced cells (CD3+/CD4+ (65.2%), CD3+/CD8+ (57.1%) and CD3+/CD4+/CD8+ (22.3%)). These results demonstrate that human CD34+ HSC transduced with the hAS8 Ube3a-expressing lentiviral vector were capable of engraftment in the NRG mice and were able to differentiate into normal T cells in the peripheral blood, spleen and thymus of engrafted mice.

As a next step in evaluating the safety of the Ube3a vector transduced cells, human B cell analyses were performed on the spleen and bone marrow of engrafted NRG mice. As displayed in **Figure 8D**, no significant difference ($P > 0.05$) in the development of CD45+/CD19+ B cells in the spleen of engrafted mice from hAS8 vector transduced human CD34+ cells were observed compared with EGFP control vector transduced or NT human CD34+ cells. On average, mice transplanted with the Ube3a vector transduced cells displayed CD45+/CD19+ (38.5%) levels in the spleen compared with mice transplanted with NT cells (CD45+/CD19+ (51.6%) and EGFP control vector transduced cells (CD45+/CD19+ (45.8%). Similarly, as displayed in **Figure 8E**, no significant difference ($P > 0.05$) in the development of CD45+/CD19+ B cells in the bone marrow of engrafted mice from hAS8 vector transduced human CD34+ cells were observed compared with EGFP control vector transduced or NT human CD34+ cells. On average, mice transplanted with the Ube3a vector transduced cells displayed CD45+/CD19+ (32.6%) levels in the bone marrow

compared with mice transplanted with NT cells CD45+/CD19+ (47.9%) and EGFP control vector transduced cells CD45+/CD19+ (39.8%). These results demonstrate that human CD34+ HSC transduced with the hAS8 Ube3a-expressing lentiviral vector were capable of engraftment in the NRG mice and were able to differentiate into normal B cells in the spleen and bone marrow of engrafted mice.

We next evaluated the levels of human macrophages and human CD34+ cells engrafted in the bone marrow of NRG mice transplanted with hAS8 Ube3a vector transduced cells. As displayed in **Figure 8F**, no significant difference ($P > 0.05$) in the development of CD45+/CD14+ macrophages or CD45+/CD34+ cells in the bone marrow of engrafted mice from hAS8 vector transduced human CD34+ cells was observed compared with EGFP control vector transduced or NT human CD34+ cells. On average, mice transplanted with the Ube3a vector-transduced cells displayed CD45+/CD14+ (19.2%) levels and CD45+/CD34+ (18.5%) levels in the bone marrow compared with mice transplanted with NT cells (CD45+/CD14+ (24.5%) and CD45+/CD34+ (13.0)) and EGFP control vector transduced cells (CD45+/CD14+ (14.6%) and CD45+/CD34+ (9.5)). These results demonstrate that human CD34+ HSC transduced with the hAS8 Ube3a-expressing lentiviral vector were capable of engraftment in the NRG mice and were able to differentiate into normal macrophages in the bone marrow of engrafted mice. These results also demonstrate that human CD34+ cells transduced with the Ube3a lentiviral vector were still present in the bone marrow of engrafted mice 6 months post-transplant.

Discussion

Currently, there is no FDA-approved therapy for AS; however, numerous therapeutic approaches are being evaluated both preclinically and clinically. While the initial preclinical study of Meng *et al*. using ASO did not observe improvements in motor abilities following ASO

treatment, the therapeutic antisense used in that study did normalize body weight and improved performance on contextual fear conditioning of AS mice when given directly into the brain by intracerebroventricular injection in adult mice (8). Another technique that modified the imprint of the antisense transcript on the paternal allele included the artificial transcription actor (ATF), S1K (10). Viral vector delivery via adeno-associated virus (AAV) has also proven successful preclinically with efficacy in long-term potentiation and contextual fear conditioning but not in rotarod or other motor assays (9). Gene-replacement therapy for AS should be a reality in the coming years. In fact, this year, two clinical trials using ASO compounds began recruitment and treatment, highlighting the groundbreaking time in AS and gene therapy research (GeneTx NCT04259281; Roche NCT04428281). Another proof-of-concept for gene-replacement therapy utilized a sophisticated tamoxifen induced Cre-line. In this work, temporally controlled Cre-dependent induction of the maternal *Ube3a* allele found improvements or rescue in rotarod and marble burying yet only when restored embryonically and at juvenile ages, not as adolescents or adults (40,46).

Our report is the first to detect rescue in multiple behavioral assays across several impaired clinically relevant domains from treatment given to neonate and adult AS mice on a congenic C57BL/6 J background, which eliminated the large influence that background strain has on motor and seizure phenotypes (36,47,48). The work presented here highlights our effort to develop the use of HSPC transduced with a lentiviral vector expressing *Ube3a*, in an innovative preclinical model of AS, which offers a promising strategy for life-long delivery of functional UBE3A through the hematopoietic system to the brain. This cross-correction approach has been successfully demonstrated for other monogenic diseases including adrenoleukodystrophy, metachromatic leukodystrophy and Sandhoff disease (22,31,32,49). In previous studies, successful

engraftment of gene-modified microglia in the brains of treated mice demonstrated that HSPC gene therapy can deliver therapeutic proteins to disease-affected cells (22,30,32–34,49). In our current study, we observed elevated levels of UBE3A in the brains of the Ube3a-HET treatment group, and rescue of motor, cognitive and EEG phenotypes following transplantation and engraftment of the genetically modified human CD34+ HSPC as neonates or adults.

The immunodeficient and *Ube3a*-deficient mice utilized in this study are capable of transplantation and engraftment of human cells following sub-lethal irradiation of neonates or busulfan treatment of adults. We chose to utilize human HSPC over mouse HSPC due to (a) early data that indicated the interleukin 2 common chain deficiency caused no behavioral outcomes in domains of interest to AS, (b) a fast forward approach to clinical translation not requiring bridging studies of mHSPC to hHSPC, (c) using human cells will allow us delineate the biological pathway that underlies cross correction, in the future, as the human cells should be distinguishable from mouse cells in brain and (d) feasibility, since an extraordinary number of mice would be required to collect donor mHSPC per subject treated mouse further in line with Animal Welfare's RRR policy. The selection of mouse strains involved numerous iterations as to confirm that no behavioral phenotypes typically attributed to the loss of *Ube3a,* were not an unintended consequence of immune alterations when deriving the immunodeficient *Ube3a*-deficient model. This resulted in the use of an *Ube3a*-deficient and *IL2* common gamma receptor chain-deficient model, $Ube3a^{mat-/pat+}$ $IL2rg^{-/y}$ allowing for the transplantation and engraftment of human cells. Next, we assessed the critical question of whether the gene-modified HSPC could prevent or rescue behavioral phenotypes in the mouse model. We performed functional experiments in cohorts treated as neonates or adults to evaluate whether providing treatment would only be useful if delivered before a critical therapeutic window early in life, or if later stage interventions could be

similarly efficacious. Finally, elevated UBE3A expression was detected in the brains of adult treated mice. A limitation to the current work is the lack of co-localization staining of neurons; however, mechanistic studies beyond the scope of this current work are ongoing.

Functional reversal of AS symptoms in treated adult mice was remarkable in subjects displaying AS phenotypes of motor deficits, coordination and gait impairments, and cognitive deficits in novel objection recognition. This was an unexpected finding, as the prevailing dogma in the AS field has highlighted the importance of critical treatment periods, suggesting that improvements in functional/behavioral phenotypes beyond a critical period would be minimal or not possible (46). These conclusions are logical and well supported by behavioral outcomes using a novel inducible genetic mutant line and physiological outcomes from this same line (43–45). Yet, our robust adult rescue in multiple behavioral and physiological domains on multiple assays challenge this interpretation and highlight improvements in performance across multiple domains on the same scale as the neonatal treated mice. Differences in behavioral rescues may not be surprising given the highly disparate mouse models, as this earlier work was performed in a tamoxifen induced Cre-line. Recent studies have demonstrated imperfections with Cre tools for numerous reasons including undesirable expression patterns, unwanted germline expression of the Cre recombinase, mosaic expression of the Cre driver complicating genotyping, and recombination beings more or less efficient depending on the floxed locus (50,51). Another difference is that the behavioral experiments in the aforementioned studies were performed in an isogenic F1 hybrid background of 129/Sv and C57BL/6 mice while ours used a congenic C57BL/6J background throughout.

In earlier work, temporally controlled Cre-dependent induction of the maternal *Ube3a* allele found improvements or rescue in rotarod and marble burying were only

observed embryonically and at juvenile ages, not as adolescents or adults (40,46). Our study also used rotarod, as it is a field gold standard assay, and we saw rotarod rescue in the neonate and adult cohorts, as well as in three additional motor tasks. While we did not perform marble burying, we performed other translational tasks such as gait mapping and EEG recordings. It is important to note, however, that not all behavioral phenotypes studied in laboratory animal models are robust, reliable, reproducible, nor optimal for enabling translational application to the clinic.

Our study, for the first time, illustrated rigorous reversal of many phenotypes in both neonate and adult treated mice using HSPC transduced with a *Ube3a*-expressing lentiviral vector. Gene modified lentiviral vectors have been applied in different clinical trials based on *ex vivo* correction of autologous HSPC and were demonstrated to be immunologically safe and therapeutically efficient in symptom correction in a wide range of single gene disorders (22,31,32). Yet still, for nearly all rare genetic disorders, including AS, there is a delay between developmental milestones not being met and an official diagnosis of a genetic syndrome. Thus, there needs to be testing of therapeutics beyond the prenatal/early neonatal state. While most AS research has highlighted this critical window, our HSPC therapeutic approach would address this oversight, as our observations of functional efficacy were nearly equivalent in neonates and adults (48).

A potential concern with the older in life approach is the busulfan conditioning cell ablation regimen used as adults (irradiation was used for the neonate transplants as analogous conditioning). We did not observe any overt side effects with the busulfan conditioning, and as it is being used clinically for other disorders, our data demonstrate strong evidence for the use of this therapy to treat AS (52).

Our data demonstrate strong evidence for the use of HSPC therapy to treat AS, which should provide long-term restoration of UBE3A in the brain. Additionally, this study challenges

the current dogma in the AS field of therapeutic treatment windows, since treatment in adults was equally as efficacious as treatment in neonates, suggesting that therapeutic treatment beyond the critical period is possible for the AS community.

Materials and Methods

Lentiviral vector production

All lentiviral vectors used were generated from a self-inactivating third generation lentiviral vector backbone called CCLc-MNDU3-x (Fig. 1A). An EGFP-alone lentiviral vector, CCLc-MNDU3-PGK-EGFP, was constructed and used as an empty vector control (Fig. 1B). To construct the Ube3a expressing lentiviral vectors, modified mouse Ube3a isoform 3 (mAS8) or modified human Ube3a isoform 1 (hAS8) were manually synthesized and cloned into pcDNA 3.1 TOPO (ThermoFisher, Grand Island, NY). The sequences of the clones were confirmed (Laragen, Culver City, CA). The mAS8 and hAS8 TOPO clones were further subcloned individually under the control of the MNDU3 promoter in the 'x' site of the CCLc-MNDU3-x-PGK-EGFP backbone (Fig. 1C and D). Experiments involving recombinant DNA were performed following the NIH guidelines.

Lentiviral vectors were produced in human embryonic kidney (HEK)-293 cells by transient transfection with a 1:5:5 ratio of the envelope vesicular stomatitis virus glycoprotein (VSVG) plasmid, a packaging plasmid (Δ8.9) containing a capsid gene and a reverse transcriptase gene, and one of the transfer plasmids, either the control EGFP alone, the mouse Ube3a, or the human Ube3a plasmids. Forty-eight hours post-transfection, cell supernatants were concentrated by ultrafiltration. Titers for total vector transducing units were calculated by transduction of HEK-293 cells and analysis of EGFP expression by flow cytometry 48 h post-transduction. Flow

cytometry was performed on a Beckman Coulter Cytomics FC500 and analyzed using CXP software.

Isolation and transduction of human CD34+ HSPC

Human CD34+ HSPC were purified from umbilical cord blood obtained from the UC Davis Umbilical Cord Blood Collection Program using Ficoll-Paque (GE Healthcare, Logan, UT) density gradient and CD34 specific magnetic bead separation (Miltenyi Biotec, Auburn, CA). The CD34+ cells were cultured for 48 h in XVIVO-10 media (Lonza, Anaheim, CA) containing 50 ng/ml Flt-3 ligand, thrombopoietin (TPO), and stem cell factor (SCF) (R&D Systems, Minneapolis, MN). After culturing for 48 h, the CD34+ cells were left either NT, transduced with the EGFP control vector, transduced with the mAS8 vector, or transduced with the hAS8 vector at an MOI of 20 and the addition of 8 mg/ml protamine sulfate for a minimum of 3 h at 37°C. The EGFP, mAS8, and the hAS8 CD34+ transduced cultures were either left unsorted or fluorescently active cell sorted (FACS) based on EGFP expression depending on the subsequent experiments in which they were utilized.

Colony-forming unit assays

The human CD34+ cells, either NT, FACS EGFP control vector, FACS mAS8 vector, or FACS hAS8 vector transduced (500 total cells) were cultured for 12 days in MethoCult medium (Stemcell Technologies, Vancouver, CA). Post-culture, total granulocyte/macrophage (GM) colonies, granulocyte/erythrocyte/megakaryocyte/macrophage (GEMM) colonies and burst forming unit-erythroid colonies (BFU-E), were counted by microscopy. Experiments were performed in triplicate.

In vitro derivation of macrophages and analysis of their phenotypic profiles

The colonies formed in the CFU assays were further differentiated into mature macrophages, in vitro, by culturing the cells in DMEM supplemented with 10% FBS, 10 ng/ml of granulocyte-macrophage colony stimulating factor (GM-CSF), 10 ng/ml macrophage colony stimulating factor (M-CSF) (R&D Systems, Minneapolis, MN) for 4 days. Macrophages were further analyzed by flow cytometry for surface expression of the macrophage cell surface markers, CD14, CD4, and HLA-DR. Macrophages were stained with a phycoerythrin (PE)-conjugated CD4, a PE-conjugated HLA-DR, or a PE-conjugated CD14 antibody (BD Biosciences, San Jose, CA). Flow cytometry was performed on a Beckman Coulter Cytomics FC500 and analyzed with CXP software. Experiments were performed in triplicate.

Western blot and ubiquitination analyses of Ube3a vector transduced cells

Human macrophages derived from the vector transduced human CD34+ cells were lysed in 1 × RIPA buffer supplemented with protease inhibitor cocktail (Millipore Sigma, St. Louis, MO) and protein concentrations were determined by Bradford assay (BioRad, Hercules, CA). For Western blots, 60 μg protein were separated on a Novex 10–20% Tris-Glycine gel (Invitrogen, Carlsbad, CA) with MOPS buffer. Protein was subsequently transferred onto a nitrocellulose membrane and protein loading was evaluated by Ponceau S stain. The membrane was rinsed with deionized water and incubated in blocking solution (5% non-fat dry milk in TBST; 50 mM Tris, 150 mM NaCl, 0.1% Tween-20) for 30 min at room temperature. Membranes were incubated with primary mouse UBE3A antibody (BD Biosciences, San Jose, CA #611416) at 1:500 dilution in blocking solution at 4°C overnight. After three 10-min washes with TBST the membrane was incubated with horseradish peroxidase conjugated rabbit anti mouse secondary antibody (1:2000 dilution in blocking solution) for 45 min at room temperature. After three more washes in TBST,

proteins were visualized with Amersham ECL Prime Western Blotting Detection Reagent (GE Healthcare, Logan, UT) using the ChemiDoc XRS Imaging System (BioRad, Hercules, CA). Cell lysates from the macrophages were further analyzed for ubiquitination of S5A using the Human E6AP/S5a Ubiquitination Kit (#K-230) (R&D Systems, Minneapolis, MN) according to the manufacturer's protocol.

Generation of an immunodeficient mouse model of AS (Ube3a$^{mat-/pat+}$ IL2rg$^{-/y}$)

Ube3a mutated immunodeficient mouse model was generated by crossing Ube3a deletion females (JAX stock #016590) with IL2rg null males (JAX stock #003174; B6.129S4-Il2rg^{tm1Wjl}/J), Ube3a$^{mat-/pat+}$ IL2rg$^{-/y}$. To identify mice, neonates were labelled by paw tattoo on postnatal day (PND) 2–3 using non-toxic animal tattoo ink (Ketchum Manufacturing Inc., Brockville, ON, Canada). At PND 5–7, tails of pups were clipped (0.5 cm) for genotyping, following the UC Davis IACUC policy regarding tissue collection. Genotyping was performed with RED Extract-N-Amp (Sigma Aldrich, St. Louis, MO) using primers R1965 GCTCAAGGTTGTATGCCTTGGTGCT, WTF1966 AGTTCTCAAGGTAAGCTGAGCTTGC, and ASF1967 TGCATCGCATTGTCTGAGTAGGTGTC for Ube3a, and IMR5330 GTGGGTAGCCAGCTCTTCAG, oIMR5331 CCTGGAGCTGGACAACAAAT, and oIMR7415 GCCAGAGGCCACTTGTGTAG for null for IL2rg. After weaning on PND 21, mice were socially housed in groups of 2–4 by sex. The resulting mice used in the experiments were identified genotypically as Ube3a$^{mat-/pat+}$ IL2rg$^{-/y}$ or Ube3a$^{mat+/pat+}$ IL2rg$^{-/y}$.

Transplantation and generation of the humanized Ube3a$^{mat-/pat+}$ IL2rg$^{-/y}$ mice

Newborn Ube3a$^{mat-/pat+}$ IL2rg$^{-/y}$ mice (2–5 days old) were irradiated with 150 rads from a Cesium source and transplanted intrahepatically with 500 000 total human CD34+ HSPC/mouse. Eight

weeks post-transplant, mice were bled via the tail vein and analyzed for engraftment by flow cytometry using a PE-CY7-conjugated anti-human CD45 antibody (BD Biosciences, San Jose, CA). Successfully engrafted mice were then evaluated for behavioral phenotypes. The order and age of testing were as follows: (1) Open field at 9 weeks of age, (2) Beam walking at 9 weeks of age, (3) Rotarod at 10 weeks of age, and (4) NOR at 11 weeks of age, (5) EEG at 15–17 weeks.

At 4–5 weeks of age, Ube3a$^{mat-/pat+}$ IL2rg$^{-/y}$ mice were treated with 20 mg/kg busulfan intraperitonially 48 and 24 h prior to transplanting with 500 000 total human CD34+ HSPC/mouse intravenously. Six weeks post-transplant, mice were bled via the tail vein and analyzed for engraftment by flow cytometry using a PE-CY7-conjugated anti-human CD45 antibody (BD Biosciences, San Jose, CA). Successfully engrafted mice were then evaluated for behavioral phenotypes. The order and age of testing were as follows: (1) Open field at 11–12 weeks of age, (2) Beam walking at 11–12 weeks of age, (3) Rotarod at 12–13 weeks of age, (4) NOR at 14–15 weeks of age.

Subjects for behavior and neurophysiology

All mice were housed in Techniplast cages (Techniplast, West Chester, PA, USA). Cages were housed in ventilated racks in a temperature (68–72°F) and humidity (~25%) controlled colony room on a 12:12 light/dark cycle. Standard rodent chow and tap water were available ad libitum. In addition to standard bedding, a Nestlet square, shredded brown paper, and a cardboard tube (Jonesville Corporation, Jonesville, MI) were provided in each cage. All experimental procedures were performed in accordance with the National Institutes of Health Guide for Care and Use of Laboratory Animals and were approved by the Institutional Animal Care and Use Committees (IACUC) #21494 (PI, Silverman) of the University of California, Davis.

Behavioral assays

Open field

General exploratory locomotion in a novel open field arena was evaluated as previously described (53,54). Briefly, each subject was tested in a VersaMax Animal Activity Monitoring System (Accuscan, Columbus, OH, USA) for 30-min in a ~30 lux testing room. Total distance traversed, horizontal activity, vertical activity and time spent in the center were automatically measured to assess gross motor abilities in mice.

Beam walking

A beam-walking motor task was conducted as previously described in (39,55,56). Fifty-nine centimeter long round rods were suspended 68 cm above a cushioned landing pad. A goal box at the end of the beam consisted of a 12 cm diameter cylinder to provide motivation to cross the beam. Each mouse was placed at one end of the beam and the time to cross to the goal box on the other end was measured. Testing sequence moved from largest diameter to smallest diameter rods in order of increased difficulty. On the day prior to testing, all animals were given two practice trials on the largest diameter round beam in order to become accustom to the procedure. On the test day, each animal was sequentially tested on three round rods (35, 18 and 13 mm). Testing sequence was based on presentations of decreasing diameter to present increasing levels of difficulty. Each mouse was given two trials on each beam, separated by ~30 min. The time to transverse the beam was recorded and averaged across the two trials for each beam. A maximum time of 60 s was assigned to individuals that failed to cross the beam in that duration. In the small number of cases where mice fell from the beam, a score of 60-s was assigned.

Rotarod

Motor coordination, balance and motor learning were tested with an accelerating rotarod (Ugo Basile, Gemonio, Italy) as previously described in (39,57). Mice were placed on a rotating cylinder that slowly accelerated from 5 to 40 revolutions per min over 5 min. Mice were given three trials per day with a 60-min inter-trial rest interval and tested for three consecutive days for a total of nine trials. Performance was scored as latency to fall off the cylinder with a maximum latency of 5 min.

Gait analysis

Treadmill gait analysis was performed using the DigiGait™ system (Mouse Specifics Inc., USA) (39,58). Mouse paws were painted with non-toxic red food coloring to augment dark green paw tattoos that generated conflict in DigiGait™ analysis 1 min prior to introduction to the walking chamber to reliably capture the entire paw surface area. Before data collection, each subject was acclimated to the Perspex walking chamber for 1 min and the treadmill was slowly accelerated to the final speed of 20 cm/s to allow mice to adjust to walking on the belt. Digital images of paw placement were recorded through a clear treadmill from the ventral plane of the animal. Mice were tested in a single session at a 20 cm/s treadmill speed maintaining a normal pace walk for WT mice. Non-performers were defined as mice who were unable to sustain walking at 20 cm/s without colliding with the posterior bumper for at least 3 s. There is no practice effect or repeated exposure, and therefore, mice were allowed retrial and retest if they were unable to adjust to walking on the belt easily. The treadmill belt and the encasing Perspex chamber were cleaned with 70% (v/v) ethanol in between tests. For each mouse, videos of ~5 s duration of all sessions were analyzed using the DigiGait™ Imaging and Analysis software v12.2 (Mouse Specifics Inc., USA).

Contrast filters were determined on a mouse-by-mouse case to facilitate consistent recognition of all four paws. All analysis was conducted in a single session by experimenter blind to genotype. Stride length (distance a paw makes during a single stride) and frequency (number of strides per second to maintain pace) were automatically calculated. Data was averaged between left and right paws for fore and hind paws.

Novel object recognition

The novel object recognition test was conducted as previously described in opaque matte white (P95 White, Tap Plastics, Sacramento, CA, USA) arenas (41 cm l x 41 cm w x 30 cm h) (39,55). The assay consisted of four sessions: a 30-min habituation session, a second 10-min habituation phase, a 10-min familiarization session and a 5-min recognition test. On Day 1, each subject was habituated to a clean empty arena for 30-min. 24-h later, each subject was returned to the empty arena for an additional 10-min habituation session. The mouse was then removed from testing arena and was placed in a clean temporary holding cage while two identical objects were placed in the arena. Subjects were returned to the testing arena and given a 10-min of familiarization period in which they had time to investigate the two identical objects. After the familiarization, phase subjects were returned to their holding cages for a 1-h interval period. One familiar object and one novel object were placed in the arena, where the two identical objects had been located during the familiarization phase. After the 1-h interval, each subject was returned to the arena for a 5-min recognition test. The familiarization session and the recognition test were recorded using Ethovision XT video tracking software (version 9.0, Noldus Information Technologies, Leesburg, VA, USA). Sniffing was defined as head facing the object with the nose point within 2 cm or less from the object. Time spent sniffing each object was scored by an investigator blind to both genotype and treatment. Recognition memory was defined as spending significantly more time

sniffing the novel object compared with the familiar object. Total time spent sniffing both objects was used as a measure of general exploration. Time spent sniffing two identical objects during the familiarization phase confirmed the lack of an innate side bias. Within genotype repeated-measures ANOVA was used to analyze novel object recognition using novel versus familiar objects as comparison. F, degrees of freedom, and P-values are reported.

EEG implantation and acquisition

These methods are described in detail by our laboratory in previous publications (58–60). Wireless EEG transmitters were implanted in anesthetized test animals using continuous isoflurane (2–4%). A 2–3 cm midline incision was made over the skull and trapezius muscles, then expanded to expose the subcutaneous space. Implants were placed in the subcutaneous pocket lateral to the spine to avoid discomfort of the animal and displacement due to movement. Attached to the implant were four biopotential leads made of a Nickel-Colbalt based alloy insulated in medical-grade silicone, making up two channels that included a signal and reference lead. These leads were threaded toward the cranial part of the incisions for EEG and EMG placement. The periosteum was cleaned from the skull using a sterile cotton-tip applicator and scalpel then two 1 mm diameter burr holes were drilled (1.0 mm anterior and 1.0 mm lateral; −3.0 mm posterior and 1.0 mm lateral) relative to bregma. Steel surgical screws were placed in the burr holes and the biopotential leads were attached by removing the end of the silicone covering and tying the lead to its respective screw. Once in place, the skull screws and lead connections were secured using dental cement. For EMG lead placement, the trapezius muscles of the animal were exposed, and each lead was looped through and sutured to prevent displacement. Finally, the incision was sutured using non-resorbable suture material and the animals were placed in a heated recovery cage where they received Carpofen (5 mg/kg; i.p.) directly after surgery and 24 h post-surgery as an analgesic.

Subjects were individually caged with ad libitum access to food and water for 1-week before EEG acquisition and monitored daily to ensure proper incision healing and recovery. Each implantation surgery took <45-min and no fatalities were observed.

EEG data acquisition, processing and analysis

After a 1-week recovery from surgical implantation, individually housed mice were assigned to PhysioTel RPC receiver plates that transmitted data from the EEG implants to a computer via the data exchange matrix using Ponemah software (Data Sciences International, St. Paul, MN). EEG and EMG data were collected at a sampling rate of 500 Hz with a 0.1 Hz high-pass and 100 Hz low-pass bandpass filter. Activity, temperature and signal strength were collected at a sampling rate of 200 Hz. Data acquired in Ponemah were read into Python and further processed with a bandpass filter from 0 to 50 Hz to focus on our frequencies of interest, as previously described (59).

Spectral analysis was performed in Python using MEG and EEG analysis and visualization (MNE) open-source software, as previously described in (59,61). Frequency bands were defined as delta 0.5–4 Hz, theta 5–9 Hz, alpha 9–12 Hz, beta 13–30 Hz and gamma 30–50 Hz. Spectral power was analyzed using the Welch's method, which windows over the signal and averages across spectral samples. For power spectral densities (PSD) investigated in Cohort 2, analysis started 3 h into recording and finished 3 h prior to the end of recording and PTZ administration, resulting in an 18-h sampling window. PSD analysis in Cohort 3 also began 3 h into recording but continued over the 3-day recording resulting in a 69-h sampling window. No statistical difference was detected in PSD within genotype between samples, therefore, both cohorts were combined. Total delta power was determined by adding the density data detected in the 0.5–4 Hz frequency range while total

power summed all the PSD data in the 0.5–50 Hz frequency range. Relative delta frequencies were calculated by dividing total delta power by total power per animal and averaging across genotype.

Immunohistochemistry labeling and analysis

Upon completion of the behavioral, motor and cognitive studies, mice were euthanized, perfused and the brain tissues were obtained, snap frozen and labeled for UBE3A, as previously described in (61). Sagittal sections (40 μM) were cryosectioned and further labeled with ImmPACT DAB Peroxidase Substrate (Vector Labs, Burlingame, CA) utilizing the Vectastain ABC Kit (HP1–26), and in conformity with recommendations from the manufacturers included protocols. In brief, to begin the process tissues underwent peroxidase quenching using a 0.3% hydrogen peroxide solution in water for 30 min, followed by immersion in a 10% blocking solution in PBS (SEA BLOCK Blocking Buffer, ThermoFisher, Grand Island, NY) for 1 h, which was followed by immersion in primary antibody UBE3A (Monoclonal Anti-UBE3A antibody produced in mouse, SAB1404508) at a concentration ratio of 1:500 with incubation overnight at 4°C. On the second day, the tissues were immersed in a biotinylated secondary antibody solution at a concentration of 1:200 with incubation for 1 h (Goat Anti-Mouse IgG Antibody, BA-9200, Vector Labs, Burlingame, CA), followed by Vectastain ABC reagent incubation for 30 min (Vector Labs, Burlingame, CA) and concluded with immersion into ImmPACT DAB Peroxidase Substrate (Vector Labs, Burlingame, CA) at manufacturers recommended concentration for 8 min. In between each step, all tissues were washed using PBST (0.1% Triton) for ~15 min. Serial sections were mounted onto uncharged slides and cover slipped using Permount Mounting Medium (ThermoFisher, Grand Island, NY). Bright field immunohistochemistry stained slides were scanned using the 20× objective (0.8, M27) with bright field illumination on an Axio Scan (Zeiss).

Transplantation of NOD-RAG1$^{-/-}$ IL2rg$^{-/y}$ Mice

NOD-RAG1$^{-/-}$ IL2rg$^{-/y}$ (NRG) mice (stock number 007799) were obtained from The Jackson Laboratory (Sacramento, CA). Two to five-day old NRG mice (N = 15 per cohort) were sublethally irradiated with 100 rads from a Cesium source and transplanted intrahepatically with either the NT, EGFP control vector transduced, or the hAS8 vector transduced human CD34+ HSPC (300 000 total cells). To determine engraftment levels, at 12 weeks post-transplant, mice were bled via the tail vein and were analyzed by flow cytometry with a PE-CY7-conjugated anti-human CD45 antibody (BD Biosciences, San Jose, CA). Flow cytometry was performed on a Beckman Coulter FC-500 and analyzed by CXP software. Mice were used in accordance with institutional and IACUC guidelines.

Engraftment and multi-lineage hematopoiesis of transplanted human CD34+ cells

To evaluate the engraftment and multi-lineage differentiation of the human CD34+ cells transduced with the hAS8 lentiviral vector, cells from the peripheral blood, bone marrow, thymus and spleen were analyzed from the transplanted NRG mice. Total cells were obtained from the above-mentioned organs and were labeled with antibodies specific for human immune cells including T cells, B cells, macrophages and CD34+ cells. The following antibodies were used in these studies: T cell antibodies used were a Brilliant violet (BV) 421-conjugated CD3 antibody, an allophycocyanin (APC) H7-conjugated CD4 antibody and an Alexa fluor (AF) 700-conjugated CD8 antibody (BD Biosciences, San Jose, CA). B cell antibodies used were a PE-CY7-conjugated CD45 antibody and a PE-conjugated CD19 antibody (BD Biosciences, San Jose, CA). Macrophage antibodies used were a PE-CY7-conjugated CD45 antibody and a PE-conjugated CD14 antibody (BD Biosciences). CD34+ cell antibodies used were a PE-CY7-conjugated CD45 antibody and a

PE-conjugated CD34 antibody (BD Biosciences, San Jose, CA). Flow cytometry was performed using a BD Fortessa and analyzed with CXP software.

References

1. Williams, C.A. (2005) Neurological aspects of the Angelman syndrome. Brain Dev., 27, 88–94.
2. Buiting, K., Williams, C. and Horsthemke, B. (2016) Angelman syndrome-insights into a rare neurogenetic disorder. Nat. Rev. Neurol., 12, 584–593.
3. Williams, C.A., Driscoll, D.J. and Dagli, A.I. (2010) Clinical and genetic aspects of Angelman syndrome. Genet. Med., 12, 385–395.
4. Chamberlain, S.J. and Lalande, M. (2010) Neurodevelopmental disorders involving genomic imprinting at human chromosome 15q11-q13. Neurobiol. Dis., 39, 13–20.
5. Matsuura, T., Sutcliffe, J.S., Fang, P., Galjaard, R.J., Jiang, Y.H., Benton, C.S., Rommens, J.M. and Beaudet, A.L. (1997) De novo truncating mutations in E6-AP ubiquiting-protein ligase gene (UBE3A) in Angelman syndrome. Nat. Genet., 15, 74–77.
6. Kishino, T., Lalande, M. and Wagstaff, J. (1997) UBE3A/E6-AP mutations cause Angelman syndrome. Nat. Genet., 15, 70–73.
7. Albrecht, U., Sutcliffe, J.S., Cattanach, B.M., Beechey, C.V., Armstrong, D., Eichele, G. and Beaudet, A.L. (1997) Imprinted expression of the murine Angelman syndrome gene, Ube3a, in hippocampal and Purkinje neurons. Nat. Genet., 17, 75–78.
8. Meng, L., Person, R.E., Huang, W., Zhu, P.J., Costa-Mattioli, M. and Beaudet, A.L. (2013) Truncation of Ube3a-ATS unsilences paternal Ube3a and ameliorates behavioral defects in the Angelman syndrome mouse model. PLoS Genet., 9, e1004039.
9. Daily, J.L., Nash, K., Jinwal, U., Golde, T., Rogers, J., Peters, M.M., Burdine, R.D., Dickey, C., Banko, J.L. and Weeber, E.J. (2011) Adeno-associated virus-mediated rescue of the cognitive defects in a mouse model for Angelman syndrome. PLoS One, 6, e27221.
10. Bailus, B.J., Pyles, B., Mcalister, M.M., O'Geen, H., Lockwood, S.H., Adams, A.N., Nguyen, J.T., Yu, A., Berman, R.F. and Segal, D.J. (2016) Protein delivery of an artificial transcription factor restores widespread Ube3a expression in an angelman syndrome mouse brain. Mol. Ther., 24, 548–555.
11. Bailus, B.J. and Segal, D.J. (2014) The prospect of molecular therapy for Angelman syndrome and other monogenic neurologic disorders. BMC Neurosci., 15, 1–7.
12. Pyles, B., Bailus, B.J., O'Geen, H. and Segal, D.J. (2019) Purified protein delivery to activate an Epingenetically silenced allele in mouse brain. Methods Mol. Biol., 1767, 227–239.

13. Ciarlone, S.L., Grieco, J.C., Agostino, D.P.D. and Weeber, E.J. (2016) Ketone ester supplementation attenuates seizure activity, and improves behavior and hippocampal synaptic plasticity in an Angelman syndrome mouse model. Neurobiol. Dis., 96, 38–46.

14. Ciarlone, S.L., Wang, X., Rogawski, M.A. and Weeber, E.J. (2017) Effects of the synthetic neurosteroid ganaxolone on seizure activity and behavioral deficits in an Angelman syndrome mouse model. Neuropharmacology, 116, 142–150.

15. Grieco, J.C., Ciarlone, S.L., Gieron-korthals, M., Schoenberg, M.R., Smith, A.G., Philpot, R.M., Heussler, H.S., Banko, J.L. and Weeber, E.J. (2014) An open-label pilot trial of minocycline in children as a treatment for Angelman syndrome. BMC Neurol., 14, 232.

16. Bird, L.M., Tan, W., Bacino, C.A., Peters, S.U., Skinner, S.A., Anselm, I., Barbieri-Welge, R., Bauer-Carlin, A., Gentile, J.K., Glaze, D.G. et al. (2012) A therapeutic trial of pro-methylation dietary supplements in Angelman syndrome. Am. J. Med. Genet. A, 155, 2956–2963.

17. van Woerden, G.M., Harris, K.D., Hojjati, M.R., Gustin, R.M., Qiu, S., de Avila Freire, R., Jiang, Y.H., Elgersma, Y. and Weeber, E.J. (2007) Rescue of neurological deficits in a mouse model for Angelman syndrome by reduction of alphaCaMKII inhibitory phosphorylation. Nat. Neurosci., 10, 280–282.

18. Weeber, E.J., Jiang, Y., Elgersma, Y., Varga, A.W., Carrasquillo, Y., Brown, S.E., Christian, J.M., Mirnikjoo, B., Silva, A., Beaudet, A.L. et al. (2003) Derangements of hippocampal calcium/calmodulin-dependent protein kinase II in a mouse model for Angelman mental retardation syndrome. J. Neurosci., 23, 2634–2644.

19. Huang, H., Allen, J.A., Mabb, A.M., Kind, I.F., Miriyala, J., Taylor-Blake, B., Sciaky, N., Dutton, J.W., Jr., Lee, H.M., Chen, X. et al. (2012) Topoisomerase inhibitors unsilence the dormant allele in Ube3a in in neurons. Nature, 481, 185–189.

20. Wynn, R.F., Mercer, J., Page, J., Carr, T.F., Jones, S. and Wraith, J.E. (2009) Use of enzyme replacement therapy (Laronidase) before hematopoietic stem cell transplantation for Mucopolysaccharidosis I: experience in 18 patients. J. Pediatr., 154, 135–139.

21. Wynn, R.F., Wraith, J.E., Mercer, J., O'Meara, A., Tylee, K., Thornley, M., Church, H.J. and Bigger, B.W. (2009) Improved metabolic correction in patients with lysosomal storage disease treated with hematopoietic stem cell transplant compared with enzyme replacement therapy. J. Pediatr., 154, 609–611.

22. Biffi, A., Montini, E., Lorioli, L., Cesani, M., Fumagalli, F., Plati, T., Baldoli, C., Martino, S., Calabria, A., Canale, S. et al. (2013) Lentiviral hematopoietic stem cell gene therapy Benefits metachromatic Leukodystrophy. Science, 341, 853–855.

23. Biffi, A. and Naldini, L. (2005) Gene therapy of storage disorders by retroviral and lentiviral vectors. Hum. Gene Ther., 16, 1133–1142.

24. Schambach, A., Zychlinski, D., Ehrnstroem, B. and Baum, C. (2013) Biosafety features of lentiviral vectors. Hum. Gene Ther., 142, 132–142.

25. Young, L.S., Searle, P.F., Onion, D. and Mautner, V. (2006) Viral gene therapy strategies: from basic science to clinical application. J. Pathol., 208, 299–318.

26. Zufferey, R., Nagy, D., Mandel, R.J., Naldini, L. and Trono, D. (1997) Multiply attenuated lentiviral vector achieves efficient gene delivery in vivo. Nat. Biotechnol., 15, 871–875.

27. Anderson, J.S., Javien, J., Nolta, J.A. and Bauer, G. (2009) Preintegration HIV-1 inhibition by a combination lentiviral vector containing a chimeric TRIM5α protein, a CCR5 shRNA, and a TAR decoy. Mol. Ther., 17, 2103–2114.

28. Barclay, S.L., Yang, Y., Zhang, S., Fong, R., Barraza, A., Nolta, J.A., Torbett, B.E., Abedi, M., Bauer, G. and Anderson, J.S. (2015) Safety and efficacy of a tCD25 Preselective combination anti-HIV lentiviral vector in human hematopoietic stem and progenitor cells. Stem Cells, 33, 870–879.

29. Walker, J.E., Chen, R.X., McGee, J., Nacey, C., Pollard, R.B., Abedi, M., Bauer, G., Nolta, J.A. and Anderson, J.S. (2012) Generation of an HIV-1-resistant immune system with CD34(+) hematopoietic stem cells transduced with a triple-combination anti-HIV lentiviral vector. J. Virol., 86, 5719–5729.

30. Biffi, A. (2012) Genetically-modified hematopoietic stem cells and their progeny for widespread and efficient protein delivery to diseased sites: the case of lysosomal storage disorders. Curr. Gene Ther., 12, 381–388.

31. Eichler, F., Duncan, C., Musolino, P.L., Orchard, P.J., De Oliveira, S., Thrasher, A.J., Armant, M., Dansereau, C., Lund, T.C., Miller, W.P. et al. (2017) Hematopoietic stem-cell gene therapy for cerebral Adrenoleukodystrophy. N. Engl. J. Med., 377, 1630–1638.

32. Beegle, J., Hendrix, K., Maciel, H., Nolta, J.A. and Anderson, J.S. (2020) Improvement of motor and behavioral activity in Sandhoff mice transplanted with human CD34+ cells transduced with a HexA/HexB expressing lentiviral vector. J. Gene Med., 22, e3205.

33. Asheuer, M., Pflumio, F., Benhamida, S., Dubart-Kupperschmitt, A., Fouquet, F., Imai, Y., Aubourg, P. and Cartier, N. (2004) Human CD34+ cells differentiate into microglia and express recombinant therapeutic protein. Proc. Natl. Acad. Sci. USA., 101, 3557–3562.

34. Sergijenko, A., Langford-Smith, A., Liao, A.Y., Pickford, C.E., McDermott, J., Nowinski, G., Langford-Smith, K.J., Merry, C.L., Jones, S.A., Wraith, J.E. et al. (2013) Myeloid/microglial driven autologous hematopoietic stem cell gene therapy corrects a Neuronopathic lysosomal disease. Mol. Ther., 21, 1938–1949.

35. Jiang, Y., Armstrong, D., Albrecht, U., Atkins, C.M., Noebels, J.L., Eichele, G., Sweatt, J.D. and Beaudet, A.L. (1998) Mutation of the Angelman ubiquitin ligase in mice causes increased cytoplasmic p53 and deficits of contextual learning and long-term potentiation. Neuron, 21, 799–811.

36. Born, H.A., Dao, A.T., Levine, A.T., Lee, W.L., Mehta, N.M., Mehra, S., Weeber, E.J. and Anderson, A.E. (2017) Strain-dependence of the Angelman syndrome phenotypes in Ube3a maternal deficiency mice. Sci. Rep., 7, 8451.

37. Berg, E.L., Pride, M.C., Petkova, S.P., Lee, R.D., Copping, N.A., Shen, Y., Adhikari, A., Fenton, T.A., Pedersen, L.R., Noakes, L.S. et al. (2020) Translational outcomes in a full gene deletion of ubiquitin protein ligase E3A rat model of Angelman syndrome. Transl. Psychiatry, 10, 39.

38. Dodge, A., Peters, M.M., Greene, H.E., Dietrick, C., Botelho, R., Chung, D., Willman, J., Nenninger, A.W., Ciarlone, S., Kamath, S.G. et al. (2020) Generation of a novel rat model of Angelman syndrome with a complete Ube3a gene deletion. Autism Res., 13, 397–409.

39. Adhikari, A., Copping, N.A., Onaga, B., Pride, M.C., Coulson, R.L., Yang, M., Yasui, D.H., LaSalle, J.M. and Silverman, J.L. (2018) Cognitive deficits in the Snord116 deletion mouse model for Prader-Willi syndrome. Neurobiol. Learn. Mem., 165, 106874.

40. Sonzogni, M., Hakonen, J., Bernabe Kleijn, M., Silva-Santos, S., Judson, M.C., Philpot, B.D., van Woerden, G.M. and Elgersma,Y. (2019) Delayed loss of UBE3A reduces the expression of Angelman syndrome-associated phenotypes. Mo. Autism, 10, 23.

41. Grieco, J.C., Gouelle, A. and Weeber, E.J. (2018) Identification of spatiotemporal gait parameters and pressure-related characteristics in children with Angelman syndrome: a pilot study. J. Appl. Res. Intellect. Disabil., 31, 1219–1224.

42. Huang, H.S., Burns, A.J., Nonneman, R.J., Baker, L.K., Riddick, N.V., Nikolova, V.D., Riday, T.T., Yashiro, K., Philpot, B.D. and Moy, S.S. (2013) Behavioral deficits in an Angelman syndrome model: effects of genetic background and age. Behav. Brain Res., 243, 79–90.

43. Sidorov, M.S., Deck, G.M., Dolatshahi, M., Thibert, R.L., Bird, L.M., Chu, C.J. and Philpot, B.D. (2017) Delta rhythmicity is a reliable EEG biomarker in Angelman syndrome: a parallel mouse and human analysis. J. Neurodev. Disord., 9, 17.

44. Judson, M.C., Wallace, M.L., Sidorov, M.S., Burette, A.C., Gu, B., van Woerden, G.M., King, I.F., Han, J.E., Zylka, M.J., Elgersma, Y. et al. (2016) GABAergic neuron-specific loss of Ube3a causes Angelman syndrome-like EEG abnormalities and enhances seizure susceptibility. Neuron, 90, 56–69.

45. den Bakker, H., Sidorov, M.S., Fan, Z., Lee, D.J., Bird, L.M., Chu, C.J. and Philpot, B.D. (2018) Abnormal coherence and sleep composition in children with Angelman syndrome: a retrospective EEG study. Mol. Autism., 9, 32.

46. Silva-santos, S., van Woerden, G.M., Bruinsma, C.F., Mientjes, E., Jolfaei, M.A., Distel, B., Kushner, S.A. and Elgersma, Y. (2015) Ube3a reinstatement identifies distinct developmental windows in a murine Angelman syndrome model. J. Clin. Invest., 125, 2069–2076.

47. Copping, N.A., Adhikari, A., Petkova, S.P. and Silverman, J.L. (2019) Genetic backgrounds have unique seizure response profiles and behavioral outcomes following convulsant administration. Epilepsy Behav., 101, 106547.

48. Sittig, L.J., Carbonetto, P., Engel, K.A., Krauss, K.S., Barrios- Camacho, C.M. and Palmer, A.A. (2016) Genetic background limits generalizability of genotype-phenotype relationships. Neuron, 91, 1253–1259.

49. Biffi, A., Capotondo, A., Fasano, S., del Carro, U., Marchesini, S., Azuma, H., Malaguti, M.C., Amadio, S., Brambilla, R., Grompe, M. et al. (2006) Gene therapy of metachromatic leukodystrophy reverses neurological damage and deficits in mice. J. Clin. Invest., 116, 3070–3082.

50. Luo, L., Ambrozkiewicz, M.C., Benseler, F., Chen, C., Dumontier, E., Falkner, S., Furlanis, E., Gomez, A.M., Hoshina, N., Huang, W.H. et al. (2020) Optimizing nervous system- specific gene targeting with Cre driver lines: prevalence of germline recombination and influencing factors. Neuron, 106, 1–29.

51. Vogt, N. (2020) Beware the unexpected in Cre drivers. Nat. Methods, 17, 364.

52. Squeri, G., Passerini, L., Ferro, F., Laudisa, C., Tomasoni, D., Deodato, F., Donati, M.A., Gasperini, S., Aiuti, A., Bernardo, M.E. et al. (2019) Targeting a pre-existing anti- transgene T cell response for effective gene therapy of MPS-I in the mouse model of the disease. Mol. Ther., 27, 1215–1227.

53. Copping, N.A., Berg, E.L., Foley, G.M., Schaffler, M.D., Onaga, B.L., Buscher, N., Silverman, J.L. and Yang, M. (2017) Touchscreen learning deficits and normal social approach behavior in the Shank3B model of Phelan-McDermid syndrome and autism. Neuroscience, 345, 155–165.

54. Gompers, A.L., Su-Feher, L., Ellegood, J., Copping, N.A., Riyadh, M.A., Stradleigh, T.W., Pride, M.C., Schaffler, M.D., Wade, A.A., Catta-Preta, R. et al. (2017) Germline Chd8 haploinsufficiency alters brain development in mouse. Nat. Neurosci., 20, 1062–1073.

55. Vogel Ciernia, A., Pride, M.C., Durbin-Johnson, B., Noronha, A., Chang, A., Yasui, D.H., Crawley, J.N. and LaSalle, J.M. (2017) Early motor phenotype detection in a female mouse model of Rett syndrome is improved by cross-fostering. Hum. Mol. Genet., 26, 1839–1854.

56. Carter, R.J., Morton, J. and Dunnett, S.B. (2001) Motor coordination and balance in rodents. Curr. Protoc. Neurosci., Chapter 8, 15, 8.12.1–8.12.14.

57. Flannery, B.M., Silverman, J.L., Bruun, D.A., Puhger, K.R., McCoy, M.R., Hammock, B.D., Crawley, J.N. and Lein, P.J. (2015) Behavioral assessment of NIH Swiss mice acutely intoxicated with tetramethylenedisulfotetramine. Neurotoxicol. Teratol., 47, 36–45.

58. Dhamne, S.C., Silverman, J.L., Super, C.E., Lammers, S.H.T., Hameed, M.Q., Modi, M.E., Copping, N.A., Pride, M.C., Smith, D.G., Rotenberg, A. et al. (2017) Replicable in vivo physiological and behavioral phenotypes of the Shank3B null mutant mouse model of autism. Mol. Autism., 8, 26.

59. Haigh, J.L., Adhikari, A., Copping, N.A., Stradleigh, T., Wade, A.A., Catta-Preta, R., Su-Feher, L., Zdilar, I., Morse, S., Fenton, T.A. et al. (2021) Deletion of a non-canonical promoter regulatory element causes loss of Scn1a expression and epileptic phenotypes in mice. Genom. Med. 13, 69.

60. Copping, N.A. and Silverman, J.L. (2021) Abnormal electrophysiological phenotypes and sleep deficits in a mouse model of Angelman Syndrome. Mol. Autism., 12, 9.

61. Judson, M.C., Sosa-Pagan, J.O., Del Cid, W.A., Han, J.E. and Philpot, B.D. (2014) Allelic specificity of Ube3a expression in the mouse brain during postnatal development. J. Comp. Neurol., 522, 1874–1896.

Figures

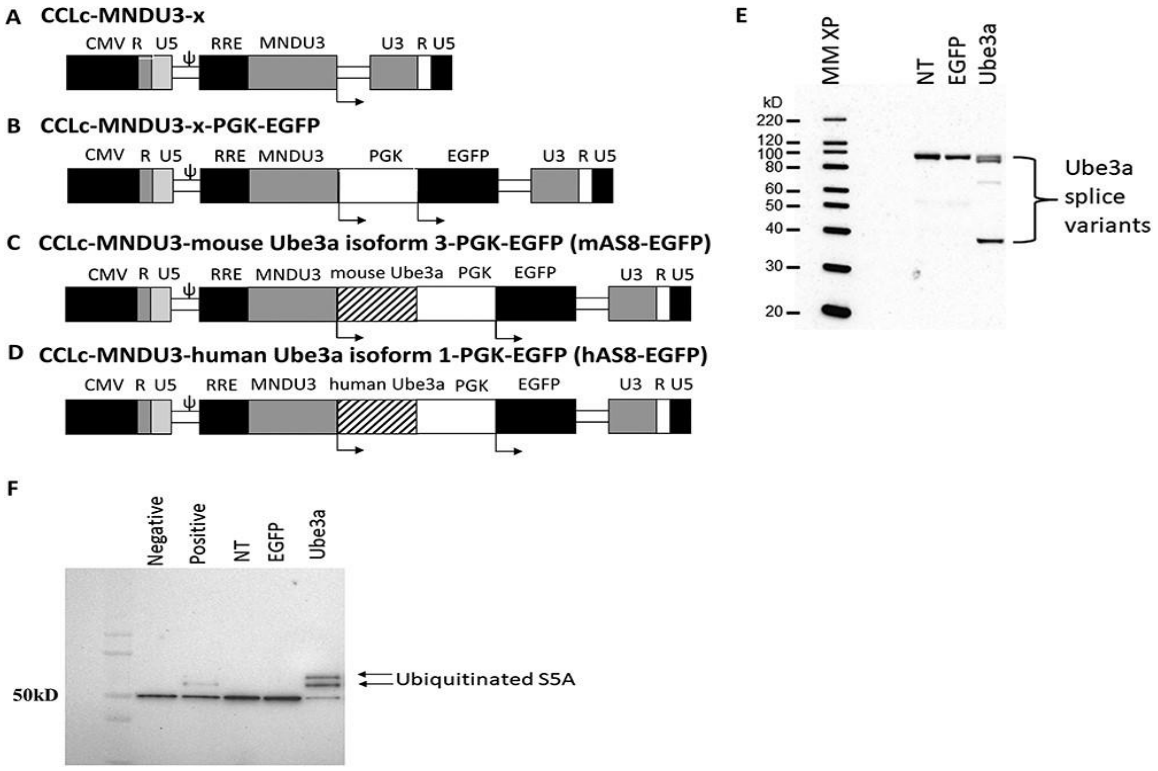

Figure 1. Schematic and functionality of the *Ube3a*-expressing lentiviral vector: (**A**) A self-inactivating lentiviral vector backbone, CCLc-MNDU3-X, was used to generate the *Ube3a* expressing lentiviral vectors. (**B**) EGFP vector used as an empty vector control. (**C**) The modified mouse *Ube3a* isoform 3 (mAS8) was cloned under the control of the MNDU3 promoter. *EGFP* was cloned downstream under the control of a PGK promoter. (**D**) The modified human *UBE3A* isoform 1 was cloned under the control of the MNDU3 promoter. *EGFP* was cloned downstream under the control of a PGK promoter. (**E**) Human CD34+ HSPC were transduced with the *Ube3a* lentivector and derived into mature macrophages. Cell extracts were then generated and evaluated for overexpression of UBE3A by western blot. (**F**) An S5A ubiquitination assay was performed on the macrophage cell extracts. Control NT, *EGFP* vector alone (EGFP) transduced cells, and negative and positive controls supplied by the manufacturer were used as controls.

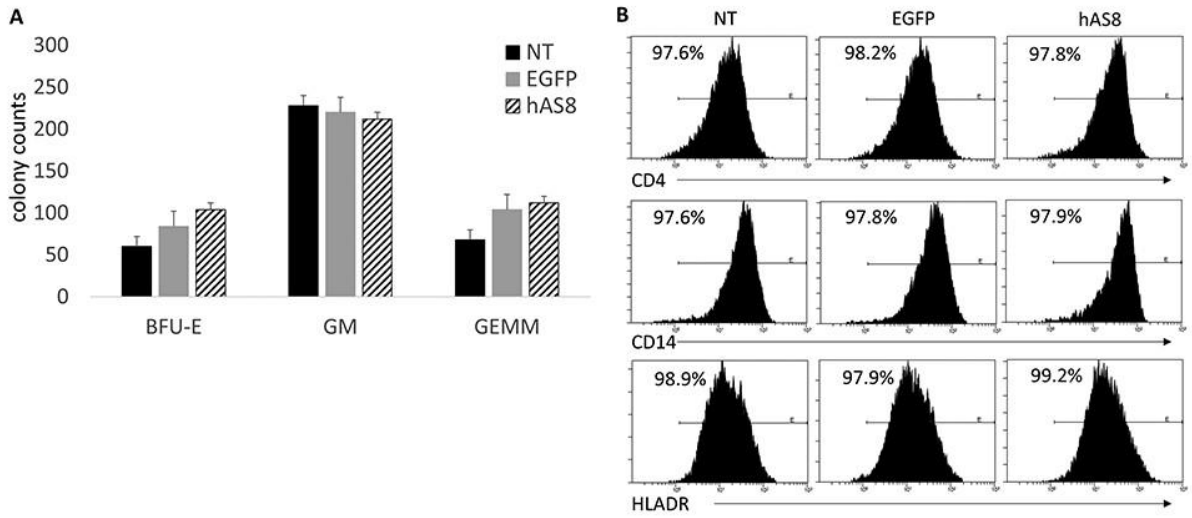

Figure 2. CFU assay and macrophage derivation of *Ube3a* vector-transduced human CD34+ HSPC: Human CD34+ HPSC were left NT or transduced with either the *EGFP* alone control vector (EGFP) or the *Ube3a* vector (hAS8). (**A**) Cells were cultured in methylcellulose media for 12 days when specific colonies (BFU-E, GM and GEMM) were counted. (**B**) CFUs were further differentiated into macrophages and analyzed by flow cytometry for the cell surface markers CD4, CD14 and HLADR.

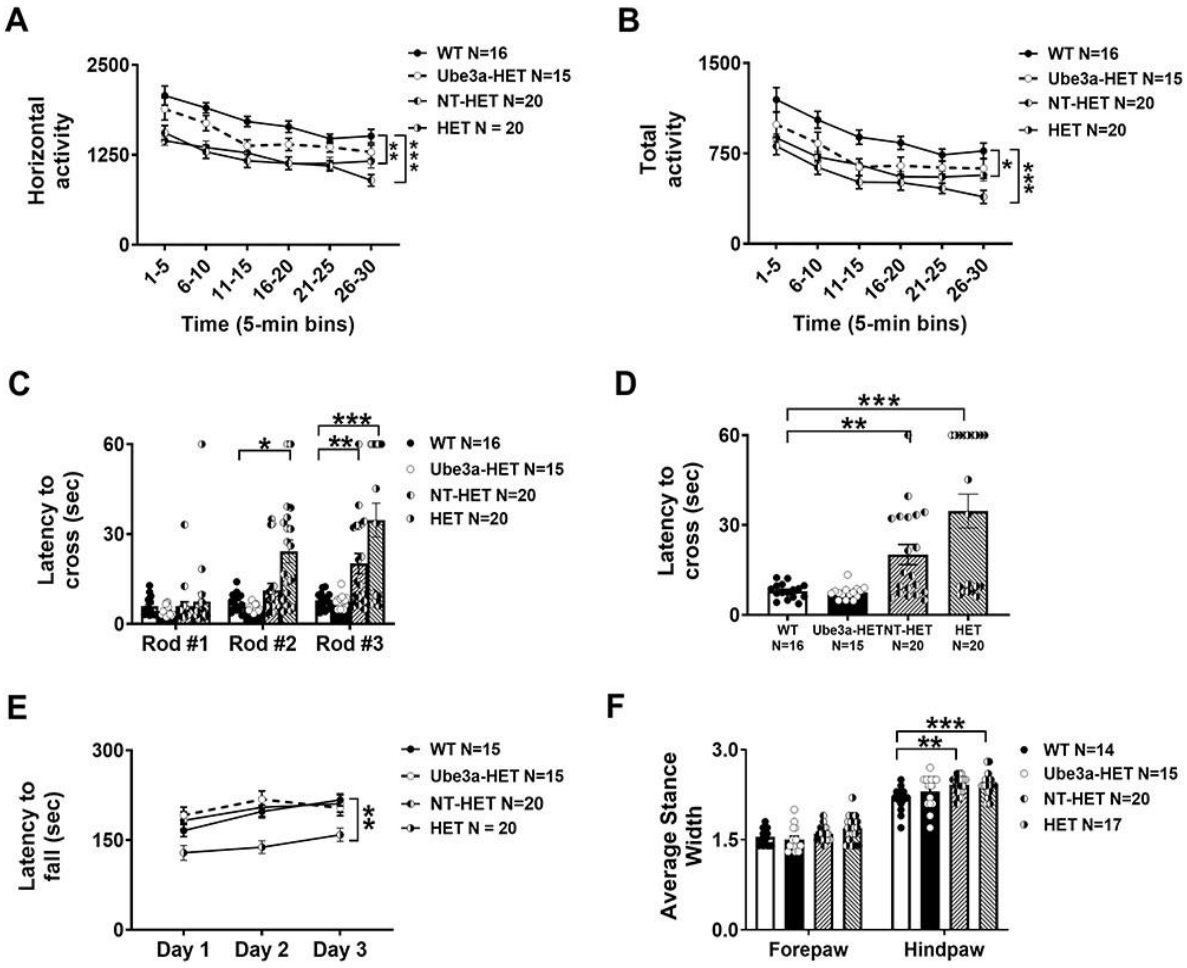

Figure 3. Locomotor ability, balance, motor coordination and gait from *Ube3a* lentivector transduced HSPC-transplanted neonates: Rigorous assessment of motor translational phenotypes using four standard motor behavioral tests in treated and untreated *Ube3a*$^{mat+/pat+}$ *IL2rg*$^{-/y}$ mice that were irradiated and transplanted as neonates with either NT (NT-HET (hatched bar) or the *Ube3a* lentivector transduced (Ube3a-HET (black bar)) human CD34+ HSPC. Eight weeks post-transplant, mice were subjected to (**A**, **B**) open field locomotion, (**C**, **D**) balance beam, (**E**) rotarod and (**F**) treadmill walking. In all tests, *Ube3a*$^{mat+/pat+}$ *IL2rg*$^{-/y}$ deficient mice transplanted with the *Ube3a* vector transduced human CD34+ HSPC (Ube3a-HET) exhibited wildtype values of performance. (A, B) Open field activity was increased by both the total distance and horizontal activity metrics. (C) Eight weeks post-transplant, mice were also tested on the beam walking assay. Beams decrease in width and are more difficult to cross going from Rod #1 to Rod #2 to Rod #3. (D) Highlight of Rod #3 of C, the most challenging coordination test with remarkable improvements. (E) Latency to fall from the rotarod was significantly improved in the *Ube3a*$^{mat+/pat+}$ *IL2rg*$^{-/y}$ mice transplanted with *Ube3a* vector-transduced human CD34+ HSPC (Ube3a-HET) compared with the NT (NT-HET) cell controls. (F) DigiGait™ analyses showed a narrowing of wide stances in the Ube3a-HET treated group.

Data are expressed as ± standard error of mean (SEM). $^{*}P < 0.05$, $^{**}P < 0.001$, $^{***}P < 0.0001$ indicate when the HET and NT-HET groups differ from the control WT group.

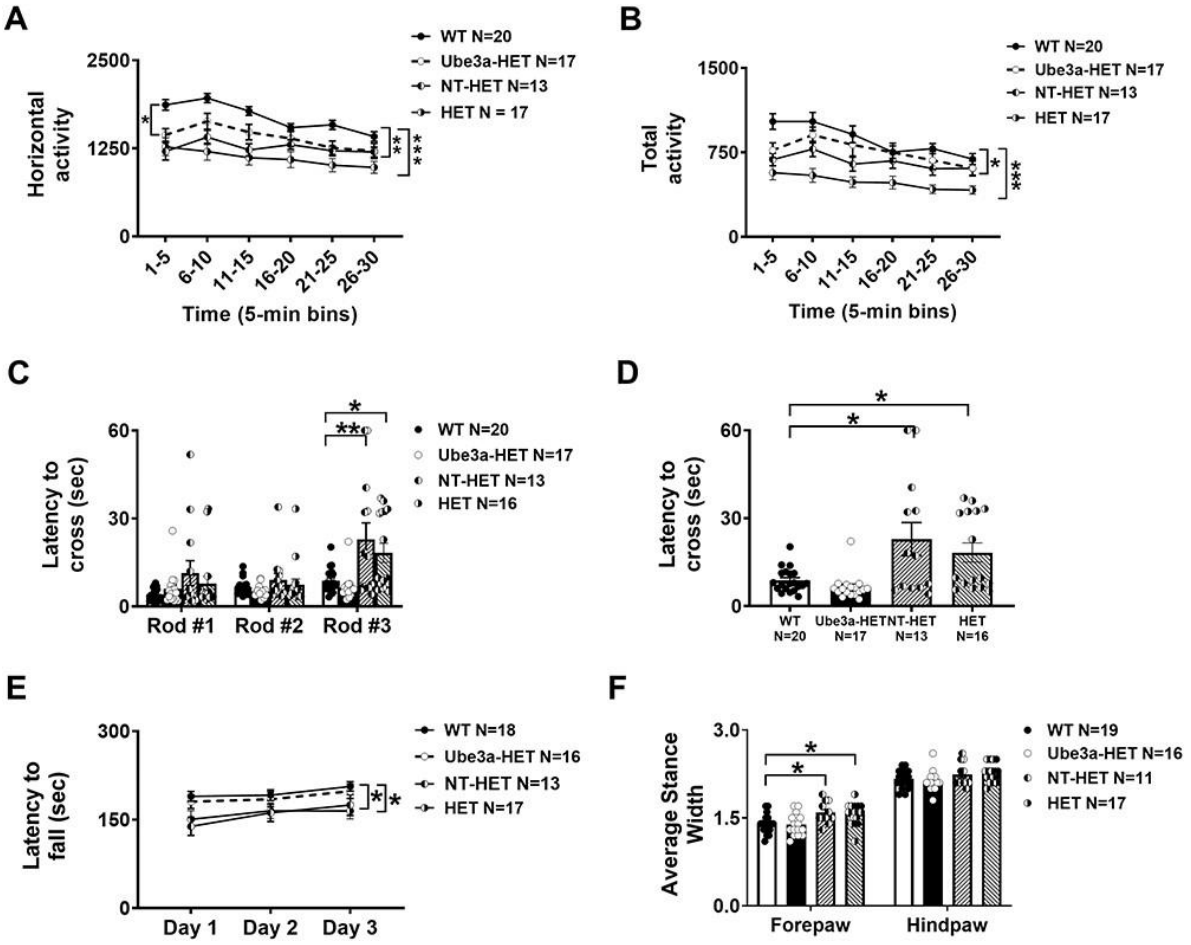

Figure 4. Locomotor ability, balance, motor coordination and gait from *Ube3a* lentivector transduced HSPC-transplanted adults: Rigorous assessment of motor translational phenotypes using four standard motor behavioral tests in treated and untreated *Ube3a*$^{mat-/pat+}$ *IL2rg*$^{-/y}$ mice that were treated with busulfan and transplanted as adults with either NT (NT-HET (hatched bar) or the *Ube3a* lentivector-transduced (Ube3a-HET (black bar)) human CD34+ HSPC. Four-five weeks old mice were conditioned with busulfan and transplanted via i.v. injection. Six weeks later mice were subjected to (**A**, **B**) open field locomotion, (**C**, **D**) balance beam, (**E**) rotarod and (**F**) treadmill walking. In all tests, *Ube3a*-deficient mice transplanted with the *Ube3a* vector-transduced human CD34+ HSPC (Ube3a-HET) exhibited wildtype values of performance. (A, B) Open field activity was increased by both the total distance and horizontal activity metrics. (C) Eight weeks post-transplant, mice were also tested on the beam walking assay. Beams decrease in width and are more difficult to cross going from Rod #1 to Rod #2 to Rod #3. (D) Highlight of Rod #3 of C. (E) Latency to fall from the rotarod was significantly improved in the *Ube3a*-deficient mice transplanted with Ube3a vector transduced human CD34+ HSPC (Ube3a-HET) compared with the NT (NT-HET) cells controls. (F) DigiGait™ analyses showed a narrowing of wide stances in the Ube3a-HET treated group.

Data are expressed as mean ± SEM. $^{*}P < 0.05$, $^{**}P < 0.001$, $^{***}P < 0.0001$ indicate when the HET and NT-HET groups differ from the control WT group.

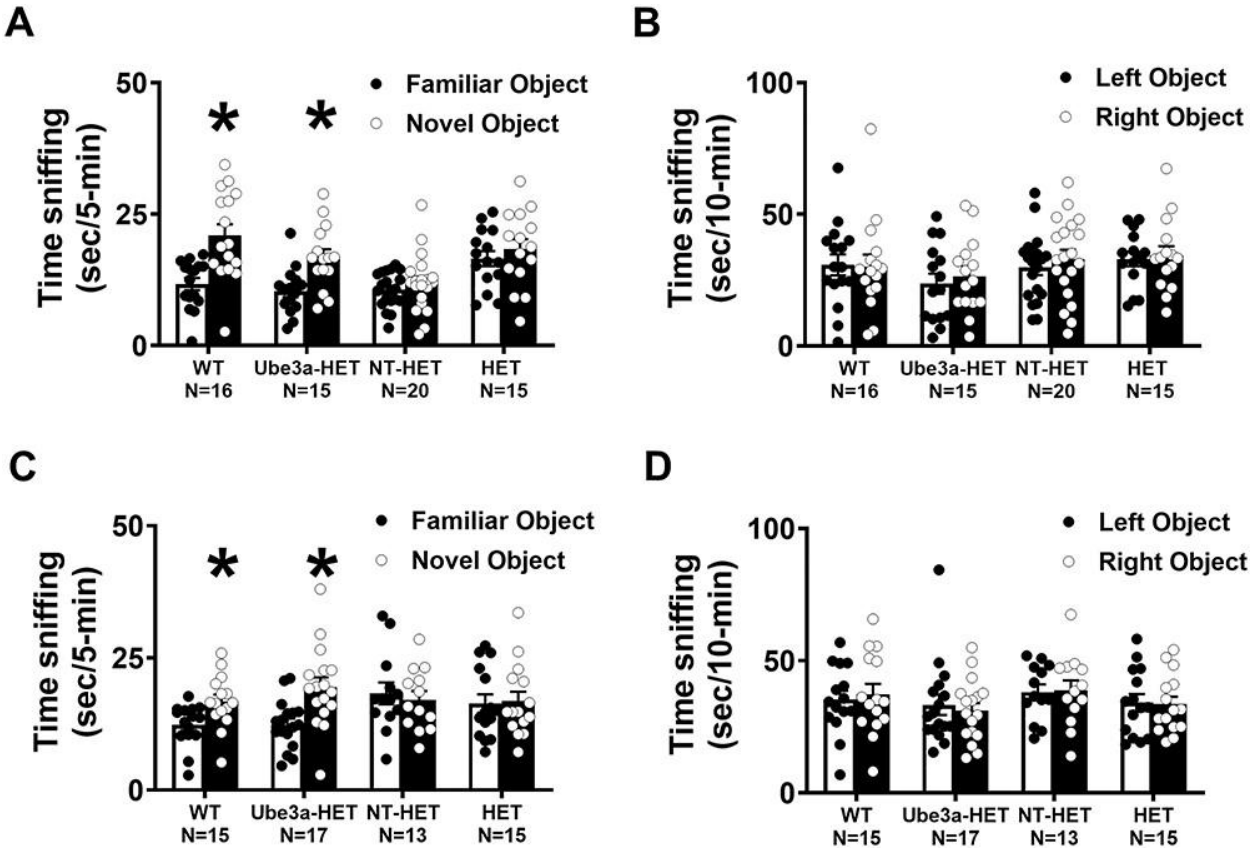

Figure 5. Novel object recognition with mice transplanted with *Ube3a* lentivector transduced HSPC: (A,B) Newborn Ube3a-deficient IL2rg-/y mice were transplanted with either nontransduced (NT-HET) or Ube3a vector-transduced (Ube3a-HET) human CD34+ HSPC. Wild type IL2rg-/y mice (WT) were used as a control. Eight weeks post-transplant, mice were assessed for learning and memory abilities using the novel object recognition test. (**A**) Ube3a-HET mice exhibited intact object recognition following a one-hour delay, similar to WT while, NT-HET mice did not spend more time with the novel object, exhibiting a lack of recognition memory. (**B**) All groups explored the two objects similarly during the familiarization phase. (**C, D**) Ube3a-deficient adult mice were transplanted with either nontransduced (NT-HET) or Ube3a vector-transduced (Ube3a-HET) human CD34+ HSPC. Wild type IL2rg-/y mice (WT) were used as a control. Six weeks post i.v. injection in adult mice, subjects were assessed for learning and memory abilities using the novel object recognition test. (C) Ube3a-HET mice exhibited intact object recognition following a one-hour delay, similar to WT while, NT-HET mice did not spend more time with the novel object, exhibiting a lack of recognition memory. (D) All groups explored the two objects similarly during the familiarization phase. $^{*}p < 0.05$, novel versus familiar.

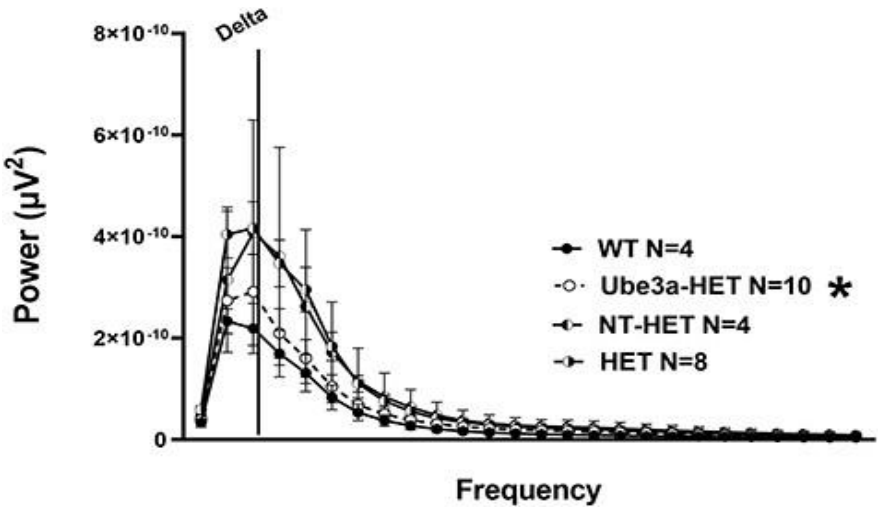

Figure 6. Delta power analysis in AS mice transplanted with *Ube3a* lentivector transduced HSPC: A PSD between using treated and untreated *Ube3a*-deficient *IL2rg*$^{-/y}$ mice that were irradiated and transplanted as neonates with either NT HET (semi-filled left) or the *Ube3a* lentivector transduced Ube3a-HET (black dotted line open circles) human CD34+ HSPC. AS mice on B6 background versus their WT background littermates illustrate observable differences in elevated delta power analogous to clinical phenotypes. Quantification of spectral power bands illustrates that treatment lowers/corrects the elevated delta spectral power toward the levels observed in WT mice.

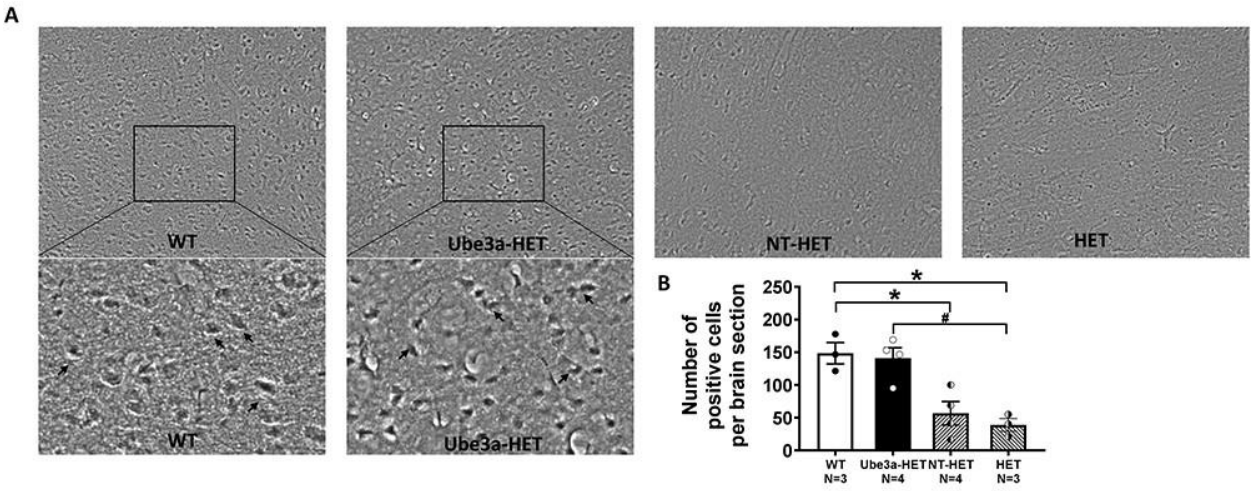

Figure 7. Immunohistochemical analysis of UBE3A expression in cortex of the mouse brain: Six weeks post-transplant in adult mice, subjects were assessed for UBE3A expression using DAB as a chromogen. (**A**) Immunohistochemical images showing expression of UBE3A in the mouse cortex of non-transplanted *Ube3a* wild type *IL2rg*$^{-/y}$ (WT) mice, those transplanted with *Ube3a* vector transduced (Ube3a-HET) human CD34+ HSPC, those transplanted with NT human CD34+ HSPC (NT-HET), and non-transplanted HET mice (HET). (**B**) A significant increase in the UBE3A positive cells, similar to the WT level, was observed in transplanted Ube3a-HET compared with NT-HET and HET when treated as adults. Data are expressed as mean ± SEM. $^{*}P < 0.05$ indicates when the HET and NT-HET groups differ from the control WT group. $^{\#}P < 0.05$ indicates when the Ube3a-HET group differs from HET group.

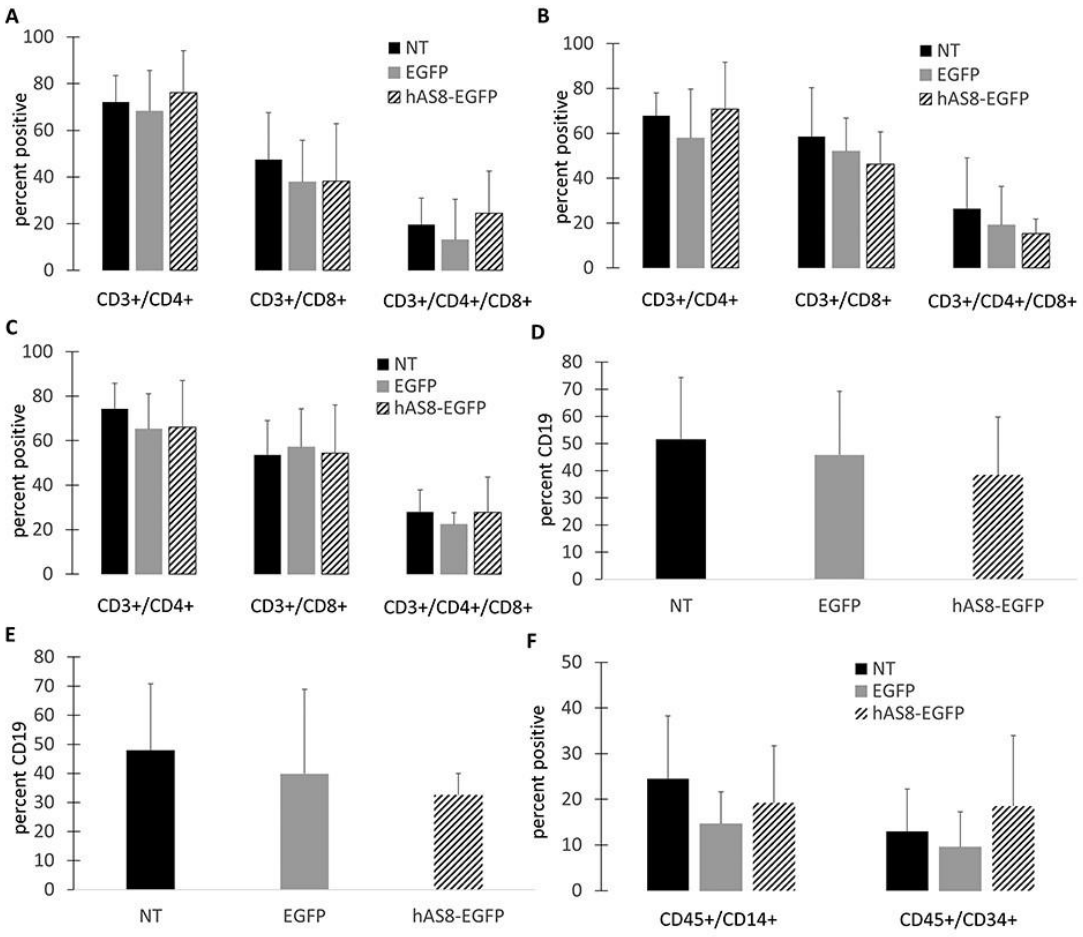

Figure 8. Engraftment and development of human immune cells in NRG mice: Human CD34+ HSPC were left NT or transduced with either the *EGFP* control (EGFP) or *Ube3a*-expressing (hAS8) lentiviral vector. Cells were transplanted into 2–5-day-old NRG mice. At 16 weeks post-transplant, mice were euthanized, and human T cells were analyzed for CD3, CD4, and CD8 expression in the (**A**) peripheral blood, (**B**) spleen, and (**C**) thymus. Human B cells were analyzed for CD45 and CD19 in the (**D**) spleen and (**E**) bone marrow. (**F**) Human macrophages (CD45/CD14) and human CD34+ HSPC (CD45/CD34) were analyzed in the bone marrow.

Supplementary Results

Analysis of motor and cognitive abilities of immunodeficient Ube3a-deficient models of AS:

To evaluate whether various immunodeficient gene knockouts affected AS phenotypes, motor and cognitive assays were performed similar to the methods described above. **Fig. S1A,B,D** demonstrated that *Rag2* mutant mice had substantial motor and cognitive deficits which would result in confounding our study of AS mice upon transplantation with the Ube3a vector transduced HSPC. This was in contrast to the *IL2rg* mutant mice which had no motor behavioral phenotype in open field over 30-minutes, summed movement, or motor coordination and learning on rotarod, Fig. S1A,B,C. The *IL2rg* mutant mice had no breeding or survival issues, readily crossed with Ube3a$^{-/+}$ dams, and produced offspring. These mice also exhibited intact cognitive abilities on the novel object recognition Fig. S1D, E. *Rag1* mutant mice had novel object recognition that was impaired by discrimination index Fig. S1F, but not within group t-tests Fig. S1D. Yet, *Rag1* null illustrated less than 5% human cell engraftment. Evaluating various degrees of immunodeficiency for AS behavioral phenotypes and human cell engraftment revealed our optimal immunodeficient strain to cross with *Ube3a* which was the *IL2rg* null mice (*IL2rg*$^{-/y}$). The crossing of the *Ube3a*$^{-/+}$ and *IL2rg*$^{-/y}$ mice generated the *Ube3a*$^{-/+}$-*IL2rg*$^{-/y}$ immunodeficient model allowed for studying the *in vivo* efficacy of the Ube3a expressing lentiviral vector in human CD34+ cells.

Supplementary Figures

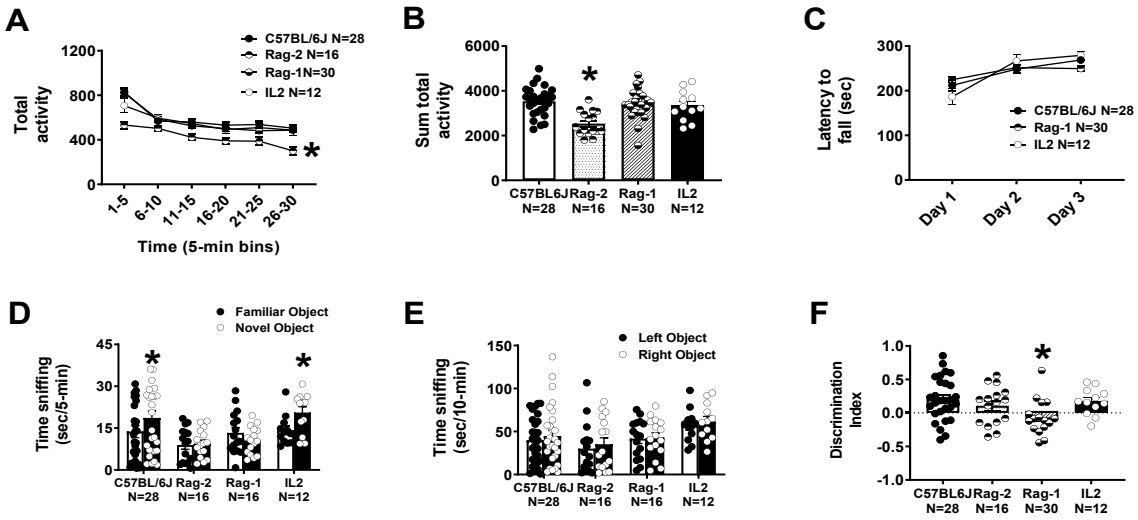

Figure S1. AS-relevant behavioral testing of host strains on a tailored battery of AS motor and cognitive: The graphs highlight host strain behavior before they had been crossed with the *Ube3a*-deficient line. *Rag2* mutant mice had substantial motor (A) and cognitive deficits (D) which would confound our study of AS mice. *Rag1* mutant mice had novel object recognition impairment by a discrimination index (F), but not within group t-tests (E). *IL2rg* mutant mice had no motor behavioral phenotype in open field over 30-minutes (A), summed movement (B), motor coordination and learning on rotarod (C). These mice had no breeding or survival issues, readily crossed with *Ube3a*-mutant dams and produced offspring. These *IL2rg* mice also exhibited intact cognitive abilities on the novel object recognition (D,E,F).

Acknowledgements

This work would not have been possible without the support and guidance that I received from many people.

I would like to express my deepest gratitude to my esteemed mentor, Dr. Jill Silverman for her guidance, time, and wisdom throughout this study. Her enthusiasm and encouragement, both personally and professionally, patience, timely advice, scientific approach, and constant support have carved my academic path since my undergraduate study. She taught me how to be a good researcher. I will be forever obliged for her mentorship.

I owe a deep sense of acknowledgement and appreciation to my incredible dissertation committee members, Dr. Joseph Anderson and Dr. Kyle Fink for their careful supervision, expert guidance, and constant feedback during my research. Dr. Anderson, my co-mentor, advised me throughout my projects and introduced me to the world of conducting Investigational New Drug enabling studies. Dr. Fink, our close collaborator, supervised my research plans as well as guided me to solidify my wet lab technical skills. I must also mention their lab members: Dr. Julie Beegle from the Anderson lab, David Cameron, Dr. Peter Deng, and Dr. Julian Halmai from the Fink lab who were always so helpful and provided me with their assistance throughout my research.

I am extremely thankful to many collaborators with whom I have had the privilege of working with over the years. I especially want to acknowledge Dr. David Segal, Dr. Alex Nord, Dr. Janine LaSalle, Dr. Jacob Ellegood, as well as their entire lab. It has been a tremendous experience getting to work with and learn from such a wonderful community of scientists.

A special acknowledgement to the support received through the Foundation for Angelman Syndrome Therapeutics and their Chief Scientific Officer Dr. Allyson Berent. I am eternally thankful to the Achievement Rewards for College Scientist Foundation for their generosity that I was afforded which made my immense career development possible.

I profusely thank my labmates: Timothy Fenton, Dr. Nycole Copping, Dr. Elizabeth Berg, and Michael Pride who all made meaningful contributions to this work. Their kind help, encouragement, and friendships truly made the process of research such an enjoyable one. The same can be said about my cohortmates: Alicia Werner, Amanda Guevara, Charles Crawford, Chih-Ting Wu, Juliana Hernandez, and Katie Murray. These past few years would not have been nearly as fun and productive without them.

Personally, I would not have accomplished this work without the enduring support of my family and friends. I would like to express my heartfelt gratitude to my parents, Ram and Deuka, for being my role models and for the numerous sacrifices they made for me and my sister. Without their love, care, and support, none of this would be possible. Their encouragement throughout my education journey has been my biggest source of inspiration, comfort, and strength. My deep appreciation goes out to my uncle and aunt, Bishnu and Indu, for providing a welcoming second home to us. I want to acknowledge my sister Astha, and my cousins Riya and Raj for the weekends full of laughter and goofiness and for always being there when needed. Ryan, my significant other, and his family for their unwavering support in every step of the way. I owe a great deal of gratitude for the warm and supportive friendships with Sean Senerchia, Dr. Stela Petkova, Danielle Kenna, Tristan Franzetti, Maneesa Subedi, Monica Choudhary, Abhay Adhikari, among many others.

I am indebted to you all. Thank you!